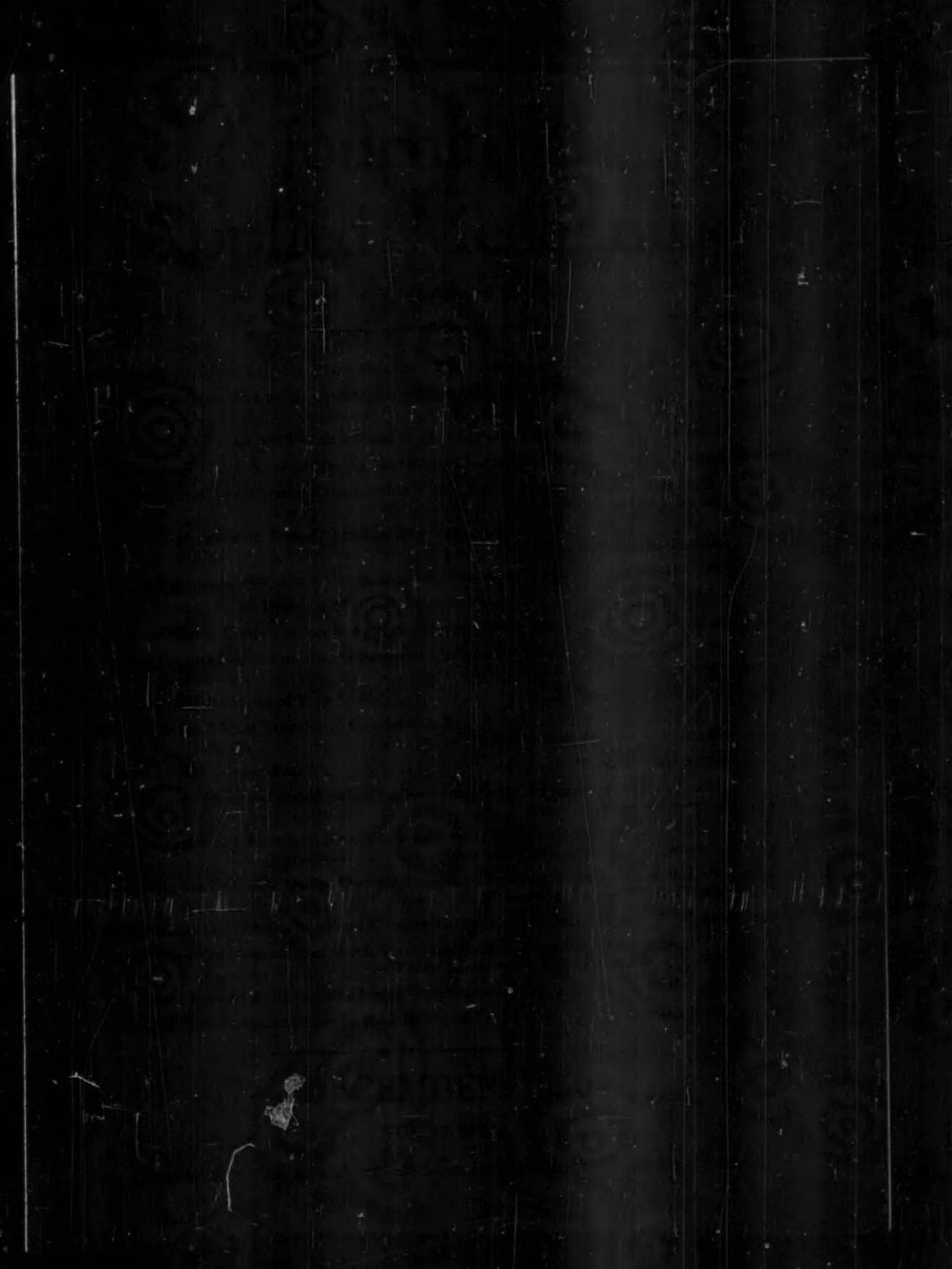

Effect of Stress-Free Edges in Plane Shear of a Flat Body

By W. T. READ,[1] MURRAY HILL, N. J.

This paper determines the tangential stiffness of a flat rectangular body, or shear pad, with a uniform relative tangential displacement on the upper and lower surfaces. The state of stress differs from pure shear in that the edges are stress-free. The correction to the stiffness in pure shear is obtained as a function of Poisson's ratio and the length-to-thickness ratio. The paper also illustrates the power of energy methods in furnishing accurate approximations with a small amount of numerical work when only over-all quantities, such as stiffness, are investigated. By manipulating energy relations and using the Prager-Synge approximate method a few hours of slide-rule computation was sufficient to determine both upper and lower bounds for the stiffness.

Introduction

THE purpose of this paper is to determine the tangential stiffness of a rectangular plate, or shear pad, defined as the tangential force on the upper and lower surfaces, Fig. 1(*a*), required to produce a uniform relative displacement of unit magnitude. The state of stress differs from pure shear in that the four edge surfaces are stress-free. This situation occurs in cemented lap joints, in shear pads for vibration isolation, and in the common test for shear modulus where the material is cemented between a pair of rigid plates. For example, at the Bell Telephone Laboratories the shear modulus and shear damping constant of plastic materials are determined by forced vibration of a flat specimen held between rigid plates which vibrate at a frequency well below the natural frequency of the specimen.

We shall determine the stiffness as a function of the shear modulus G, Poisson's ratio ν, and the relative dimensions; or, specifically, the correction, which must be applied to the stiffness-shear modulus relation for pure shear, will be determined as a function of ν and the length-to-thickness ratio. By manipulating simple energy relations and using an approximate energy method, recently developed by W. Prager and J. L. Synge,[2] both upper and lower bounds are determined for the stiffness. The small amount of numerical calculation involved can be carried out by slide rule in a few hours.

Energy and Stiffness Corrections

It will be convenient to consider the state of stress as the sum of a state of pure shear and a correction state, Fig. 1, which must

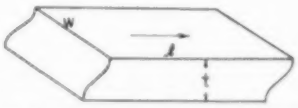

Fig. 1(*a*) Pad With Uniform Tangential Displacement of Upper Surface Relative to Lower (End surfaces are stress-free.)

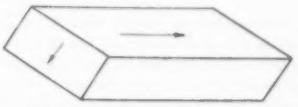

Fig. 1(*b*) Same Pad as (*a*) in Pure Shear

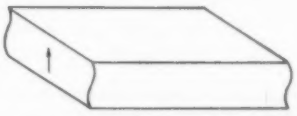

Fig. 1(*c*) Correction State of Stress = Difference Between Total and Pure-Shear States

be superposed on pure-shear to satisfy the boundary conditions. Since the pure-shear state gives the correct displacement on the upper and lower surfaces and gives no normal stress at the ends, the correction state is defined by the condition that it remove the pure shear stress at the ends, give no normal stress at the ends, and no displacement on the upper and lower surfaces.

In this section we shall find the stiffness correction in terms of the energy in the correction state and the ratio of the length l to the thickness t. If the width w is large in comparison to the thickness then the assumption of plane strain is a valid approximation, and an equilibrium state of stress can be represented by an Airy stress function. If φ is the total stress function, φ_p the pure-shear stress function, and φ_c the correction stress function then $\varphi = \varphi_p + \varphi_c$ with similar additive relations for the displacements, stresses, and strains but not for the energies.

To determine the relation between the energy W_p of pure shear, the energy W_c of the correction state, and the energy W of the combined or total state of stress, we begin with the combined state and subtract from it the correction state leaving the body in a state of pure shear; or, in physical terms, we begin with a uniform relative displacement on the upper and lower surfaces and stress-free ends and superpose a uniform shearing stress on the ends—this uniform shear being the negative of the shear defining the correction state. In this process a positive amount of work W_c is done on the end surfaces by the negative correction stresses acting through the negative correction displacements. No work is done on the upper and lower surfaces which remain fixed. Thus in adding an amount of energy W_c to the initial energy W, we have produced the state of pure shear having energy W_p, so that

$$W_p = W + W_c \quad \ldots\ldots\ldots\ldots\ldots\ldots\ldots\ldots [1]$$

---

[1] Bell Telephone Laboratories, Inc.

[2] "Approximations in Elasticity Based on the Concept of Function Space," by W. Prager and J. L. Synge, *Quarterly of Applied Mathematics*, vol. 5, October, 1947, pp. 241–269.

Presented at the National Conference of the Applied Mechanics Division, Purdue University, Lafayette, Ind., June 22–24, 1950, of The American Society of Mechanical Engineers.

Discussion of this paper should be addressed to the Secretary, ASME, 29 West 39th Street, New York, N. Y., and will be accepted until January 10, 1951, for publication at a later date. Discussion received after the closing date will be returned.

Note: Statements and opinions advanced in papers are to be understood as individual expressions of their authors and not those of the Society. Manuscript received by the Applied Mechanics Division September 16, 1949. Paper No. 50—APM-6.

Since the energy of every state of stress is necessarily positive, the total energy is less than the pure-shear energy, as would be expected from the fact that the pure-shear state is defined by more constraints than the total state. Since stiffness is proportional to energy for a given displacement, the assumption of pure shear gives a stiffness which is too large. If k is the stiffness per unit width and d the displacement of the upper surface relative to the lower, and the W's are energies per unit width, then

$$W = \frac{1}{2} kd^2 \quad W_p = \frac{Gd^2 l}{2t} \qquad [2]$$

and from Equation [1]

$$k = k_0 (1 - \epsilon) \qquad [3]$$

where $k_0 = Gl/t$ is the static stiffness in pure shear and

$$\epsilon = \frac{2t}{l} \frac{W_c}{Gd^2}$$

is a dimensionless correction term. Since W_c is proportional to Gd^2, the analysis can be simplified by taking $G = 1$ and $d = 2$ with unit positive displacement on the upper surface and unit negative displacement on the lower surface. Also, since the correction term does not depend upon the absolute size but on the relative dimensions, the half-thickness may be taken as the unit of length. Then since energy depends upon the square of the linear scale factor

$$\epsilon = \frac{1}{2R} W_c \qquad [4]$$

where R is the length to thickness ratio and W_c is now a dimensionless quantity giving the energy per unit width in a pad with unit half-thickness unit shear modulus, unit negative shear stress, and no normal stress on the ends, and no displacement of the upper and lower surfaces.

Relation to a Semi-Infinite Pad

In this section we shall express ϵ in terms of R and the energy in a semi-infinite pad.

The energy W_c depends upon ν and R. However, as R increases, W_c approaches a constant value, since the total state of stress approaches pure shear in the interior, and the self-energy of the correction state is concentrated in the ends; the energy in each end approaching the energy in a semi-infinite pad with fixed upper and lower surfaces and with unit negative shear at the end. How rapidly W_c approaches twice the energy W_0 in the semi-infinite pad depends upon how rapidly the correction stress decays in moving from the ends toward the interior. We shall show that, in the semi-infinite pad, the stress decays with distance from the end x approximately as e^{-3x} where x is measured in terms of the half-thickness. When $x = 3$, the stress in the center has declined to $e^{-9} = 0.00012$ of its value at the end, so that the state of stress in the semi-infinite pad will be a good approximation to the correction state of stress in one end of the finite pad, even for a length-to-thickness ratio as low as 3. Thus we take $W_c = 2W_0$, which gives

$$\epsilon = \frac{W_0}{R} \qquad [5]$$

and proceed to calculate W_0, the energy in a semi-infinite pad with fixed upper and lower surfaces and unit negative shear stress and no normal stress on the end.

Upper Bound for Energy in Semi-Infinite Pad

In this section we shall determine an upper bound for the energy in the semi-infinite pad. In the following section the lower bound will be found and the interval of uncertainty reduced.

Taking an xy-co-ordinate system as shown in Fig. 2, and calling u and v the components of displacement in the x and y-

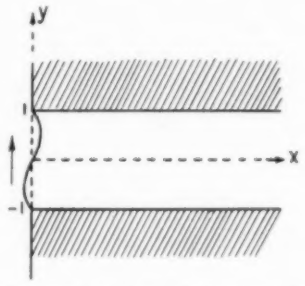

Fig. 2 Semi-Infinite Pad With Unit Negative Shear at End and No Displacement of Upper and Lower Surfaces

directions, respectively, the boundary conditions on displacement are

$$u = v = 0 \qquad [6]$$

when $y = \pm 1$. Calling σ_x, σ_y, and τ_{xy} the stress components, the boundary conditions on stress are

$$\sigma_x = 0, \quad \tau_{xy} = -1 \qquad [7]$$

when $x = 0$. In addition, we have the requirement that the stress vanish at infinity.

In this problem the boundary conditions are mixed, partly stress, partly displacement. For such problems exact solutions are usually impractical. Instead, we shall use the approximate method of Prager and Synge,[2] which furnishes both upper and lower bounds for the energy so that W_0 may be determined with a known uncertainty.

To find the upper bound, we construct an approximate state of stress, defined by components of stress which satisfy the equilibrium conditions and the boundary conditions on stress, but not necessarily the compatibility conditions, that is, the corresponding strains, which are determined through Hooke's law, need not represent displacements. Now consider the state of stress defined by the difference between the actual stress and strain and the approximate stress and strain.

The energy corresponding to any state of stress and strain which satisfies Hooke's law is positive, independently of whether the stress satisfies equilibrium or the strain, compatibility. Thus the energy in the artificial state defined by the difference between the actual and approximate stresses is positive, and we have the inequality

$$W_0 + W_a - 2W_{0a} > 0 \qquad [8]$$

where W_a is the self-energy of the approximate state of stress and $W_{0a} = W_{a0}$ is the interaction energy, which has the negative sign, because we are considering the state defined by the difference between the actual and the approximate states. Since the approximate stress satisfies equilibrium, W_{0a} may be transformed to the surface integral of the work done by the approximate surface stress acting through the actual displacement. The actual displacement vanishes on the upper and lower surfaces, which therefore give no contribution to W_{0a}. However, on the end surface the approximate stress satisfies the boundary conditions and is therefore equal to the actual stress so that W_{0a} is equal

to the work done by the actual surface stress acting through the actual displacement, that is, $W_{0s} = W_0$ and Equation [8] becomes

$$W_0 < W_s \quad [9]$$

and we have an upper bound for W_0 and therefore a lower bound for k.

Since the approximate stress satisfies equilibrium, the stress components can be derived from a stress function. By taking

$$\frac{-y}{a} e^{-ax}$$

as a stress function, we obtain the stress components

$$\left.\begin{aligned} \sigma_x &= 0 \\ \sigma_y &= -ay\, e^{-ax} \\ \tau_{xy} &= -e^{-ax} \end{aligned}\right\} \quad [10]$$

which satisfy the boundary conditions at $x = 0$ and appear to be physically reasonable; σ_y being a compression in the upper half of the disk and tension in the lower half, and the stress approaching zero exponentially away from the end. The parameter a is determined to make W_s a minimum. Computing the strain and the energy density and integrating with respect to x from 0 to ∞ and with respect to y from -1 to 1 and minimizing with respect to a, we obtain

$$W_0 < W_s = \sqrt{\frac{1-\nu}{6}} \quad [11]$$

with an optimum a of

$$\sqrt{\frac{6}{1-\nu}}$$

Double Bounds for the Energy

In this section we shall obtain a lower bound for the energy and then, by using more complex approximate solutions, reduce the gap between the upper and lower bounds.

To obtain a lower bound we construct approximate displacements which satisfy the boundary conditions on displacement. The corresponding stress components are calculated from the strain components using Hooke's law and need not satisfy either the equilibrium conditions or the boundary conditions on stress.

Since the energy in a state of stress defined by the difference between the actual and approximate displacements must be positive, we have as before

$$W_0 + W_d - 2W_{0d} > 0 \quad [12]$$

where W_d is the self-energy of the approximate displacement solution and $W_{0d} = W_{d0}$ is the interaction energy of the actual stress and the approximate strain. Since the actual stress satisfies equilibrium and the approximate strain, compatibility W_{0d} can be transformed to the surface integral of the work done by the actual surface stress acting through the approximate displacement. However, the approximate displacement satisfies the boundary conditions on displacement and therefore vanishes on the upper and lower surfaces, so that these give no contribution to W_{0d}. On the end surfaces the actual surface stress is known from the boundary conditions on stress, so that W_{0d} is known and we have a lower bound

$$W_0 > 2W_{0d} - W_d \quad [13]$$

If we multiply the approximate displacement by a constant c, we have a more general displacement which also satisfies the boundary conditions, that is, which vanishes on $y = \pm 1$. Since W_{0d} varies with c and W_d with c^2, if we maximize $2W_{0d} - W_d$ with respect to c we obtain the lower limit

$$W_0 > \frac{(W_{0d})^2}{W_d} \quad [14]$$

which is independent of the magnitude of the approximate displacement.

The negative unit shear stress at the end acting in the direction of positive v, gives

$$W_{0d} = \frac{1}{2}\int_{-1}^{1} v(0, y)\, dy \quad [15]$$

where $v(0, y)$ is the approximate vertical displacement at $x = 0$.

Since the only applied force acts in the vertical direction, as a first approximation to the displacement we take

$$\left.\begin{aligned} u &= 0 \\ v &= (1 - y^2)\, e^{-bx} \end{aligned}\right\} \quad [16]$$

which gives $W_{0d} = 2/3$.

Calculating the self-energy and maximizing with respect to b gives

$$W_0 > \frac{1}{6}\sqrt{\frac{5(1-2\nu)}{1-\nu}} \quad [17]$$

with an optimum b of

$$\sqrt{\frac{5(1-\nu)}{1-2\nu}}$$

The case of an incompressible material, where $\nu = 1/2$, will be considered separately. In the range $\nu = 1/4$ to $\nu = 1/2$, the agreement between the upper and lower bounds is encouraging for a first approximation, Fig. 3. With $\nu = 1/4$ we have

$$0.304 < W_0 < 0.354 \quad [18]$$

and for $\nu = 1/3$

$$0.263 < W_0 < 0.333 \quad [19]$$

Even more encouraging is the agreement between the parameters a and b, which indicate the rate of decay of the stress. For $\nu = 1/4$, $a = 2.83$, and $b = 2.74$; for $\nu = 1/3$, $a = 3.00$, and $b = 3.16$. From Equations [3] and [5], a length-to-thickness ratio of 7, and $\nu = 1/4$, we have

$$0.949 < \frac{k}{k_0} < 0.957 \quad [20]$$

so that k can be determined from the known k_0 with an uncertainty of less than 0.5 per cent.

For shorter pads and greater accuracy, we take more complicated approximate solutions involving more parameters. As a second approximation, we add to the stress function the function $(A + By^2)\, x^2 y e^{-ax}$, which gives zero normal and shear components of stress on the end, so that the stress-boundary conditions are still satisfied. Then minimizing the upper bound with respect to A and B, and adding to u and v the displacements

$$\left.\begin{aligned} u &= Dy(1 - y^2)e^{-ax} \\ v &= 0 \end{aligned}\right\} \quad [21]$$

which satisfy the displacement boundary conditions, and maximizing the lower bound with respect to D, we obtain for $\nu = 1/4$ and $a = 2.83$

$$0.321 < W_0 < 0.340 \quad [22]$$

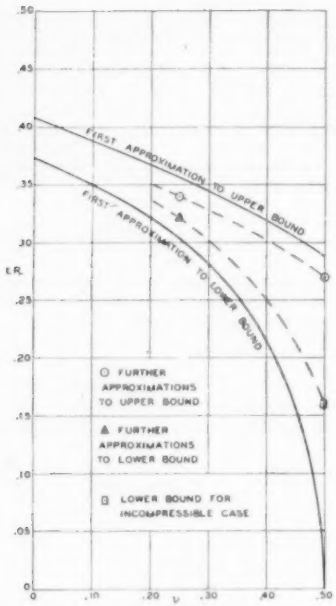

FIG. 3 VARIATION OF ϵR WITH POISSON'S RATIO ν
[$(1 - \epsilon)$ is ratio of actual stiffness to stiffness in pure shear, R is length-to-thickness ratio.]

so that, even for a length-to-thickness ratio as low as 3, the stiffness can be determined with an accuracy of ± 0.3 per cent.

INCOMPRESSIBLE MATERIAL

For an incompressible body we use the same stress functions, which give $W_0 < 0.27$. In this case the stress decreases more rapidly and a is around 4. To determine the lower bound we must choose displacements which satisfy the incompressibility condition

$$\frac{\partial u}{\partial x} + \frac{\partial w}{\partial y} = 0 \quad \ldots\ldots\ldots\ldots\ldots\ldots [23]$$

This may be done by choosing a displacement function ψ where

$$\left.\begin{aligned} u &= \frac{\partial \psi}{\partial y} \\ v &= -\frac{\partial \psi}{\partial x} \end{aligned}\right\} \quad \ldots\ldots\ldots\ldots\ldots\ldots [24]$$

By taking

$$\psi = (1 - y^2)^2 e^{-ax} \quad \ldots\ldots\ldots\ldots\ldots\ldots [25]$$

which satisfies the displacement boundary conditions, we obtain

$$W_0 < 0.15$$

By adding to this the function

$$B(1 - y^2)^2 x e^{-ax} \quad \ldots\ldots\ldots\ldots\ldots\ldots [26]$$

which also satisfies the boundary conditions, and maximizing with respect to B, the lower bound was raised to 0.16. Thus

$$0.16 < W_0 < 0.27 \quad \ldots\ldots\ldots\ldots\ldots\ldots [27]$$

This result was used to determine the shear modulus and shear damping constant of a plastic material from measurements of the impedance of a specimen held between two rigid plates, one of which vibrates in its own plane at a frequency well below the natural frequency of the specimen. For a rectangular specimen with a length-to-thickness ratio of 3, the actual shear modulus and damping constant of the plastic are 7 ± 2 per cent larger than those computed by neglecting the edge effect and assuming that the body deforms in pure shear. Due to the restrictions on choice of approximate displacements, the interval of uncertainty here is somewhat greater than for the compressible case; but the accuracy was, nevertheless, sufficient for practical purposes.

The results as a function of ν are plotted in Fig. 3.

ACKNOWLEDGMENT[1]

The author wishes to thank Professor Prager for valuable suggestions regarding the application of energy methods to this problem.

[1] This paper is an abridged version of a thesis submitted in partial fulfillment for the master of science degree at Brown University, Providence, R. I., in the Graduate Division of Applied Mathematics.

The Stresses Around a Small Opening in a Beam Subjected to Pure Bending

By J. A. JOSEPH[1] and J. S. BROCK,[2] WASHINGTON, D. C.

This paper contains an exact closed solution for the stress distribution around a small opening in the web of a beam that is subjected to pure bending. The complex variable method of solution for plane stress problems (Muschelišvili) is outlined. It is applied to the case of a general ovaloid opening (Greenspan). Curves showing the tangential stresses around the boundary are given for several common openings found in engineering structures.

Nomenclature

The following nomenclature is used in the paper:

- (x, y) = Cartesian co-ordinates
- (α, β) = orthogonal curvilinear co-ordinates in general, and ovaloid co-ordinates in particular
- $z = x + iy$
- $w = \alpha + i\beta$
- $\zeta = e^{w}$
- $\sigma = e^{s\beta}$
- J = stretch ratio
- χ = angle in z-plane between tangent to curve β = const and x-axis
- s, t, r = real parameters
- $T = t + \frac{tr}{s} - \frac{s}{2}$
- Φ, Ψ = potential functions of complex variable z
- φ, ψ = potential functions of complex variable ζ
- F = Airy stress function
- σ_x, σ_y / $\sigma_\alpha, \sigma_\beta$ = normal stresses; σ_γ is normal to surface for which γ = const, etc.
- $\tau_{xy}, \tau_{\alpha\beta}$ = shear stresses
- A_n, B_n / a_n, b_n = complex constants
- M = applied bending moment
- y_0 = half-height of opening at $x = 0$
  $= s - t + r$
- I = moment of inertia of beam
- h = height of beam
- — = bar above, indicates conjugate complex

Introduction

The purpose of this paper is to obtain an exact solution for the stress concentrations at the boundary and in the neighborhood of an ovaloid opening in the web of a beam that is subjected to pure bending, Fig. 1.

The beam is considered to be of infinite extent in the x-direction and large (compared to the height of the opening) but of finite extent in the y-direction. The center of the opening is on the neutral axis; however, this is no limitation. The stress distribution when the opening is above or below the neutral axis can be obtained by taking the known solutions of a uniform compression or tension field (1)[3] and superimposing it upon the solution considered here. The opening treated herein is called an ovaloid, defined in detail later, and may be made to represent closely several common openings which occur in engineering structures.

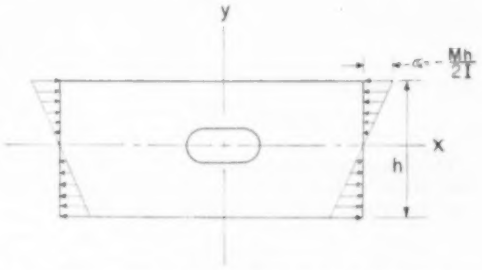

Fig. 1 Distribution of Bending Load on Beam Containing an Opening

The method of solution used is that known as the complex-variable method, associated with the name of N. I. Muschelišvili. For a detailed treatment see Sokolnikoff (2).

This problem of bending in the cases of circular and elliptical openings has been solved by using Airy stress functions, the circle by Tuzi (3), and the ellipse by Neuber (4).

Curvilinear Co-Ordinates

With the notation of the complex variable, a mapping function of the form

$$z = f(\zeta) = c\zeta + \sum_{0}^{n} \frac{c_n}{\zeta^n} \qquad [1]$$

where $z = x + iy$ and $\zeta = e^{w} = e^{\alpha + i\beta}$ transforms continuously points in the $\zeta(\alpha, \beta)$-plane into points in the $z(x, y)$-plane. In

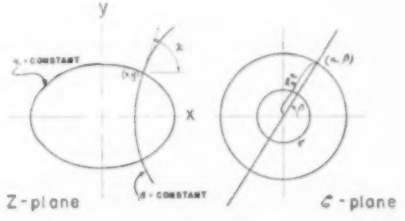

Fig. 2 Geometry and Notation for Transformation of Co-Ordinates

[1] Operations Analyst, Headquarters, U. S. Air Force.

[2] Physicist, David Taylor Model Basin.

Presented at the Conference of the Applied Mechanics Division, Purdue University, Lafayette, Ind., June 22–24, 1950, of The American Society of Mechanical Engineers.

Discussion of this paper should be addressed to the Secretary, ASME, 29 West 39th Street, New York, N. Y., and will be accepted until January 10, 1951, for publication at a later date. Discussion received after the closing date will be returned.

Note: Statements and opinions advanced in papers are to be understood as individual expressions of their authors and not those of the Society. Manuscript received by the Applied Mechanics Division June 20, 1949. Paper No. 50—APM-3.

[3] Numbers in parentheses refer to the Bibliography at the end of the paper.

particular (see Fig. 2), points on a circle of radius e^{α}, α held constant, defined by the position angles β, will transform into points (x, y) on a closed curve, defined by the functional form in Equation [1]. Also, the radial line defined by β = const transforms into a curve that is orthogonal to those for which α = const. The case when $\alpha = 0$ is of importance; it defines the unit circle γ in the ζ-plane and transforms, by proper selection of the form of Equation [1], into the shape of the opening to be studied. A special symbol σ is given to those ζ-values which lie on this circle

$$\sigma = e^{i\beta} \quad \ldots\ldots [2]$$

so that the conjugate of σ

$$\bar{\sigma} = e^{-i\beta} = \frac{1}{\sigma}$$

The transformation defined in Equation [1] describes the relation between an increment dz in the z-plane and an increment dw in the ζ-plane. The ratio, expressed in polar form

$$\frac{dz}{dw} = Je^{i\chi} \quad \ldots\ldots [3]$$

defines J, the stretch ratio and χ, the angle between the tangent to the curve β = const and the x-axis.[6] To obtain J and χ, we differentiate Equation [1]

$$\frac{dz}{dw} = \frac{dz}{d\zeta}\frac{d\zeta}{dw} = \frac{dz}{d\zeta}\zeta \quad \ldots\ldots [4]$$

and from Equation [3]

$$Je^{i\chi} = \zeta z'(\zeta) \quad \ldots\ldots [5]$$

where the prime indicates differentiation with respect to the variable in parentheses. The conjugate of Equation [5] is

$$Je^{-i\chi} = \bar{\zeta}z'(\bar{\zeta}) \quad \ldots\ldots [6]$$

provided that $z = f(\zeta)$ has real coefficients and parameters. By multiplication of Equations [5] and [6], we get

$$J^2 = z'(\zeta)z'(\bar{\zeta})\zeta\bar{\zeta} = z'(\zeta)z'(\bar{\zeta})e^{2\alpha} \quad \ldots\ldots [7]$$

and by division, we get

$$e^{2i\chi} = \frac{z'(\zeta)}{z'(\bar{\zeta})}e^{2i\beta} \quad \ldots\ldots [8]$$

In general, in plane problems of elasticity, the technique which follows can be applied to any mapping function of the form of Equation [1].

A discussion of the transformation used in the present problem follows. Consider the mapping function due to Greenspan (1)

$$z = s\zeta + \frac{t}{\zeta} + \frac{r}{\zeta^3} \quad \ldots\ldots [9]$$

where s, t, and r are real constants that are determined by the proportions of the opening. As before, $z = x + iy$ and

$$\zeta = e^{\alpha + i\beta}$$

then

$$\left.\begin{aligned} x &= (se^{\alpha} + te^{-\alpha})\cos\beta + re^{-3\alpha}\cos 3\beta \\ y &= (se^{\alpha} - te^{-\alpha})\sin\beta - re^{-3\alpha}\sin 3\beta \end{aligned}\right\} \quad \ldots\ldots [10]$$

When $\alpha = 0$, Equations [10] define the general ovaloid opening. Several special cases occur as follows: (*a*) if $r = t = 0$, a circular opening of radius s is defined; (*b*) if $r = 0$, an ellipse is defined; (*c*) if $t = 0$ and r is negative, a square with fillets can be approximated; (*d*) if $t = 0$ and r is positive, the preceding "square" is rotated 45 deg. In the general case, equations of the form of Equations [10], for α equal to zero, define ovaloids when by proper choice of the constants s, t, r, the equations can be made to approximate an opening of the common structural hole shown in Fig. 3, which is made up of a rectangle and two semicircles.

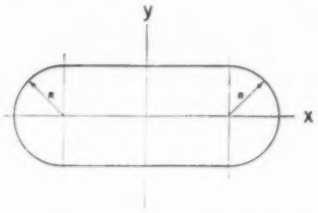

FIG. 3 COMMON STRUCTURAL OPENING WHICH MAY BE APPROXIMATED BY OVALOID EQUATION

From Equation [9]

$$z'(\zeta) = s - \frac{t}{\zeta^2} - \frac{3r}{\zeta^4} \quad \ldots\ldots [11]$$

and J and χ can be obtained, in general, from Equations [7] and [8]. When $\alpha = 0$, we use the subscript zero and from Equation [7]

$$J_0^2 = s^2 + t^2 + 9r^2 - (2st - 6rt)\cos 2\beta - 6sr\cos 4\beta \quad \ldots\ldots [12]$$

TECHNIQUE OF METHOD OF THE COMPLEX VARIABLE FOR OBTAINING STRESSES

In order to obtain the stresses in plane problems in elasticity by using the method of the complex variable, two potential functions have to be determined. It is possible to write these two functions in the following general form

$$\left.\begin{aligned} \Phi(z) &= \sum_{1}^{k} A_n z^n + \sum_{1}^{\infty} \frac{a_n}{z^n} \\ \Psi(z) &= \sum_{1}^{k'} B_n z^n + \sum_{1}^{\infty} \frac{b_n}{z^n} \end{aligned}\right\} \quad \ldots\ldots [13]$$

where the A_n, a_n, B_n, b_n, are constants, possibly complex. The solution is thus reduced to the evaluation of these constants. Since z is a simple series in ζ, we could also have defined Φ and Ψ in terms of ζ with the same form as Equations [13], but different constant coefficients, of course. For the present problem the form given in Equations [13] is preferable. The values of A_n, B_n will be determined by the normal stresses σ_x, σ_y and the shear stresses τ_{xy} at infinity; the values of a_n, b_n will be determined by the values of A_n and B_n, and also by the normal stress σ_α and the shear stress $\tau_{\alpha\beta}$ at the boundary of the opening. Once the two complex potential functions are completely determined by the boundary conditions, the stresses in the plane can be obtained by differentiation. These functions therefore play a role similar to the Airy stress function. In fact, the Airy stress function corresponding to the two complex potential functions is

$$F(x, y) = Re\,[\bar{z}\Phi(z) + \int \Psi(z)\,dz] \quad \ldots\ldots [14]$$

where Re signifies "the real part of" and $\bar{z}$ is the conjugate of z. The stresses, in terms of the two functions, are

[6] Reference (5), §2.32, et seq.

$$\left.\begin{aligned}\sigma_y + \sigma_x &= 2[\Phi'(z) + \Phi'(\bar{z})]\\ \sigma_y - \sigma_x + 2i\tau_{xy} &= 2[\bar{z}\Phi''(z) + \Psi'(z)]\end{aligned}\right\} \quad \ldots\ldots [15]$$

In order to study the stresses σ_α (normal to the curves α = const), and σ_β (normal to the curves β = const) and the shear stresses $\tau_{\alpha\beta}$, the usual transformation equations of stresses,[5] tell us that

$$\left.\begin{aligned}\sigma_y + \sigma_x &= \sigma_\beta + \sigma_\alpha\\ \sigma_y - \sigma_x + 2i\tau_{xy} &= (\sigma_\beta - \sigma_\alpha + 2i\tau_{\alpha\beta})\, e^{-2i\alpha}\end{aligned}\right\} \quad \ldots [16]$$

In terms of the potential functions in ζ

$$\left.\begin{aligned}\sigma_\beta + \sigma_\alpha &= 2[\Phi'(z) + \Phi'(\bar{z})]\\ \sigma_\beta - \sigma_\alpha + 2i\tau_{\alpha\beta} &= 2[z(\bar{\zeta})\Phi''(z) + \Psi'(z)]\,\frac{z'(\zeta)}{z'(\bar{\zeta})}\, e^{2i\beta}\end{aligned}\right\} \quad \ldots [17]$$

where the functions of z on the right are to be expressed in terms of $\zeta(\alpha, \beta)$ co-ordinates as follows: for the sake of simplicity we write $\Phi(z) = \Phi[z(\zeta)] = \varphi(\zeta)$, and differentiation is with respect to the variable in parentheses

$$\left.\begin{aligned}\Phi'(z) &= \frac{\varphi'(\zeta)}{z'(\zeta)}\\ \Psi'(z) &= \frac{\psi'(\zeta)}{z'(\zeta)}\\ \Phi''(z) &= \frac{\varphi''(\zeta)}{[z'(\zeta)]^2} - \frac{\varphi'(\zeta)z''(\zeta)}{[z'(\zeta)]^3}\end{aligned}\right\} \quad \ldots\ldots [18]$$

If, at the opening, the normal stresses σ_α and the shear stresses $\tau_{\alpha\beta}$ are zero, which is the case at a free boundary, it can be shown that

$$\varphi(\sigma) + \frac{z(\sigma)}{z'\left(\frac{1}{\sigma}\right)}\,\bar{\varphi}'\left(\frac{1}{\sigma}\right) + \bar{\psi}\left(\frac{1}{\sigma}\right) = 0 \ldots\ldots [19]$$

Two fundamental theorems from complex-variable theory (Cauchy-type integrals) are important in the determination of $\varphi(\zeta)$ and $\psi(\zeta)$. These are as follows.[6]

Theorem 1. Let $f(\zeta)$ be continuous in the closed region $|\zeta| \leq 1$ and analytic in the interior, with the possible exception of the point $\zeta = 0$, where $f(\zeta)$ has the structure

$$f(\zeta) = \frac{A_1}{\zeta} + \frac{A_2}{\zeta^2} + \ldots + \frac{A_n}{\zeta^n} + g(\zeta)$$

and where $g(\zeta)$ is analytic; then

$$\frac{1}{2\pi i}\int_\gamma \frac{f(\sigma)}{\sigma - \zeta}\,d\sigma = -\frac{A_1}{\zeta} - \frac{A_2}{\zeta^2} - \ldots - \frac{A_n}{\zeta^n} \text{ for } |\zeta| > 1$$

where γ is the unit circle $\sigma = e^{i\beta}$.

Theorem 2. If $f(\zeta)$ is continuous in the closed region $|\zeta| \geq 1$ and analytic in the region exterior to γ, with the possible exception of the point $\zeta = \infty$ where $f(\zeta)$ has the structure

$$f(\zeta) = A_0 + A_1\zeta + A_2\zeta^2 + \ldots + A_n\zeta^n + \sum_{k=1}^{\infty}\frac{B_k}{\zeta^k}$$

then

$$\frac{1}{2\pi i}\int_\gamma \frac{f(\sigma)}{\sigma - \zeta}\,d\sigma = -f(\zeta) + A_0 + A_1\zeta + A_2\zeta^2 + \ldots + A_n\zeta^n \text{ for } |\zeta| > 1$$

[5] Reference (5), p. 135.
[6] Reference (2), pp. 144–145.

The form of the mapping function, Equation [1], having been determined, the technique for determining the coefficients in the series expressions for Φ and Ψ is as follows:

Step 1 Insert the expressions for the stresses at infinity in the left of Equations [15], and insert Φ and Ψ, defined in Equations [13] in the right of Equations [15], and let z become infinite in a prescribed direction. This will determine A_n and B_n in terms of the applied loading or stresses.

Step 2 Insert Equation [1] written for the boundary into Equations [13], obtaining $\varphi(\sigma)$ and $\psi(\sigma)$ with a_n and b_n as yet undetermined. Obtain $\varphi'(\sigma)$.

Step 3 Write Equation [19] introducing only $z(\sigma)$, $z'\left(\frac{1}{\sigma}\right)$, $\bar{\varphi}'\left(\frac{1}{\sigma}\right)$, and $\bar{\psi}\left(\frac{1}{\sigma}\right)$.

Step 4 Multiply this equation by $d\sigma/[2\pi i(\sigma - \zeta)]$ and integrate around γ using Theorems 1 and 2. This expression will contain $\varphi(\zeta)$, and, in general, m of the a_n's.

Step 5 Repeat Step 4 after multiplying by $\sigma d\sigma/[2\pi i(\sigma - \zeta)]$.

Step 6 Repeat Step 4 after multiplying by $\sigma^2 d\sigma/[2\pi i(\sigma - \zeta)]$.

Step 7 And so on until multiplication by $\sigma^m d\sigma/[2\pi i(\sigma - \zeta)]$.

Step 8 Steps 4 through 7 yield $(m + 1)$ linear equations in $\varphi(\zeta)$, and m unknown a_n's which can be solved simultaneously, thus determining $\varphi(\zeta)$.

Step 9 Using $\varphi(\zeta)$, now known, write the conjugate of Equation [19] and integrate around γ after multiplying by $d\sigma/[2\pi i(\sigma - \zeta)]$. Use Theorems 1 and 2 to determine $\psi(\zeta)$.

Step 10 Insert $\varphi(\zeta)$ and $\psi(\zeta)$ in Equations [17] and solve for the stresses σ_α, σ_β, and $\tau_{\alpha\beta}$. Note that $(\sigma_\beta)_{\alpha=0}$ could have been obtained after Step 8, once $\varphi(\zeta)$ had been determined, by using the first of Equations [17], since at a free boundary $(\sigma_\alpha)_{\alpha=0} = 0$.

In other words

$$(\sigma_\beta)_{\alpha=0} = 2\left[\frac{\varphi'(\sigma)}{z'(\sigma)} + \frac{\bar{\varphi}'(1/\sigma)}{z'(1/\sigma)}\right] \ldots\ldots [20]$$

Using this technique the solution of the bending problem for beams with ovaloid openings follows.

General Ovaloid Opening in a Beam Subjected to Pure Bending

Step 1 From Equations [13], letting z go to infinity in the x-direction

$$\left.\begin{aligned}\Phi'(z)_{z=\infty} &= \left[\sum_1^k n A_n z^{n-1}\right]_{z=\infty}\\ \Phi''(z)_{z=\infty} &= \left[\sum_2^k n(n-1)A_n z^{n-2}\right]_{z=\infty}\\ \Psi'(z)_{z=\infty} &= \left[\sum_1^k n B_n z^{n-1}\right]_{z=\infty}\end{aligned}\right\} \ldots\ldots [21]$$

The boundary conditions at $x = \infty$ are $\sigma_x = -My/I$, $\sigma_y = 0$, $\tau_{xy} = 0$. Inserting Equations [21] into the first of Equations [15] along with these boundary conditions gives

$$-\frac{My}{I} = 2\left[\sum_1^k n A_n(x + iy)^{n-1} + \sum_1^k n \bar{A}_n(x - iy)^{n-1}\right]_{x=\infty}$$

This requires that $A_n = 0$ for $n = 1, 3, 4, \ldots\ldots, k$ but for

$n = 2$, $A_2 = (Mi)/(8I)$. Likewise inserting Equations [21] into the second of Equations [15] gives

$$\frac{My}{I} = 2\left[(x - iy)\,2A_2 + \sum_1^{k'} n\,B_n(x + iy)^{n-1}\right]_{z=\infty}$$

This requires that $B_n = 0$ for $n = 1, 3, 4, \ldots\ldots k'$ but for $n = 2$, $B_2 = -A_2 = -(Mi)/(8I)$. Therefore the potential functions for pure bending

$$\left.\begin{aligned}\Phi(z) &= \frac{Mi}{8I}\,z^2 + \sum_1^{\infty}\frac{a_n}{z^n}\\ \Psi(z) &= -\frac{Mi}{8I}\,z^2 + \sum_1^{\infty}\frac{b_n}{z^n}\end{aligned}\right\}\quad\ldots\ldots\ldots[22]$$

give the applied stresses at infinity for any opening, regardless of shape.

Step 2 On the boundary of the opening, we have for φ

$$(\sigma_\beta)_{\alpha=0} = -\frac{Ms}{I}\left[\frac{(s^2 + 6rT - 2tT - 12r^2)\sin\beta - (2rt - st + s^2)\sin 3\beta + rs\sin 5\beta}{s^2 + t^2 + 9r^2 - (2st - 6rt)\cos 2\beta - 6rs\cos 4\beta}\right]\quad\ldots\ldots[27]$$

$$\varphi(\sigma) = \frac{Mi}{8I}\left(s\sigma + \frac{t}{\sigma} + \frac{r}{\sigma^3}\right)^2 + \sum_1^{\infty}\frac{a_n}{\left(s\sigma + \frac{t}{\sigma} + \frac{r}{\sigma^3}\right)^n}$$

$$\psi'\left(\frac{1}{\sigma}\right) = -\left[\frac{Mi}{4I}\left(\frac{s}{\sigma} + t\sigma + r\sigma^3\right) + \sum_1^{\infty}\frac{na_n}{\left(\frac{s}{\sigma} + t\sigma + r\sigma^3\right)^{n+1}}\right]z'\left(\frac{1}{\sigma}\right)$$

with a similar expression for $\overline{\psi}(1/\sigma)$.

Step 3 The boundary condition, Equation [19] becomes

$$\varphi(\sigma) - \frac{s\sigma^4 + t\sigma^2 + r}{\sigma^3}\left[\frac{Mi}{4I}\left(\frac{s}{\sigma} + t\sigma + r\sigma^3\right) + \sum_1^{\infty}\frac{na_n}{\left(\frac{s}{\sigma} + t\sigma + r\sigma^3\right)^{n+1}}\right] + \frac{Mi}{8I}\left(\frac{s}{\sigma} + t\sigma + r\sigma^3\right)^2 + \sum_1^{\infty}\frac{b_n}{\left(\frac{s}{\sigma} + t\sigma + r\sigma^3\right)^n} = 0\quad\ldots\ldots[23]$$

Step 4 Multiplying by $d\sigma/[2\pi i(\sigma - \zeta)]$, integrating, and using Theorems 1 and 2, we get

$$-\varphi(\zeta) + \frac{Mi}{8I}\left[s^2\zeta^2 + 2t\left(1 + \frac{r}{s}\right)\frac{s}{\zeta^2} + \frac{2rs}{\zeta^4} - \frac{s^2}{\zeta^2}\right] + \frac{ra_1}{s^2\zeta} = 0\quad\ldots\ldots[24]$$

Steps 5–8 Multiplying by $\sigma d\sigma/[2\pi i(\sigma - \zeta)]$ and integrating, readily shows that $a_1 = 0$; therefore

$$\varphi(\zeta) = \frac{Mis}{4I}\left[\frac{s\zeta^2}{2} + \frac{T}{\zeta^2} + \frac{r}{\zeta^4}\right]\quad\ldots\ldots[25]$$

where

$$T = t + \frac{tr}{s} - \frac{s}{2}$$

Step 9 Writing the conjugate of Equation [19] and using Equation [25] gives

$$-\frac{Mis}{4I}\left[\frac{s}{2\sigma^2} + T\sigma^2 + r\sigma^4 + \frac{\sigma^3(s + t\sigma^2 + r\sigma^4)}{s\sigma^4 - t\sigma^2 - 3r}\left(s\sigma - \frac{2T}{\sigma^3} - \frac{4r}{\sigma^5}\right)\right] + \psi(\sigma) = 0$$

Multiplying this by $d\sigma/[2\pi i(\sigma - \zeta)]$ and integrating around γ gives

$$\psi(\zeta) = \frac{Mis}{4I}\left[r\zeta^4 + T\zeta^2 + \frac{s}{2\zeta^2} - \frac{s\zeta^4 - 2T - \frac{4r}{\zeta^2}}{s\zeta^4 - t\zeta^2 - 3r}(s + t\zeta^2 + r\zeta^4)\right]\quad\ldots\ldots[26]$$

Step 10 From Equation [20], the tangential stresses around the opening are

Inserting Equations [25] and [26] into Equation [14] gives the Airy stress function

$$\left.\begin{aligned}F(\alpha,\beta) &= \frac{Ms}{4I}\left[g_1(\alpha)\sin\beta + g_2(\alpha)\sin 3\beta + g_3(\alpha)\sin 5\beta\right]\\ &\text{where}\\ g_1(\alpha) &= -\frac{s^2e^{2\alpha}}{2} + (s^2 - 2Tr + Tt + 3r^2)e^{\alpha} + \left(3rT - \frac{s^2}{2} - 2Tt - 4r^2\right)e^{-\alpha} + Tte^{-3\alpha} - Tre^{-5\alpha} + r^2e^{-7\alpha}\\ g_2(\alpha) &= \left(\frac{st - Ts + rt}{3}\right)e^{3\alpha} - \frac{ste^{\alpha}}{2} + Tse^{-\alpha} + \left(\frac{st}{6} - \frac{2Ts}{3} - \frac{4rt}{3}\right)e^{-3\alpha} + tre^{-5\alpha}\\ g_3(\alpha) &= \left(-\frac{e^{-\alpha}}{2} + e^{-3\alpha} - \frac{e^{-\alpha}}{2}\right)rs\end{aligned}\right\}\quad..[28]$$

Equations [27] and [28] agree with Tuzi's results for the circle, and with Neuber's results for the ellipse. It is of interest to observe that along the x-axis the normal stresses σ_α and σ_β are zero, whereas $\tau_{\alpha\beta}$ is not zero and may be obtained directly from the second of Equations [17], upon putting $\beta = 0$. Furthermore, along the y-axis $\tau_{\alpha\beta}$ is zero and σ_α and σ_β may be obtained by addition and subtraction of Equations [17], upon putting $\beta = \pi/2$.

Numerical Cases

Following Greenspan, we obtain the tangential stresses due to bending σ_t, along the inner boundary, $\alpha = 0$, for four simple cases.

Case 1 (Fig. 4). Ovaloid hole, major axis horizontal for which $s = 1.586$, $t = 0.478$, $r = -0.079$. These are consistent with Greenspan's values of p, q, and r, where $s = (p + q)/2$, $t = (p - q)/2$, and the r is the same in both systems. Then from Equation [27]

$$\frac{\sigma_t}{-My_0/I} = \frac{4.504\sin\beta - 2.591\sin 3\beta - 0.193\sin 5\beta}{2.798 - 1.741\cos 2\beta + 0.752\cos 4\beta}$$

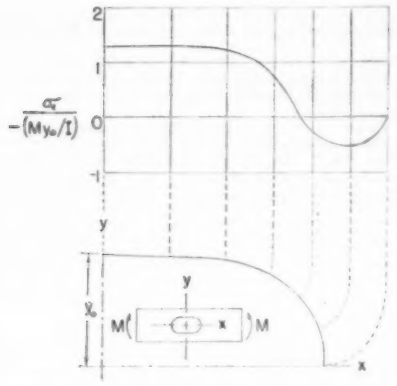

FIG. 4 OVALOID HOLE, MINOR AXIS VERTICAL
(Distribution along boundary of stress due to pure bending.)

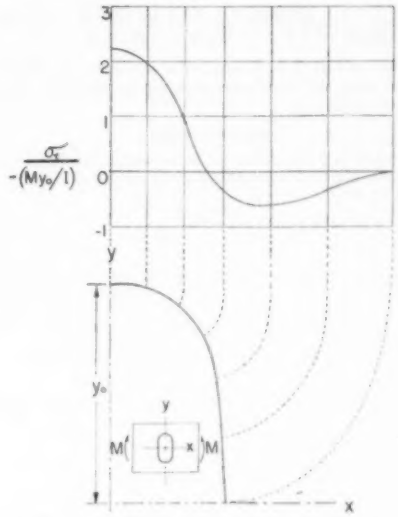

FIG. 5 OVALOID HOLE, MAJOR AXIS VERTICAL
(Distribution along boundary of stress due to pure bending.)

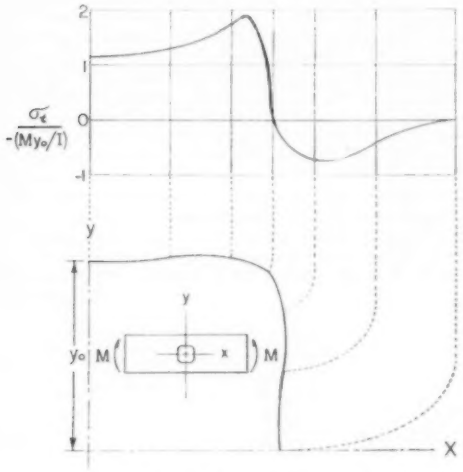

FIG. 6 SQUARE HOLE, SIDE VERTICAL
(Distribution along boundary of stress due to pure bending.)

where $y_o = s - t + r$ = one-half height of the opening; and the reference stress $-My_o/I$ is the stress σ_x at $x = \infty$, $y = y_o$.

Case 2 (Fig. 5). Ovaloid hole, major axis vertical; $s = 1.586$, $t = -0.478$, $r = -0.079$, then

$$\frac{\sigma_t}{-My_o/I} = \frac{1.456 \sin \beta - 2.674 \sin 3\beta - 0.100 \sin 5\beta}{2.798 + 1.741 \cos 2\beta + 0.752 \cos 4\beta}$$

Case 3 (Fig. 6). Square hole, side vertical; $s = 1$, $t = 0$, $r = -0.14$; then

$$\frac{\sigma_t}{-My_o/I} = \frac{1.378 \sin \beta - 1.163 \sin 3\beta - 0.163 \sin 5\beta}{1.176 + 0.84 \cos 4\beta}$$

Case 4 (Fig. 7). Square hole, diagonal vertical; $s = 1$, $t = 0$, $r = 0.14$; then

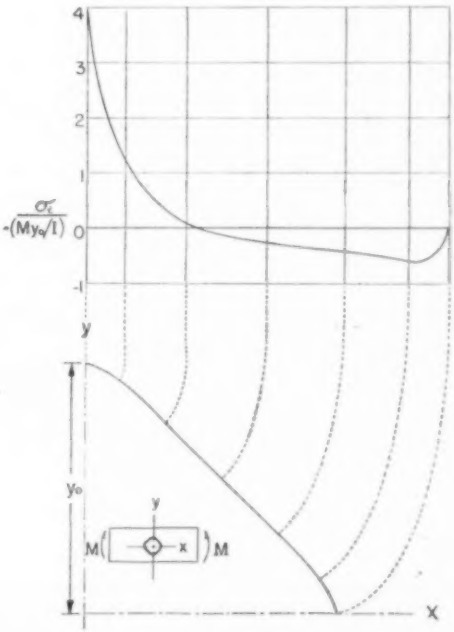

FIG. 7 SQUARE HOLE, DIAGONAL VERTICAL
(Distribution along boundary of stress due to pure bending.)

$$\frac{\sigma_t}{-My_0/I} = \frac{0.298 \sin \beta - 0.877 \sin 3\beta + 0.123 \sin 5\beta}{1.176 - 0.84 \cos 4\beta}$$

In each of Figs. 4, 5, 6, and 7, the values of $\sigma_t/(-My_0/I)$ are plotted along the development of one quadrant of the inner boundary of the plate.

BIBLIOGRAPHY

1 "Effect of a Small Hole on the Stresses in a Uniformly Loaded Plate," by Martin Greenspan, *Quarterly Applied Mathematics*, vol. 2, 1944, pp. 60–71.

2 "Mathematical Theory of Elasticity," by I. S. Sokolnikoff, (mimeographed lecture notes), Brown University, Providence, R. I., 1941.

3 "Effect of a Circular Hole on the Stress Distribution of a Beam Under Uniform Bending Moment," by Ziro Tuzi, Sci. papers of the Tokyo Institute of Physical and Chemical Research, vol. 9, Aug. 20, 1928, pp. 65–89.

4 "Theory of Notch Stresses," by H. Neuber, David Taylor Model Basin, Translation no. 74, by F. A. Raven and J. S. Brock, November, 1945. (Distributed by J. W. Edwards, Ann Arbor, Mich.)

5 "A Treatise on Photoelasticity," by E. G. Coker and L. N. G. Filon, Cambridge University Press, London, England, 1931.

Torsion of a Circular Shaft With a Number of Longitudinal Notches

By H. OKUBO,[1] SENDAI, JAPAN

The object of this paper is to find a solution for the torsion problem of a circular shaft with a number of longitudinal semicircular notches. By using elementary functions the author has been able to simplify the numerical calculations in contrast to previous work in similar cases by other writers.

GRONWALL[2] has worked out a solution for a circular section with one notch in the form of an orthogonal circle, and Weber[3] has obtained a solution for the section with one notch in the form of a semicircle which has its center on the bounding circle. Subsequently, Shepherd[4] obtained a solution for a circular section with one notch and that with two, using elliptic functions. According to his method, the calculation is found to be very complicated, since the evaluation of functions must be carried out by expanding in series. Accordingly, it is desired to find the solution in a simpler form more convenient for numerical calculations, since the section of a spline shaft in practical use sometimes is in the form of a circle with a number of semicircular notches. In this paper, we shall find a solution for a shaft with m notches, in a simpler form by using elementary functions.

We consider a plane harmonic function ϕ which becomes a uniform magnitude p in m intervals, distributed in equal distances and vanishes elsewhere, on the bounding circle of the section, as shown in Fig. 1. If we denote the central angle contained by a circular arc where ϕ becomes uniform in magnitude, by $2h$, the boundary condition is

$$\left.\begin{aligned} \phi &= p, \ \frac{2k\pi}{m} + h > \theta > \frac{2k\pi}{m} - h \\ &= 0, \ \frac{2(k+1)\pi}{m} - h > \theta > \frac{2k\pi}{m} + h \end{aligned}\right\} \text{ at } r = 1$$

where

$$k = 0, 1, 2, \ldots, m-1$$

which is transformed into

$$\phi = \frac{mhp}{\pi} + \frac{2p}{\pi} \sum_{n=1}^{\infty} \frac{\sin nmh}{n} \cos nm\theta, \text{ at } r = 1$$

Putting $2hp = P$, and considering the limiting case when h approaches zero, it becomes

$$\phi = \frac{Pm}{\pi} \left(\frac{1}{2} + \sum_{n=1}^{\infty} \cos nm\theta \right) \text{at } r = 1 \qquad [1]$$

The function ϕ which satisfies the boundary condition, Equation [1], is

$$\phi = \frac{Pm}{\pi} \left(\frac{1}{2} + \sum_{n=1}^{\infty} r^{nm} \cos nm\theta \right)$$

which can be transformed into

$$\phi = \frac{P(1 - r^{2m})}{1 + r^{2m} - 2r^m \cos m\theta} \qquad [2]$$

If we put $m = 1$ and $P = -a^2/2$ in Equation [2], then we have the solution for a circular shaft with one semicircular notch of radius a, which was obtained previously by Weber. When $m \geq 2$, the notches are not strictly in a form of a semicircle, but are in a slightly different form. The deviation from a semicircle, however, is very small and can be considered as a semicircle practically, as will be seen in the example to be shown later.

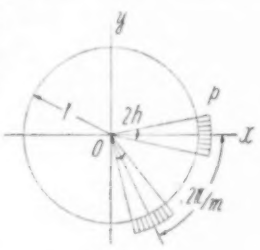

FIG. 1

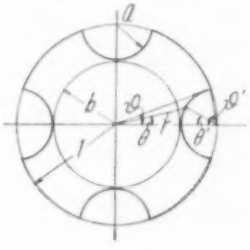

FIG. 2

The equation which represents the boundary of the section is

$$\phi - \frac{r^2}{2} = \text{const} = -\frac{1}{2}$$

or

$$\frac{P(1 - r^{2m})}{1 + r^{2m} - 2r^m \cos m\theta} + \frac{1}{2}(1 - r^2) = 0 \qquad [3]$$

If b represents the distance from the center of the section to the bottom of each notch, as is shown in Fig. 2, P is determined as

$$P = -\frac{(1 - b^2)(1 - b^m)}{2(1 + b^m)} \qquad [4]$$

---

[1] Institute of High Speed Mechanics, Tōhoku University.

[2] "On the Influence of Keyways Under Stress Distribution in Cylindrical Shafts," by T. H. Gronwall, Trans. American Mathematical Society, vol. 20, 1919, pp. 234–244.

[3] "Die Lehre der Drehungsfestigkeit," by C. Weber, *Forschungsarbeiten*, no. 249, 1921, 70 pp.

[4] "The Torsion and Flexure of Shafting With Keyways or Cracks," by W. M. Shepherd, Proceedings of the Royal Society of London, series A, vol. 138, 1932, pp. 607–634.

Presented at the National Conference of the Applied Mechanics Division, Purdue University, Lafayette, Ind., June 22–24, 1950, of THE AMERICAN SOCIETY OF MECHANICAL ENGINEERS.

Discussion of this paper should be addressed to the Secretary, ASME, 29 West 39th Street, New York, N. Y., and will be accepted until January 10, 1951, for publication at a later date. Discussion received after the closing date will be returned.

NOTE: Statements and opinions advanced in papers are to be understood as individual expressions of their authors and not those of the Society. Manuscript received by the Applied Mechanics Division June 27, 1949. Paper No. 50—APM-7.

and the equation which represents the peripheries of the notches is

$$(1 - b^2)(1 - b^m)(1 + r^2 + r^4 + \ldots\ldots + r^{2m-2}) = (1 + b^m)(1 + r^{2m} - 2r^m \cos m\theta) \ldots [5]$$

From Equation [5] we can readily obtain the radius of curvature ρ at the bottom of the notch as

$$\rho = \frac{b^2}{b - \left(\frac{d^2r}{d\theta^2}\right)_0} \ldots\ldots [6]$$

where

$$\left(\frac{d^2r}{d\theta^2}\right)_0 = \frac{m^2b^{m-1}(1 - b^2)(1 + b^m)}{(1 - b^m)(1 + mb^{m-2} - mb^m - b^{2m})}$$

The stresses on the cross section are given by

$$\tau_{zx} = G\alpha\left(\frac{\partial\phi}{\partial y} - y\right), \quad \tau_{yz} = -G\alpha\left(\frac{\partial\phi}{\partial x} - x\right) \ldots\ldots [7]$$

where G and α represent the modulus of elasticity in shear and the angle of twist per unit length, respectively.

The stress on the cross section becomes its maximum at the bottoms of the notches, and the magnitude is

$$\tau_{max} = G\alpha\left[b + \frac{mb^{m-1}(1 - b^2)}{1 - b^{2m}}\right] \ldots\ldots [8]$$

The moment of the couple is generally given by[b]

$$M = G\alpha\left(J - \mathscr{I}\psi\frac{\partial\phi}{\partial s}\,ds\right) \ldots\ldots [9]$$

where ψ is a function conjugate with ϕ, viz.

$$\psi = -\frac{2P_0r^m \sin m\theta}{1 + r^{2m} - 2r^m \cos m\theta} = \frac{r^m \sin m\theta}{1 + r^2 + r^4 + \ldots + r^{2m-2}}$$

J is the polar moment of inertia of the cross section with respect to the axis of z, and the integral is taken around the bounding curve of the section. The evaluation of the integral is complicated except in the case when $m = 1$, and so it is rather convenient to use the method of numerical calculation for it.

Assuming that the notch is strictly in the form of a semicircle of radius a, we can simplify the calculation as follows (see Fig. 2)

$$r \sin\theta = a \sin\theta', \; r\cos\theta = 1 - a\cos\theta', \; ds = ad\theta'$$

$$\frac{\partial\phi}{\partial s} = \frac{\partial}{\partial s}\left\{-\frac{1}{2}(1 - r^2)\right\} = \sin\theta'$$

Since $\partial\phi/\partial s$ vanishes on the bounding circle, we can transform Equation [9] into

$$M = G\alpha\left(J - 2ma\int_0^{\theta'}\psi \sin\theta' d\theta'\right) \ldots\ldots [10]$$

[b] "A Treatise on the Mathematical Theory of Elasticity," by A. E. H. Love, fourth edition, Cambridge University Press, London, England, 1927, p. 312.

We shall investigate the form of the notches in detail in one example in the following:

When $m = 2$, the equation which represents the peripheries of notches is

$$\cos 2\theta = \frac{1 + r^4}{2r^2} - \frac{(1 - b^2)^2(1 + r^2)}{2(1 + b^2)r^2} \ldots\ldots [11]$$

and the corresponding case treated by Shepherd is

$$\cos 2\theta = \frac{k^2(1 + r^4)}{2r^2} \ldots\ldots [12]$$

In the particular case when $b = 0.625$, we shall compare the forms of notches represented by Equations [11] and [12]. In this case $k = 0.6778$. Points on the periphery of each notch and a semicircle of radius 0.375, represented by polar co-ordinates, and the radius of curvature at the bottom of each notch, calculated by each equation, are given in Table 1.

From Table 1 we can see that the deviation of the form of the notch from the semicircle is very small in the case treated by the author, while in the case treated by Shepherd it is not so small.

Assuming $b = 0.625$, the radii of curvature, the maximum stresses and the moments of the couple, calculated by Equations [6], [8], and [9] for several values of m are given in Table 2. The results show that the influence of the number of notches on the form of the notch is not perceptible, but the stress distribution around the notch varies in accordance with the number of notches.

TABLE 1

r		0.6250	0.6537	0.7307	0.8365	0.9533	1	ρ
θ	Semicircle	0°	10° 12′	17° 33′	21° 16′	21° 58′	21° 37′	0.375
	Author	0°	10° 10′	17° 28′	21° 8′	21° 48′	21° 26′	0.369
	Shepherd	0°	10° 9′	17° 40′	21° 53′	23° 32′	23° 40′	0.363

The magnitude of the maximum stress decreases accordingly as the number of notches increases, as is shown in Table 2.

TABLE 2

No. of notches, m	1	2	3	4
ρ	0.375	0.369	0.366	0.371
$\tau_{max}/G\alpha$	1.625	1.524	1.384	1.234
$M/G\alpha$	1.255	0.965	0.725	0.546

Next, as an application of Equation [2], we shall introduce an approximate solution for a circular section with shallow notches of any form. If 2ϑ denotes the angle contained by both ends of each notch at the center of the section, a function ϕ which satisfies the boundary condition may be represented by a certain curve in the interval 2ϑ on the bounding circle, and its effect on the stress distribution is not affected perceptibly by the replacement of ϕ by a function ϕ_1, which has $2n + 2$ discontinuous points in the interval 2ϑ, as shown in Fig. 3. The function ϕ_1 can be replaced by the sum of the functions, each of which has a concentrated value P_j of the magnitude equal to the shaded area of the corresponding narrow rectangle, at a point h_j on the bounding circle. Hence the solution ϕ can be expressed approximately in the form as follows

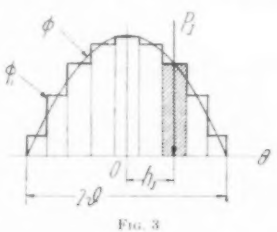

FIG. 3

$$\phi = (1 - r^{2m})\left[\frac{P_0}{1 + r^{2m} - 2r^m \cos m\theta} + \sum_{j=1}^{n} P_j \left\{\frac{1}{1 + r^{2m} - 2r^m \cos m(\theta + h_j)} + \frac{1}{1 + r^{2m} - 2r^m \cos m(\theta - h_j)}\right\}\right] \quad \ldots\ldots [13]$$

The unknown constants P_j contained in Equation [13] are determined from the condition that $\phi = -\frac{1}{2}(r^2) = -\frac{1}{2}$, at $2n + 1$ points on the periphery of the notch.

As a simple example, we shall obtain an approximate solution for the cross section shown in Fig. 4. The vertical sides of the boundary are given by the equation $x = \pm b$ and the other two sides are arcs of the circle of radius unity.

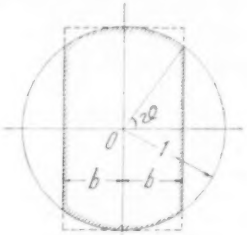

FIG. 4

In this case Equation [13] becomes

$$\phi = (1 - r^4)\left[\frac{P_0}{1 + r^4 - 2r^2 \cos 2\theta} + \sum_{j=1}^{n} P_j \left\{\frac{1}{1 + r^4 - 2r^2 \cos 2(\theta + h_j)} + \frac{1}{1 + r^4 - 2r^2 \cos 2(\theta - h_j)}\right\}\right] \quad \ldots\ldots [14]$$

and the equation which represents the peripheries of the notches is

$$\frac{P_0}{1 + r^4 - 2r^2 \cos 2\theta} + \sum_{j=1}^{n} P_j \left[\frac{1}{1 + r^4 - 2r^2 \cos 2(\theta + h_j)} + \frac{1}{1 + r^4 - 2r^2 \cos 2(\theta - h_j)}\right] = -\frac{1}{(1 + r^2)} \quad \ldots\ldots [15]$$

Let us assume that the angle contained at the center by both ends of the vertical side st is 60° or $\vartheta = 30°$, and 0, 1, 2, 3, 4, 5 represent the intersecting points of the line st and the radii dividing the central angle into 12 equal parts. Then the coordinates of the points are as given in Table 3.

TABLE 3

	0	1	2	3	4	5
r	0.85717	0.86045	0.87039	0.88740	0.91218	0.94578
ϑ	0°	5°	10°	15°	20°	25°

[6] The approximate solution ϕ has no singular points within the bounding circle. Subsequently, the solution [13] is not valid when the exact solution has singular points within the domain bounded by the circle and the periphery of each notch. On this account, this method often fails in case of a section with deep notches. The solution which is valid in these cases will be given in a later report.

If we choose h_j as is shown in Fig. 5, then $h_1 = 5°$, $h_2 = 10°$, $h_3 = 15°$, $h_4 = 20°$, $h_5 = 25°$.

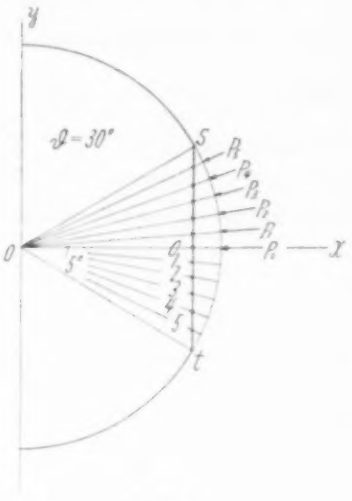

FIG. 5

Inserting these numerical values into Equation [15], and solving the simultaneous equations, we have

$$P_0 = -0.005305,\ P_1 = -0.005139,\ P_2 = -0.004571,$$
$$P_3 = -0.003698,\ P_4 = -0.002598,\ P_5 = -0.001254$$

The stress becomes its maximum at the center of the vertical side and the magnitude is

$$\tau_{max} = -4bG\alpha\left\{-\frac{1}{4} + \frac{P_0}{(1 - b^2)^2} + 2\sum_{j=1}^{5} \frac{P_j[(1 + b^4)\cos 2h_j - 2b^2]}{(1 + b^4 - 2b^2 \cos 2h_j)^2}\right\} \quad \ldots\ldots [16]$$

Putting $b = 0.85717$ in Equation [16], and inserting the numerical values of P_j, we have

$$\tau_{max} = 1.190\, G\alpha$$

When $\vartheta = 45°$, if we choose the points on st, as in Table 4, and

TABLE 4

	0	1	2	3	4	5
r	0.70711	0.71242	0.72875	0.75742	0.80085	0.86322
ϑ	0°	7°	14°	21°	28°	35°

h_j as $h_1 = 7°$, $h_2 = 14°$, $h_3 = 21°$, $h_4 = 28°$, $h_5 = 35°$, then, by a similar calculation, it becomes

$$P_0 = -0.01679,\ P_1 = -0.01559,\ P_2 = -0.01439,$$
$$P_3 = -0.01110,\ P_4 = -0.00781,\ P_5 = -0.00451$$

The magnitude of the maximum stress is

$$\tau_{max} = 1.137\, G\alpha$$

When $\vartheta = 60°$, if we choose the points on st, as in Table 5 and

TABLE 5

	0	1	2	3	4	5
r	0.50000	0.50771	0.53209	0.57735	0.65271	0.77786
θ	0°	10°	20°	30°	40°	50°

h_j as $h_1 = 10°$, $h_2 = 20°$, $h_3 = 30°$, $h_4 = 40°$, $h_5 = 50°$, then we have

$$P_0 = -0.04210,\ P_1 = -0.03722,\ P_2 = -0.03344,$$
$$P_3 = -0.02470,\ P_4 = -0.01491,\ P_5 = -0.00560$$

The corresponding maximum stress is

$$\tau_{max} = 0.9252\ G\alpha$$

Assuming the distance $2b$ between the vertical sides to be constant (for the convenience of calculations, b is taken as unity), the relation between the maximum stress and the form of the section is obtained from the foregoing numerical results. Curve I in Fig. 6 shows the relation. For the sake of comparison, we took up the case of a rectangular section which circumscribes the section of the former case (the rectangle is shown by dotted lines in Fig. 4). The relation between τ_{max} and ϑ in the latter case is shown in Curve II in Fig. 6. From the figure, we can see that the discrepancy between each case becomes very small when ϑ becomes larger than 60 deg.

ACKNOWLEDGMENT

The grant in aid for scientific research of the Education Department of Japan has been given to the present study.

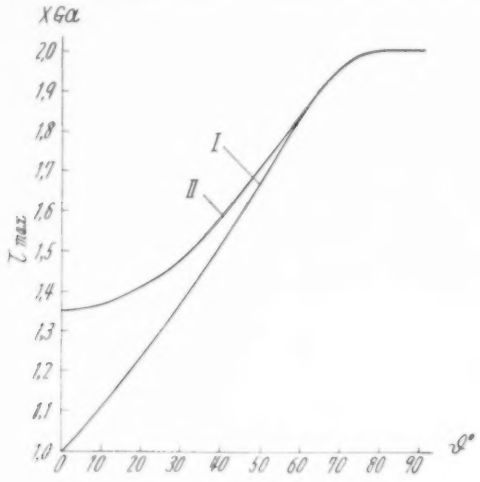

FIG. 6

Vibrations of Elastic Systems Having Hereditary Characteristics

By ENRICO VOLTERRA,[1] CHICAGO, ILL.

Results of experiments carried out on plastics and rubberlike materials at high rate of straining are given. It is shown that the dynamic stress-strain (σ, ϵ) relationship for those materials can be expressed by the formula

$$\sigma = f(\epsilon) + \int_0^t \phi(t-\tau)\frac{d\epsilon(\tau)}{d\tau}\,d\tau$$

The first term represents the static stress-strain relationship, while the second depends on the rate of straining $\frac{d\epsilon}{dt}$. As a first approximation it is supposed that the materials follow Hooke's law when statically stressed. Equation [1] then becomes

$$\sigma = E\epsilon + \int_0^t \phi(t-\tau)\frac{d\epsilon(\tau)}{d\tau}\,d\tau$$

Materials which follow the second equation are called materials with "hereditary characteristics." Vibrations of single-degree-of-freedom systems having hereditary characteristics are considered. Methods of finding the hereditary function $\phi(t)$ from forced vibrations are given. Free and forced vibrations of simply supported beams having hereditary characteristics are studied.

Introduction

THE hypothesis of proportionality between forces and displacements, generally admitted in the mathematical theory of elasticity, is not perfectly verified in practice. The same applies to any other hypothesis based on the correspondence between stress and strain and dependent on the existence of an elastic potential.

Experience shows that every dynamic phenomenon in an elastic body is always accompanied by an internal mechanical dissipation of energy and that the existence of an elastic potential in the ordinary sense is not admissible.

It is well known that an elastic body repeatedly stressed becomes hot. If an elastic body set in vibration is left to itself, its vibrations damp out with time even if the body is kept in a vacuum. If an elastic body is submitted to forced oscillations, a positive work of the exciting forces has to be spent in order to keep the amplitudes of the oscillations constant with time. The reason for the heating of the body, for the damping out of vibrations, and for the expenditure of external work is the internal dynamic friction. Although this dissipation of mechanical energy can be accepted in a qualitative way, it is more difficult to translate the problem into mathematical terms.

As is well known, two principal hypotheses have been proposed to explain the phenomenon of internal dynamic friction, namely, (a) the viscous theory, and (b) the hereditary theory.

The theory of viscous friction is the oldest and has been until recent times the most generally employed.

Coulomb was the first to propose it. Considered again by Voigt and Routh, it has been proposed more recently by Plank after dynamic experiments on low-carbon steels (1).[2]

Many experimentalists have tried to give to this theory an experimental confirmation. In the viscous theory it is admitted that in solid bodies there exist some viscous actions which can be compared to the viscosity of fluids. These viscosity effects should be proportional to the first derivative of the strain with respect to time. The coefficient of proportionality (constant for each material at a constant temperature) is called "coefficient of viscosity." In the case of normal deformation, therefore, the relation between stress (σ) and strain (ϵ) is expressed by

$$\sigma = E\epsilon + A\frac{d\epsilon}{dt} \qquad [1]$$

Two Japanese physicists, Kotaro Honda and Seibei Konno, have determined the constants A, for different metals at room temperature. The correponding values are given in Table 1, together with Young's modulus E for those materials

TABLE 1 CONSTANTS A AND YOUNG'S MODULUS E FOR VARIOUS MATERIALS

Material	$E \times 10^6$ psi	$A \times 10^6$ psi
Steel	30	0.70–4.00
Copper	17	0.70
Nickel	30	0.44
Brass	13	0.22
Aluminum	10	0.12

Vibrations of a single-degree-of-freedom system, having viscous damping therefore are represented by

$$\frac{d^2q(t)}{dt^2} + 2\lambda\frac{dq(t)}{dt} + a^2q(t) = Q(t) \qquad [2]$$

If the external force Q is supposed to be periodical: $Q = Q_0 \sin \omega t$ a particular integral of Equation [2], which represents the forced vibration is

$$q = \sin(\omega t - \varphi)$$

where

$$C = \frac{Q_0}{\sqrt{(a^2-\omega^2)^2 + 4\omega^2\lambda^2}} \qquad [2a]$$

$$\tan\varphi = \frac{2\omega\lambda}{a^2-\omega^2} \qquad [2b]$$

By multiplying Equation [2] by dq and integrating between 0 and t the relation

[1] Associate Professor, Illinois Institute of Technology. Mem. ASME.

Presented at the Annual Conference of the Applied Mechanics Division, Purdue University, Lafayette, Ind., June 22–24, 1950, of THE AMERICAN SOCIETY OF MECHANICAL ENGINEERS.

Discussion of this paper should be addressed to the Secretary, ASME, 29 West 39th Street, New York, N. Y., and will be accepted until January 10, 1951, for publication at a later date. Discussion received after the closing date will be returned.

NOTE: Statements and opinions advanced in papers are to be understood as individual expressions of their authors and not those of the Society. Manuscript received by the Applied Mechanics Division August 10, 1949. Paper No. 50—APM-8.

[2] Numbers in parentheses refer to the Bibliography at the end of the paper.

$$\int_0^t q'q''dt + a^2 \int_0^t qq'dt + 2h \int_0^t q'^2dt = \int_0^t Qq'dt \ldots [3]$$

is obtained. The term

$$E - E_0 = \int_0^t q'q''dt + a^2 \int_0^t qq'dt$$

of Equation [3] represents the variation of the total energy in the interval $(0, t)$, the term

$$E_\delta = 2h \int_0^t q'^2dt$$

is a positive quantity; while

$$W = \int_0^t Qq'dt$$

represents the work done by the external force in the same interval of time. Therefore Equation [3] can be written

$$E - E_0 + E_\delta = W \ldots [4]$$

Equation [4] demonstrates the following principle: For a mechanical system having viscous damping, the work of the external force always exceeds the variation of the mechanical energy by a positive quantity. If $W = 0$, the work of the external force is not entirely transformed into mechanical energy, but always a residual part of this work remains untransformed. If $W = 0$, Equation [4] demonstrates the principle that the mechanical energy is constantly decreasing.

The "hereditary theory" was first advanced by Boltzmann in the year 1876 (2). It attributes the loss of work due to internal damping to the elastic delay (*Elastische Nachwirkung*), for which the deformation follows the applied force.

From this delay it follows that the deformation instead of depending only on the actual applied stress, as it should by Hooke's law, depends on all the stresses which have been applied on the elastic body. Now, if in a physical or mechanical problem the future state of a system depends only on the actual state or on an infinitely near state, the phenomenon is said to be "nonhereditary." The problems connected with those phenomena are solved by ordinary differential or by partial differential equations.

However, when the future state of the phenomenon depends not only upon the values of some parameters at the actual time, but also upon all the values in a precedent instant, the phenomenon is said to be "hereditary." The problems connected with this phenomenon are solved by integro-differential equations (3).

For the sake of simplicity, let us consider a system having only one degree of freedom. Let q be Lagrange's parameter.

The influence of the past, that is, of all values preceding the instant t, can be taken into account by introducing in the equation of the problem a term

$$y(t) = \int_{-\infty}^t \phi(t,\tau)q(\tau)d\tau$$

if "linear heredity" is supposed. The function $\phi(t,\tau)$ is called "hereditary nucleus" (or hereditary or memory function), and $y(t)$, which depends on all values of $q(t)$ in the interval $-\infty \leq \tau \leq t$ is a "functional." Often the function $\phi(t,\tau)$ depends only on the difference $(t - \tau)$. It can then be written $\phi(t,\tau) = \phi(t - \tau)$. If all the far "memory" in the time preceding the instant $(t - T_0)$ can be neglected, i.e., the function $\phi(t - \tau)$, T_0 being the period of heredity, then

$$\int_{-\infty}^t \phi(t,\tau)q(\tau)d\tau = \int_{t-T_0}^t \phi(t - \tau)q(\tau)d\tau = \int_0^{T_0} \phi(\tau)q(t - \tau)d\tau$$

The equation of vibrations for a single-degree system in the hereditary case is therefore

$$\frac{d^2q(t)}{dt^2} + a^2q(t) + \int_0^{T_0} \phi(t - \tau)q(\tau)d\tau = Q(t) \ldots [5]$$

the stress-strain relationship being in this case

$$s = Ee + \int_0^t \phi(t - \tau)e(\tau)d\tau \ldots [6]$$

The integro-differential Equation [5] generally can be resolved by a successive-approximations method or by transforming it into a "Volterra's integral equation" (3).

As the function $\phi(t)$ is, in general, a function decreasing with time, it can be represented by a sum of exponentials

$$\phi(t) = \sum_1^n A_\varepsilon e^{-\alpha_\varepsilon t} \ldots [7]$$

Substituting in the integro-differential Equation [5], the development of $\phi(t)$ given by Equation [7], Equation [5] can be easily solved (4). In fact, by differentiating Equation [5] n times, the integrals are eliminated and a differential linear equation with constant coefficients of $(n + 2)$ order is obtained (n being the number of terms of the development of Equation [7]).

It is easy to see what relation subsists (at least from a mathematical point of view) between the two theories, namely, that of the viscous and that of the hereditary damping. In fact Equation [5] can be written in the following form

$$\frac{d^2q(t)}{dt^2} + a^2q(t) = \int_0^{T_0} \phi(\tau)q(t - \tau)d\tau + Q(t) \ldots [8]$$

By developing $q(t - \tau)$ in a Taylor series in the vicinity of t one obtains

$$q(t - \tau) = q(t) - \tau \frac{dq(t)}{dt} + \frac{\tau^2}{2!} \frac{d^2q(t)}{dt^2} - \frac{\tau^3}{3!} \frac{d^3q(t)}{dt^3} + \ldots . [9]$$

Substituting Equation [9] in [8], one gets the following equation

$$\frac{d^2q(t)}{dt^2} + a^2q(t) = Q(t) + \sum_1^n {}_K p_K \frac{d^Kq(t)}{dt^K} \ldots \ldots [10]$$

p_K being constants, defined by

$$p_K = \frac{(-K)^K}{K!} \int_0^{T_0} \tau^K \phi(\tau)d\tau$$

Therefore the viscous aspect is contained in the hereditary one when the powers of τ greater than the first are neglected.

The differential equation which is obtained in the hereditary case, being of a greater order than the second, two constants of integration, i.e., initial position, q and initial velocity $(dq)/(dt)$, are no more sufficient to specify the problem. It is necessary to have a number of constants equal to the degree of the differential equation. In fact, in an hereditary problem not only the initial conditions q and $(dq)/(dt)$ for $t = 0$, but also the past history must be known. Now, if all the derivatives of the function $q(t)$ at $t = 0$ are known, and in addition the analyticity of the function $q(t)$ is admitted, the function $q(t)$ is uniquely determined by the Taylor development given by Equation [9]. It is also possible for hereditary systems to establish a fundamental energy relation (5) expressed by

$$E - E_0 + \int_0^t E_\delta \, dt = W \ldots [11]$$

where $E = E_p + E_K$ represents the mechanical energy; sum of the potential internal energy

$$E_p = \frac{1}{2} mq^2(t) - \frac{1}{2}\int_0^{\tau_0} \phi(\tau)[q(t) - q(t-\tau)]^2 d\tau$$

where

$$(m = a^2 + \int_0^{\tau_0} \phi[\tau]d\tau \text{ is a positive quantity})$$

and of the kinetic energy

$$E_K = \frac{1}{2}\left[\frac{dq(t)}{dt}\right]^2$$

W being the work of the external force in the interval of time $(0, t)$ while E_δ is a positive quantity expressed by

$$E_\delta = -\frac{1}{2}\int_0^{\tau_0} \phi'(\tau)[q(t) - q(t-\tau)]^2 d\tau$$

Equation [11] demonstrates that during vibrations of systems having hereditary characteristics, there is dissipation of energy.

Experimental Results on Plastic and Rubberlike Materials

During the late war experiments on some plastics and rubberlike materials at high rate of loading were carried out in Cambridge, England, under the supervision of Sir Geoffrey Taylor, FRS (6).

Short cylinders of the materials to be tested were placed on the plane end of a steel bar hung as a ballistic pendulum. Another bar, also hung as a ballistic pendulum, was made to impinge upon it. The distance between the two bars was photographed by a camera using a rotating drum.

From the photographs it was possible to deduce the displacements of the two ends of the specimen; by a double differentiation, the force acting on it during impact; and finally, the dynamic stress-strain relationship of the material. The details of the experimental method employed already have been described by the author (7), and therefore will not be repeated here.

Fig. 1 shows some of the results obtained with polythene. The stress-strain curve $\sigma = f(\epsilon)$ obtained in static compression tests, using specimens with lubricated ends, is also shown in the same figure. From the analysis of the dynamic stress-strain curves in Fig. 1, one finds that the quantities

$$\sigma_d = \sigma - \sigma_s = \sigma - f[\epsilon]$$

(where σ is the dynamic stress, $f[\epsilon]$ the static stress, and σ_d the pure dynamic stress) are dependent upon all the values taken by the function

$$\frac{d\epsilon(\tau)}{d\tau}$$

(variation of the strain with respect to time), when the time τ varies in the interval $(0, t)$. In other words, the quantity $\sigma - f(\epsilon)$ is a "functional" of the function

$$\frac{d\epsilon(\tau)}{d\tau}$$

in the interval $(0, t)$. One can then write, using the classical notation

$$\sigma - f(\epsilon) = F\left|\left[\frac{d\epsilon(\tau)}{d\tau}\right]_0^t\right|$$

or

$$\sigma - f(\epsilon) = \int_0^t \phi(\tau)\frac{d\epsilon(t-\tau)}{d\tau}d\tau = \int_0^t \phi(t-\tau)\frac{d\epsilon(\tau)}{d\tau}d\tau \quad [12]$$

FILM NO.	DATE	SYMBOL	INITIAL SPEED inch/sec	TEMPERATURE °F	TIME OF IMPACT 10^3 sec
1	1-5-45	●	12.33	61°	16.48
2	1-5-45	●	17.44	61°	16.48
4	1-6-45	●	21.36	62°	16.00
3	1-5-45	✚	24.65	62°	16.48
5	1-8-45	●	30.20	60°	16.95
1	1-8-45	▲	37.00	59°	16.65

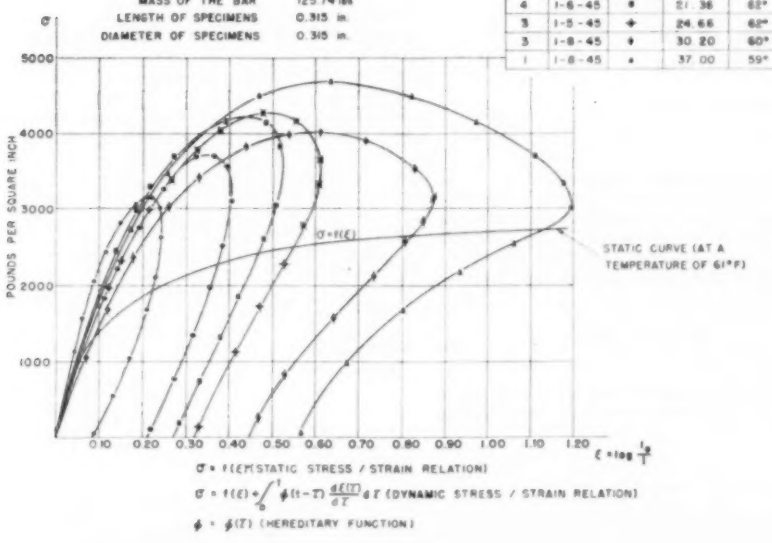
MASS OF THE BAR 125.74 lbs
LENGTH OF SPECIMENS 0.315 in.
DIAMETER OF SPECIMENS 0.315 in.
σ
5000
4000
3000
2000
1000
POUNDS PER SQUARE INCH
0.10 0.20 0.30 0.40 0.50 0.60 0.70 0.80 0.90 1.00 1.10 1.20
ε = log l₀/l
σ=f(ε)
STATIC CURVE (AT A TEMPERATURE OF 61°F)
σ = f(ε) (EMPIRICAL STATIC STRESS / STRAIN RELATION)
σ = f(ε) + ∫₀ᵗ φ(t−τ) dε(τ)/dτ dτ (DYNAMIC STRESS / STRAIN RELATION)
φ = φ(t) (HEREDITARY FUNCTION)

Fig. 1

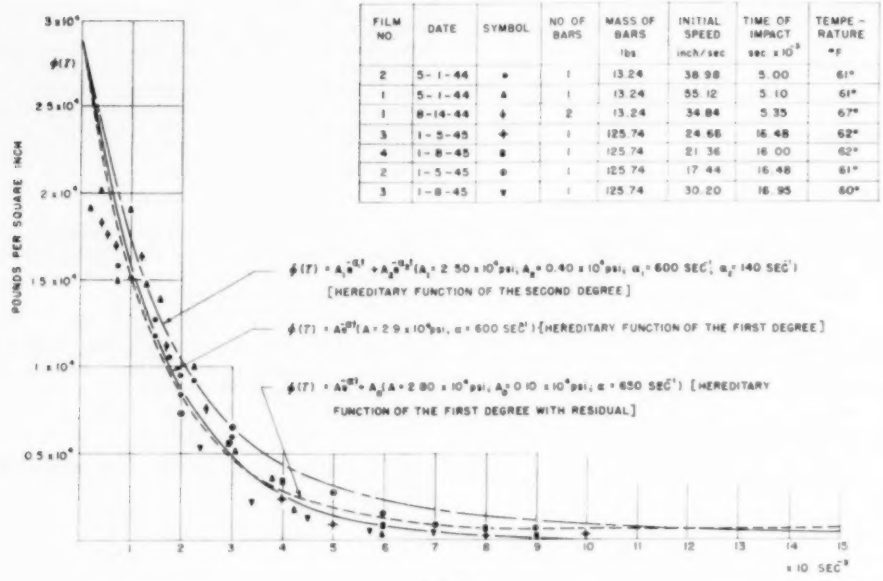
3 x 10⁴
φ(T)
2.5 x 10⁴
2 x 10⁴
1.5 x 10⁴
1 x 10⁴
0.5 x 10⁴
POUNDS PER SQUARE INCH
1
2
3
4
5
6
7
8
9
10
11
12
13
14
15
x 10⁻³ SEC
φ(T) = A₁e^(−α₁T) + A₂e^(−α₂T) (A₁ = 2.50 x 10⁴ psi, A₂ = 0.40 x 10⁴ psi, α₁ = 600 SEC⁻¹, α₂ = 140 SEC⁻¹)
[HEREDITARY FUNCTION OF THE SECOND DEGREE]
φ(T) = Ae^(−αT) (A = 2.9 x 10⁴ psi, α = 600 SEC⁻¹) [HEREDITARY FUNCTION OF THE FIRST DEGREE]
φ(T) = Ae^(−αT) + A₀ (A = 2.80 x 10⁴ psi, A₀ = 0.10 x 10⁴ psi, α = 650 SEC⁻¹) [HEREDITARY FUNCTION OF THE FIRST DEGREE WITH RESIDUAL]

FILM NO.	DATE	SYMBOL	NO. OF BARS	MASS OF BARS lbs	INITIAL SPEED inch/sec	TIME OF IMPACT sec x 10⁻³	TEMPERATURE °F
2	5-1-44	•	1	13.24	38.98	5.00	61°
1	5-1-44	▲	1	13.24	55.12	5.10	61°
1	8-14-44	♦	2	13.24	34.84	5.35	67°
3	1-5-45	✚	1	125.74	24.66	16.48	62°
4	1-8-45	■	1	125.74	21.36	16.00	62°
2	1-5-45	●	1	125.74	17.44	16.48	61°
3	1-8-45	▼	1	125.74	30.20	16.95	60°

FIG. 2

where $\phi(t)$ is an unknown function which takes account of the whole strain history of the material up to the time t.

By analyzing the experiments on "polythene," using Relation [12], it was found that the function $\phi(t)$ could be represented over the range of the experiments by the following formulas

$$\phi(t) = Ae^{-\alpha t} = 2.9(10^4)e^{-600t} \text{ psi}$$

(hereditary function of the first degree)

$$\phi(t) = A_1e^{-\alpha_1 t} + A_2e^{-\alpha_2 t} = [2.50e^{-600t} + 0.40e^{-140t}]10^4 \text{ psi}$$

(hereditary function of second degree)

$$\phi(t) = Ae^{-\alpha t} + A_0 = [2.8e^{-650t} + 0.10]10^4 \text{ psi}$$

(hereditary function of the first degree with residual).

The values of $\phi(t)$ found by analyzing the experimental values for polythene are given in Fig. 2. From the figure it is seen that the period T_0 of the heredity of polythene at room temperature is of about 10×10^{-2} sec. From Equation [12] it follows that the dynamic stress-strain relationship for plastics and rubberlike materials can be expressed as follows

$$\sigma = f(\epsilon) + \int_0^t \phi(t-\tau)\frac{d\epsilon(\tau)}{d\tau}d\tau \quad \ldots\ldots [13]$$

If in a first approximation it is supposed that the material follows Hooke's law $f(\epsilon) = E\epsilon$, when stressed statically, then Equation [13] becomes

$$\sigma = E\epsilon + \int_0^t \phi(t-\tau)\frac{d\epsilon(\tau)}{d\tau}d\tau = E\epsilon + \int_0^t \phi(\tau)\frac{d\epsilon(t-\tau)}{d\tau}d\tau \quad \ldots\ldots [14]$$

From a mathematical point of view Equation [14] is identical with Equation [6]. In fact, since $t = 0$, $\epsilon = 0$, by an integration of parts in Equation [14] one gets

$$\sigma = [E + \phi(0)]\epsilon(t) + \int_0^t \phi'(t-\tau)\epsilon(\tau)d\tau \quad \ldots\ldots [15]$$

Direct Determination of Dynamic Stress-Strain Curves

Once the hereditary function $\phi(t)$ of a given material has been determined, it is possible to calculate directly the stress-strain curve during a dynamic test. Suppose that the material follows Equation [14], call l_0 the initial length of the specimen, A_0 the initial cross-section area, $l = l_0 - s$ the length of the specimen at the instant t, and m the mass of the impinging bars. The following integro-differential equation holds

$$m\frac{d^2s(t)}{dt^2} + \frac{EA_0}{l_0}s + \frac{A_0}{l_0}\int_0^t \phi(t-\tau)\frac{ds(\tau)}{d\tau}d\tau = 0 \quad \ldots [16]$$

In the case of heredity of the first degree, $\phi(t) = Ae^{-\alpha t}$, by differentiating Equation [16] the following equation

$$m\frac{d^3s(t)}{dt^3} + \alpha m\frac{d^2s(t)}{dt^2} + \frac{(E+A)A_0}{l_0}\frac{ds(t)}{dt} + \frac{A_0}{l_0}\alpha Es(t) = 0 \quad [17]$$

is obtained.

Its solution is

$$s = C_1e^{-\gamma t} + C_2e^{-pt}\cos qt + C_3e^{-pt}\sin qt$$

where $-\gamma$; $-p + iq$; $-p - iq$ are the roots of the algebraic equation

$$x^3 + \alpha x^2 + \frac{(E+A)A_0}{l_0m}x + \frac{A_0E\alpha}{l_0m} = 0$$

From the initial conditions

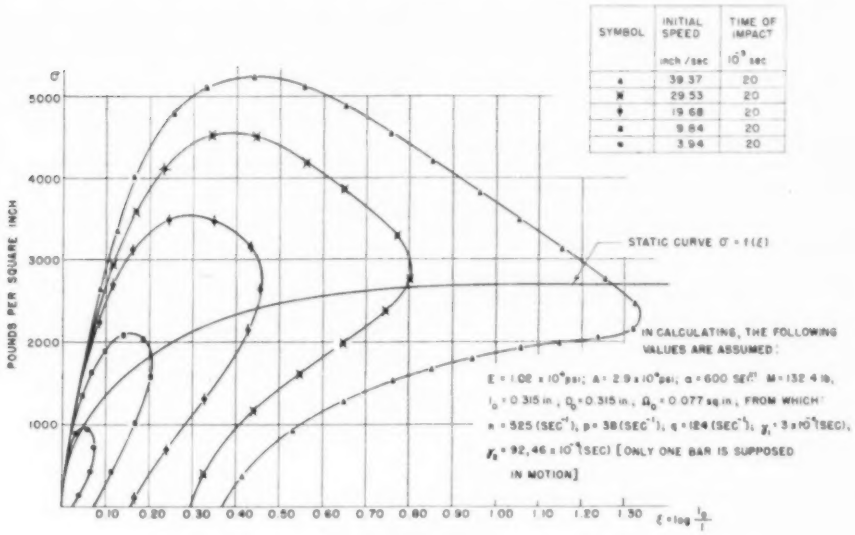
SYMBOL | INITIAL SPEED inch/sec | TIME OF IMPACT 10^{-5} sec
▲ 39.37 20
✖ 29.53 20
✦ 19.68 20
■ 9.84 20
● 3.94 20
σ
POUNDS PER SQUARE INCH
5000
4000
3000
2000
1000
STATIC CURVE σ = f(ε)
IN CALCULATING, THE FOLLOWING VALUES ARE ASSUMED:
E = 1.02 x 10⁶ psi; A = 2.9 x 10⁶ psi; α = 600 SEC⁻¹; M = 132.4 lb,
l₀ = 0.315 in.; D₀ = 0.315 in.; Ω₀ = 0.077 sq.in.; FROM WHICH:
n = 525 (SEC⁻¹), p = 38 (SEC⁻¹), q = 124 (SEC⁻¹); γ₁ = 3 x 10⁻⁵ (SEC),
γ₂ = 92.46 x 10⁻⁵ (SEC) [ONLY ONE BAR IS SUPPOSED IN MOTION]
0.10 0.20 0.30 0.40 0.50 0.60 0.70 0.80 0.90 1.00 1.10 1.20 1.30
ε = log l₀/l

Fig. 3

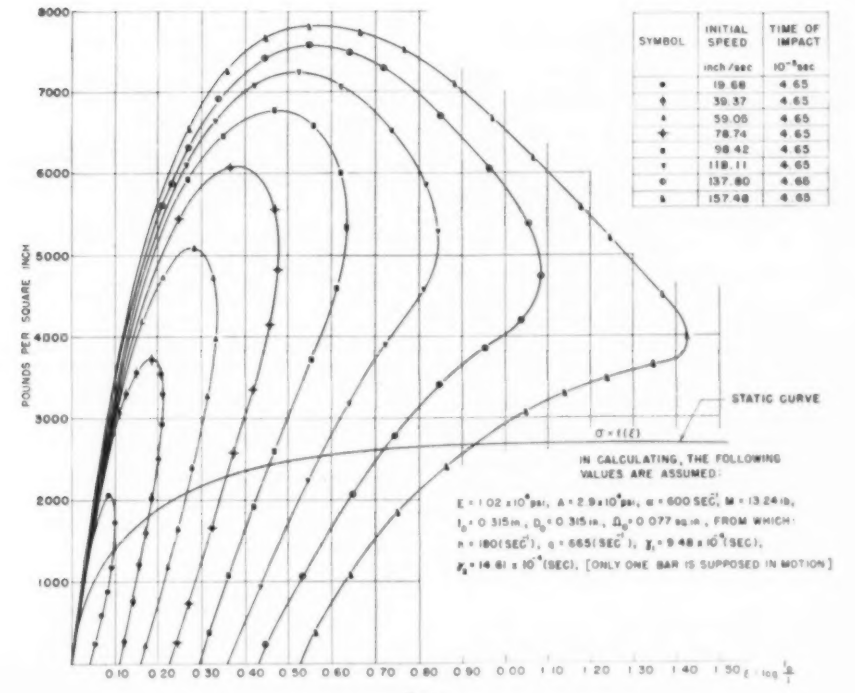
SYMBOL | INITIAL SPEED inch/sec | TIME OF IMPACT 10^{-5} sec
● 19.68 4.65
✦ 39.37 4.65
▲ 59.05 4.65
✚ 78.74 4.65
■ 98.42 4.65
▼ 118.11 4.65
○ 137.80 4.65
△ 157.48 4.65
POUNDS PER SQUARE INCH
8000
7000
6000
5000
4000
3000
2000
1000
STATIC CURVE
σ = f(ε)
IN CALCULATING, THE FOLLOWING VALUES ARE ASSUMED:
E = 1.02 x 10⁶ psi; A = 2.9 x 10⁶ psi; α = 600 SEC⁻¹; M = 13.24 lb,
l₀ = 0.315 in.; D₀ = 0.315 in.; Ω₀ = 0.077 sq.in.; FROM WHICH:
n = 180 (SEC⁻¹), q = 665 (SEC⁻¹); γ₁ = 9.48 x 10⁻⁵ (SEC),
γ₂ = 14.61 x 10⁻⁵ (SEC). [ONLY ONE BAR IS SUPPOSED IN MOTION]
0.10 0.20 0.30 0.40 0.50 0.60 0.70 0.80 0.90 1.00 1.10 1.20 1.30 1.40 1.50
ε = log l₀/l

Fig. 4

$$s = 0; \quad \frac{ds}{dt} = v_0; \quad \frac{d^2s}{dt^2} = 0$$

it follows $C_1 = \gamma_1 v_0$; $C_2 = -\gamma_1 v_0$; $C_3 = \gamma_2 v_0$ where

$$\gamma_1 = \frac{2p}{q^2 + (r-p)^2}; \quad \gamma_2 = \frac{q^2 + r^2 - p^2}{q[q^2 + (r-p)^2]}$$

Figs. 3 and 4 show the stress-strain curves for polythene, calculated on the assumption that the impinging masses m are 132 lb and 13.2 lb, respectively, and for different speeds. The calculated curves closely coincide with those found experimentally, therefore giving a confirmation of the dynamic stress-strain relationship found for plastics and rubberlike materials.

Forced Vibrations of Single-Degree-of-Freedom Hereditary Systems: Determination of Hereditary Function $\phi(t)$ Directly From Forced Vibrations

Indicating by $q = q(t)$ Lagrange's co-ordinate, the following equation holds

$$\frac{d^2q(t)}{dt^2} + a^2q(t) + b^2 \int^t \phi(t-\tau) \frac{dq(\tau)}{d\tau} d\tau = Q(t) \quad [18]$$

a^2 and b^2 being constants.

If the external force is sinusoidal, $Q(t) = Q_0 \sin \omega t$; and if the hereditary function is of the first degree $\phi(t) = Ae^{-\alpha t}$, Equation [18] becomes

$$\frac{d^2q(t)}{dt^2} + a^2q(t) + b^2 \int_0^t e^{-\alpha(t-\tau)} \frac{dq(\tau)}{d\tau} d\tau = Q_0 \sin \omega t \quad [19]$$

By differentiating Equation [19] one gets

$$\frac{d^3q(t)}{dt^3} + \alpha \frac{d^2q(t)}{dt^2} + (a^2 + b^2) \frac{dq(t)}{dt} + \alpha a^2 q(t) = \alpha Q_0 \sin \omega t + \omega Q_0 \cos \omega t \quad [20]$$

Let a particular solution (forced vibration) of Equation [20] be

$$q = C \sin (\omega t - \varphi)$$

One finds

$$C = Q_0 \frac{\sqrt{[\alpha^2(a^2 - \omega^2) - \omega^2 \{\omega^2 - (a^2 + b^2)\}]^2 + (\alpha\omega b^2)^2}}{\alpha^2(a^2 - \omega^2)^2 + \omega^2[\omega^2 - (a^2 + b^2)]^2}$$

$$\tan \varphi = \frac{\alpha\omega b^2}{\alpha^2(a^2 - \omega^2) - \omega^2[\omega^2 - (a^2 + b^2)]} \quad [21]$$

Let

$$\gamma = \frac{b}{a}; \quad \vartheta = \frac{\alpha}{a}; \quad x = \frac{\omega}{a}$$

The values of the functions Ca^2/Q_0 and φ are shown in Figs. 5, 6, 7, 8, 9, and 10, for $\vartheta = 0.10$, 1.00, and 10; x variable between 0 and 10; and γ variable between 0.25 and 4. On the same graphs the dotted lines represent the corresponding values for viscous damping (from Equations [2a] and [2b]).

If one puts in Equations [21], $a = \omega$, one gets

$$\tan \varphi = \frac{a}{a}; \quad C = \frac{Q_0}{b^2} \sqrt{1 + \left(\frac{\alpha}{a}\right)^2} = \frac{Q_0}{b^2 \cos \varphi} \quad [22]$$

and finally

$$\alpha = (a \tan \varphi)_{\omega = a}$$

$$b = \left[\sqrt{\frac{Q_0}{C \cos \varphi}}\right]_{\omega = a} \quad [23]$$

Equations [22] and [23] show the possibility of determining the hereditary characteristics of a material, i.e., the constants α and b from forced vibrations once that the constant a has been determined from static tests.

More generally, in order to find the function $\phi(t)$ directly from forced vibrations, let us suppose that

$$Q(t) = \sum_1^\infty{}_r \{A_r \sin rt + B_r \cos rt\}$$

Let T_0 be the period of heredity. Equation [18] becomes

$$\frac{d^2q(t)}{dt^2} + a^2q(t) + b^2 \int_{t-T_0}^t \phi(\tau) \frac{dq(t-\tau)}{d\tau} d\tau = Q(t)$$

or

$$\frac{d^2q(t)}{dt^2} + a^2q(t) = Q(t) + b^2 \int_0^{T_0} \phi(\tau) \frac{dq(t-\tau)}{d\tau} d\tau$$

Let

$$q(t) = \sum_1^\infty{}_r (\alpha_r \sin r\nu t + \beta_r \cos r\nu t)$$

then

$$\left.\begin{aligned} \alpha_r &= \frac{1}{\Delta_r} \{A_r [a^2 - (r\nu)^2 - r\nu G_r] - B_r r\nu L_r\} \\ \beta_r &= \frac{1}{\Delta_r} \{B_r [a^2 - (r\nu)^2 - r\nu G_r] + A_r r\nu L_r\} \end{aligned}\right\} \quad [24]$$

where

$$\Delta_r = [a^2 - (r\nu)^2 - r\nu G_r]^2 + (r\nu L_r)^2$$

$$L_r = \int^{T_0} \phi(\tau) \cos r\nu\tau d\tau$$

$$G_r = \int_0^{T_0} \phi(\tau) \sin r\nu\tau d\tau$$

Let us suppose that the external force has the period equal to the period T_0 of the heredity. One measures $q(t)$ and obtains by harmonic analysis, αr and βr. With A_r and B_r known, one can calculate the values of G_r and L_r by means of Equation [24]

$$L_r = \int_0^{T_0} \phi(\tau) \cos \frac{2\pi r}{T_0} \tau d\tau$$

$$G_r = \int_0^{T_0} \phi(\tau) \sin \frac{2\pi r}{T_0} \tau d\tau$$

But as Lr and Gr are the coefficients of the Fourier development of the unknown function $\phi(t)$, one obtains by harmonic composition

$$\phi(t) = \frac{2}{T_0} \sum_r \left[L_r \cos \frac{2\pi r}{T_0} t + G_r \sin \frac{2\pi r}{T_0} t \right]$$

Transverse Free and Forced Vibrations of Simply Supported Beams Having Hereditary Characteristics

For transverse vibrations of a beam the following integro-differential equation holds (8)

$$\frac{\partial^2 u(x,t)}{\partial t^2} + a^2 \left[\frac{\partial^4 u(x,t)}{\partial x^4} + \frac{1}{E} \int_0^t \phi(t-\tau) \frac{\partial^2(x,\tau)}{\partial x, \partial \tau} d\tau \right] = p'(x,t) \quad [25]$$

where $a^2 = EI/m$; EI being the flexural rigidity of the bar, m the mass per unit length, $p'(x,t) = p(x,t)/m$; where $p(x,t)$ repre-

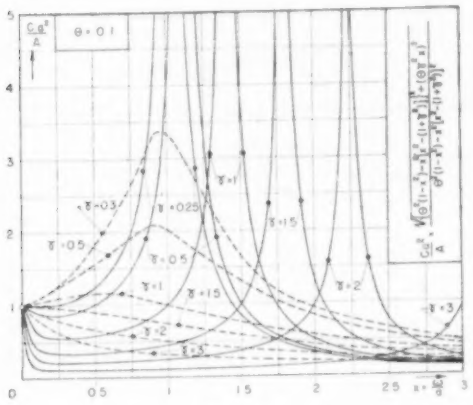

FIG. 5

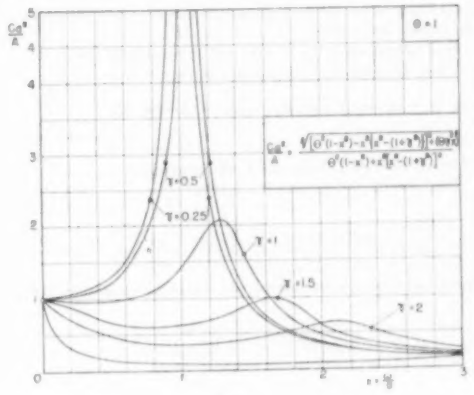

FIG. 6

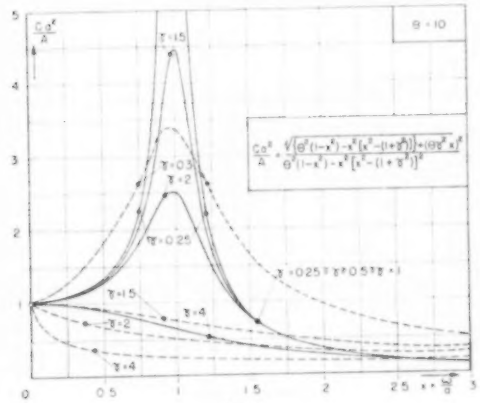

FIG. 7

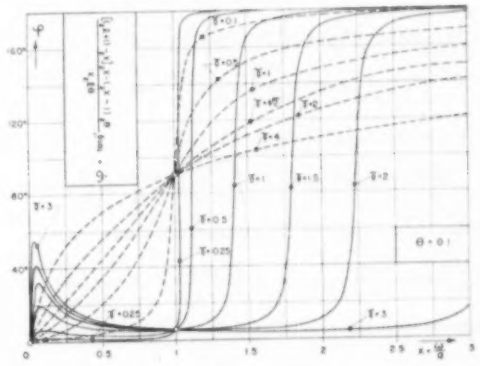

FIG. 8

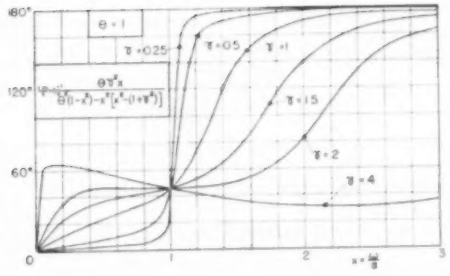

FIG. 9

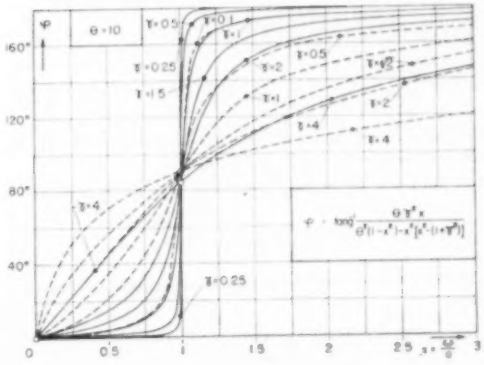

FIG. 10

sents the external force acting on the unit length of the beam, l is the length of the beam.

Free vibrations, $[p'(x,t) = 0]$ will be considered first.

Using the methods of separation of variables, let

$$u(x,t) = [A_1 \cos Kx + A_2 \sin Kx + A_3 \cosh Kx + A_4 \sinh Kx]f(t)$$

where A_i $(i = 1, 2, 3, 4)$ and K are constants.

The solution of Equation [25] is then

$$\frac{d^2f(t)}{dt^2} + a^2K^4\left[f(t) + \frac{1}{E}\int_0^t \phi(t-\tau)\frac{df(\tau)}{d\tau}\,d\tau\right] = 0$$

If the bar is simply supported, the following conditions hold

$$(u)_{x=0} = 0 \qquad \left(\frac{\partial^2 u}{\partial x^2}\right)_{x=0} = 0$$

$$(u)_{x=l} = 0 \qquad \left(\frac{\partial^2 u}{\partial x^2}\right)_{x=l} = 0$$

from which it follows

$$K_i = \frac{i\pi}{l}$$

The solution of Equation [25] is then found to be

$$u(x,t) = \sum_1^\infty A_i \sin\frac{i\pi x}{l} f_i(t)$$

In the case in which $\phi(t) = Ae^{-\alpha t}$ one gets

$$\frac{d^2f_i(t)}{dt^2} + K_i{}^4a^2\left[f_i(t) + \frac{A}{E}\int_0^t e^{-\alpha(t-\tau)}\frac{df_i(\tau)}{d\tau}\,d\tau\right] = 0 \quad [26]$$

Differentiating Equation [26] with respect to t, there results

$$\frac{d^3f_i(t)}{dt^3} + \alpha\frac{d^2f_i(t)}{dt^2} + \left[K_i{}^4a^2 + \frac{A}{E}\right]\frac{df_i(t)}{dt} + \alpha K_i{}^4f_i(t) = 0 \quad [27]$$

Substituting in Equation [27], $f_i(t) = e^{r_i t}$ the algebraic equation

$$r_i{}^3 + \alpha r_i{}^2 + \left[K_i{}^4a^2 + \frac{A}{E}\right]r_i + \alpha K_i{}^4a^2 = 0 \quad [28]$$

is obtained.

The discriminant of Equation [28] is positive. Therefore, of the three roots one $-r_i$, will be real, while the two others $-p_i + iq_i$, $-p_i - iq_i$ will be complex conjugate.

The solution of Equation [25] will then be

$$u(x,t) = \sum_1^\infty \sin\frac{i\pi x}{l}\left[C_{i1}e^{-r_i t} + C_{i2}e^{-p_i t}\cos q_i t + C_{i3}e^{-p_i t}\sin q_i t\right]$$

The initial conditions for determining the constants C_{ij}: $(j = 1, 2, 3)$ are as follows:

1 For $t = 0$, the initial configuration of the beam is known

$$u(x,0) = \sum_1^\infty A_i \sin\frac{i\pi x}{l}$$

2 For $t = 0$, the initial velocities of all points of the beam are known

$$\frac{\partial u(x,0)}{\partial t} = \sum_1^\infty A_i{}' \sin\frac{i\pi x}{l}$$

3 For $t = 0$, the following relationship is satisfied

$$\frac{\partial^2 u(x,0)}{\partial t^2} + a^2\frac{\partial^4 u(x,0)}{\partial x^4} = 0$$

The values for the constants C_{ij} are found to be as follows

$$C_{i1} = \frac{A_i{}'}{A_i(p_i - r_i)} + a^2\left(\frac{\pi}{l}\right)^4\frac{A_i}{(2p_ir_i - p_i{}^2 - r_i{}^2 - q_i{}^2)} + \frac{A_i{}'(r_i + p_i)}{A_i(2p_ir_i - p_i{}^2 - r_i{}^2 - q_i{}^2)}$$

$$C_{i2} = \frac{A_i{}'}{A_i(r_i - p_i)} + a^2\left(\frac{\pi}{l}\right)^4\frac{A_i}{p_i{}^2 + r_i{}^2 + q_i{}^2 - 2p_ir_i} + \frac{A_i{}'(r_i + p_i)}{A_i(2p_ir_i - p_i{}^2 - r_i{}^2 - q_i{}^2)}$$

$$C_{i3} = \frac{A_i(r_i - p_i)}{q_i(2p_ir_i - p_i{}^2 - r_i{}^2 - q_i{}^2)}a^2\left(\frac{\pi}{l}\right)^4 + \frac{A_i{}'(r_i{}^2 - p_i{}^2)}{A_iq_i(2p_ir_i - p_i{}^2 - r_i{}^2 - q_i{}^2)}$$

If the external load is distributed along the beam in a sinusoidal manner and varies harmonically with the time, then

$$p(x,t) = p_0 \sin\frac{\pi x}{l}\sin 2\pi nt \quad [29]$$

If heredity of the first degree is supposed, Equation [25] becomes

$$\frac{\partial^2 u(x,t)}{\partial t^2} + a^2\left[\frac{\partial^4 u(x,t)}{\partial x^4} + \frac{A}{E}\int_0^t e^{-\alpha(t-\tau)}\frac{\partial^4 u(x,t)}{\partial x^4\partial\tau}\,d\tau\right] = p_0{}'\sin\frac{\pi x}{l}\sin 2\pi nt \quad [30]$$

where

$$\left(p_0{}' = \frac{p_0}{m}\right)$$

Putting in this case

$$u(x,t) = p_0 \sin\frac{\pi x}{l} f(t) \quad [31]$$

and substituting Equation [31] in [30]

$$\frac{d^2f(t)}{dt^2} + a^2\left(\frac{\pi}{l}\right)^4 f(t) + a^2\left(\frac{\pi}{l}\right)^4\frac{A}{E}\int_0^t e^{-\alpha(t-\tau)}\frac{df(\tau)}{d\tau}\,d\tau = \sin 2\pi nt \quad [32]$$

By differentiating Equation [32] there results

$$\frac{d^3f(t)}{dt^3} + \alpha\frac{d^2f(t)}{dt^2} + a^2\left(\frac{\pi}{l}\right)^4\left(1 + \frac{A}{E}\right)\frac{df(t)}{dt} + \alpha a^2\left(\frac{\pi}{l}\right)^4 f(t) = \alpha\sin 2\pi nt + 2\pi n\cos 2\pi nt \quad [33]$$

Let us assume as a particular solution of Equation [30]

$$u'(x,t) = p_0{}'D\sin\frac{\pi x}{l}\sin(2\pi nt - \varphi) \quad [34]$$

one finds

$$\tan \varphi = \frac{2\pi n \alpha a^2 \left(\frac{\pi}{l}\right)^4 \frac{A}{E}}{(2\pi n)^2 \left\{(2\pi n)^2 - a^2\left(\frac{\pi}{l}\right)^4\left(1+\frac{A}{E}\right)\right\} + a^2\left\{(2\pi n)^2 - a^2\left(\frac{\pi}{l}\right)^4\right\}} \quad [35]$$

$$D = \frac{\sqrt{\left[(2\pi n)^2\left\{(2\pi n)^2 - a^2\left(\frac{\pi}{l}\right)^4\left(1+\frac{A}{E}\right)\right\} + a^2\left\{(2\pi n)^2 - a^2\left(\frac{\pi}{l}\right)^4\right\}\right]^2 + \left[2\pi n \alpha a^2\left(\frac{\pi}{l}\right)^4 \frac{A}{E}\right]^2}}{(2\pi n)^2\left\{(2\pi n)^2 - a^2\left(\frac{\pi}{l}\right)^4\left(1+\frac{A}{E}\right)\right\}^2 + a^2\left\{(2\pi n)^2 - a^2\left(\frac{\pi}{l}\right)^4\right\}^2} \quad [36]$$

The general integral of Equation [30] will then be

$$u(x,t) = p_0 D \sin\frac{\pi x}{l} \sin(2\pi n t - \varphi) + [C_1 e^{-rt} + C_2 e^{-pt} \sin qt + C_3 e^{-pt} \cos qt] \sin\frac{\pi x}{l} \quad [37]$$

The constants C_1, C_2, and C_3 have to be determined from the following initial conditions

$(t = 0)\ u(x,0) = 0$

$$\frac{\partial u(x,0)}{\partial t} = 0$$

$$\frac{\partial^2 u(x,0)}{\partial t^2} + a^2 \frac{\partial^2 u(x,0)}{\partial x^4} = 0$$

One therefore finds

$$C_1 = p_0 D \sin\varphi - C_3$$

$$C_2 = \frac{r p_0 D \sin\varphi}{q} - \frac{2\pi n p_0 D \cos\varphi}{q} + \frac{p-r}{q} C_3$$

$$C_3 = \frac{(2\pi n)^2 p_0 D \sin\varphi + 4p_0 \pi n p D \cos\varphi + r^2 p_0 D \sin\varphi - 2pr p_0 D \sin\varphi}{r^2 + 2p(p-r)}$$

In Equation [37] the first term represents the forced vibration, and the terms between brackets, the damped free vibration. The foregoing solution for forced vibration in a simply supported beam, having hereditary characteristics, can be applied to the study of traveling loads on simply supported girders (8). This may be accomplished by making use of the method of harmonic analysis developed by Sir Charles Inglis, for elastic beams (9).

Conclusions

In this paper a short review has been given of the principal mathematical theories so far proposed to explain the complex phenomenon of internal dynamic friction of elastic bodies. It has been shown how the viscous and hereditary theories are related.

Experiments carried out on plastics and rubberlike materials have been described. The dynamic stress-strain relationship expressed by the formula

$$\sigma = f(\epsilon) + \int_0^t \phi(t-\tau)\frac{d\epsilon(\tau)}{d\tau}\,d\tau$$

which has been found for those materials, has perhaps a more general character and very probably could express the dynamic stress-strain relationship for many metallic materials as well.

It would therefore be desirable to carry out further research; in particular, the study of the dynamic behavior of materials, especially metals, at different temperatures would be most interesting.

The work presented here shows how the hereditary function $\phi(t)$ of a material having hereditary characteristics may be directly determined from the study of its forced vibrations.

Bibliography

1 "Über innere Reibung fester Korper, insbesondere der Metalle," by W. Voigt, *Annalen der Physik*, vol. 47, 1892, p. 671.

"Betrachtungen über dynamische Zugbeanspruchung," by Rudolph Plank, *Forschungsarbeiten*, vol. 133, 1913, pp. 21–46.

"Applied Elasticity," by S. Timoshenko and J. M. Lessels, Constable and Company, Ltd., London, England, 1928, p. 419.

2 "Zur Theorie der elastische Nachwirkung," by L. Boltzmann, *Annalen der Physik*, vol. 7, 1876, p. 624.

"Physikalische Grundlagen der Festigkeitlehre," by T. von Kármán, Enciclopedia der Mathematischen Wissenschaft—IV, vol. 11, pp. 697–770.

"Plasticity," by A. Nadai, McGraw-Hill Book Company, Inc., New York, N. Y., and London, England, 1939, p. 29.

3 "Vibrazioni elastiche nel caso della eredità," by V. Volterra, Rendiconti Accademia dei Lincei, vol. 21, serie 5, 1912.

"Lecons sur les équations intégrales et les équations intégro-differentielles," by V. Volterra, Gauthier-Villars, Paris, France, 1913.

"Saggi Scientifici," by V. Volterra, Zanichelli-Bologna, Italy, 1924.

"La Teoria dei Funzionali applicata ai Fenomeni Ereditari," by V. Volterra, Atti Congresso Internazionale di Matematica di Bologna, vol. 10, 1928.

"Theory of Functionals and of Integral and Integro-Differential Equations," by V. Volterra, Blackie and Son, London, England, 1930.

4 "On the Numerical Solutions of Integral Equations," by E. T. Whittaker, Proceedings of the Royal Society of London, series A, vol. 94, 1918.

"Sulla Teoria delle oscillazioni elastiche con eredità," by D. Graffi, "Il Nuovo Cimento," 1928.

5 "Energia nei Fenomeni Elastici Ereditari," by V. Volterra, *Acta Pontificia Academia Scientiarum*, vol. 4, 1940, p. 14.

6 "The Testing of Materials at High Rates of Loading," by G. I. Taylor, James Forrest Lecture 1946, *Journal of the Institution of Civil Engineers*, London, England, 1946.

7 "On the Dynamic Stress-Strain Relationship for Plastic and Elastic Materials," by E. Volterra, Sixth International Congress of Applied Mechanics, Paris, France, 1946.

"Sulla relazione dinamica tra sforzi specifici e deformazioni specifiche per i materiali elastici e plastici," by E. Volterra, *Giornale del Genio Civile-Fascicolo*, vol. 3, 1946, pp. 1–59.

"Alcuni risultati di prove dinamiche sui materiali," by E. Volterra, La Rivista del Nuovo Cimento, vol. 4, 1948, pp. 1–28.

8 "Problemi dinamici della trave in regime ereditario," by E. Volterra, Rendiconti Accademia dei Lincei-Fascicoli 1 e 2, vol. 2, 1947.

9 "Theory of Transverse Oscillations in Girders," by C. E. Inglis, Proceedings of the Institution of Civil Engineers, London, England 1924.

Plastic Biaxial Stress-Strain Relations for Alcoa 24S-T Subjected to Variable-Stress Ratios

By JOSEPH MARIN[1] and B. J. KOTALIK,[2] STATE COLLEGE, PA.

Usually plastic biaxial stress-strain relations for metals have been determined for tests in which the ratios of the principal stresses have been maintained essentially constant. This paper presents biaxial plastic stress-strain relations for both constant and variable-stress ratios. The purpose of conducting the variable-stress-ratio tests is to attempt to prove whether the flow- or deformation-type theory is the correct theory for predicting plastic stress-strain relations. The paper also gives a comparison between the actual and theoretically predicted values of the biaxial yield, ultimate and fracture strengths, and the biaxial ductility. Various ratios of biaxial tensile stresses were investigated by subjecting tubular specimens to axial tension and internal pressure. The test results showed that the yield-strength values agree best with the distortion-energy theory. For the prediction of the plastic stress-strain relations the deformation-type theory was found to be in approximate agreement with the test results for both the constant- and variable-stress-ratio tests.

Introduction

THE information available on plastic stress-strain relations for metals subjected to combined stresses is very limited. There are two main purposes for obtaining such data. For some metals used in the form of sheets, such as aluminum and steel plates, cold-forming operations are used which produce biaxial stresses and strains in the plastic range. In these forming procedures, it is desirable to know what the limiting bending strains are so that rupture does not occur. To obtain these formability limits, more information is desired on biaxial plastic stress-strain relations for metals. Plastic stress-strain relations are also of value in the design of certain machine and structural parts which are subjected to an initial state of stress producing plastic flow.

The purpose of this paper is to present data for an aluminum alloy subjected to biaxial tensile stresses. In the tests made, both variable and constant biaxial-stress ratios were investigated.

Material Tested

The material used was originally a fully heat-treated aluminum alloy, designated as 24S-T, and was fabricated in tubular extruded form. The extrusions had originally a 2-in. ID and a $^1/_8$-in. wall thickness. For this alloy, the nominal chemical composition, in addition to aluminum and normal impurities, consists of 4.4 per cent copper, 1.5 per cent magnesium, and 0.6 per cent manganese. The mechanical properties of 24S-T Alcoa, as furnished by the manufacturer, are tensile strength, 68,000 psi; yield strength (0.2 per cent offset), 44,000 psi; modulus of elasticity, 10.6×10^6 psi; per cent elongation (in 2 in.), 14 per cent; and Poisson's ratio, 0.33. After the specimens were machined they were annealed and reheat-treated in order to remove the directional properties present in the extruded tubes.

Tests of Thin-Walled Tubes Subjected to Internal Pressure and Axial Tension

Specimen. The specimens, Fig. 1, were machined from tubular stock 16 ft long, 2 in. ID, and $^1/_4$ in. wall thickness. The specimens had an intermediate length of 11 in. of reduced wall thickness of 0.100 ± 0.002 in. The internal surface was left in the extruded form. The wall-thickness values were measured for six positions around the periphery, and at five positions along the tube length, using an apparatus described elsewhere.[3] The ratio of the wall thickness to diameter of specimen was about 0.05, so that the biaxial stresses throughout the wall were essentially uniform. The diameter-length ratio was about 0.18, thereby providing a sufficiently long section of the specimen free from bending stresses produced by end restraints.

FIG. 1 TUBULAR SPECIMEN FOR COMBINED-STRESS TESTS

Testing Machine. The testing machine used for this investigation has been described in detail.[3] Fig. 2 illustrates the essential parts of the machine. A motor M applies a direct tensile load to a pulling rod R, which is attached to a lever beam B. The lever B transmits an axial load to the specimen S, through spherical seats SS. The spherical seats are used to insure axiality of loading. A hydraulic pressurizing oil was used to apply an internal pressure to the specimen by means of an injection pump unit P, as shown in Fig. 3. The rate of pressure application was controlled by the rheostat of a motor generator set MG, and by means of a release valve which discharged surplus oil

---

[1] Professor of Engineering Mechanics, Department of Engineering Mechanics, The Pennsylvania State College. Mem. ASME.

[2] Graduate Student, Department of Engineering Mechanics, The Pennsylvania State College.

Presented at the Annual Conference of the Applied Mechanics Division, Purdue University, Lafayette, Ind., June 22–24, 1950, of THE AMERICAN SOCIETY OF MECHANICAL ENGINEERS.

Discussion of this paper should be addressed to the Secretary, ASME, 29 West 39th Street, New York, N. Y., and will be accepted until January 10, 1951, for publication at a later date. Discussion received after the closing date will be returned.

NOTE: Statements and opinions advanced in papers are to be understood as individual expressions of their authors and not those of the Society. Manuscript received by the Applied Mechanics Division, September 16, 1949. Paper No. 50—APM-16.

[3] "Biaxial Plastic Stress-Strain Relations for 24S-T Aluminum Alloy," by J. Marin, J. H. Faupel, V. L. Dutton, and M. W. Brossman, Technical Note 1536, NACA, May, 1948, 96 pp.

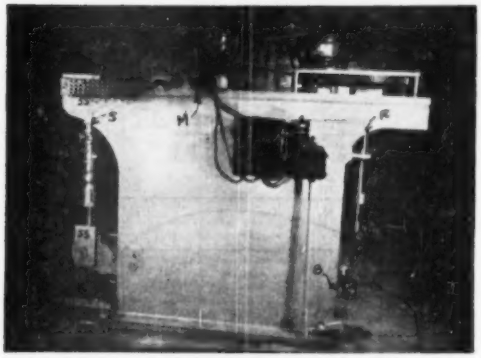

FIG. 2 COMBINED-STRESS TESTING MACHINE

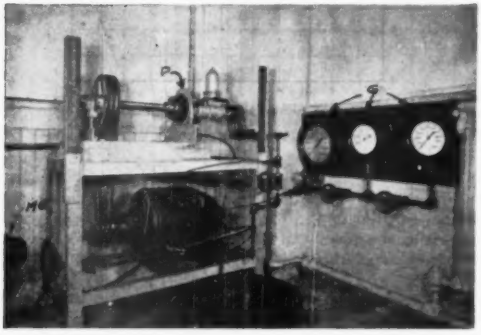

FIG. 3 INTERNAL PRESSURE UNIT FOR COMBINED-STRESS TESTS

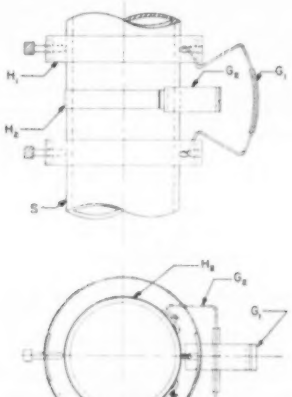

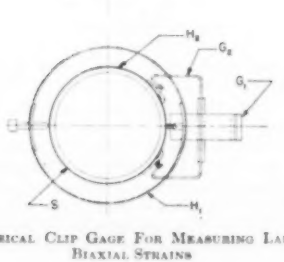

FIG. 4 ELECTRICAL CLIP GAGE FOR MEASURING LARGE PLASTIC BIAXIAL STRAINS

into the oil-supply reservoir. Three U. S. Bourdon gages, G, were used for measuring the oil pressure.

The pulling rod R was calibrated by placing in the testing machine a calibrated rod in place of the specimen. The pressure gages were also calibrated before they were used for this test program.

Method of Strain Measurement. The elastic strains were measured with two SR-4 electric strain gages of $^{12}/_{16}$-in. gage lengths. One gage measured the longitudinal strain, and the other measured the lateral strain for a region near the central part of the specimen. Specially designed clip-type gages were used to measure the plastic strains in both the longitudinal and lateral directions as illustrated in Fig. 4, and described in footnote 3. Clip gage G_1 measured the longitudinal plastic strains, and G_2 the lateral strains. It was necessary to use clip gages since the SR-4 electric strain gages used had a maximum range of about 0.015 in. per in., and the plastic strains greatly exceeded this value. The final strains at rupture were measured to 0.01 in. by means of dividers and a scale. The circumferential plastic strain measured represented an average value for the outer circumference of the tube, while the longitudinal plastic strain was measured over a 2-in. strain gage.

Method of Testing. In preparation for a test, the elastic SR-4 gages and calibrated clip gages are placed on a specimen. The specimen is then inserted in the testing machine and filled with oil in preparation for internal pressure application. Two types of tests were made; one in which the ratio of the internal pressure to the axial load was maintained essentially constant and the other in which this ratio was varied. The foregoing types of test will be designated later in this paper as the constant- and variable-stress-ratio tests.

For either type of test the specimen was loaded to predetermined values up to rupture. At the end of each load interval, the strains were measured in both the longitudinal and lateral directions.

Test Results—Tests With Constant-Stress Ratios. The relations between the true stress and strain for both the longitudinal and transverse principal stresses are shown in Fig. 5. Fig. 5 shows the true-stress-strain diagrams for tests in which the principal stress ratio was kept essentially constant.

The true stresses were determined, based upon the actual and not the original values of wall thickness and diameter, that is, for an axial load P and internal pressure p, the longitudinal and transverse stresses are, respectively

$$\sigma_1 = \frac{P}{\pi d_p t_p} + \frac{p d_p}{4 t_p} \quad \ldots\ldots [1]$$

$$\sigma_2 = \frac{p d_p}{2 t_p} \quad \ldots\ldots [2]$$

where d_p and t_p are the actual internal-diameter and wall-thickness values at the loads considered. The values of the dimensions d_p and t_p can be expressed in terms of the original values of the internal diameter and wall thickness and the measured nominal strains e_1 and e_2 in the longitudinal and lateral directions. The values of the wall thickness t_p and internal diameter d_p have been shown to be[4]

$$t_p = \frac{t}{1 + e_1 + e_2} \quad \ldots\ldots [3]$$

$$d_p = (d + 2t)(1 + e_2) - 2t_p \quad \ldots\ldots [4]$$

Placing the measured values of the original dimensions of the

[4] Appendix C, of reference (3).

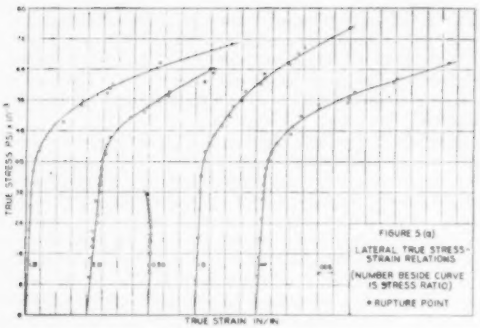
TRUE STRESS PS, psi x 10^-3
TRUE STRAIN IN/IN
FIGURE 5 (a)
LATERAL TRUE STRESS-STRAIN RELATIONS
(NUMBER BESIDE CURVE IS STRESS RATIO)
• RUPTURE POINT

FIG. 5(a)

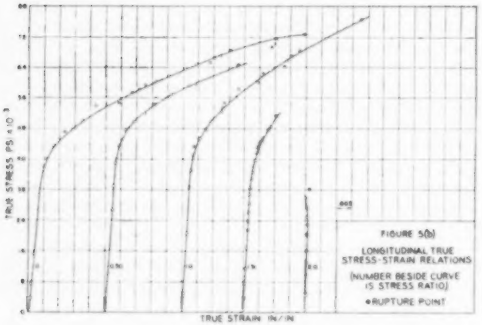

FIG. 5(b)

internal diameter d, wall thickness t, and the nominal strains e_1 and e_2 in Equations [3] and [4], the values of t_p and d_p can be determined. Then by Equations [1] and [2] the true stresses σ_1 and σ_2 are found. The true strains ϵ_1 and ϵ_2, corresponding to nominal strains e_1 and e_2 can be shown to be[8]

$$\epsilon_1 = \log_e (1 + e_1) \quad [5]$$

$$\epsilon_2 = \log_e (1 + e_2) \quad [6]$$

The true stresses as calculated by Equations [1] and [2], and the true strains as obtained by Equations [5] and [6], are plotted in Fig. 5.

For the elastic range or for small strains the stresses can be obtained by Equations [1] and [2] by replacing t_p by t and d_p by d. For the elastic range and small strains, the values of ϵ_1 and ϵ_2, as obtained by Equations [5] and [6], become equal to e_1 and e_2, respectively, and the measured nominal strains, therefore, can be plotted.

The "biaxial yield strengths" for various values of the biaxial stress ratios, as obtained from Fig. 5, are tabulated in Table 1. These strengths are determined based upon an equivalent offset strain.[9] A comparison of the biaxial yield strengths as

[9] "A New Method of Defining Failure in Members Subjected to Combined Stresses," by J. Marin, Trans. American Society of Metals, vol. 29, 1941, p. 1013; or "Mechanical Properties of Materials and Design," McGraw-Hill Book Company, Inc., New York, N. Y., 1942.

TABLE 1 YIELD STRESSES FOR CONSTANT BIAXIAL STRESS RATIOS

Biaxial stress ratio $\alpha = \sigma_2/\sigma_1$	Yield stress σ_{1y} (psi)	Yield stress σ_{2y} (psi)	Yield stress σ_{3y} (psi)	Stress ratios $x = \sigma_{1y}/\sigma_y$	Stress ratios $y = \sigma_{3y}/\sigma_y$
0 Longitudinal tension	41700	0	0	1.00	0
0.50	46900	24000	—2400	1.13	0.58
1.00	46250	44600	—4400	1.11	1.07
1.31	41900	44000	—4400	1.01	1.06
2.00	22200	44400	—4400	0.53	1.07

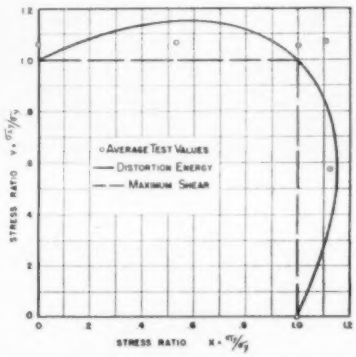

FIG. 6 COMPARISON OF YIELD STRENGTHS WITH THEORIES OF FAILURE

based on Table 1 with the stress, shear, and distortion-energy theories is given in Fig. 6. In Fig. 6, σ_y represents the yield stress in axial tension. An examination of Fig. 6 shows that the distortion-energy theory is in good agreement with the test results.

The "biaxial nominal ultimate strength" based on the original cross section, and the "true fracture strengths," based upon the dimensions at fracture, are given in Tables 2 and 3 for various biaxial-stress ratios. Figs. 7 and 8 give a comparison of these strength values with the maximum-shear or stress theories and shows that there is reasonably good agreement between test results and theory. In Fig. 7, σ_u represents the nominal ultimate stress, and in Fig. 8, σ_r is the true fracture stress. Average test values indicated in Figs. 6, 7, and 8, represent average of three tests.

The "plastic stress-strain relations" are compared with the deformation theory in Fig. 9. Fig. 9 shows the relation[9] between the significant stress $\bar{\sigma}$ and the significant strain ϵ where

$$\bar{\sigma} = \sqrt{\tfrac{1}{2}[(\sigma_1 - \sigma_2)^2 + (\sigma_2 - \sigma_3)^2 + (\sigma_3 - \sigma_1)^2]} \quad [7]$$

and

$$\epsilon = \sqrt{\tfrac{2}{3}(\epsilon_1^2 + \epsilon_2^2 + \epsilon_3^2)} \quad [8]$$

where σ_1, σ_3, and σ_2 are the true longitudinal, lateral, and radial stresses, respectively; and ϵ_1, ϵ_3, and ϵ_2 are the true longitudinal, lateral, and radial strains, respectively. In Fig. 9 a plot of the significant stress and strain for each stress ratio is given. Fig. 10 gives the significant stress-strain plots for all the constant-stress-ratio tests, using the same origin for all tests. If the deformation theory is correct all the foregoing stress plots should coincide with the uniaxial true stress-strain relation. From an engineering point of view, the agreement between the stress-strain relations shows that the deformation theory can be

TABLE 2 NOMINAL ULTIMATE STRESSES FOR CONSTANT STRESS RATIOS

Biaxial stress ratio $\alpha = \sigma_2/\sigma_1$	Nominal ultimate stress σ_{1u} (psi)	Nominal ultimate stress σ_{2u} (psi)	Stress ratios $x = \sigma_{1u}/\sigma_{1u}$	Stress ratios $y = \sigma_{2u}/\sigma_{1u}$
0	66900	0	1.00	0
Longitudinal tension				
0.50	62150	30000	0.93	0.45
1.00	64900	63000	0.97	0.94
1.31	46400	60000	0.69	0.90
2.00	29500	59000	0.44	0.88

TABLE 3 TRUE FRACTURE STRESSES FOR CONSTANT-STRESS RATIOS

Biaxial stress ratio $\alpha = \sigma_2/\sigma_1$	True fracture stress σ_{1f} (psi)	True fracture stress σ_{2f} (psi)	Stress ratios $x = \sigma_{1f}/\sigma_{1f}$	Stress ratios $y = \sigma_{2f}/\sigma_{1f}$
0	72890	0	1.00	0
Longitudinal tension				
0.50	64640	31320	0.89	0.43
1.00	72610	74940	1.00	1.03
1.31	51170	70620	0.70	0.97
2.00	31970	63940	0.44	0.88

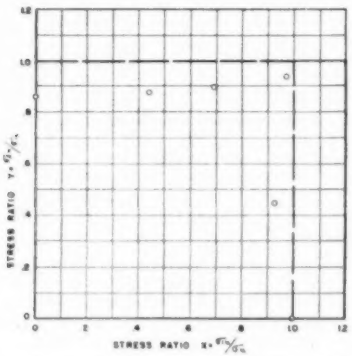

FIG. 7 COMPARISON OF NOMINAL BIAXIAL ULTIMATE STRENGTHS WITH MAXIMUM-STRESS THEORY

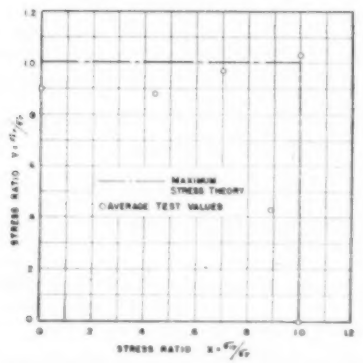

FIG. 8 COMPARISON OF TRUE BIAXIAL FRACTURE STRESSES WITH MAXIMUM-STRESS THEORY

considered to give a fair approximation for the plastic stress-strain relations under combined stresses.

"Ductility" values under biaxial stresses can be determined

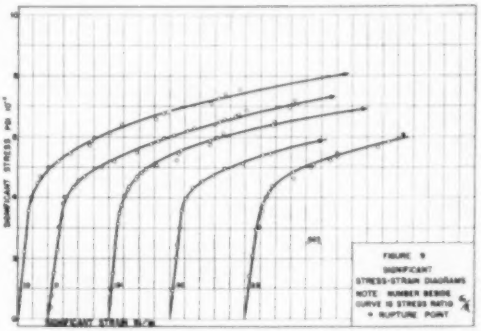

FIG. 9

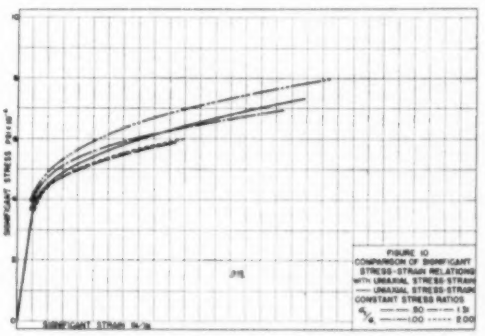

FIG. 10

TABLE 4 NOMINAL AND TRUE DUCTILITIES FOR CONSTANT BIAXIAL STRESS RATIOS

Biaxial stress ratio	Nominal ductility in./in.	True ductility in./in.
0	0.086	0.083
Longitudinal tension		
0.50	0.039	0.038
1.00	0.055	0.054
1.31	0.065	0.063
2.00	0.035	0.034

theoretically based on the deformation theory and the stress theory.[3] Table 4 lists the values of the measured nominal and true ductilities for the various biaxial stress ratios considered. These values correspond to the maximum principal strains at fracture. Table 4 shows that the experimental values of the ductilities do not agree with the theoretical values. The discrepancy may be due to the presence of a nonuniform state of stress at the necked-down section of the specimens prior to fracture, the recording of an average strain for a 2-in. gage length (other than a local strain), or the inadequacy of the theory used for obtaining the theoretical strain values.

Test Results—Tests With Variable-Stress Ratios. The true stress-strain relations for the variable-stress-ratio tests are shown in Fig. 11. In these tests the internal pressure was first applied to a preselected magnitude. Axial load was then applied to the specimen to fracture, while the internal pressure was kept constant.

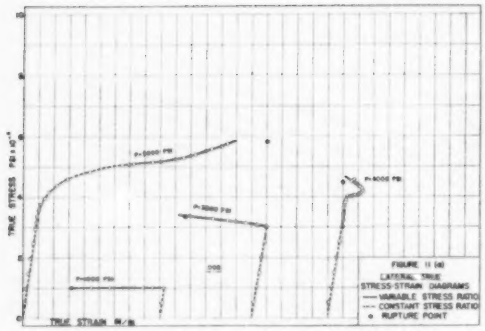

FIG. 11(a)

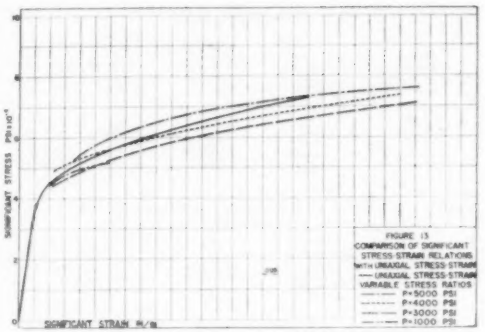

FIG. 13

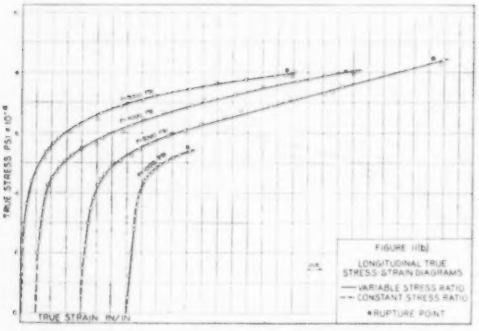

FIG. 11(b)

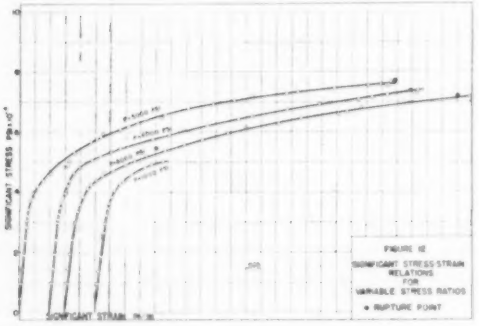

FIG. 12

Fig. 12 shows the relation between the significant stress and significant strains for the various tests as obtained, based upon Equations [7] and [8]. A comparison of the significant stress-strain relations in Fig. 12, with the simple tension true stress-strain values is shown in Fig. 13. The agreement between the stress-strain relations in Fig. 13 shows that from an engineering point of view, the deformation theory is a good approximation, that is, true stresses and strains with variable biaxial tensile-stress ratios can be predicted by the deformation theory.

The constants k and n used to obtain the theoretical values of

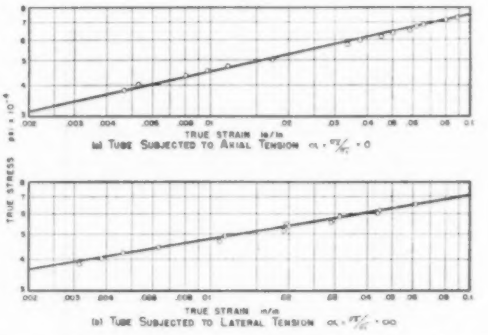

FIG. 14 TRUE STRESS-STRAIN RELATIONS FOR TENSION TESTS

the ductility[3] were calculated based on the log-log plots in Fig. 14, that is, the true stress-strain relations in Fig. 14 are defined by $\sigma = k\delta^n$ where σ = the true stress, and δ = the true strain.

CONCLUSIONS

For the annealed and reheat-treated 24S-T aluminum-alloy tubing tested, and for biaxial tensile stresses, it was found that:

1 The biaxial yield strengths can be approximately predicted by the distortion-energy theory.

2 The nominal ultimate and true fracture biaxial strengths are in approximate agreement with the maximum-shear or stress theories.

3 The values of the biaxial nominal and true ductilities are less than the values for simple tension and do not agree with values predicted by the deformation theory.

4 For both the constant and variable biaxial stress-ratio tests, and for engineering purposes, the plastic stress-strain relations can be predicted approximately by the deformation theory.

ACKNOWLEDGMENTS

The testing machine used for this investigation was designed and built under the sponsorship and financial assistance of the National Advisory Committee for Aeronautics. The data presented represents a part of a master's thesis prepared by B. F. Kotalik under the direction of Joseph Marin. The authors wish to express their thanks to V. L. Dutton, research assistant, for help in conducting the tests, and to Homer Johnson for preparing the specimens.

Beam Vibrations With Time-Dependent Boundary Conditions

By R. D. MINDLIN[1] and L. E. GOODMAN,[2] NEW YORK, N. Y.

A procedure is described for extending the method of separation of variables to the solution of beam-vibration problems with time-dependent boundary conditions. The procedure is applicable to a wide variety of time-dependent boundary-value problems in systems governed by linear partial differential equations.

Introduction

IT happens frequently that vibration problems have to deal with continuous systems of which one or more boundaries are constrained to undergo displacements or tractions which vary with time. Simple examples include a cantilevered beam whose clamped end experiences a lateral-displacement pulse, a rod subjected at its ends to varying longitudinal pressure, or a plate whose edge is twisted by an oscillating edge moment. In other cases the time-dependence of the boundary condition is itself the object of investigation as when one structural element interacts with another, or when we wish to infer the state of strain at one end of a structure from continuous measurements made at another end. All of these problems are characterized by the fact that the boundary conditions are not "stationary" and on this account, solutions are not, in general, obtainable by the classical method of separation of variables, although solutions do appear in the literature for a number of special problems of this type.[3]

The present paper includes these solutions as special cases. In it is developed a general method by means of which the time-dependence is removed from the boundary conditions. The remaining problem then can be solved by any one of the classical or numerical methods available for handling the free- or forced-vibration problem. The method is here developed for and applied to the problem of the flexural vibrations of beams. It is equally applicable to time-dependent boundary-value problems in the flexural vibrations of plates, the torsional vibrations of shafts and, in fact, in a wide variety of systems governed by linear partial differential equations.

Problems of this type have been solved by the method of Laplace transform, but the present method employs more elementary mathematical techniques and is applicable in certain cases where the transforms do not exist or their inverses are not known.

Statement of Problem

Consider a structure whose displacement is governed by the equation

$$a^2 \frac{\partial^4 w}{\partial x^4} + \frac{\partial^2 w}{\partial t^2} = \frac{q(x)p(t)}{\rho A} \qquad [1]$$

This is the case if the structure is a prismatic beam executing flexural vibrations according to the simple Bernoulli-Euler or classical theory of flexure. Then the symbols have the meanings

- w = deflection of beam
- x = position along beam; $x = 0$ is one end of beam, $x = l$ is the other end
- ρ = density
- A = cross-sectional area of beam
- a^2 = $EI/\rho A$, where E and I are Young's modulus and the second moment of area of the cross section of the beam, respectively
- $q(x)p(t)$ = external load per unit length of beam. If the load does not vary with time, $p(t) = 1$

The method to be described applies equally well if the rotatory inertia, shear, damping, and elastic foundation terms are included in the differential equation, but they are omitted for simplicity.

In the following development, the symbol D_i is used to represent a linear differential operator of order 0, 1, 2, or 3, as the boundary conditions of the problem dictate, that is, $D_i[w]$ stands for w, or $\partial w/\partial x$, or $\partial^2 w/\partial x^2$, or $\partial^3 w/\partial x^3$, or a linear combination of these operations. With this notation the boundary conditions can be written

$$\left.\begin{aligned} D_i[w(0,t)] &= f_i(t), \quad i = 1,2 \\ D_i[w(l,t)] &= f_i(t), \quad i = 3,4 \end{aligned}\right\} \qquad [2]$$

For example, if the beam in question is a cantilever clamped at $x = 0$

$$D_1 = 1,\ D_2 = \partial/\partial x,\ D_3 = \partial^2/\partial x^2,\ D_4 = \partial^3/\partial x^3$$

while the displacement and slope at $x = 0$, and the moment and shear at $x = l$ may be required to vary with time according to $f_i(t)$. Linear combinations of the operators occur, for example, when the end of the beam is spring-restrained against displacement or rotation.

The initial conditions of the motion are specified by two arbitrary functions

$$\left.\begin{aligned} w(x,0) &= w_0(x) \\ \left.\frac{\partial w}{\partial t}\right]_{t=0} &= \dot{w}_0(x) \end{aligned}\right\} \qquad [3]$$

A difficulty in solving problems of this type by the method of separation of variables arises when not all of the functions $f_i(t)$ vanish. The method of separation of variables breaks down when applied directly because it is not possible to satisfy Equations [2] by adjustment of the x-dependent function.

Method of Solution

The foregoing difficulty may be resolved by separating the solution into two parts, one of which is later adjusted so as to simplify the boundary conditions on the other. We take

---

[1] Professor of Civil Engineering, Columbia University, and Consultant, Bell Telephone Laboratories, Inc., Murray Hill, N. J. Mem. ASME.

[2] Instructor in Civil Engineering, Columbia University.

[3] See references (1) to (4). Numbers in parentheses refer to the Bibliography at the end of the paper.

Contributed by the Applied Mechanics Division and presented at the Annual Meeting, New York, N. Y., November 27–December 2, 1949, of The American Society of Mechanical Engineers.

Discussion of this paper should be addressed to the Secretary, ASME, 29 West 39th Street, New York, N. Y., and will be accepted until January 10, 1951, for publication at a later date. Discussion received after the closing date will be returned.

Note: Statements and opinions advanced in papers are to be understood as individual expressions of their authors and not those of the Society. Manuscript received by the Applied Mechanics Division July 18, 1949. Paper No. 49—A-19.

$$w = \zeta(x, t) + \sum_{i=1}^{4} f_i(t) g_i(x) \quad [4]$$

Substituting Equation [4] into Equation [1] we find that ζ must satisfy the differential equation

$$a^2 \frac{\partial^4 \zeta}{\partial x^4} + \frac{\partial^2 \zeta}{\partial t^2} = \frac{q(x)p(t)}{\rho A} - \sum_{i=1}^{4} (a^2 f_i g_i^{IV} + \ddot{f}_i g_i) \quad [5]$$

where Roman superscripts indicate differentiations with respect to x, and dots indicate differentiations with respect to time.

In addition, the assumed expression for w, Equation [4], must satisfy the boundary conditions, Equations [2]. Hence

$$\left.\begin{aligned} D_i[\zeta(0, t)] &= f_i(t) - \sum_{j=1}^{4} D_i[g_j(0)] f_j(t), \quad i = 1,2 \\ D_i[\zeta(l, t)] &= f_i(t) - \sum_{j=1}^{4} D_i[g_j(l)] f_j(t), \quad i = 3,4 \end{aligned}\right\} \quad [6]$$

Finally, the initial conditions, Equations [3], become

$$\left.\begin{aligned} \zeta(x, 0) &= w_0 - \sum_{i=1}^{4} f_i(0) g_i(x) \\ \left.\frac{\partial \zeta}{\partial t}\right]_{t=0} &= \dot{w}_0 - \sum_{i=1}^{4} \dot{f}_i(0) g_i(x) \end{aligned}\right\} \quad [7]$$

The functions $g_i(x)$ are now chosen so as to reduce to zero the right-hand sides of Equations [6]. To assure this, it is sufficient to satisfy the 16 conditions

$$\left.\begin{aligned} D_1[g_1(0)] &= 1 & D_1[g_2(0)] &= 0 \\ D_2[g_1(0)] &= 0 & D_2[g_2(0)] &= 1 \\ D_3[g_1(l)] &= 0 & D_3[g_2(l)] &= 0 \\ D_4[g_1(l)] &= 0 & D_4[g_2(l)] &= 0 \\ D_1[g_3(0)] &= 0 & D_1[g_4(0)] &= 0 \\ D_2[g_3(0)] &= 0 & D_2[g_4(0)] &= 0 \\ D_3[g_3(l)] &= 1 & D_3[g_4(l)] &= 0 \\ D_4[g_3(l)] &= 0 & D_4[g_4(l)] &= 1 \end{aligned}\right\} \quad [8]$$

or, in more abbreviated notation

$$\left.\begin{aligned} D_j[g_i(0)] &= \delta_{ij}, \quad j = 1,2, \quad i = 1,2,3,4 \\ D_j[g_i(l)] &= \delta_{ij}, \quad j = 3,4, \quad i = 1,2,3,4 \end{aligned}\right\} \quad [9]$$

where $\delta_{ij} = 0$ for $i \neq j$ and $\delta_{ij} = 1$ for $i = j$. Each column of Equations [8] provides four conditions on one of the four functions g_i. In order to be certain of being able to satisfy these conditions in all cases the g_i are taken to be polynomials of the fifth degree in x

$$g_i = a_i + b_i x + c_i x^2 + d_i x^3 + e_i x^4 + f_i x^5, \; i = 1,2,3,4 \quad [10]$$

choosing the coefficients according to the following rule:

"Substitute each of the g_i in the appropriate (ith) column of Equations [8]. In each case, there will result a set of four linear algebraic equations governing the coefficients of the particular function g_i. If more than four of the constants $a_i \ldots f_i$ appear in these expressions, reduce to four the number which do appear by setting equal to zero the coefficient of the term of highest degree in x and also, if necessary, the coefficient of the term of second highest degree. If any of the constants $a_i \ldots f_i$ does not appear, set it equal to zero." In this way the four conditions on the coefficients of each of the g_i will always be expressed by means of four linear, independent, algebraic equations in four unknowns. These equations determine the constants of Equations [10] so as to satisfy Equations [8]. With this choice of the functions g_i, the boundary conditions expressed by Equations [6] become those of a "stationary" problem

$$\left.\begin{aligned} D_i[\zeta(0, t)] &= 0 \quad i = 1,2 \\ D_i[\zeta(l, t)] &= 0 \quad i = 3,4 \end{aligned}\right\} \quad [11]$$

Usually only a third-degree polynomial is required for the functions g_i. The additional terms are included to accommodate exceptional cases as, for example, when time-dependent moment and shear are prescribed at both ends of the beam. It should be noticed, also, that it is necessary only to compute those of the g_i for which the corresponding $f_i(t)$ do not vanish.

It remains to find the function $\zeta(x, t)$ satisfying the differential equation, Equation [5], the boundary conditions, Equations [11], and the initial conditions, Equations [7]. This can be done in the classical manner. We seek a solution in the form

$$\zeta = \sum_{n=1}^{\infty} X_n T_n \quad [12]$$

where

$$X_n = X_n(x), \quad T_n = T_n(t)$$

and assume that the functions X_n will be orthogonal[4] with respect to the interval $0,l$ so that $q(x)$, $g_i(x)$ and $g_i^{IV}(x)$ can be expanded in series of functions X_n by means of the expansion formulas

$$\left.\begin{aligned} q(x) &= \sum_{n=1}^{\infty} Q_n X_n \\ g_i(x) &= \sum_{n=1}^{\infty} G_{in} X_n \\ g_i^{IV}(x) &= \sum_{n=1}^{\infty} G_{in}^* X_n \end{aligned}\right\} \quad [13]$$

where the constants Q_n, G_{in}, and G_{in}^* are given by the expressions

$$\left.\begin{aligned} Q_n &= \frac{\int_0^l q(x) X_n dx}{\int_0^l X_n^2 dx} \\ G_{in} &= \frac{\int_0^l g_i(x) X_n dx}{\int_0^l X_n^2 dx}, \quad i = 1, 2, 3, 4 \\ G_{in}^* &= \frac{\int_0^l g_i^{IV}(x) X_n dx}{\int_0^l X_n^2 dx}, \quad i = 1, 2, 3, 4 \end{aligned}\right\} \quad [14]$$

After substituting Equations [12] and [13] in Equation [5] and separating variables, the equations governing X_n and T_n are readily solved

$$X_n = C_n \cos \frac{m_n x}{l} + D_n \sin \frac{m_n x}{l} + E_n \cosh \frac{m_n x}{l} + F_n \sinh \frac{m_n x}{l} \quad [15]$$

$$T_n = A_n \cos \omega_n t + B_n \sin \omega_n t + \frac{1}{\omega_n} \int_0^t P_n(\tau) \sin \omega_n (t - \tau) d\tau \quad [16]$$

[4] The conditions under which the functions X_n are orthogonal with respect to the interval $0,l$ are well known (5). It is sufficient to note that this is the case if the ends of the beam are fixed or free or simply supported or restrained against translation or rotation by linear springs. These include all the types of end conditions which can arise from Equation [11]. In a private communication, Dr. R. W. Hamming has shown how to extend the method to nonorthogonal functions by introducing the adjoint equation.

where

$$P_n(\tau) = Q_n \frac{p(\tau)}{\rho A} - \sum_{i=1}^{4} [G_{in} \ddot{f}_i(\tau) + a^2 G_{in}{}^* f_i(\tau)], \quad m_n{}^2 = \frac{\omega_n l^2}{a}$$

Equations [15], [16], and [12] determine the form of ζ. The constants of integration C_n, D_n, E_n, and F_n are adjusted to satisfy the simple boundary conditions, Equations [11], which also determine the transcendental equation governing m_n and hence the natural frequencies ω_n. This part of the solution is identical with the free-vibration case. The initial conditions given in Equations [7] serve to determine the constants of integration A_n and B_n. Since

$$\zeta(x, 0) = \sum_{n=1}^{\infty} A_n X_n$$

$$\left.\frac{\partial \zeta}{\partial t}\right]_{t=0} = \sum_{n=1}^{\infty} B_n X_n \omega_n$$

we must have

$$\left.\begin{aligned} A_n &= \frac{\int_0^l \left[w_0 - \sum_{i=1}^{4} f_i(0) g_i(x)\right] X_n dx}{\int_0^l X_n{}^2 dx} \\ B_n &= \frac{\int_0^l \left[\dot{w}_0 - \sum_{i=1}^{4} \dot{f}_i(0) g_i(x)\right] X_n dx}{\omega_n \int_0^l X_n{}^2 dx} \end{aligned}\right\} \quad \ldots\ldots [17]$$

This completes the formal solution of the problem.

Applications of the Method

Example 1. As a first illustration, consider the vibrations which arise when the "free" end of a cantilever beam is actuated by a cam. Taking the fixed end of the beam at $x = l$, the boundary conditions are

$$w(0, t) = f_1(t), \quad \left.\frac{\partial^2 w}{\partial x^2}\right]_{x=0} = \left.\frac{\partial w}{\partial x}\right]_{x=l} = w(l, t) = 0$$

where $f_1(t)$ is the transverse displacement enforced by the cam. For convenience take $w_0 = \dot{w}_0 = 0$. Applying the rule of the previous section we have

$$g_1 = 1 - \frac{3x}{2l} + \frac{x^3}{2l^3} \quad \ldots\ldots [18]$$

Application of the boundary conditions to Equation [15] yields

$$X_n = \sinh m_n \sin \frac{m_n x}{l} - \sin m_n \sinh \frac{m_n x}{l} \quad \ldots\ldots [19]$$

where

$$\tan m_n = \tanh m_n$$

From Equation [14]

$$G_{1n} = 2/[m_n(\sinh m_n - \sin m_n)]$$

and from Equations [17]

$$A_n = -f_1(0) G_{1n}$$

$$B_n = -\dot{f}_1(0) G_{1n}/\omega_n$$

so that a general solution of this problem is

$$w = f_1(t)\left(1 - \frac{3x}{2l} + \frac{x^3}{2l^3}\right) - \sum_{n=1}^{\infty} \frac{2X_n}{m_n(\sinh m_n - \sin m_n)} \left[f_1(t) - \omega_n \int_0^t f_1(\tau) \sin \omega_n(t - \tau)\, d\tau\right] \quad \ldots\ldots [20]$$

Special cases of this general solution may be obtained by substituting the corresponding values of f_1 in Equation [20] (6).

Example 2. The clamped end of a cantilever beam undergoes a damped sine-wave displacement transient, starting from rest. As before, we take the clamped end of the beam at $x = l$; then we are given

$$D_1 = \frac{\partial^2}{\partial x^2}, \quad D_2 = \frac{\partial^3}{\partial x^3}, \quad D_3 = 1, \quad D_4 = \frac{\partial}{\partial x}$$

$$f_1 = f_2 = f_4 = 0, \quad f_3 = Ae^{-\beta t} \sin \omega_f t$$

From Equations [15] and [16]

$$X_n = \left(\sin \frac{m_n x}{l} + \sinh \frac{m_n x}{l}\right)(\cos m_n + \cosh m_n) - \left(\cos \frac{m_n x}{l} + \cosh \frac{m_n x}{l}\right)(\sin m_n + \sinh m_n)$$

$$\cos m_n \cosh m_n = -1$$

$$g_3 = 1$$

$$G_{3n} = [(\coth m_n - \cot m_n) m_n]^{-1}$$

$$A_n = 0$$

$$B_n = -AG_{3n} \frac{\omega_f}{\omega_n}$$

$$T_n = -A \frac{\omega_f}{\omega_n} G_{3n} \sin \omega_n t - \frac{1}{\omega_n} G_{3n} \int_0^t \ddot{f}_3(\tau) \sin \omega_n(t - \tau)\, d\tau$$

and a complete solution is

$$w = Ae^{-\beta t} \sin \omega_f t + \sum_{n=1}^{\infty} \frac{AX_n}{m_n(\coth m_n - \cot m_n)} [\omega_f L \sin(\omega_n t - \varphi_1) + \omega_n L e^{-\beta t} \sin(\omega_f t + \varphi_2) - e^{-\beta t} \sin \omega_f t] \quad \ldots\ldots [21]$$

$$L = \omega_n \{[\beta^2 + (\omega_f + \omega_n)^2][\beta^2 + (\omega_f - \omega_n)^2]\}^{-1/2}$$

$$\varphi_1 = \tan^{-1} 2\beta\omega_n/(\beta^2 + \omega_f{}^2 - \omega_n{}^2)$$

$$\varphi_2 = \tan^{-1} 2\beta\omega_f/(\beta^2 + \omega_n{}^2 - \omega_f{}^2)$$

A Special Case

When the time-dependent functions in the boundary conditions are simple circular or hyperbolic or exponential functions, it is sometimes advantageous to choose the $g_i(x)$ in other than polynomial forms. Although these cases can be handled by the general method described in the preceding sections, the solution may be put in a form more suitable for computation by means of the following device:

If, for example, the $f_i(t)$ are simple trigonometric functions, then

$$\ddot{f}_i(t) = -k^2 f_i(t)$$

If we choose

$$\varphi_i(x) = a_i \sin \sqrt{\frac{k}{a}}\, x + b_i \cos \sqrt{\frac{k}{a}}\, x + c_i \cosh \sqrt{\frac{k}{a}}\, x + d_i \sinh \sqrt{\frac{k}{a}}\, x \quad \ldots\ldots [22]$$

then the right-hand side of Equation [5] will reduce to zero (except for the distributed-load term, if any), and at the same time the constants $a_i \ldots . d_i$ of Equations [22] may be adjusted so as to satisfy the 16 conditions given in Equations [8]. Having removed the time-dependence in this manner, the solution proceeds exactly as before except that the summations with respect to i do not appear in Equation [16].

This variant of the general method takes advantage of a special form of the time-dependence of the boundary conditions, and therefore cannot be used in general. Where it can be employed, it serves to remove from the summation sign the forced part of the solution. This part of the solution is expressed in closed form.

Example 3. As a simple example of the special method, consider a simply supported beam, initially at rest, one of whose ends $x = l$, is subjected to an oscillating bending moment of amplitude M and frequency ω_f. In this case the given quantities are

$$D_1 = 1, \; D_2 = \frac{\partial^2}{\partial x^2}, \; D_3 = 1, \; D_4 = EI \frac{\partial^2}{\partial x^2}$$

$$f_1 = f_2 = f_3 = 0, \; f_4 = -M \sin \omega_f t$$

$$w_0 = \dot{w}_0 = 0$$

The constants of Equation [22] are to be adjusted so as to satisfy the conditions expressed by Equations [8]. When this is done

$$M\varphi_4(x) = \frac{M}{EI} \frac{a}{2\omega_f} \left[\sinh \sqrt{\frac{\omega_f}{a}}\, x \operatorname{cosech} \sqrt{\frac{\omega_f}{a}}\, l - \sin \sqrt{\frac{\omega_f}{a}}\, x \operatorname{cosec} \sqrt{\frac{\omega_f}{a}}\, l \right] \quad \ldots\ldots [23]$$

Equation [23] gives directly, in closed form, the amplitude of the steady state or forced vibration. It remains to complete the solution by writing out the transient. From Equation [15], together with the boundary conditions of Equations [11]

$$X_n = \sin \frac{n\pi x}{l}, \quad \omega_n = \frac{n^2\pi^2 a}{l^2}$$

From Equations [16] and [17]

$$A_n = 0$$

$$B_n = \frac{M}{EI} \frac{2\omega_f a}{n\pi} \frac{(-1)^n}{\omega_n^2 - \omega_f^2}$$

$$T_n = B_n \sin \omega_n t$$

The complete solution of the problem is therefore

$$w = -\frac{M}{EI} \frac{a}{2\omega_f} \left[\sinh \sqrt{\frac{\omega_f}{a}}\, x \operatorname{cosech} \sqrt{\frac{\omega_f}{a}}\, l - \sin \sqrt{\frac{\omega_f}{a}}\, x \operatorname{cosec} \sqrt{\frac{\omega_f}{a}}\, l \right] \sin \omega_f t + \frac{M}{EI} \frac{a}{2\omega_f} \frac{4}{\pi} \sum_{n=1}^{\infty} \frac{(-1)^n}{n \left(\frac{\omega_n^2}{\omega_f^2} - 1 \right)} \sin \frac{n\pi x}{l} \sin \frac{n^2\pi^2 a t}{l^2} \quad \ldots\ldots [24]$$

BIBLIOGRAPHY

1 "Sur les vibrations d'un système quelconque de points matériels," by J. M. C. Duhamel, *Journal de l'École Polytechnique*, Cah. 23, Paris, France, 1834, pp. 1–36.

2 "Solution de divers problèmes de Mécanique, etc.," by E. Phillips, *Journal de Math.*, Paris, France, vol. 9, 1864, pp. 25–83.

3 "L'Élasticité des Corps Solides," by A. Clebsch, with notes by B. de Saint Venant, Paris, France, 1883, pp. 538–547.

4 "History of the Theory of Elasticity," by I. Todhunter and K. Pearson, Cambridge, England, 1886, vol. 1, p. 486; vol. 2, part 1, pp. 240–241, 470–472.

5 "Theory of Sound," by Lord Rayleigh, The Macmillan Company, London, England, second edition, vol. 1, 1894, p. 262.

6 "Vibration of a Cantilever Beam With Prescribed End Motion," by G. A. Nothmann, Trans. ASME, vol. 70, 1948, p. 327.

Temperature Distribution in a Steady, Laminar, Preheated Air Jet

By CHIA-SHUN YIH,[1] VANCOUVER, B. C., CANADA

This paper contains an exact closed solution for the temperature distribution in a preheated air jet when the flow is steady and laminar. Both the two-dimensional and the axially symmetrical cases have been treated. The solution is immediately applicable to other similar problems of diffusion.

Introduction

THE velocity distribution in a steady laminar air jet issuing from either a slit or a small hole in a plane wall was obtained in 1933 by Schlichting[2] who used the boundary-layer equations as the equations of motion. In 1937 Bickley[3] gave a closed solution for the axial-symmetry case. In the present paper the air issuing from the opening is supposed to have a temperature difference from the air surrounding the jet, and the resulting temperature distribution is sought. If the additional velocity induced by the nonuniformity of temperature distribution is small as compared with the velocity obtained for isothermal jets, it can be neglected and the velocity distribution can be assumed to be practically the same as obtained by Schlichting and Bickley. Under this assumption, the equation for temperature distribution can be solved easily.

It should be noted that the solution is directly applicable not only to precooled air jets but also to problems where some property other than heat is undergoing diffusion. For instance, if oxygen is being discharged through a small slit or a small hole into an open space filled with nitrogen, the concentration of oxygen at different points in the jet can be obtained directly from the corresponding solution by making the necessary changes of physical constants.

It may be remarked that although the true line or point source cannot be realized, the solutions are still valid at a distance sufficiently large as compared with the dimension of the opening.

Two-Dimensional Case

In a plane perpendicular to the slit, the trace of the slit is taken as the origin, the center line of the air jet the x-axis, and the trace of the wall as the y-axis. The velocities in the x- and y-directions are, respectively, denoted by u and v. Using ψ for the stream function, ν for the kinematic viscosity, ρ for the density, and $M = \int_{-\infty}^{\infty} \rho u^2 dy$ for the momentum flux per unit length of the slit, the Schlichting-Bickley solution of the system (with proper boundary conditions)

$$\left.\begin{aligned} u\frac{\partial u}{\partial x} + v\frac{\partial u}{\partial y} &= \nu\frac{\partial^2 u}{\partial y^2} \\ u = \frac{\partial \psi}{\partial y}, \quad v &= -\frac{\partial \psi}{\partial x} \end{aligned}\right\} \qquad [1]$$

gives

$$u = \left(\frac{3M^2}{32\rho^2\nu x}\right)^{1/3} \operatorname{sech}^2 \xi \qquad [2]$$

$$v = \left(\frac{M\nu}{6\rho x^2}\right)^{1/3} (2\xi \operatorname{sech}^2\xi - \tanh \xi) \qquad [3]$$

where

$$\xi = \left(\frac{M}{48\rho\nu^2}\right)^{1/3} \frac{y}{x^{2/3}}$$

Denoting by T_0 the original temperature of the free space into which the heated air jet is discharged, by T the temperature at any point of the free space, and by θ the quantity $(T - T_0)/T_0$, the equation for temperature distribution can be written

$$u\frac{\partial \theta}{\partial x} + v\frac{\partial \theta}{\partial y} = \alpha\left(\frac{\partial^2 \theta}{\partial x^2} + \frac{\partial^2 \theta}{\partial y^2}\right) \qquad [4]$$

where $\alpha = k/(\rho c_v)$ is the thermometric conductivity, k being the thermal conductivity and c_v the specific heat at constant volume. Assuming, as in the case of velocity, that $\partial^2\theta/\partial x^2$ is uniformly small as compared with $\partial^2\theta/\partial y^2$ (the assumption being justifiable a posteriori) Equation [4] can be written

$$u\frac{\partial \theta}{\partial x} + v\frac{\partial \theta}{\partial y} = \alpha\frac{\partial^2 \theta}{\partial y^2} \qquad [5]$$

The flux of temperature difference per unit length of the slit with T_0 as the datum temperature, is defined to be

$$H = \int_{-\infty}^{\infty} u(T - T_0)dy = T_0\int_{-\infty}^{\infty} u\theta dy \qquad [6]$$

which, in view of the steadiness of motion, must be independent of x. A dimensional analysis shows that θ must be a function of the three dimensionless quantities $H/(T_0\nu)$, $(\rho\nu^2)/(Mx)$, and ξ. In order that the right side of Equation [6] can be reduced to H, it is readily seen that θ must be of the following functional form

$$\theta = \left(\frac{H}{T_0\nu}\right)\left(\frac{\rho\nu^2}{Mx}\right)^{1/3} t(\xi) \qquad [7]$$

where the function $t(\xi)$ is to be determined from Equation [5].

Substitution of Equations [2], [3], and [7] in [5] gives, after simplification

$$-2\sigma[t(\xi)\operatorname{sech}^2\xi + t'(\xi)\tanh\xi] = t''(\xi) \qquad [8]$$

where $\sigma = \nu/\alpha$ is the Prandtl number. As $t'(0) = 0$, integration of Equation [8] gives

[1] Department of Mathematics, University of British Columbia.

[2] "Laminare Strahlensbreitung," by H. Schlichting, *Zeitschrift der Angewandte Mathematik und Mechanik*, vol. 13, 1933, pp. 260–263.

[3] "The Plane Jet," by W. G. Bickley, *Philosophical Magazine*, series 7, vol. 23, 1937, pp. 727–731. The foregoing papers are available in condensed form in S. Goldstein's "Modern Developments in Fluid Dynamics," Great Britain Aeronautical Research Committee, Oxford, England, vol. 1, 1938, pp. 145–148.

Presented at the National Conference of the Applied Mechanics Division, Purdue University, Lafayette, Ind., June 22–24, 1950, of The American Society of Mechanical Engineers.

Discussion of this paper should be addressed to the Secretary, ASME, 29 West 39th Street, New York, N. Y., and will be accepted until January 10, 1951, for publication at a later date. Discussion received after the closing date will be returned.

Note: Statements and opinions advanced in papers are to be understood as individual expressions of their authors and not those of the Society. Manuscript received by the Applied Mechanics Division July 25, 1949. Paper No. 50—APM-5.

$$f'(\xi) = -2\sigma f(\xi) \tanh \xi$$

A second integration then yields

$$f(\xi) = C \operatorname{sech}^{2\sigma}\xi \quad [9]$$

where C is to be determined from Equation [6]. Substitution of Equations [9] and [7] in [6] gives

$$C = \frac{1}{(36)^{1/3}\int_0^\infty \operatorname{sech}^{2+2\sigma}\xi d\xi} \quad [10]$$

Equation [7] then becomes

$$\theta = \frac{CH}{T_0}\left(\frac{\rho}{M\nu x}\right)^{1/3} \operatorname{sech}^{2\sigma}\xi$$

or

$$T - T_0 = CH\left(\frac{\rho}{M\nu x}\right)^{1/3} \operatorname{sech}^{2\sigma}\xi \quad [11]$$

where C is given by Equation [10]. For $\sigma = 1$, $C = 0.455$. For air under normal conditions $\sigma = 0.733$, and by numerical integration $C = 0.421$.

It may be noted that when $\sigma = 1$, the solution for θ is of exactly the same functional form with respect to ξ as that for u, as it should be, since Equations [5] and the first of Equations [1] are exactly the same for $\nu = \alpha$. From Equation [11] the use of the boundary-layer Equation [5] can be justified a posteriori.

Axially Symmetrical Case

In a plane containing the center line of the jet, the opening is taken as the origin and the center line of the jet as the x-axis from which r is measured in a radial direction. The longitudinal and radial velocities are denoted by u and v, respectively. Using ψ now for Stokes' stream function, Schlichting's solution of the system (with proper boundary conditions)

$$u\frac{\partial u}{\partial x} + v\frac{\partial u}{\partial r} = \frac{\nu}{r}\frac{\partial}{\partial r}\left(r\frac{\partial u}{\partial r}\right)$$
$$u = \frac{1}{r}\frac{\partial \psi}{\partial r}, \quad v = -\frac{1}{r}\frac{\partial \psi}{\partial x} \quad [12]$$

gives

$$u = \frac{3}{8\pi}\frac{M}{\rho\nu x}\frac{1}{\left(1 + \frac{1}{4}\eta^2\right)^2} \quad [13]$$

$$v = \frac{1}{4}\left(\frac{3M}{\pi\rho}\right)^{1/2}\frac{1}{x}\frac{\eta\left(1 - \frac{1}{4}\eta^2\right)}{\left(1 + \frac{1}{4}\eta^2\right)^2} \quad [14]$$

where

$$\eta = \frac{1}{4}\left(\frac{3M}{\pi\rho\nu^2}\right)^{1/2}\frac{r}{x}$$

M now being the total momentum flux and is equal to $\int_0^\infty 2\pi r\rho u^2 dr$. Retaining the meanings of T_0, α, and θ, and under the assumption that $\partial^2\theta/\partial x^2$ is uniformly small as compared with

$$\frac{1}{r}\frac{\partial}{\partial r}\left(r\frac{\partial \theta}{\partial r}\right)$$

the equation for temperature distribution can be written as

$$u\frac{\partial \theta}{\partial x} + v\frac{\partial \theta}{\partial r} = \frac{\alpha}{r}\frac{\partial}{\partial r}\left(r\frac{\partial \theta}{\partial r}\right) \quad [15]$$

The total flux of temperature difference, with T_0 as the datum temperature, is defined to be

$$H = \int_0^\infty 2\pi r u(T - T_0)dr = 2\pi T_0 \int_0^\infty ru\theta dr \quad [16]$$

which, in view of the steadiness of motion, must be independent of x. A dimensional analysis shows that θ must be a function of the three dimensionless quantities

$$\frac{H}{T_0\nu x}, \quad \frac{M}{\rho\nu^2}, \quad \text{and } \eta$$

In order that the right side of Equation [16] can be reduced to H, it is readily seen that θ must be of the following functional form

$$\theta = \frac{H}{T_0\nu x}f(\eta) \quad [17]$$

where the function $f(\eta)$ is to be determined from Equation [15].

Substitution of Equations [13], [14], and [17] in Equation [15] gives, after simplification

$$\frac{-2\eta f(\eta)}{\left(1 + \frac{1}{4}\eta^2\right)^2}\frac{\eta^2 f'(\eta)}{1 + \frac{1}{4}\eta^2} = \frac{1}{\sigma}[f'(\eta) + \eta f''(\eta)]$$

which can be immediately integrated to

$$\frac{\eta^2 f(\eta)}{1 + \frac{1}{4}\eta^2} = \frac{\eta f'(\eta)}{\sigma}$$

the constant integration being zero, since $f(\eta)$ and $f'(\eta)$ are both finite for $\eta = 0$. A second integration yields

$$f(\eta) = \frac{C}{\left(1 + \frac{1}{4}\eta^2\right)^{2\sigma}} \quad [18]$$

By substitution of Equations [17] and [18] in [16], C can be readily determined to be $(1 + 2\sigma)/(8\pi)$. Equation [17] then becomes, by virtue of Equation [18]

$$\theta = \frac{1 + 2\sigma}{8\pi}\frac{H}{T_0\nu x}\frac{1}{\left(1 + \frac{1}{4}\eta^2\right)^{2\sigma}}$$

or

$$T - T_0 = \frac{1 + 2\sigma}{8\pi}\frac{H}{\nu x}\frac{1}{\left(1 + \frac{1}{4}\eta^2\right)^{2\sigma}} \quad [19]$$

It may be noted that when $\sigma = 1$, the solution for θ is of exactly the same functional form with respect to η as that for u, as it should be, since Equation [15] is exactly the same as the first of Equations [12] for $\nu = \alpha$. From Equation [19], the use of the boundary-layer Equation [15] can be justified a posteriori.

Conclusion

The temperature distributions of a two-dimensional and an axially symmetrical preheated air jet, when the flow is steady and laminar, are given in closed forms by Equations [11] and [19], respectively, where the symbols M and H have different meanings as defined in the foregoing for each case.

Elastic Torsion in the Presence of Initial Axial Stress

By J. N. GOODIER,[1] STANFORD UNIVERSITY, STANFORD, CALIF.

The torsional rigidity, for small elastic torsion, of bars of thin-walled open section, is, in general, altered by initial tension, compression, bending, or other axial stress. This appears in the increase of torsional stiffness of strips due to tension, in the decrease to zero in open sections which buckle torsionally as columns, and also has an influence on lateral buckling of beams. This paper contains an extension of the Saint Venant solution for ordinary torsion to the problem of torsion in the presence of initial axial stress with any distribution on the cross section. The results are confirmed by tests, and validate the intuitively derived formulas which are in use.

Introduction

THE torsional buckling of compressed bars of open thin-walled section demonstrates that torsional stiffness can be diminished to the vanishing point by thrust. Tension will increase it. An axial stress varying over the cross section—bending, residual, or thermal stress—may have either effect, according to the variation of the stress and the shape of the section.

The effect of tension on the torsional stiffness of strips was observed by L. R. Wilberforce and A. Campbell (1)[2] in 1913, and a simple theory was given by J. C. Buckley (2) in 1914. Essentially the same theory was proposed in 1929 by H. Wagner (3) to account for the torsional buckling of compressed aircraft stiffeners. It involved certain special assumptions. In the untwisted form the "fibers" have compressive stress in them. In the twisted form the fibers run through a cross section in a twisted pattern. The fibers are supposed to carry their compressive stresses with them. These stresses, acting on a cross section, being no longer parallel to the axis, form a couple about the axis as well as a force resultant (the thrust). It is also supposed that the Saint Venant shear stresses of torsion, corresponding to the geometrical twist, appear on the cross section in company with the fiber stresses. This point of view (combined with an approximate analysis of nonuniform torsion) led to a formula for the critical thrust for torsional buckling which agrees well with test results (4). It was extended by Kappus (5) to unsymmetrical sections, which buckle by twisting combined with bending. It was employed by the author (6) in a theory of lateral buckling of unsymmetrical sections in bending.

That it is a hypothesis can be shown as follows: The twisted pattern of fiber stress may be regarded as the normal stress on a nonplane section made up of elements of area to which the fibers are normal. The shear stresses on this section are taken as the Saint Venant stresses corresponding to the geometrical twist. This is essentially Wagner's representation. Instead of this, let the compressed bar be twisted, and then a strictly plane cross section made, normal to the axis of the twist. The normal stress on this section is strictly parallel to the axis and its moment about it is zero. It is equally plausible to take the shear stresses on this section as, again, those of Saint Venant. But then the torsion would be unaffected by the thrust. In fact, however, at torsional buckling, the shear stresses on this plane section are so far from having the Saint Venant values that they form zero axial moment. It is evident that in this and related problems, the precise definition of the cross section under consideration is a matter of the first importance.

A solution of the problem of torsion in the presence of uniform axial stress, without special assumptions, has been obtained by Biot (7) from general equations for small deformation in the presence of initial stress, which follow by linearization from his general nonlinear equations of elasticity. The torsional rigidity found is the same as that obtainable from Wagner's hypothesis.

A solution for initial axial stress nonuniform over the cross section is derived in the present paper. It yields the same torsional rigidity as does Wagner's hypothesis, and thus validates the terms obtained from this hypothesis in the equations of lateral buckling from a state of pure flexure, or pure flexure combined with thrust (eccentric thrust) (6).

Choice of General Equations

The differential equations of equilibrium, and the boundary conditions of equilibrium, in terms of stress, are the same for a solid which has undergone a finite deformation as they are for small deformation, provided co-ordinates, areas, and normals employed in the specification of stress and the boundary conditions are those of the final state. When the undeformed boundary is given, it is expedient to use the co-ordinates of the undeformed state as independent variables, and the equations are then transformed into a formally less simple set involving the displacements. The precise form obtained depends upon which of several available choices is made for the specification of stress. Two distinct formulations of the general equations are available, (*a*) by Trefftz (8) and Kappus (9), (*b*) by Biezeno and Hencky (10), Biot (11); these have been discussed further by Neuber (12), and Prager (13). The problem in hand is solvable in each of these two sets of equations. Of the two, the solution found in terms of (*a*) is considerably simpler than the solution found in terms of (*b*). Only the former is given here.

Let Ox, Oy, Oz be fixed rectangular axes, and x, y, z, the co-ordinates of a particle of the body in the initial state (either the unstrained state, or a state of initial stress). Three line elements dx, dy, dz, in the interior, form an infinitesimal rectangular block, which in the deformation is displaced and strained into an infinitesimal parallelepiped. The force vector on any one face is resolved into (nonorthogonal) components parallel to the edges of the parallelepiped. These components, divided by the original

---

[1] Professor of Theoretical and Applied Mechanics, Stanford University. Mem. ASME.

[2] Numbers in parentheses refer to Bibliography at end of paper.

This paper presents results obtained in the course of research carried out under a contract (N6-ONR-251) between the Office of Naval Research and Stanford University.

Presented at the Annual Conference of the Applied Mechanics Division, Purdue University, Lafayette Ind., June 22-24, 1950, of The American Society of Mechanical Engineers.

Discussion of this paper should be addressed to the Secretary, ASME, 29 West 39th Street, New York, N. Y., and will be accepted until January 10, 1951, for publication at a later date. Discussion received after the closing date will be returned.

Note: Statements and opinions advanced in papers are to be understood as individual expressions of their authors and not those of the Society. Manuscript received by the Applied Mechanics Division August 29, 1949. Paper No. 50—APM-4.

area of the face, are Trefftz's stress components ($k_{\mu\nu}$; $\mu, \nu = x, y, z$). They form a symmetric tensor.

The differential equations of equilibrium (in the absence of body force) are three of the type

$$\left.\begin{aligned}&\frac{\partial}{\partial x}\left[k_{xx}\left(1+\frac{\partial u}{\partial x}\right)+k_{xy}\frac{\partial u}{\partial y}+k_{xz}\frac{\partial u}{\partial z}\right]\\&+\frac{\partial}{\partial y}\left[k_{yx}\left(1+\frac{\partial u}{\partial x}\right)+k_{yy}\frac{\partial u}{\partial y}+k_{yz}\frac{\partial u}{\partial z}\right]\\&+\frac{\partial}{\partial z}\left[k_{zx}\left(1+\frac{\partial u}{\partial x}\right)+k_{zy}\frac{\partial u}{\partial y}+k_{zz}\frac{\partial u}{\partial z}\right]=0\end{aligned}\right\}\quad\ldots[1]$$

the other two being obtained by cyclic permutation $x \to y \to z \to x$, $u \to v \to w \to u$; u, v, w are the displacement components, i.e., the particle at x, y, z, moves to $x+u, y+v, z+w$.

The boundary conditions of equilibrium are three of the type

$$\left.\begin{aligned}&\alpha\left[k_{xx}\left(1+\frac{\partial u}{\partial x}\right)+k_{xy}\frac{\partial u}{\partial y}+k_{xz}\frac{\partial u}{\partial z}\right]\\&+\beta\left[k_{yx}\left(1+\frac{\partial u}{\partial x}\right)+k_{yy}\frac{\partial u}{\partial y}+k_{yz}\frac{\partial u}{\partial z}\right]\\&+\gamma\left[k_{zx}\left(1+\frac{\partial u}{\partial x}\right)+k_{zy}\frac{\partial u}{\partial y}+k_{zz}\frac{\partial u}{\partial z}\right]=p_x\end{aligned}\right\}\quad\ldots[2]$$

α, β, γ being the direction cosines of an element dS of boundary surface at $x\ y\ z$, all in the "initial" state, and $p_x dS$ the x-component of boundary force in the final state, on the element into which dS is deformed and displaced. The other two are obtained by cyclic permutation, including $\alpha \to \beta \to \gamma \to \alpha$.

The initial state may be taken to be one of initial stress given by ordinary Cartesian components $S_{\mu\nu}$, and for the final state we may write

$$k_{\mu\nu} = S_{\mu\nu} + s_{\mu\nu}\quad\ldots[3]$$

$s_{\mu\nu}$ being stress increments accompanying the displacement. Inserting Equation [3] in the equations of the type of Equation [1], and dropping nonlinear terms such as $s_{xx}\,\partial u/\partial x$, we obtain three equations, valid for small deformation from the initial state, of the type

$$\left.\begin{aligned}&\frac{\partial s_{xx}}{\partial x}+\frac{\partial s_{xy}}{\partial y}+\frac{\partial s_{xz}}{\partial z}+\frac{\partial}{\partial x}\left[S_{xx}\frac{\partial u}{\partial x}+S_{xy}\frac{\partial u}{\partial y}\right.\\&\left.+S_{xz}\frac{\partial u}{\partial z}\right]+\frac{\partial}{\partial y}\left[S_{xy}\frac{\partial u}{\partial x}+S_{yy}\frac{\partial u}{\partial y}+S_{yz}\frac{\partial u}{\partial z}\right]\\&+\frac{\partial}{\partial z}\left[S_{xz}\frac{\partial u}{\partial x}+S_{yz}\frac{\partial v}{\partial y}+S_{zz}\frac{\partial u}{\partial z}\right]=0\end{aligned}\right\}\quad\ldots[4]$$

Since equilibrium in the initial state requires satisfaction of the three equilibrium equations of the type

$$\frac{\partial S_{xx}}{\partial x}+\frac{\partial S_{xy}}{\partial y}+\frac{\partial S_{xz}}{\partial z}=0\quad\ldots[5]$$

Equation [4] may be written

$$\begin{aligned}&\frac{\partial s_{xx}}{\partial x}+\frac{\partial s_{xy}}{\partial y}+\frac{\partial s_{xz}}{\partial z}+S_{xx}\frac{\partial^2 u}{\partial x^2}+S_{yy}\frac{\partial^2 u}{\partial y^2}+S_{zz}\frac{\partial^2 u}{\partial z^2}\\&+2S_{xy}\frac{\partial^2 u}{\partial x\partial y}+2S_{yz}\frac{\partial^2 u}{\partial y\partial z}+2S_{zx}\frac{\partial^2 u}{\partial z\partial x}=0\end{aligned}\quad\ldots[6]$$

In the boundary condition, Equation [2], p_x may be replaced by $f_x + \Delta f_x$, where f_x is the value for the initial state, so that

$$f_x = \alpha S_{xx} + \beta S_{xy} + \gamma S_{xz}\quad\ldots[7]$$

On inserting Equation [3], dropping such nonlinear terms as $s_{xx}\,\partial u/\partial x$ and taking account of Equation [7], the boundary conditions become three of the type

$$\begin{aligned}&\alpha s_{xx}+\beta s_{xy}+\gamma s_{xz}+\alpha\left[S_{xx}\frac{\partial u}{\partial x}+S_{xy}\frac{\partial u}{\partial y}+S_{xz}\frac{\partial u}{\partial z}\right]\\&+\beta\left[S_{xy}\frac{\partial u}{\partial x}+S_{yy}\frac{\partial u}{\partial y}+S_{yz}\frac{\partial u}{\partial z}\right]+\gamma\left[S_{xz}\frac{\partial u}{\partial x}\right.\\&\left.+S_{yz}\frac{\partial u}{\partial y}+S_{zz}\frac{\partial u}{\partial z}\right]=\Delta f_x\end{aligned}\quad\ldots[8]$$

The stress increments will be taken as related to the accompanying deformation by the usual linear stress-strain relations of the homogeneous isotropic elastic solid, of the types

$$E\frac{\partial u}{\partial x}=s_{xx}-\nu(s_{yy}+s_{zz}),\quad G\left(\frac{\partial v}{\partial x}+\frac{\partial u}{\partial y}\right)=s_{xy}\quad\ldots[9]$$

Solution for Torsion

We now seek a solution of the sets of equations typified by Equations [6], [8], and [9], to represent small torsion of a uniform bar in the presence of initial stress $S_{\mu\nu}$, by postulating

$$u=-\theta yz,\quad v=\theta xz,\quad w=w(x,y)\quad\ldots[10]$$

with θ (the twist per unit length) a constant, exactly as in the Saint Venant torsion theory. As in that theory, Equations [10] substituted in the stress-strain relations of the type of Equation [9] yield only two nonzero stress components

$$s_{zx}=G\left(\frac{\partial w}{\partial x}-\theta y\right),\quad s_{yz}=G\left(\frac{\partial w}{\partial y}+\theta x\right)\quad\ldots[11]$$

and these are independent of z.

The last six terms on the left of Equation [6], and its two companion equations, are reduced by Equations [10] to

$$-2S_{yz}\theta,\quad 2S_{xz}\theta,\quad S_{xx}\frac{\partial^2 w}{\partial x^2}+2S_{xy}\frac{\partial^2 w}{\partial x\partial y}+S_{yy}\frac{\partial^2 w}{\partial y^2}$$

respectively. These vanish if the initial stress consists of axial stress S_{zz} only. To satisfy the equilibrium Equations [5] of the initial state, there being no body force, it is then necessary that S_{zz} be independent of z. If S_{zz} is due to applied forces, these must be end loads consisting of uniform thrust or tension, and bending couples. S_{zz} is then a linear function of x and y. But S_{zz} may also be residual or thermal stress with a less simple distribution.

With S_{zz} a function of x and y only, the torsion stresses, Equation [11], satisfy all three equations of the type of Equation [6] provided

$$\frac{\partial s_{xz}}{\partial x}+\frac{\partial s_{yz}}{\partial y}=0\quad\ldots[12]$$

which represents the last one.

Applying the boundary conditions, Equations [8], to the curved surface of the bar,[1] we have $\gamma = 0$, and, since the surface is free, $\Delta f_x = 0$, etc. The first two of the three are now identically satisfied. The third reduces to

$$\alpha s_{xz}+\beta s_{yz}=0\quad\ldots[13]$$

But Equations [10], [11], [12], and [13] are the equations of the Saint Venant torsion theory. It follows that when θ is prescribed, w, s_{xz}, s_{yz}, are determined in terms of it exactly as in that

[1] Taken as exactly cylindrical in spite of the initial stress.

theory. This does not mean, however, that the torsion is unaffected by the initial stress. We have yet to evaluate the torque required to maintain this torsion, and this is affected.

The z-component of force per unit initial area, acting on the end $z = 0$ of the bar, Fig. 1, in the direction of the fixed x-axis

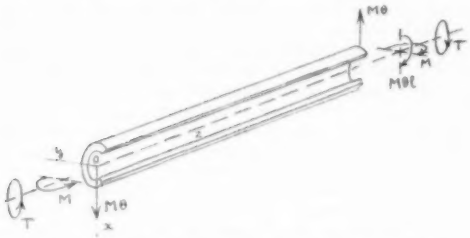

FIG. 1 LOADING IMPLIED BY SAINT VENANT DISPLACEMENT

is obtained as $f_x + \Delta f_x$, f_x being given by Equation [7], and Δf_x by Equation [8], with $\alpha = \beta = 0$, $\gamma = -1$, and similarly for the other components. Then

$$\Delta f_x = -s_{zx} + S_{zz}\theta y\,; \quad \Delta f_y = -s_{yz} - S_{zz}\theta x\,; \quad f_z + \Delta f_z = -S_{zz} \ldots\ldots [14]$$

f_x and f_y being now zero.

The force resultant in the x-direction on the end $z = 0$ is

$$F_x = -\iint s_{zx}\,dxdy + \theta \iint S_{zz} y\,dxdy$$

The first integral vanishes as in the Saint Venant theory. The second is the moment of the initial axial stress about the x-axis. Thus

$$F_x = \theta \iint S_{zz} y dxdy\,; \quad F_y = -\theta \iint S_{zz} x dxdy\,; \quad F_z = -\iint S_{zz} dxdy \ldots\ldots [15]$$

The end force distribution specified by Equation [14] forms a moment not only about the z-axis (torque), but also about the x- and y-axes. In computing these we recall that by definition the components, Equations (14), when multiplied by $dx\,dy$ give force elements which act on the element of area as it is in the final state, with displacement u, v, w. Thus the torque is (as in Fig. 1, on the left-hand end $z = 0$)

$$T = \iint [\Delta f_x(y + v) - \Delta f_y(x + u)]\,dxdy \ldots\ldots [16]$$

But u, v, vanish at $z = 0$. At any other cross section the products $\Delta f_x \cdot v$, $\Delta f_y \cdot u$ are of the second order in the small quantities of the torsion, and may be dropped, as have similar quantities already in the linearization of the differential equations and boundary conditions. Then, using Equations [14]

$$T = \iint (-s_{zx} y + s_{yz} x)\,dxdy + \theta \iint S_{zz}(x^2 + y^2)\,dxdy \ldots [17]$$

The first integral is the Saint Venant torque corresponding to the twist θ and may be written $GC\theta$, GC being the ordinary torsional rigidity. Thus

$$T = GC\theta + \theta \iint S_{zz} r^2 dxdy \ldots\ldots [18]$$

with $r^2 = x^2 + y^2$.

The final bending moment, on the left-hand end, formed by $f_x + \Delta f_x$ is identical with the bending moment of the initial stress distribution, by Equation [14], and the vanishing of u and v at that end.

The distribution of force in the final state on the right-hand end $z = l$ is given by Equations [14] with the signs on the right reversed, since $\alpha = \beta = 0$, $\gamma = 1$. The force resultants and the torque (moment about the z-axis) are given by Equations [15] and [18] with signs reversed. The bending moments show a difference. The moment about the x-axis, in the sense of M on the end $z = l$ in Fig. 1, is

$$M_x = \iint S_{zz}(y + v)\,dxdy = \iint S_{zz} y dxdy + \theta l \iint S_{zz} x dxdy \ldots\ldots [19]$$

The first integral in the last member of Equation [19] represents the initial bending moment about the x-axis. The second represents the initial bending moment about the y-axis.

Similarly, the final bending moment about the y-axis (right-handed looking out) is

$$M_y = -\iint S_{zz}(x + u)dxdy = -\iint S_{zz} x dxdy - \theta l \iint S_{zz} y dxdy \ldots\ldots [20]$$

The interpretation of Equations [19 and 20] is that the initial bending moment has simply been carried round with the torsional rotation of the end $z = l$. The transverse forces F_x and F_y of Equations [15], and their reversed counterparts on the end $z = l$ are required to preserve equilibrium.

We find, therefore, that the simple torsional deformation, Equations [10], is maintained not by torque alone, but by torque with modifications of the initial bending moment, and associated shearing forces. Initial stress due to tension or thrust, and pure bending in one principal plane, will now be considered separately.

INITIAL TENSION OR THRUST (S_{zz} CONSTANT)

The solution obtained holds for any choice of the z-axis, the axis of the torsional rotations, parallel to the generators of the curved surface. If the z-axis is now taken to be the axis of centroids, the transverse forces F_x, F_y of Equations [15] vanish, as do the moments, Equations [19] and [20]. The torsion is maintained by the initial uniform axial stress together with the torque, Equation [18], which becomes

$$T = (GC + S_{zz}J)\theta \ldots\ldots [21]$$

where J is the polar moment of inertia of the section about the centroid. This is the same as Biot's result (7). The stress components he employs also have the Saint Venant distribution corresponding to the twist θ. But the two solutions are not identical, because the stress specification differs from that of Trefftz; Equation [21] of course has a significance independent of the stress specification. It confirms Wagner's hypothesis for this problem.

A change of the axis of torsion, from the centroidal axis to a parallel axis, can be effected by a small rigid-body rotation, as in the Saint Venant theory. In the present problem the tensile or compressive forces on the ends must be carried round with the small rotation, so that the whole system, bar and loads, is merely placed in a new position without essential change.

INITIAL BENDING STRESS ABOUT A PRINCIPAL AXIS

Choice of the axis of torsion being free, it is taken for this case as coincident with the axis of shear centers, as is convenient in considering combinations of torsion and bending in general. Ox, Oy are taken parallel to centroidal principal axes. The initial stress is due to bending couples M (in the horizontal plane, Fig. 1; the other actions shown are not present initially), producing the initial stress

$$S_{zz} = \frac{M}{I_x}(y - y_0) \ldots\ldots [22]$$

y_0 being the y-co-ordinate of the centroid, and I_x the moment of inertia about a centroidal axis parallel to Oz.

It is easily verified that the forces F_y, F_z of Equations [15] now vanish, and F_z becomes $M\theta$, which is shown in Fig. 1.

The torque, Equation [18], becomes

$$T = \left(GC + \frac{\kappa M}{I_x}\right)\theta \qquad [23]$$

where

$$\kappa = \int\int yr^2 dx dy - A\rho^2 y_0$$

and $A\rho^2$ is the polar moment of inertia about the shear center. This agrees with the result obtained from Wagner's hypothesis (6). The bending moment on the end $z = 0$ is identical with that of the initial state.

On the right-hand end $z = l$, we have from Equations [19], [20], and [22]

$$M_x = M,\ M_y = -M\theta l \qquad [24]$$

in addition to the force $F_z = -M\theta$ and the torque $-T$.

The final loading on the bar, represented by all these actions, is shown in Fig. 1. The moments, Equations [24], represent the initial bending moment rotated through the torsional rotation θl of the right-hand end.

It is possible to mount and load the bar in such a way that the initial bending moment on the end $z = l$ remains unrotated as the bar is twisted, as when the moment is applied through a bearing in which the bar may turn, Fig. 2. In that case the solution

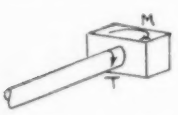

Fig. 2 Loading With Bending Moment in a Fixed Plane

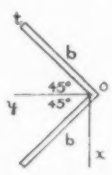

Fig. 3 Angle Section

must be amended by removing the moment $M\theta l$, and the associated shear forces $M\theta$ of Fig. 1. On the assumption of superposition as valid for a first approximation, this is equivalent to imposing equal and opposite actions, producing a "cantilever" bending of the bar, in the vertical plane, concave upward. The slope of one end relative to the other in this bending is (approximately) $(M\theta l^2)/(2EI_y)$, I_y being the moment of inertia of the section about a centroidal axis parallel to Oy. The ratio of this to the slope of one end relative to the other in the initial bending is $\theta I_x/2I_y$. It is small if I_x and I_y are of the same order of magnitude but may be appreciable if I_y is much less than I_x, as in a thin strip.

Such secondary bending is to be expected when the right-hand end of the bar rotates but the applied moment does not, for the latter then has components about both (rotated) principal axes of the section.

Torsional Rigidity

The principal effect of the initial stress on the torsion is in the the change of torsional rigidity. In the absence of initial stress (Saint Venant torsion), the stress and torque are the same for all axes of torsion parallel to the generators. In the presence of initial stress, the torque is given by Equation [18] for arbitrary distribution of S_{zz} on the section, and depends upon the position of the axis of torsion (Oz) through the term r^2 in the integral. This is not surprising when it is observed that the torque is the moment of all loads on one end about Oz and that the initial stress S_{zz} becomes inclined to Oz in the torsional deformation. The simple Cartesian component S_{zz} of the initial state is replaced by the Trefftz component k_{zz}, of the same magnitude, since $k_{zz} = S_{zz} + s_{zz}$, and in the torsional solution s_{zz} is zero. But the Trefftz component has the direction of the "fiber." In this, and in the existence of Saint Venant shear stress on the warped cross section, the present solution agrees with Wagner's hypothetical representation of the stress. The shear-stress components s_{xz} and s_{yz} of the present solution are also of course of Trefftz's type. They have the directions assumed after the torsional deformation by line elements dx, dy of the initial state. But for the small torsion considered they are not significantly different from Cartesian components.

It is known that for uniform tension or thrust the second term on the right of Equation [18], or [21], can be comparable to the first for thin-walled open sections (7). For closed or solid sections the first term is so large that the second can be neglected. Similar remarks apply for initial bending stress. There is then, however, the further consideration that the second term in Equation [18], or [23] may vanish on account of section symmetry. The quantity κ in Equation [23] vanishes in the following cases: (*a*) symmetry about both principal axes; (*b*) point-symmetry (e.g., Z-section); (*c*) symmetry about Oz only. It does not vanish, however, when there is symmetry about Oy only, i.e., symmetry about the principal axis in the plane of the bending. Symmetry about an axis means of course that both centroid and shear center lie on this axis.

As an example, the thin angle section indicated in Fig. 3 has $\kappa = tb^4/6\sqrt{2}$. Writing Equation [23] as

$$T = \left(1 + \frac{\kappa M}{GCI_x}\right) GC\theta \qquad [25]$$

the term $(\kappa M)/(GCI_x)$ becomes $(\sigma\, b^2)/(2\,G\,t^2)$ where σ is the bending stress in the extreme fiber. For $\sigma = 2 \times 10^4$ psi, $G = 4 \times 10^6$ psi, $b/t = 10$, the term is $^1/_4$. This represents an increase of torsional rigidity if the bending is such that the apex of the angle is in compression, a decrease if it is in tension.

Measurements

Tests carried out at Stanford University on the torsional rigidity of strips in tension, and angle sections in pure bending, have shown excellent agreement with Equation [18] in the special forms of Equations [21] and [25] appropriate to the tests.

A strip of 618-T Dural, $1^1/_2$ in. $\times$ $^1/_{32}$ in. $\times$ 30 in., was tested in torsion under tensile stresses up to 20,000 psi. At this stress the torsional rigidity is 4.5 times the ordinary (zero axial stress) value.

A 90-deg-angle section bar 1 in. $\times$ 1 in. $\times$ $^1/_{32}$ in. was tested in torsion under bending moments up to values which doubled the ordinary torsional rigidity.

It is expected that these, and further tests showing the influence of these changes of torsional rigidity on the buckling behavior, will be reported in a later paper.

Bibliography

1 "On Vibration Galvanometers With Unifilar Torsional Control," by A. Campbell, Proceedings of the Physical Society, London, England, vol. 25, 1913, pp. 203–205.

2 "Bifilar Property of Twisted Strips," by J. C. Buckley, *Philosophical Magazine*, vol. 28, 1914, pp. 778–787.

3 "Torsion and Buckling of Open Sections," by H. Wagner, NACA, TM no. 807, 1936 (Translation).

4 "Experimental Study of Torsional Column Failure," by A. S. Niles, NACA, TM no. 733, 1939, and references cited therein.

5 "Twisting Failure of Centrally Loaded Open-Section Columns in the Elastic Range," by R. Kappus, NACA, TM no. 851, 1938 (translation).

6 "Torsional and Flexural Buckling of Bars of Thin-Walled Open Section Under Compressive and Bending Loads," by J. N. Goodier, JOURNAL OF APPLIED MECHANICS, Trans. ASME, vol. 64, 1942, p. A-103.

7 "Increase of Torsional Stiffness of a Prismatical Bar Due to Axial Tension," by M. A. Biot, *Journal of Applied Physics*, vol. 10, 1939, pp. 860–864.

8 "Zur Theorie der Stabilität des elastischen Gleichgewichts," by E. Trefftz, *Zeitschrift für angewandte Mathematik und Mechanik*, vol. 12 1933, pp. 160–165.

9 "Zur Elastizitätstheorie endlicher Verschiebungen," by R. Kappus, *Zeitschrift für angewandte Mathematik und Mechanik*, vol. 19, 1939, pp. 344–360.

10 "On the General Theory of Elastic Stability," by C. B. Biezeno and H. Hencky, Proceedings Koninklijke Akademie van Wetenschappen te Amsterdam, vol. 31, 1928, pp. 569–578, 579–592.

11 "Non-Linear Theory of Elasticity and the Linearized Case for a Body Under Initial Stress," by M. A. Biot, *Philosophical Magazine*, vol. 27, 1939, pp. 468–489.

12 "Die Grundgleichungen der elastischen Stabilität in allgemeinen Koordinaten und ihre Integration," by H. Neuber, *Zeitschrift für angewandte Mathematik und Mechanik*, vol. 23, 1943, pp. 321–330.

13 "The General Variational Principle of the Theory of Structural Stability," by W. Prager, *Quarterly Applied Mathematics*, vol. 4, 1947, pp. 378–384.

Torsional Stress Concentration in Angle and Square Tube Fillets

By J. H. HUTH,[1] STANFORD UNIVERSITY, CALIF.

This paper points out the wide variation in the results of previous investigations into the stress concentration at the fillets of angle sections subjected to uniform torsion. The relaxation method is applied and new results are given (not in agreement with previous results) for both angle sections and thin-walled square tube sections. These results are believed to be within about 4 per cent of the correct values, and they cover a complete range of fillets of all sizes. Also, the maximum shearing stress and torsional rigidity are given for a prismatical bar whose cross section is formed by a circular quadrant tangent to two sides of a square. It is pointed out that the stress concentration in angle sections with generous fillets may be lowered considerably by rounding off the outside corner in such a way as to keep the thickness of the section everywhere approximately constant.

Introduction

THE problem is that of determining the shearing-stress concentration at the fillet of an angle section subjected to uniform torsion.

Angle Sections. Fig. 1 shows the results of previous investigations of this problem.[2] They were carried out either experimentally with the aid of the soap-film analogy, or analytically, using certain simplifying assumptions. The wide variation in these results prohibits the drawing of any definite conclusions, and indicates the need for applying a method in which the accuracy depends only upon the degree of refinement of a numerical process. Therefore the relaxation method has been used, and the results are indicated in Figs. 1 and 2 by the heavy line. These results are believed to be accurate to within about 4 per cent of the true values over the entire range.

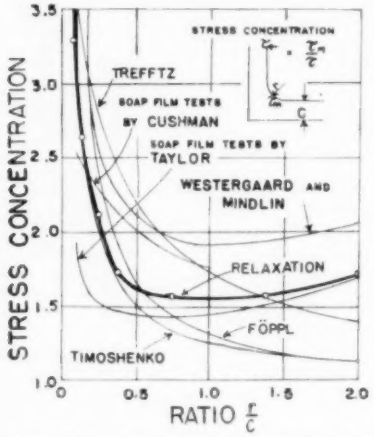

FIG. 1 STRESS CONCENTRATION IN FILLETS OF ANGLE SECTIONS SUBJECTED TO UNIFORM TORSION

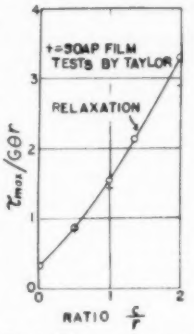

FIG. 2 EXTENSION OF THE RANGE OF FIG. 1 TO INCLUDE FILLETS OF VERY LARGE RADIUS

(Stress concentration for any given value of r/c may be computed by taking corresponding ordinate from this curve and multiplying it by r/c.)

Thin-Walled Square Tubes. The shearing-stress concentration at the fillets of a thin-walled square tube was also investigated by the relaxation method, and the results are indicated by the heavy line in Fig. 3. As noted in Fig. 3, these results are valid only for the case in which the length of the side of the tube is very great (at least 15 to 20 times as great) in comparison with either the wall thickness or the radius of curvature of the fillets. The other curve in

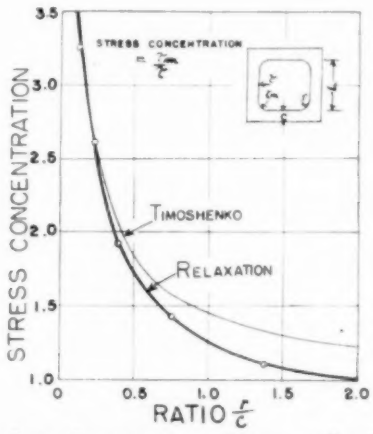

FIG. 3 STRESS CONCENTRATION IN FILLETS OF THIN-WALLED SQUARE TUBES SUBJECTED TO UNIFORM TORSION

(These results are valid only for case in which L is much greater than either c or r.)

[1] Graduate Student, Div. of Engrg. Mech., Stanford University.

Presented at the National Meeting of the Applied Mechanics Division, Purdue University, Lafayette, Ind., June 22–24, 1950, of THE AMERICAN SOCIETY OF MECHANICAL ENGINEERS.

Discussion of this paper should be addressed to the Secretary, ASME, 29 West 39th Street, New York, N. Y., and will be accepted until January 10, 1951, for publication at a later date. Discussion received after the closing date will be returned.

NOTE: Statements and opinions advanced in papers are to be understood as individual expressions of their authors and not those of the Society. Manuscript received by the Applied Mechanics Division August 15, 1949. Paper No. 50—APM-9.

[2] The results of previous investigations were obtained from the paper, "Structural Beams in Torsion," by I. Lyse and B. G. Johnston Lehigh University Publication, vol. 9, no. 10, 1935, p. 477.

Fig. 3 was computed from a formula given by Timoshenko.[3] His curve approaches the limiting case of a stress concentration of unity asymptotically as the ratio of fillet radius to wall thickness increases. It is believed that the accuracy of these results is about the same as in the case of the angle sections.

Theory Needed for the Treatment of Angle Sections

In calculating the shearing stress, use was made of the stress function ϕ which may be defined as follows:[4]

1 To satisfy the equation

$$\frac{\partial^2\phi}{\partial x^2} + \frac{\partial^2\phi}{\partial y^2} = -2G\theta$$

within the cross-sectional area, where G represents the shearing modulus and θ the angle of twist per unit length.

2 $$\tau_{xz} = +\frac{\partial\phi}{\partial y}; \quad \tau_{yz} = -\frac{\partial\phi}{\partial x}$$

where τ represents the shearing stress.

Actually, it was more convenient to work with ψ which is defined by

$$\psi = \phi/G\theta$$

For singly connected regions, it is permissible to take ψ as being equal to zero on the boundary. Therefore the problem amounts to solving the equation

$$\frac{\partial^2\psi}{\partial x^2} + \frac{\partial^2\psi}{\partial y^2} = -2 \qquad [1]$$

with the added condition that ψ be equal to zero on the boundary of the region as shown in Fig. 4.

At a large distance from the fillet, the solution to Equation [1] will approach the form[4]

$$\psi = \frac{c^2}{4} - y^2$$

and therefore far from the fillet, we may write

$$\tau_{max} = G\theta\left(\frac{\partial\psi}{\partial y}\right)_{y=-\frac{c}{2}} = cG\theta$$

while at the fillet

$$\tau_{max} = G\theta\left(\frac{\partial\psi}{\partial s}\right)_{s=0}$$

Consequently, the stress concentration may be written as

$$\left(\frac{\partial\psi}{\partial s}\right)_{s=0}\Big/c = \frac{\tau_{max}\text{ at fillet}}{cG\theta}$$

An analytical solution for ψ in the entire region of Fig. 3 would present formidable difficulties. Therefore the relaxation method[4] was applied to obtain the results given in Figs. 1, 2, and 3.

Concerning the accuracy of the results, the author has previously solved the problem of the torsion of a prismatical bar of square cross section by the relaxation method, and has found that for a net size comparable to that used in this problem the error in the maximum shearing stress was in the order of 3.5 per cent of the exact value, the approximate value being too low. In addition, for one value of r/c, the problem of the angle section was reworked using a finer net and the results from the two nets were found to be in close agreement, (actually about a 2 per cent variation). Consequently, the author feels that the error in the stress concentration probably does not exceed about 4 per cent.

[3] "Theory of Elasticity," by S. P. Timoshenko, McGraw-Hill Book Company, New York, N. Y., first edition, 1934, pp. 228–284.

[4] "Relaxation Methods in Theoretical Physics," by R. V. Southwell, Clarendon Press, London, England, first edition, 1946, pp. 38–102.

General Discussion of Results for Angle Sections

Calculation of Stress Concentration for Very Generous Fillets. If c is held constant while the ratio of r to c is permitted to increase, the section as a whole will become larger and larger. However, if θ is held constant and all the linear dimensions of the cross section are multiplied by a constant k, then the shearing stress at every point in the cross section will be multiplied by the same constant k. As a result of this, the curve of stress concentration versus the ratio r/c depends only upon the shape and not upon the size of the cross section; that is, we can always scale down the cross section to a fixed value of r without changing the stress concentration.

Then it is apparent that as the ratio r/c increases it is permissible to think of the fillet radius as being fixed while the leg thickness decreases. The larger the ratio r/c, therefore, the less will be the influence of the legs on τ_{max}. Consequently, for large values of the ratio r/c, the maximum shearing stress in the angle cross section may be calculated by using a section bounded by two sides of a square and a tangent circle as shown in Fig. 5. The maximum shearing stress for the section in Fig. 5 was computed by the relaxation method and found to be equal to $0.31\,G\theta r$, while the torsional modulus of rigidity was found to be equal to $0.00326\,Gr^4$. For very generous fillets, then, it would seem more logical to take the section in Fig. 5 as the basis of the comparison. This may be done by plotting $\tau_{max}/rG\theta$ versus c/r as in Fig. 2. Then, for c/r equal to zero, the curve must come to a value of $\tau_{max}/rG\theta$ equal to 0.31.

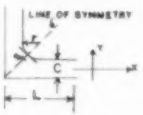

Fig. 4 Angle-Section Detail

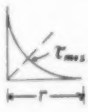

Fig. 5 Special Section Used in Computing the Stress Concentration in Very Generous Fillets of Angle Sections

Other points on the curve of Fig. 2 may be obtained by taking the ordinate of any point on Fig. 1 and dividing by the corresponding value of the ratio r/c. In other words, Fig. 2 merely represents another way of plotting the results given in Fig. 1. However, it brings the region of large fillets into the origin so that it is possible to use the further information gained from the limiting case represented in Fig. 5.

By means of Fig. 2 we then have extended the range of the results to indefinitely large fillets for, obviously, the entire range from r/c equal to 2 to r/c equal to ∞ is covered in the region in Fig. 2 from c/r equal to $\frac{1}{2}$ to c/r equal to 0. In order to obtain the stress concentration corresponding to a given value of r/c, it is necessary only to take the ordinate at the corresponding value of c/r from Fig. 2 and multiply by the value of r/c.

In addition, the conformity of the curve of Fig. 2 to the limit value for c/r equal to zero represents a check on the calculations, as the limit value was computed independently from Fig. 5. A few points are also plotted in Fig. 2 from Taylor's soap-film tests. They indicate that these tests were more accurate for large-fillet radii than for small radii.

Comment on Timoshenko's Results for Angle Sections. The results of the relaxation process are in very good agreement with Timoshenko's results for small radii of curvature. Timoshenko's results[3] are based upon the assumption, among others, that the shearing stress becomes equal to zero at a point at a distance equal to $c/2$ in along the line of symmetry from the fillet. The curves in Fig. 6 show, in fact, that this assumption is correct only for fillets with small radii of curvature.

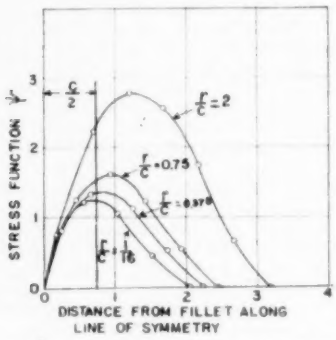

FIG. 6 VARIATION OF THE FUNCTION ψ ALONG LINE OF SYMMETRY NORMAL TO THE FILLET OF AN ANGLE SECTION
(Unit distance equals $\frac{1}{4}c$, and is measured from fillet.)

Comment on Lowering the Stress Concentration in Angle Sections. Fig. 8 shows the lines of shearing stress for both angle and thin-walled square-tube sections. The prominence of the closed contours for large fillets in the case of the angle sections suggests the possibility of lowering the stress concentration by rounding off the outside corner. The stress concentration for a section as shown in Fig. 9, with r/c equal to 2, was found from the relaxation method to be approximately equal to 1.07. This is much lower than the minimum of the curve given in Fig. 1. Consequently, it appears that the stress concentration in angle sections can be brought near to unity by the use of generous fillets combined with removal of the outside corner (as in Fig. 9 or by rounding) so as to keep the thickness of the section everywhere approximately constant. For an angle section in which the outside corner has been rounded off so as to keep the thickness of the section everywhere equal to c, the lines of shearing stress much more closely resemble those in thin-walled square tubes.

THEORY NEEDED FOR THE TREATMENT OF THIN-WALLED SQUARE TUBES

For doubly connected regions it is necessary to add to Equation [1] the following condition in order to insure continuity of displacements

$$\oint \tau ds = 2AG\theta \quad \ldots\ldots\ldots\ldots\ldots\ldots\ldots\ldots [2]$$

Here A represents the area of the region enclosed by the line integral of τ. This line integral could be evaluated along any closed curve enclosing the hole. However, for convenience, it may be evaluated along the inner boundary of the cross section where it is known that the shearing stress will be parallel to the line element. Then A merely becomes equal to the cross-sectional area of the tube hole. The additional requirement of Equation [2] can be shown to be equivalent to choosing properly

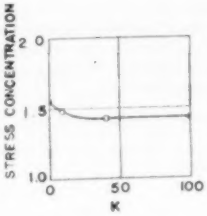

FIG. 7 (*left*) VARIATION OF STRESS CONCENTRATION WITH PARAMETER K, FOR FIXED LEG THICKNESS AND RADIUS OF CURVATURE OF FILLET

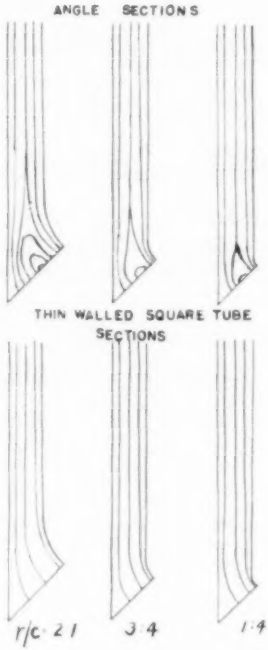

FIG. 8 (*left*) CONTOUR LINES FOR THE FUNCTION ψ
(These contour lines are the lines of shearing stress for the cross section.)

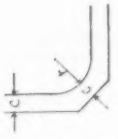

FIG. 9 ANGLE SECTION WITH LOW STRESS CONCENTRATION

a constant K for a given value[3] of L, where K represents a fixed value assigned to ψ on the outer boundary of the cross section with the value on the inner boundary being equal to zero. A large value of L will require a large value of K.

It was necessary then to calculate the effect of K on the stress concentration. In other words, for a fixed ratio of r/c, (r/c equal to $^3/_4$), K was varied corresponding to different values of L and the stress concentration computed in each case. The results of these computations are shown in Fig. 7. They indicate, as expected, that for L sufficiently long compared to both r and c, the stress concentration becomes independent of L. In all cases then, the value of K was chosen sufficiently large to insure that any further increase in the length L would not affect the stress concentration.

ACKNOWLEDGMENTS

This work was carried out under a Fellowship from the Standard Oil Company of Indiana. The problems were suggested by Dr. J. N. Goodier who also made many helpful comments.

Natural Frequencies of Continuous Beams of Uniform Span Length

By R. S. AYRE[1] and L. S. JACOBSEN,[2] STANFORD, CALIF.

A simple graphical network is used to determine the natural frequencies of flexural vibration of continuous beams having any number of spans of uniform length. The network is based upon a relatively few calculated values.

Introduction

THE classical method of solution for the natural frequencies of flexural vibration of beams is well known.[3] The method is, in general, a laborious one when there is more than one span. However, in the case of continuous beams of "uniform" span length there exists a definite pattern of frequency. Once this pattern has been established, the frequency of any mode of a beam of any number of equal spans may be determined by a graphical network method, to an accuracy of at least three significant figures. The network has known boundaries and a few known control points. It applies directly to the following three conditions of support of the extreme ends of the beam: (1) Both ends simply supported, (2) both ends rigidly clamped, (3) one end rigidly clamped and one end simply supported. Furthermore, the network may be used as a guide in estimating the frequencies of beams of unequal span length or of beams with end restraints intermediate between those mentioned. The effects of shear distortion and of rotatory inertia are discussed briefly in the Appendix.

The difficult part of the classical method lies in the calculation of the roots of the frequency equation. Once these have been determined the frequencies follow from the simple expression

$$f_i = \frac{(n_i\pi)^2}{2\pi l^2}\sqrt{\frac{EIg}{A\gamma}} \qquad [1]$$

where

f_i = natural frequency of the ith mode in cycles per second (cps)

$n_i\pi$ = ith root of frequency equation, where n_i is a dimensionless number

l = length of each span

E = modulus of elasticity

I = moment of inertia of beam cross section with reference to its neutral axis

γ = weight of material of beam per unit of volume

g = acceleration due to gravity

The network is a plot of the number n_i as a function of the number of spans, k: n_i is used, rather than n_i^2, because of the resulting near symmetry of the net.

Relationships Among Natural Modes

Extreme Ends Simply Supported. The first step is to sketch as many of the known natural-mode deflection shapes as possible, at the same time writing down the known values of n_i and noting the required number of inflection points, Fig. 1. It is evident that the fundamental mode shape, regardless of the number of spans, is equivalent to the fundamental of the single-span beam. Similarly, the $1 + k$ mode, regardless of k, is equivalent to the second mode of the single-span case; the $1 + 2k$ mode is equivalent to the third of the single-span beam, etc. Symmetry tells us that the second mode for the two-span case is equivalent to the fundamental of a single-span beam with one end clamped and the other simply supported. In the case of three spans, the second mode has a stationary inflection point at the mid-point of the beam; the mode is equivalent to the fundamental of a two-span, simply supported beam, with one span of length l and the other of length $l/2$. A reduced equivalent to the third mode exists but it is not of much practical interest. Considering the four-span case next, we see that the third mode corresponds to the second of the two-span beam with ends simply supported. Furthermore, the second and fourth modes correspond, respectively, to the fundamental and second of a two-span beam with one extreme end clamped and the other simply supported.

The six-span beam is particularly interesting since the natural modes of beams of one, two, and three spans all appear again in the six-span case. It can be shown that the fourth mode is equivalent to the second of the two-span case, and the third and fifth modes to the second and third of the three-span beam. The second and sixth modes are new forms which originate with the six-span beam and can be expected to appear again only when k is divisible by 6. In the five-span case, k is divisible only by 1 and 5, consequently we can expect to find already known shapes only in the single-span beam. Modes 2, 3, 4, and 5 originate with the five-span beam and appear again only when k is divisible by 5.

An interesting pattern is developing: (1) The values of n_i for modes of numbers 2 to k, and when $k \geq 2$, arrange themselves nearly symmetrically about the number 1.250. (2) There are $k - 1$ inflection points in the fundamental mode, each being located at an interior support. With each increase in the number i of the mode, a new point of inflection appears, in fact there are $k + i - 2$ inflection points in any mode. In order to make room for each new point the inflection points redistribute themselves in a symmetrical manner. (3) As the number of the mode is increased, the shape is alternately symmetrical and antisymmetrical.

[1] Acting Associate Professor of Mechanical Engineering, Stanford University. Mem. ASME.

[2] Professor of Mechanical Engineering, Stanford University. Mem. ASME.

[3] See, for example: (*a*) "Theory of Sound," Lord Rayleigh, London, first edition, vol. 1, 1877; recently republished by Dover Publications, New York, N. Y., 1945. (*b*) "Vibration Problems in Engineering," by S. Timoshenko, second edition, D. Van Nostrand Company, Inc., New York, N. Y., 1937. (*c*) "Dynamik der Stabwerke," by K. Hohenemser and W. Prager, J. Springer, Berlin, 1933. (*d*) "The Transverse Vibrations of Beams and the Whirling of Shafts Supported at Intermediate Points," by E. R. Darnley, *Philosophical Magazine*, vol. 41, 1921, p. 81.

Presented at the Annual Conference of the Applied Mechanics Division, Purdue University, Lafayette, Ind., June 22–24, 1950, of The American Society of Mechanical Engineers.

Discussion of this paper should be addressed to the Secretary, ASME, 29 West 39th Street, New York, N. Y., and will be accepted until January 10, 1951, for publication at a later date. Discussion received after the closing date will be returned.

Note: Statements and opinions advanced in papers are to be understood as individual expressions of their authors and not those of the Society. Manuscript received by the Applied Mechanics Division October 26, 1949. Paper No. 50—APM-21.

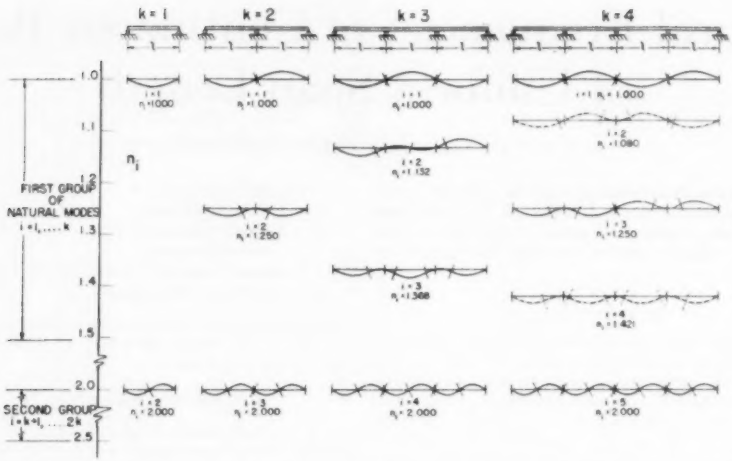

FIG. 1 NATURAL-MODE DEFLECTION SHAPES, CONTINUOUS BEAMS WITH EXTREME ENDS SIMPLY SUPPORTED: SPANS OF UNIFORM LENGTH

(The shapes were calculated from theory for beams of one, two, and three spans; these were extended, where applicable, to beams of a greater number of spans. The amplitudes are arbitrary. The calculated shapes and inflection points are shown in full line, the estimated shapes and points of inflection in dashed line. The calculated values of n_i are also shown. Vertical spacing of diagrams is proportional to n_i, i.e., to square root of frequency.)

Grouping of the Natural Modes. The natural modes fall in groups, with as many modes in each group as there are spans in the beam. The first group of modes is associated with the fundamental, the second group with the $1 + k$ mode, etc. Since a single-span beam has an infinite number of natural modes a beam of k spans has $k \cdot \infty$ modes. The values of n_i for the second group, exclusive of the $1 + k$ mode, are nearly symmetrically distributed about the number 2.250, which is n_i for the second natural mode of a single-span beam with one end clamped and the other simply supported. The grouping of the modes is repeated in the following approximate intervals: $n_i = 1.0$ to 1.5, 2.0 to 2.5, 3.0 to 3.5, etc.[4]

Extreme Ends Clamped. Now compare the shapes and the n_i values of beams with both extreme ends clamped, Fig. 2, with those for simply supported beams. Notice that the first row of the n_i values in Fig. 1 has disappeared in Fig. 2; that the second n_i in each column of Fig. 1, where $k \leq 2$, becomes the first in the corresponding column of Fig. 2; that the third n_i, where $k \leq 3$, now becomes the second, etc.; and that a new row of n_i values (of constant value, 1.506), corresponding to the kth mode appears in Fig. 2. The kth mode is equivalent to the fundamental of the single-span beam with both ends clamped. The $2k$ mode ($n_i = 2.500$) is equivalent to the second mode of the single-span beam with both ends clamped. The theoretical equivalence in the n_i values of the two types of beams can be demonstrated by a comparison of the frequency equations.

The relationship between the shapes of the two classes of beams is obvious when the number of spans is even, but not so when the number is odd. For example, a simple geometric change makes the shape of the "fundamental" mode of the two-span "clamped" beam exactly equivalent to that of the "second" mode of the two-span "simply supported" beam, but the geometry of the first- and second-mode shapes of the "three-span" clamped beam does not have an obvious relationship to that of the second and third-mode shapes of the corresponding beam with simple end supports. In both examples, however, resort to the frequency equations shows the equivalence in natural frequency.

One Extreme End Clamped, Other Simply Supported. Already it has been remarked, in connection with Fig. 1, that some of the modes are equivalent to those of beams with one extreme end simply supported and the other clamped. Similar equivalence can be seen in Fig. 2.

CONSTRUCTION OF NETWORK

The network for the first group is shown to large scale in Fig. 3. The repetitive nature of the network is indicated in Fig. 4. The large-scale network was carried out to a large number of spans in order to provide adequate checking. The twenty-four-span case is a desirable stopping point since it includes natural mode forms which originate in beams of one, two, three, four, six, eight, and twelve spans; thus all modes up through the twelve-span case have repeated themselves at least once in the network. The curves of the network are difficult to construct only in the region of the upper and lower boundaries. In order to guide the drafting in these areas cross-plots were made of n_i, and of the difference between successive values of n_i, as functions of i. Two examples of cross-plotting have been shown in Fig. 5.

The network for the first group is slightly asymmetrical, while those for the higher groups are symmetrical within the limits of at least four significant figures. Hence the network of the first group does not quite repeat itself. However, the lower half of the first net repeats to nearly four-figure accuracy in the higher group nets, and if it is mirrored over it also repeats as the upper halves of the higher nets. Tables 1, 2, and 3 list values of n_i, as determined from the net, for beams of from one to twelve spans.

[4] The trend of deviation from the approximate values is indicated by the following listing to eight significant figures, of the controlling values of n_i (based on Rayleigh's "Theory of Sound"):

1.0000000	2.0000000	3.0000000	4.0000000	5.000000
1.2498763	2.2499998	3.2500000	4.2500000	5.250000
1.5056187	2.4997527	3.5000107	4.4999996	5.500000

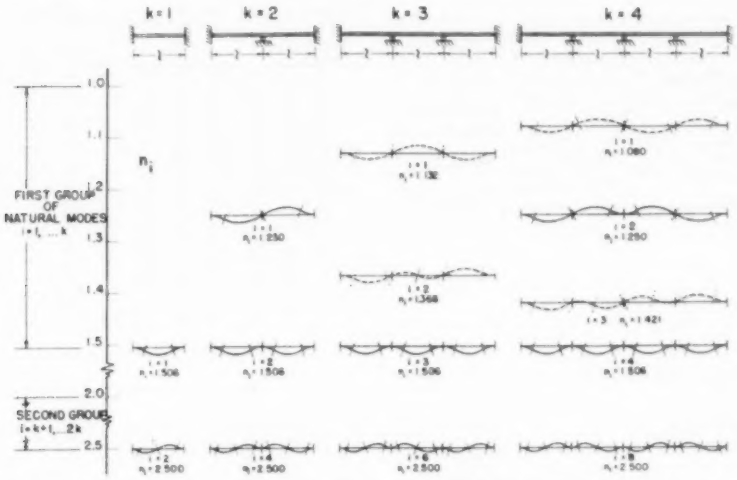

FIG. 2 NATURAL-MODE DEFLECTION SHAPES, CONTINUOUS BEAMS WITH EXTREME ENDS CLAMPED; SPANS OF UNIFORM LENGTH

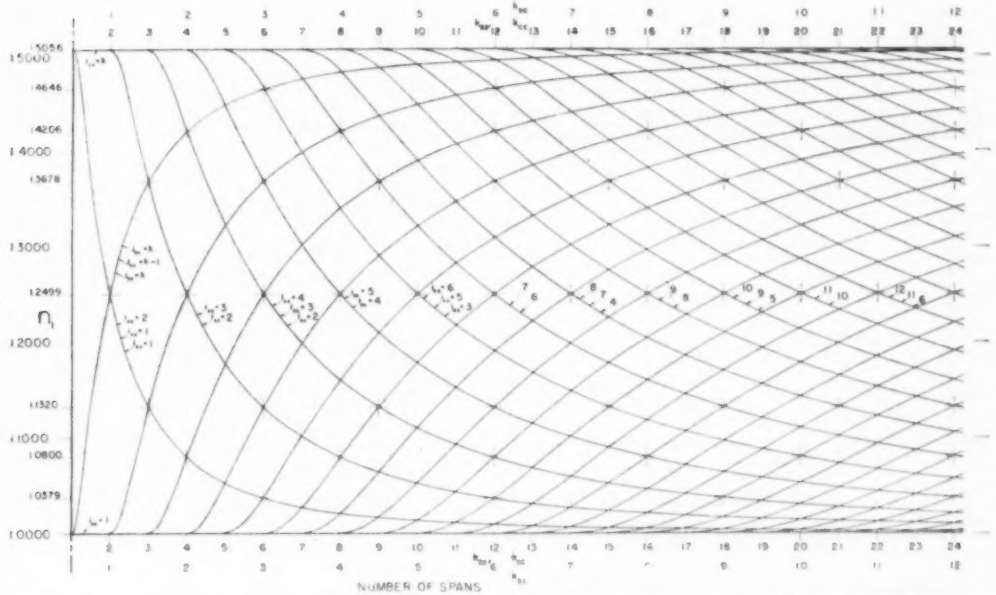

(n_i = ith root of frequency equation divided by π; k = number of spans; i = number of natural mode. Subscripts refer to type of support at extreme ends of beam: ss = both ends simply supported; cc = both ends clamped; sc = one end simply supported, other end clamped.

Each intersection, or point of tangency with horizontal boundaries, is a solution. The crosses indicate computed values of n_i. Note that net is nearly symmetrical about line, n_i = 1.2499.)

FIG. 3 THE n_i, k NETWORK FOR FIRST GROUP OF MODES (i = 1, 2, 3, ... k)

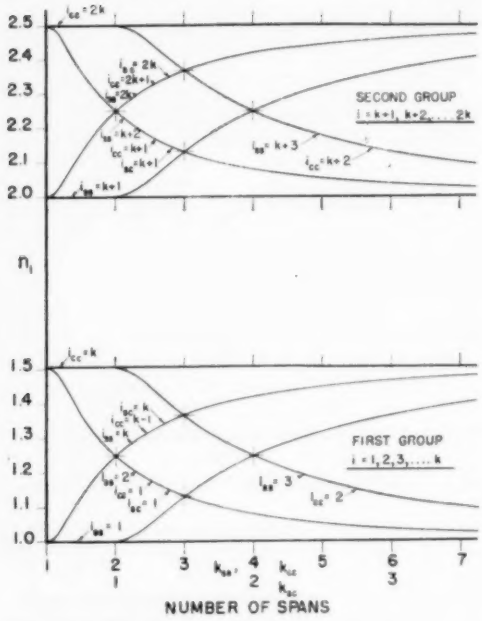

FIG. 4 REPETITIVE NATURE OF NETWORK

(The network repeats itself in the approximate intervals, n_i = 1.000 to 1.500, 2.000 to 2.500, 3.000 to 3.500, etc., with near symmetry about the lines, n_i = 1.250, 2.250, 3.250, etc. Lower half of lower network may be used to reconstruct upper and lower halves of any of upper networks.)

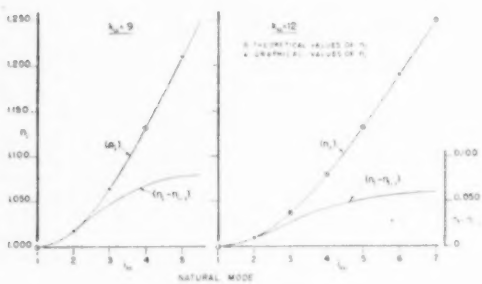

FIG. 5 CROSS-PLOTTING

(Construction of the network of Fig. 3 required several adjustments in order to "balance" all intersections of net. Final adjustment was based on cross-plots of type shown here.)

The tables cover only the first two groups of modes but can easily be extended to any higher group.

ACKNOWLEDGMENT

The authors are indebted to Messrs. C. S. Hsu and Melvin Zaid, graduate students in Mechanical Engineering, for assistance in the calculations and graphical construction. This investigation is a part of a contract held by Stanford University and sponsored by the Office of Naval Research.

TABLE 1 VALUES OF n_{ki} BOTH EXTREME ENDS SIMPLY SUPPORTED[a]

i \ k	1	2	3	4	5	6	7	8	9	10	11	12
1	1.000	**1.00**	**1.00**	**1.00**	**1.00**	**1.00**	**1.00**	**1.00**	**1.00**	**1.00**	**1.00**	**1.00**
2	2.000	2.25	1.13	1.06	1.03	1.02	1.01	1.01	1.00	1.00	1.00	1.00
3	3.000	**2.00**	2.37	1.25	1.13	1.08	1.05	1.03	1.02	1.01	1.01	1.00
4	4.000	4.25	**2.00**	2.12	1.25	1.13	1.08	1.05	1.03	1.02	1.01	1.01
5	5.000	**3.00**	3.13	**2.00**	2.06	1.25	1.13	1.08	1.05	1.03	1.02	1.01
6	6.000	6.25	4.37	3.06	**2.00**	2.03	1.25	1.13	1.08	1.05	1.03	1.02
7	7.000	**4.00**	**3.00**	4.06	3.03	**2.00**	2.02	1.25	1.13	1.08	1.05	1.03
8	8.000	8.25	6.13	4.06	4.03	3.00	**2.00**	2.02	1.25	1.13	1.08	1.05
9	9.000	**5.00**	5.37	**3.00**	4.22	4.13	3.03	**2.00**	2.02	1.25	1.13	1.08
10	10.000	10.25	**4.00**	5.06	5.03	5.25	4.13	3.03	**2.00**	2.02	1.25	1.13
11	11.000	**6.00**	6.13	5.06	5.84	6.03	5.25	4.13	3.03	**2.00**	2.02	1.25
12	12.000	12.25	7.37	**4.00**	5.84	6.84	6.03	5.25	4.13	3.03	**2.00**	2.02
13	13.000	**7.00**	**5.00**	6.06	**4.00**	5.84	6.84	6.03	5.25	4.13	3.03	**2.00**
14	14.000	14.25	8.63	6.06	6.84	**4.00**	5.84	6.84	6.03	5.25	4.13	3.03
15	15.000	**8.00**	6.13	**5.00**	6.84	6.84	**4.00**	5.84	6.84	6.03	5.25	4.13
16	16.000	16.25	9.87	8.06	7.84	8.84	6.84	**4.00**	5.84	6.84	6.03	5.25
17	17.000	**9.00**	7.37	**6.00**	**5.00**	**4.00**	**4.00**	5.84	6.84	6.03	5.25	4.13
18	18.000	18.25	**8.00**	8.06	7.84	8.84	**4.00**	5.84	6.84	6.03	5.25	4.13
19	19.000	**10.00**	8.63	**7.00**	**6.00**	**5.00**	5.84	6.84	6.03	5.25	4.13	3.03
20	20.000	20.25	11.11	8.06	8.84	8.84	6.84	**4.00**	5.84	6.84	6.03	5.25
21	21.000	**11.00**	9.37	**8.00**	**7.00**	**6.00**	**5.00**	5.84	6.84	6.03	5.25	4.13
22	22.000	22.25	**10.00**	9.06	8.84	9.84	**6.00**	6.84	6.03	5.25	4.13	3.03
23	23.000	**12.00**	9.87	**8.00**	**7.00**	**6.00**	**5.00**	5.84	6.84	6.03	5.25	4.13
24	24.000	24.25	12.37	9.06	9.84	9.84	7.84	**4.00**	5.84	6.84	6.03	5.25
25	25.000	**13.00**	**9.00**	**7.00**	**6.00**	**5.00**	**5.00**	**4.00**	**4.00**	**3.00**	**3.00**	**3.00**

[a] Each bold face value of n_{ki} is lowest value in its group.

TABLE 2 VALUES OF n_{ki} BOTH EXTREME ENDS CLAMPED[a]

i \ k	1	2	3	4	5	6	7	8	9	10	11	12
1	1.52	**1.25**	**1.13**	**1.08**	**1.05**	**1.04**	**1.03**	**1.02**	**1.02**	**1.02**	**1.01**	**1.01**
2	2.50	1.71	1.37	1.25	1.18	1.13	1.10	1.08	1.06	1.05	1.04	1.04
3	3.50	**2.25**	1.53	1.42	1.32	1.25	1.20	1.16	1.13	1.11	1.09	1.08
4	4.50	2.75	**2.13**	1.53	1.45	1.37	1.30	1.25	1.21	1.18	1.15	1.13
5	5.50	**3.25**	3.21	**2.08**	1.51	1.46	1.40	1.34	1.29	1.25	1.22	1.19
6	6.50	3.75	3.50	3.25	**2.06**	1.53	1.47	1.42	1.37	1.32	1.28	1.25
7	7.50	**4.25**	**3.13**	3.42	3.11	**2.04**	1.53	1.48	1.44	1.39	1.35	1.31
8	8.50	4.75	4.21	3.42	3.17	3.13	**2.03**	1.53	1.49	1.45	1.41	1.37
9	9.50	**5.25**	5.21	**3.08**	3.45	3.25	3.10	**2.02**	1.53	1.49	1.46	1.42
10	10.50	5.75	**4.13**	4.25	3.99	4.21	3.29	3.06	**2.02**	1.53	1.49	1.46
11	11.50	**6.25**	6.37	**5.08**	**5.05**	4.46	4.21	3.26	3.06	**2.02**	1.53	1.49
12	12.50	6.75	**5.13**	5.25	5.99	**5.04**	4.47	4.21	3.26	3.06	**2.01**	1.53
13	13.50	**7.25**	7.37	**6.08**	6.32	6.04	**5.05**	4.47	4.21	3.26	3.06	**2.01**
14	14.50	7.75	**6.13**	6.25	6.99	7.04	6.05	5.47	4.21	4.26	3.06	3.06
15	15.50	**8.25**	8.37	**7.08**	7.32	**6.04**	6.05	**5.05**	5.47	4.21	4.26	3.06
16	16.50	8.75	**7.13**	7.25	**6.99**	7.04	**6.05**	6.05	**5.05**	5.47	4.21	4.26
17	17.50	**9.25**	9.37	**8.08**	8.32	8.04	7.05	**6.05**	6.05	**5.05**	5.47	4.21
18	18.50	9.75	**8.13**	8.25	**7.99**	**8.04**	**7.05**	7.05	**6.05**	6.05	**5.05**	5.47
19	19.50	**10.25**	**9.13**	**9.08**	**8.99**	9.04	**8.05**	**8.05**	7.05	**6.05**	6.05	**5.05**
20	20.50	20.75	10.37	9.25	9.99	**8.04**	8.05	8.05	**7.05**	7.05	**6.05**	6.05
21	21.50	**11.25**	11.37	**10.08**	**10.05**	10.05	**9.05**	**9.05**	8.05	**7.05**	7.05	**6.05**
22	22.50	22.75	**12.13**	10.25	10.99	**10.04**	9.05	9.05	**8.05**	8.05	**7.05**	7.05
23	23.50	**12.25**	12.37	**11.08**	11.32	11.04	**10.05**	**10.05**	9.05	**8.05**	8.05	**7.05**
24	24.50	24.75	**13.13**	11.25	**11.99**	**12.04**	10.05	10.05	**9.05**	9.05	**8.05**	8.05
25	25.50	**13.25**	**13.13**	**12.08**	12.32	12.04	**11.05**	**11.05**	10.05	**9.05**	9.05	**8.05**

[a] Each bold face value of n_{ki} is lowest value in its group.

TABLE 3 VALUES OF n_{ki} ONE EXTREME END SIMPLY SUPPORTED, OTHER EXTREME END CLAMPED[a]

i \ k	1	2	3	4	5	6	7	8	9	10	11	12
1	1.25	**1.08**	**1.04**	**1.02**	**1.02**	**1.01**	**1.01**	**1.01**	**1.00**	**1.00**	**1.00**	**1.00**
2	2.25	1.62	1.25	1.15	1.11	1.08	1.06	1.05	1.04	1.03	1.02	1.02
3	3.25	**2.08**	1.66	1.34	1.25	1.19	1.15	1.12	1.10	1.08	1.07	1.06
4	4.25	2.62	**2.04**	1.66	1.39	1.31	1.25	1.20	1.17	1.14	1.12	1.11
5	5.25	**3.08**	3.01	**2.02**	1.69	1.52	1.35	1.30	1.25	1.21	1.18	1.16
6	6.25	6.62	3.46	2.16	**2.02**	1.69	1.52	1.36	1.33	1.29	1.25	1.23
7	7.25	**4.08**	**3.04**	3.34	2.11	**2.01**	1.53	1.45	1.40	1.36	1.32	1.29
8	8.25	8.62	5.63	3.63	3.25	2.09	**2.01**	1.53	1.46	1.41	1.37	1.34
9	9.25	**5.08**	5.46	**3.32**	3.62	3.19	2.09	**2.01**	1.53	1.47	1.43	1.39
10	10.25	10.62	**4.04**	5.15	4.63	3.31	3.15	2.09	**2.00**	1.53	1.48	1.44
11	11.25	**6.08**	6.25	5.34	**3.02**	4.62	3.25	3.12	2.06	**2.00**	1.53	1.48
12	12.25	6.62	6.46	5.63	5.22	**3.99**	4.39	3.25	3.10	2.03	**2.00**	1.53
13	13.25	**7.08**	**5.04**	**4.02**	4.75	**3.01**	3.96	4.39	3.25	3.10	**3.01**	**2.00**
14	14.25	7.62	7.25	6.15	5.39	5.05	4.99	3.98	4.39	3.25	3.12	3.02
15	15.25	**8.08**	7.46	**6.34**	5.63	5.19	**5.01**	4.45	3.93	4.21	3.12	3.06
16	16.25	8.62	**6.04**	6.64	**4.02**	5.31	5.06	**4.02**	4.45	3.79	4.21	3.12
17	17.25	**9.08**	8.75	**7.02**	6.11	**5.07**	**5.01**	5.06	**4.02**	4.45	3.79	4.21
18	18.25	9.62	8.46	8.16	**6.25**	6.19	5.25	**5.01**	5.06	**4.02**	4.45	3.79
19	19.25	**10.08**	**7.04**	**7.34**	6.39	**6.01**	**5.25**	5.42	**5.01**	5.06	**4.02**	4.45
20	20.25	20.62	10.25	8.46	**8.02**	6.77	6.26	**5.01**	5.42	**5.01**	5.06	**4.02**
21	21.25	**11.08**	11.46	**8.04**	**8.02**	**7.01**	6.39	6.42	**5.01**	5.42	**5.01**	5.06
22	22.25	22.62	**8.04**	9.25	9.11	8.01	**7.01**	**6.01**	6.42	**5.01**	5.42	**5.01**
23	23.25	**12.08**	12.25	**9.34**	9.51	**8.01**	8.01	6.42	**6.01**	6.42	**5.01**	5.42
24	24.25	24.62	**9.04**	10.25	**9.27**	9.01	**8.01**	**7.01**	6.42	**6.01**	6.42	**5.01**
25	25.25	**13.08**	**9.04**	**7.02**	9.34	**5.01**	8.01	**4.01**	**4.01**	6.42	**6.01**	6.42

[a] Each bold face value of n_{ki} is lowest value in its group.

Appendix

EFFECT OF SHEAR DISTORTION AND OF ROTATORY INERTIA

The effect of shear distortion and of rotatory inertia is to reduce the natural frequencies. If the effect is small it may be approximated by multiplying the right-hand side of Equation [1] by the following factor[5]

[5] Derived from Equation [150], p. 342, reference 3(b).

$$[1 - n_s^2(r/l)^2(\pi^2/2)(1 + \alpha E/G)]$$

where the additional notation is

G = modulus of elasticity in shear
α = shear deflection coefficient
r = radius of gyration of beam cross section

When α and E/G are constant, the subtracted term varies as the square of the characteristic number n_s of the natural mode and as the square of the r/l ratio. Strictly speaking, the foregoing applies only to the sinusoidally shaped modes; however, it indicates the general trend in the other modes.

For a simply supported beam of rectangular cross section with $\alpha = 3/2$ and $d/l = 1/20$, where d is the depth of the beam, and taking $E/G = 8/3$, the frequency correction factor becomes

$$(1 - 0.00513\ n_s^2)$$

or 0.995 for the fundamental modes, 0.980 for all modes with $n_s = 2.00$, etc.

On the General Theory of Thin Shells

By W. R. OSGOOD[1] and J. A. JOSEPH,[2] WASHINGTON, D. C.

In the general theory of shells expressions are obtained for the changes of curvature and the twist, and revisions are introduced in the equations of equilibrium.

Introduction

In examining Love's general theory of thin plates and shells,[3] we were struck by the unsymmetrical character of his "change of curvature" τ. Langhaar[4] also recently called attention to the lack of symmetry. Other authors over a period of years in specific problems have disagreed with the use Love makes of his "change of curvature" κ_1, κ_2, and τ. Lamb,[5] back in 1890, by considerations somewhat different from those of Love, obtained expressions for these quantities that do not agree with Love's but appear to be correct.

Love's equations of equilibrium also contain inconsistencies.

It is the purpose of this paper to re-examine certain parts of the general theory of thin shells. Following Love's concepts, we shall derive expressions for the changes of curvature and the twist, and we shall present new equations of equilibrium. The notation is that of Love wherever possible.

Geometrical Considerations

It will be necessary to introduce certain components of strain and of rotation, which we begin by doing.

The middle surface of the shell in the unstrained state is regarded as a curved surface, and the families of curves which are lines of curvature are designated by α = const and β = const. The lengths of linear elements of the lines of curvature are $Bd\beta$ and $Ad\alpha$, respectively, where A and B are, in general, functions of α, β. In the deformed state, "the curves that were lines of curvature become two families of curves, traced on the strained middle surface, which cut each other at an angle that may differ slightly from a right angle."[3] We denote the cosine of the angle by $\bar{\omega}$ and recognize it as the shearing strain corresponding with the directions of α and β, and we denote by e_1 and e_2 the linear strains of elements which lie along the curves β = const and α = const. Love shows that

$$\left.\begin{aligned} e_1 &= \frac{1}{A}\frac{\partial u}{\partial \alpha} + \frac{v}{AB}\frac{\partial A}{\partial \beta} - \frac{w}{R_1'} \\ e_2 &= \frac{1}{B}\frac{\partial v}{\partial \beta} + \frac{u}{AB}\frac{\partial B}{\partial \alpha} - \frac{w}{R_2'} \\ \bar{\omega} &= \frac{1}{A}\frac{\partial v}{\partial \alpha} + \frac{1}{B}\frac{\partial u}{\partial \beta} - \frac{u}{AB}\frac{\partial A}{\partial \beta} - \frac{v}{AB}\frac{\partial B}{\partial \alpha} \end{aligned}\right\} \quad \ldots [1]$$

where "u, v, w denote the components of displacement of any point on the unstrained middle surface referred to the tangents at the point to the curves β = const and α = const, and the normal at the point to the surface,"[3] and R_1, R_2 denote the principal radii of curvature of the unstrained surface, R_1 being associated with the curve β = const.

We now introduce in the strained shell a right-handed system of moving axes of x, y, z with the origin at a point (α, β) of the middle surface, the axis of z normal to the surface, the axis of x tangent to the curve β = const, and the axis of y tangent to the surface and at right angles to the axis of x.[6] When the origin of this system of axes moves in the direction of α, i.e., along the curve β = const, the directions of the axes change. The components of rotation of the system, referred to the instantaneous positions of the axes of x, y, z, are denoted by $p_1'd\alpha$, $q_1'd\alpha$, $r_1'd\alpha$, so that p_1', q_1', r_1' are the components of the rate of rotation. Otherwise stated, p_1', q_1', r_1' are the components of the rate of rotation of the normal section β = const of the shell as one proceeds in the direction of α. When the origin of the system of axes moves along the curve α = const, the components of rotation, referred to the instantaneous positions of the axes of x, y, z, are denoted by $p_2'd\beta$, $q_2'd\beta$, $r_2'd\beta$, that is, p_2', q_2', r_2' are the components of the rate of rotation of the normal sections β = const of the shell as one proceeds along α = const in the direction of β. Note that p_2', q_2', r_2' are not the analogs of p_1', q_1', r_1'. Love shows that[7]

$$\left.\begin{aligned} p_1' &= \frac{\partial}{\partial \alpha}\left(\frac{1}{B}\frac{\partial w}{\partial \beta} + \frac{v}{R_2}\right) - \frac{1}{B}\frac{\partial A}{\partial \beta}\left(\frac{1}{A}\frac{\partial w}{\partial \alpha} + \frac{u}{R_1}\right) \\ &\quad - \frac{1}{R_1}\left(\frac{\partial v}{\partial \alpha} - \frac{u}{B}\frac{\partial A}{\partial \beta}\right) \\ q_1' &= -\frac{A}{R_1} - \frac{\partial}{\partial \alpha}\left(\frac{1}{A}\frac{\partial w}{\partial \alpha} + \frac{u}{R_1}\right) \\ &\quad - \frac{1}{B}\frac{\partial A}{\partial \beta}\left(\frac{1}{B}\frac{\partial w}{\partial \beta} + \frac{v}{R_2}\right) \\ r_1' &= -\frac{1}{B}\frac{\partial A}{\partial \beta} + \frac{\partial}{\partial \alpha}\left(\frac{1}{A}\frac{\partial v}{\partial \alpha} - \frac{u}{AB}\frac{\partial A}{\partial \beta}\right) \\ &\quad + \frac{A}{R_1}\left(\frac{1}{B}\frac{\partial w}{\partial \beta} + \frac{v}{R_2}\right) \end{aligned}\right\} \quad \ldots [2]$$

[1] Senior Research Engineer, Armour Research Foundation, formerly Senior Structural Engineer, David Taylor Model Basin. Mem. ASME.

[2] Operations Analyst, Headquarters United States Air Force.

[3] "A Treatise on the Mathematical Theory of Elasticity," by A. E. H. Love, Dover Publications, New York, N. Y., 1944, chapt. 24.

[4] "A Strain-Energy Expression for Thin Elastic Shells," by H. L. Langhaar, Trans. ASME, vol. 71, 1949, p. 183.

[5] "On the Deformation of an Elastic Shell," by Horace Lamb, Proceedings of the London Mathematical Society, vol. 21, 1891, p. 119.

Presented at the Annual Conference of the Applied Mechanics Division, Purdue University, Lafayette, Ind., June 22–24, 1950, of The American Society of Mechanical Engineers. Manuscript received by the Applied Mechanics Division September 2, 1949. Paper No. 50—APM-14.

[6] The α,β-system of co-ordinates is considered to be embedded in the shell; once an α-line, always an α-line!

[7] In passing, attention is called to the first two of Love's Equations [11].[3] An error evidently has been introduced in editions subsequent to the first (1893); in the first edition these equations correctly contain an additional term in each, to read

$$r_1' = \frac{\partial \bar{\omega}}{\partial \alpha} + \frac{\bar{\omega}}{B}\frac{\partial B}{\partial \alpha} - (1 + e_1 - e_2)\frac{1}{B}\frac{\partial A}{\partial \beta} - \frac{A}{B}\frac{\partial e_1}{\partial \beta}$$

$$r_2' = -\frac{\bar{\omega}}{A}\frac{\partial A}{\partial \beta} + (1 - e_1 + e_2)\frac{1}{A}\frac{\partial B}{\partial \alpha} + \frac{B}{A}\frac{\partial e_2}{\partial \alpha}$$

Only in this form do they agree with the expressions for r_1' and r_2' in the sets of Equations [2] and [3] herewith.

Discussion of this paper should be addressed to the Secretary, ASME, 29 West 39th Street, New York, N. Y., and will be accepted until January 10, 1951, for publication at a later date. Discussion received after the closing date will be returned.

and

$$\left.\begin{aligned} p_2' &= \frac{B}{R_2} + \frac{\partial}{\partial\beta}\left(\frac{1}{B}\frac{\partial w}{\partial\beta} + \frac{v}{R_2}\right) \\ &\quad + \frac{1}{A}\frac{\partial B}{\partial\alpha}\left(\frac{1}{A}\frac{\partial w}{\partial\alpha} + \frac{u}{R_1}\right) \\ q_2' &= -\frac{\partial}{\partial\beta}\left(\frac{1}{A}\frac{\partial w}{\partial\alpha} + \frac{u}{R_1}\right) + \frac{1}{A}\frac{\partial B}{\partial\alpha}\left(\frac{1}{B}\frac{\partial w}{\partial\beta} + \frac{v}{R_2}\right) \\ &\quad - \frac{B}{AR_2}\left(\frac{\partial v}{\partial\alpha} - \frac{u}{B}\frac{\partial A}{\partial\beta}\right) \\ r_2' &= \frac{1}{A}\frac{\partial B}{\partial\alpha} + \frac{\partial}{\partial\beta}\left(\frac{1}{A}\frac{\partial v}{\partial\alpha} - \frac{u}{AB}\frac{\partial A}{\partial\beta}\right) \\ &\quad - \frac{B}{R_2}\left(\frac{1}{A}\frac{\partial w}{\partial\alpha} + \frac{u}{R_1}\right) \end{aligned}\right\} \quad \ldots [3]$$

If now the usual assumption is made, according to which the linear elements of the shell that are initially normal to the unstrained middle surface remain straight, become normal to the strained middle surface, and suffer no extension, then it can be shown that the components of strain referred to the directions of x and y are[6]

$$\left.\begin{aligned} e_{xx} &= \frac{1}{1 - z/R_1}\left[e_1 + z\left(\frac{1}{R_1} + \frac{q_1'}{A}\right)\right] \\ e_{yy} &= \frac{1}{1 - z/R_2}\left[e_2 + z\left(\frac{1}{R_2} - \frac{p_2'}{B}\right)\right] \\ e_{xy} &= \frac{\tilde{\omega}}{1 - z/R_2} + z\left[\frac{q_2'}{B(1 - z/R_2)} - \frac{p_1'}{A(1 - z/R_1)}\right] \end{aligned}\right\} \quad \ldots [4]$$

or to first powers in z

$$\left.\begin{aligned} e_{xx} &= e_1 + z\left[(1 + e_1)\frac{1}{R_1} + \frac{q_1'}{A}\right] \\ e_{yy} &= e_2 + z\left[(1 + e_2)\frac{1}{R_2} - \frac{p_2'}{B}\right] \\ e_{xy} &= \tilde{\omega} + z\left(\frac{\tilde{\omega}}{R_2} + \frac{q_2'}{B} - \frac{p_1'}{A}\right) \end{aligned}\right\} \quad \ldots\ldots [5]$$

Changes of Curvature and Twist

If we define k_1, k_2, and $2t$ as the negatives of the coefficients of z in the expressions for e_{xx}, e_{yy}, and e_{xy}, respectively, we have

$$\left.\begin{aligned} e_{xx} &= e_1 - zk_1 \\ e_{yy} &= e_2 - zk_2 \\ e_{xy} &= \tilde{\omega} - 2zt \end{aligned}\right\} \quad \ldots\ldots [6]$$

On expanding k_1, k_2, and t in terms of the components of the displacements by means of Equations [1], [2], and [3], we find

$$\left.\begin{aligned} k_1 &= \frac{u}{A}\frac{\partial}{\partial\alpha}\left(\frac{1}{R_1}\right) + \left(\frac{1}{R_1} - \frac{1}{R_1}\right)\frac{v}{AB}\frac{\partial A}{\partial\beta} \\ &\quad + \frac{1}{A}\frac{\partial}{\partial\alpha}\left(\frac{1}{A}\frac{\partial w}{\partial\alpha}\right) + \frac{1}{AB^2}\frac{\partial A}{\partial\beta}\frac{\partial w}{\partial\beta} + \frac{w}{R_1^2} \\ k_2 &= \left(\frac{1}{R_1} - \frac{1}{R_2}\right)\frac{u}{AB}\frac{\partial B}{\partial\alpha} + \frac{v}{B}\frac{\partial}{\partial\beta}\left(\frac{1}{R_2}\right) \\ &\quad + \frac{1}{A^2B}\frac{\partial B}{\partial\alpha}\frac{\partial w}{\partial\alpha} + \frac{1}{B}\frac{\partial}{\partial\beta}\left(\frac{1}{B}\frac{\partial w}{\partial\beta}\right) + \frac{w}{R_2^2} \\ t &= \frac{1}{2B}\left[\frac{\partial}{\partial\beta}\left(\frac{u}{R_1}\right) - \frac{1}{R_2}\frac{\partial u}{\partial\beta}\right] + \frac{1}{2A}\left[\frac{\partial}{\partial\alpha}\left(\frac{v}{R_2}\right)\right. \\ &\quad \left. - \frac{1}{R_1}\frac{\partial v}{\partial\alpha}\right] + \frac{1}{AB}\left(\frac{\partial^2 w}{\partial\alpha\,\partial\beta} - \frac{1}{A}\frac{\partial A}{\partial\beta}\frac{\partial w}{\partial\alpha} - \frac{1}{B}\frac{\partial B}{\partial\alpha}\frac{\partial w}{\partial\beta}\right) \end{aligned}\right\} \quad \ldots [7]$$

These equations take the place of Love's Equations [26] for κ_1, κ_2, and τ; in particular, the expression for the twist t is self-symmetrical. The equations agree with Love's equations only when the deformation of the middle surface is inextensional, that is, when $e_1 = e_2 = \tilde{\omega} = 0$. Equations [7] are equivalent to corresponding expressions obtained by Lamb.[5] If the radical in the fourth of Langhaar's Equations [11][4] is expanded by the binomial theorem, the negative of the coefficient of z in his equation is $2t$.

Equations of Equilibrium

We turn now to the equations of equilibrium. They are obtained by considering the equilibrium of an element of the shell bounded by the faces and by the surfaces formed by the aggregates of the normals drawn to the middle surface at points of a curvilinear quadrilateral, which is made up of two neighboring arcs of each of the families of curves α and β. We denote the bounding curves of the curvilinear quadrilateral by α, $\alpha + \delta\alpha$,

[6] Equations [4] can be obtained by equating coefficients of l^2, m^2, and lm in Love's Equation [29] and his preceding equation for r_1^2, and putting ξ, η, and ζ, and their derivatives equal to zero.

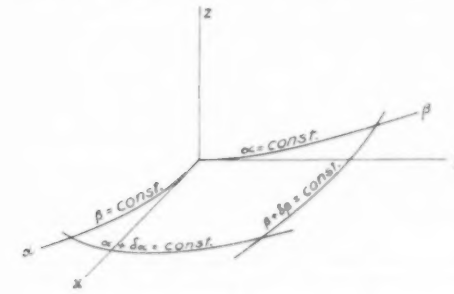

Fig. 1

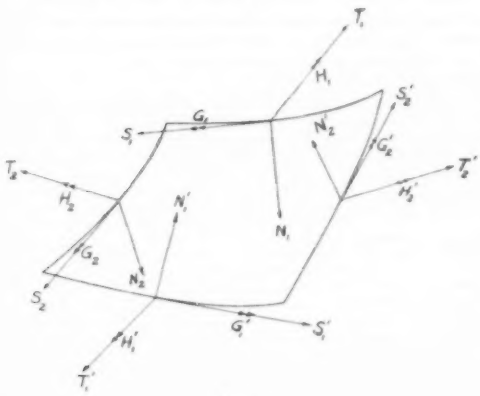

Fig. 2

β, $\beta + \delta\beta$. Fig. 1 shows the middle surface of such an element in the unstrained state with fixed axes of x, y, z which coincide with the tangents to β and α at their point of intersection and the normal to the middle surface at this point. Fig. 2 shows the middle surface of the same element in the strained state with the stress-resultants T, S, and N and the stress-couples G and H, those acting on the edges $\alpha + \delta\alpha$ and $\beta + \delta\beta$ being distinguished by primes.

In writing the equations of equilibrium of the element, the components of rotation of one edge relative to the opposite edge enter. The components of rotation of the edge $\beta + \delta\beta$ relative to the edge β are

$$p_2'\delta\beta, \quad q_2'\delta\beta, \quad r_2'\delta\beta$$

The components of rotation of the edge $\alpha + \delta\alpha$ relative to the edge α can be expressed similarly as

$$p_1'\delta\alpha, \quad q_1'\delta\alpha, \quad r_1'\delta\alpha,$$

where p_1', q_1', r_1' are analogous to p_2', q_2', r_2'. In fact, p_1', q_1', and r_1' are symmetrically related to q_2', p_2', and r_2', respectively (actually $q_1' = q_1'$). Thus from Equations [3] we may write immediately

$$\left.\begin{aligned}
&\frac{\partial(T_1B)}{\partial\alpha} - \frac{\partial(S_2A)}{\partial\beta} - (r_1'S_1B + r_2'T_2A) + (q_1'N_1B + q_2'N_2A) + ABX' = 0\\
&\frac{\partial(S_1B)}{\partial\alpha} + \frac{\partial(T_2A)}{\partial\beta} - (p_1'N_1B + p_2'N_2A) + (r_1'T_1B - r_2'S_2A) + ABY' = 0\\
&\frac{\partial(N_1B)}{\partial\alpha} + \frac{\partial(N_2A)}{\partial\beta} - (q_1'T_1B - q_2'S_2A) + (p_1'S_1B + p_2'T_2A) + ABZ' = 0
\end{aligned}\right\} \quad \ldots [9]$$

$$\left.\begin{aligned}
&\frac{\partial(H_1B)}{\partial\alpha} - \frac{\partial(G_2A)}{\partial\beta} - (G_1Br_1' + H_2Ar_2') + (N_2 + L')AB + N_1ABm_1 = 0\\
&\frac{\partial(G_1B)}{\partial\alpha} + \frac{\partial(H_2A)}{\partial\beta} + (H_1Br_1' - G_2Ar_2') - (N_1 - M')AB - N_2ABl_2 = 0\\
&G_1Bp_1' + G_2Aq_2' - (H_1Bq_1' - H_2Ap_2') + (S_1 + S_2)AB + (T_2 - T_1)AB\bar{\omega} = 0
\end{aligned}\right\} \quad \ldots [10]$$

$$\left.\begin{aligned}
p_1' &= \frac{\partial}{\partial\alpha}\left(\frac{1}{B}\frac{\partial w}{\partial\beta} + \frac{v}{R_2}\right) - \frac{1}{B}\frac{\partial A}{\partial\beta}\left(\frac{1}{A}\frac{\partial w}{\partial\alpha} + \frac{u}{R_1}\right)\\
&\quad + \frac{A}{BR_1}\left(\frac{\partial u}{\partial\beta} - \frac{v}{A}\frac{\partial B}{\partial\alpha}\right)\\
q_1' &= -\frac{A}{R_1}\frac{\partial}{\partial\alpha}\left(\frac{1}{A}\frac{\partial w}{\partial\alpha} + \frac{u}{R_1}\right)\\
&\quad - \frac{1}{B}\frac{\partial A}{\partial\beta}\left(\frac{1}{B}\frac{\partial w}{\partial\beta} + \frac{v}{R_2}\right)\\
r_1' &= -\frac{1}{B}\frac{\partial A}{\partial\beta} - \frac{\partial}{\partial\alpha}\left(\frac{1}{B}\frac{\partial u}{\partial\beta} - \frac{v}{AB}\frac{\partial B}{\partial\alpha}\right)\\
&\quad + \frac{A}{R_1}\left(\frac{1}{B}\frac{\partial w}{\partial\beta} + \frac{v}{R_2}\right)
\end{aligned}\right\} \quad \ldots [8]$$

When the deformation of the middle surface is inextensional, p_1', q_1', r_1' are equal to p_1', q_1', r_1', respectively.

We may now express the conditions of equilibrium of the element by resolving the stress resultants on the edges in the direction of the axes of x, y, z in the conventional manner.[3] In addition to the terms obtained by Love there should be included in the equations of moments three more terms arising from the shearing deformation and the rotation. Such terms are introduced by Sanden and Tölke[3] but, we believe, incorrectly. The terms are N_1ABm_1, $-N_2ABl_2$, and $(T_2 - T_1)AB\bar{\omega}$, where m_1 and l_2 are, respectively, the rotations about the axis of z of the edges β = const and α = const of the element

$$m_1 = \frac{1}{A}\frac{\partial w}{\partial\alpha} - \frac{u}{AB}\frac{\partial A}{\partial\beta}, \quad l_2 = \frac{1}{B}\frac{\partial u}{\partial\beta} - \frac{v}{AB}\frac{\partial B}{\partial\alpha}.$$

m_1 is given on page 522 of Love[3] and l_2 is the symmetrical expression for the other edge. We arrive finally at the equations of equilibrium

where X', Y', Z', and L', M' denote the components, parallel to the axes of x, y, z, of the forces and couple-resultant of the externally applied forces per unit of area of the middle surface. Equations [9] and [10] differ from Love's Equations [45] and [46] in that they contain besides the additional terms mentioned, the components p_1', q_1', r_1' of the rate of rotation as defined by Equation [8] rather than the components p_1', q_1', r_1' defined by Equations [2] ($q_1' = q_1'$). When the deformation of the middle surface is inextensional and irrotational, Equations [9] and [10] reduce to Love's Equations [45] and [46].

The literature contains many solutions of problems of shells in which inextensibility is assumed in part of a solution and extensibility in another part of the same solution. Solutions of this kind may be justified when the extension of the middle surface is sufficiently small or when, on the basis of experience and sequentially acquired intuition, the investigator knows what he is about; but it is at least more logical to carry a solution through, if possible, with inextensibility assumed throughout or with extensibility assumed either throughout or at least consistently. Equations [7], [8], [9], and [10] give in general form the new information needed for extensional solutions.

[3] "Über Stabilitätsprobleme dünner, kreiszylindrischer Schalen," by K. v. Sanden and F. Tölke, *Ingenieur-Archiv*, vol. 3, 1932, p. 24.

NOTE: Statements and opinions advanced in papers are to be understood as individual expressions of their authors and not those of the Society.

Momentum and Mass Transfer in Coaxial Gas Jets[1]

By WALTON FORSTALL, JR.,[2] and ASCHER H. SHAPIRO,[3] CAMBRIDGE, MASS.

The mixing at constant pressure of a circular jet with an annular coaxial stream has been studied for conditions of nearly common density and temperature, but differing initial velocities. By using 10 per cent by volume of helium as a tracer in the inner stream, the mixing region was mapped with respect to both material and momentum transfer. It is concluded that material diffuses more rapidly than momentum; that the principal independent variable determining the shape of the mixing region is the velocity ratio of the streams; and that the integral method of Squire and Trouncer, using experimentally determined constants, is adequate for predicting approximate values of concentration and velocity in the mixing region of a jet flowing into a moving medium of the same density. Data for widely different experiments of various investigators show that the turbulent Prandtl and the Schmidt numbers are both within ±10 per cent of 0.70, independent of the nature of the experiment and the magnitudes of the laminar Prandtl and Schmidt numbers.

Nomenclature

The following nomenclature is used in the paper (see also Fig. 1):

- a = radius of primary-jet nozzle
- c = mixing length coefficient from Squire and Trouncer (see Bibliography ref. 66)
- c_p = specific heat at constant pressure
- D = diameter of primary-jet nozzle ($2a$), also laminar coefficient of mass diffusion
- D_t = turbulent coefficient of mass diffusion
- f = a function
- k = laminar coefficient of heat conductivity
- k_t = turbulent coefficient of heat conductivity
- L = value of x/D for end of potential core
- N_A = mass flow by diffusion, concentration per unit time per unit area
- Q_A = heat flow, energy per unit time per unit area
- r = radial distance from jet axis
- $r_{m v}$ = radius where velocity is arithmetic average of its value on axis and in secondary stream, for a given x
- $r_{m \xi}$ = radius where concentration is one half the axial concentration at a given x
- $r_{o v}$ = radius of outer edge of velocity profile
- $r_{o \xi}$ = radius of outer edge of concentration profile
- T = temperature, deg F abs
- U = time average velocity in axial direction
- U_c = velocity on axis at a given x
- U_p = velocity of primary stream at $x = 0$
- U_s = velocity of undisturbed secondary stream
- x = axial distance downstream from jet exit measured parallel to axis
- y = distance perpendicular to x-direction
- λ = velocity ratio, U_s/U_p
- μ = viscosity
- ν = kinematic viscosity
- ν_t = turbulent coefficient of kinematic viscosity
- ξ = concentration of helium by volume
- π = number of radians in a semicircle
- ρ = density
- σ = dimensionless slope coefficient, defined by Equations [4] and [5]
- τ = shear stress

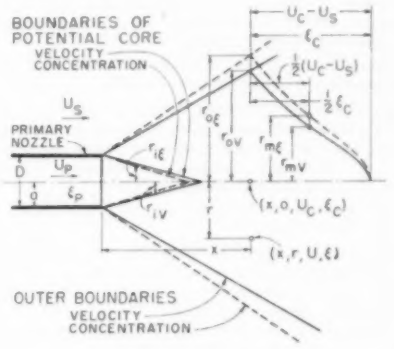

Fig. 1 Sketch Illustrating Nomenclature

Introduction

Nature of Problem. The spreading of a jet, such as in the mixing of two coaxial streams, is of interest from at least two viewpoints: (*a*) Its study should lead to a better understanding of free turbulence and the mechanism of turbulent diffusion. (*b*) The information obtained can be used in certain fields of engineering design, for example, combustion chambers, jet pumps, thrust augmenters, mixing tanks, and the disposal of waste gases.

The subject of spreading of jets may be subdivided according to the following classifications, where items in italics indicate conditions applying to the tests reported here:

[1] This paper is based on "Material and Momentum Transfer in Coaxial Gas Streams," by Walton Forstall, Jr., Sc.D. thesis in Department of Mechanical Engineering, Massachusetts Institute of Technology, June, 1949.

[2] Formerly Research Associate in Mechanical Engineering, Gas Turbine Laboratory, Massachusetts Institute of Technology. Now Associate Professor of Mechanical Engineering, Carnegie Institute of Technology, Pittsburgh, Pa. Jun. ASME.

[3] Associate Professor of Mechanical Engineering, Massachusetts Institute of Technology. Mem. ASME.

Presented at the Annual Conference of the Applied Mechanics Division, Purdue University, Lafayette, Ind., June 22–24, 1950, of The American Society of Mechanical Engineers.

Discussion of this paper should be addressed to the Secretary, ASME, 29 West 39th Street, New York, N. Y., and will be accepted until January 10, 1951, for publication at a later date. Discussion received after the closing date will be returned.

Note: Statements and opinions advanced in papers are to be understood as individual expressions of their authors and not those of the Society. Manuscript received by the Applied Mechanics Division July 28, 1949. Paper No 50—APM-13.

Geometry of flow (see sketches in Table 1)
- Two-dimensional planar
  - Doubly infinite
  - Symmetric
- *Three-dimensional axially symmetric*

Secondary stream
- Stationary
- *Moving*

Primary and secondary streams
- Alike
- Different as to
  - *Velocity*
  - *Chemical composition*
  - Temperature
  - Density

Diffusing property
- *Momentum*
- *Material*
- Temperature

Initial turbulence
- Primary stream
- Secondary stream
- *No initial turbulence*

State of mixing region
- Laminar
- *Turbulent*

Previous Work. For the convenience of workers in this field, an extensive Bibliography is given at the end of the paper,[4] covering the most important analytical and experimental work related to the fields of mixing and jets. Table 1 is presented as a guide to the Bibliography and as an indication of how previous work falls into the classifications of the foregoing outline.

Analytical. The three principal lines of analytical attack on the jet spreading problem may be outlined briefly as follows:

1 Point-source diffusion of momentum, material, or temperature, using equations and solutions well known from the study of heat flow (67, 75, 76, 84).[4] This method is valid only at distances downstream from the point of initial mixing which are large compared to the initial jet width.

2 Boundary-layer form of the Navier-Stokes equations, into which are inserted various transport theories.

(*a*) Momentum transport, using the mixing-length concept.
(*b*) Vorticity transport, using the mixing-length concept.
(*c*) Constant exchange coefficient, using the concepts of "turbulent" coefficients of viscosity, thermal conductivity, and diffusion.
(*d*) Kármán similarity theory.
(*e*) Statistical theory.

Most of the extensive literature on jets and wakes is concerned with this approach. For an excellent summary of the mathematical steps and the assumptions involved in each of the theories just listed, see reference (65).

3 Integral equations of motion (Kármán momentum equations). (See references 4, 17, 18, 38, 53, 54, 66).

All these approaches have been of some utility in studying the various types of jet problems. However, for the case we are concerned with here, that of two moving streams which are axially symmetric, only the third approach has thus far proved practical. The resulting solution, first worked out for the velocity field by Squire and Trouncer (66), is therefore the most suitable for comparison with experimental results. Briefly, the method and its premises are as follows:

The equations of motion are written in integral form by equating the change in total momentum flux between two adjacent transverse sections of the jet to the turbulent shear stress acting on the jet between these sections. In evaluating the momentum flux at various sections, Squire and Trouncer made two assumptions, namely, (*a*) that the velocity profile in dimensionless form is identical for all values of x, and (*b*) that the velocity profile plausibly may be represented by a cosine curve. For determining the turbulent shear stress, they assumed in essence that this stress is proportional to the square of the difference in velocities between the center and edge of the jet. With these premises, the entire velocity field is worked out in terms of the ratio of stream velocities and one proportionality constant which must be determined experimentally. The validity of these premises and the question of variation of shear-stress proportionality constant with stream velocity ratio will be examined in the light of the experimental data of this paper.

Experimental. Table 1 shows that scarcely any experimental work has been done on the important practical case of two round moving jets and, in particular, no comparisons of material and momentum transfer for this case have been made. Most of the previous researches have been concerned with a single jet discharging into a stationary medium, and the most common measurements of mixing have been in respect to velocity and temperature.

Objectives. 1 To obtain useful design information for the transfer of momentum and mass between two coaxial gas streams.

2 To enlarge the understanding of the mechanism of turbulent mixing.

3 To test experimentally the analytical formulation of Squire and Trouncer.

Acknowledgments

This work was carried out as part of the Guided Missiles Program at the Massachusetts Institute of Technology, under sponsorship of the Navy Department, Bureau of Ordnance. The help of Mr. Dumont Rush and of the staff of the M.I.T. Gas Turbine Laboratory is gratefully acknowledged.

Method of Investigation

Description of Apparatus and Techniques. The apparatus was designed and constructed to permit measurement of material and momentum transfer from a circular jet (primary) into an annular stream (secondary). The secondary stream was room air at normal pressure and temperature, and the primary stream was room air at normal pressure and temperature with about 10 per cent by volume of helium added as a tracer. A schematic flow diagram is shown in Fig. 2.

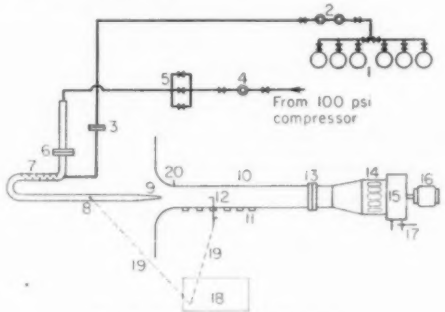

Fig. 2 Schematic Flow Diagram

(Helium tanks at 2000 psia 1, helium reducing valves 2, orifice for monitoring helium flow 3, primary-air reducing valve 4, primary-air control manifold 5, orifice for monitoring primary air 6, baffles for mixing helium and primary air 7, primary mixture-sampling probe 8, primary nozzle 9, 4-in-diam mixing tunnel 10, access holes for Pitot tube and sampling probe 11, Pitot tube 12, metering orifice for tunnel flow 13, by-pass holes at blower inlet 14, centrifugal blower 15, motor 16, blast gate at blower discharge 17, helium-analysis bench 18, sampling lines 19, static-pressure tap 20.)

[4] Numbers in parentheses refer to the Bibliography at the end of the paper.

TABLE 1 BIBLIOGRAPHICAL CHART OF PREVIOUS WORK ON JETS

	Year	Reference Number	TWO DIMENSIONAL PLANAR												THREE DIMENSIONAL					
			DOUBLY INFINITE						SYMMETRIC						AXIALLY SYMMETRIC					
			NO SECOND.			WITH SECOND.			NO SECOND.			WITH SECOND.			NO SECOND.			WITH SECOND.		
			ξ	U	T	ξ	U	T	ξ	U	T	ξ	U	T	ξ	U	T	ξ	U	T
ZIMM	1921	82														E				
BETZ	1923	7														E				
TOLLMIEN	1926	73		A						A						A				
RUDEN	1933	56														E	E			
SCHLICHTING	1933	59								A						A				
FÖRTHMANN	1934	27		E						E										
BROWN	1935	89							E											
KUETHE	1935	35					A									B				
ABRAMOVICH	1935	I		A						A						A				
PREDVODITELEV	1936	50														E				
BICKLEY	1937	8								A										
BICKNELL	1937	85							E	E										
HOWARTH	1938	32								A	A					A	A			
TOMOTIKA	1938	74														A				
ABRAMOVICH	1939	3		A	A															
VOORHEIS	1939	80														E				
LIN	1940	39								A	A					A	A			
REICHARDT	1941	52		A																
VICTORIN	1941	78																	E	
SCHMIDT	1941	61								A	A					B	B			
GÖRTLER	1942	30					A			A										
BINNIE	1942	9													E					
REICHARDT	1942	53								A						A				
CORRSIN	1943	16														E	E			
McELROY	1943	43														E				
SQUIRE	1944	66																	A	
PABST	1944	46																	E	E
SZABLEWSKI	1944	69														B				
TUVE	1945	77								E						E				
SQUIRE	1945	65					A	A		A	A					A	A			
CLEEVES	1946	14														E	E			
LENHART	1946	36													E					
RIBNER	1946	54																	A	
CHOU	1947	12								A										
CITRINI	1947	13														E				
DEODATI	1947	18																	A	
LIEPMANN	1947	38		B																
HINZE	1948	31													B	B	B			
ROUSE	1948	4								B						B				
CHAPMAN	1948	10		A																
CORRSIN	1948	17														B	B			
BARON	1948	84													A	A	A			
TAYLOR, J.F.	1948	88														E				
ALEXANDER	1948	83														E				

A Mathematical analysis
E Experimental investigation
B Both analytical and experimental

ξ Diffusion of material
U Diffusion of momentum
T Diffusion of temperature

"Second." refers to a secondary stream which is moving.
Reference number refers to the listing in the bibliography.

The tunnel was a 4-in-diam copper tube, mounted horizontally, with a baffle board and rounded entrance to provide a uniform flat velocity profile for the secondary air streaming in from the room. The tunnel exit was connected to the inlet of a single-stage centrifugal blower. Eighteen small access holes spaced axially 2 in. apart permitted the insertion of a Pitot tube into the tunnel.

For the primary jet, air was supplied from a compressor and helium from a bank of six bottles. The air and helium were thoroughly mixed by a series of baffles in the piping and emerged into the secondary stream from either of two interchangeable nozzles, one being 1/4 in. diam., the other, 1 in. diam.

Each primary nozzle had a smooth transformation from the 2-in. pipe line to which it was attached, and the latter contained a honeycomb so as to produce a uniform stream approaching the nozzle. Thus, except for small unavoidable boundary layers on the inside and outside of the primary nozzle, both jets had flat velocity profiles at the beginning of mixing.

The Pitot-static tube used for velocity and concentration traverses was 0.065 in. OD stainless steel, with four 0.010-in-ID static holes and a 0.020-in-ID impact hole. The Pitot tube was clamped into a specially designed micrometer screw traversing mechanism graduated in 0.001 in.

Samples were withdrawn from the stream through the impact hole of the Pitot tube and passed into apparatus suitable for determining the helium content. This measurement was carried out in a standard thermal conductivity cell manufactured by Leeds and Northrup and used in a circuit developed for this investigation (57). The accuracy of helium measurement was about one part in a thousand.

Since helium has an unusually large laminar coefficient of mass diffusion, it was suspected that the use of helium as a tracer might give an exaggerated picture of turbulent mass transfer. However, calculations for some typical runs showed that the experimental coefficient of diffusion is of the order of 30 sq cm per sec, as compared with the laminar coefficient of 0.45 sq cm per sec, thus demonstrating that molecular diffusion played an insignificant role compared with turbulent diffusion. This conclusion is further supported by the work of Hinze (31).

Range of Experimental Variables. For various values of primary and secondary velocity, measurements of velocity and concentration were made at a large number of points throughout the mixing region and extending downstream as far as 136 jet diameters. Table 2 gives the velocities employed in each of five series of runs.

TABLE 2 VELOCITIES USED IN FIVE SERIES OF RUNS

Series	U_p fps	U_s fps	U_s/U_p	$U_p - U_s$ fps	$1/2(U_p + U_s)$ fps
C	180	90	0.50	90	135
D	120	90	0.75	30	105
E	120	30	0.25	90	75
F	90	45	0.50	45	67.5
G	225	45	0.20	180	135

Results

Profile Shapes. Fig. 3 illustrates typical experimental data arranged in the form of velocity and concentration profiles. Faired curves were drawn through the observed points, and these curves were used in all subsequent calculations.

To compare shapes, the profiles were made dimensionless and normalized by plotting $(U - U_s)/(U_c - U_s)$ and ξ/ξ_c versus $r/r_{m\tau}$ and $r/r_{m\xi}$, respectively. When fully normalized in this manner, all profiles downstream from the end of the potential core were strikingly similar, both for velocity and concentration. Furthermore, this profile shape may be represented rather well by any one of several simple mathematical expressions, as illustrated in Figs. 4(*a*), (*b*), and (*c*). The shaded region is the same

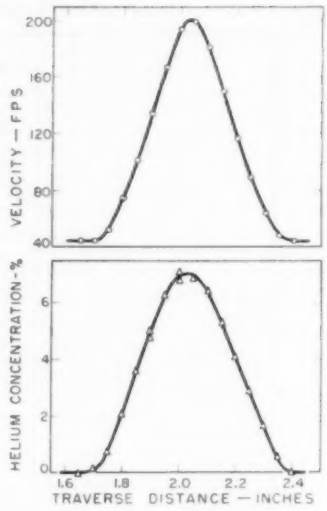

Fig. 3 Typical Velocity and Concentration Data Found From a Radial Traverse, and Plotted in Form of Velocity and Concentration Profiles

(Data shown here were obtained with the 1/4-in. primary nozzle, at $x/D = 8$, with $U_p = 225$ fps, and $U_s = 45$ fps.)

in all the charts and includes all the points from all the velocity and concentration profiles of series G, for values of x/D larger than 6. This composite profile is compared with the following mathematical representations, which are shown as broad lines in each figure:

Fig. 4(*a*) (cosine curve)

$$\frac{U - U_s}{U_c - U_s} = \frac{1}{2}\left(1 + \cos\frac{\pi r}{2r_{m\tau}}\right); \quad \sigma = 1.57 \qquad [1]$$

Fig. 4(*b*) (three-halves power curve)

$$\frac{U - U_s}{U_c - U_s} = \left[1 - 0.293\left(\frac{r}{r_{m\tau}}\right)^{3/2}\right]^3; \quad \sigma = 1.37 \qquad [2]$$

Fig. 4(*c*) (error curve)

$$\frac{U - U_s}{U_c - U_s} = \left[\frac{1}{2}\right]^{(r/r_{m\tau})^2}; \quad \sigma \leqq 1.39 \qquad [3]$$

It should be noted that the broadening of the shaded band near the base of the experimental profiles is not significant, because the experimental accuracy in determining $(U - U_s)$ and ξ is very poor near the edge of the jet. With this in mind, the following conclusions may be reached:

(*a*) The fully normalized velocity and concentration profiles are substantially alike in shape.

(*b*) Both the fully normalized velocity and concentration profiles have shapes which are substantially independent of x/D.

(*c*) The data for series C, D, E, and F, which for brevity are not included here, show that the shape of the fully normalized velocity and concentration profiles is independent of velocity ratio.

(*d*) Fig. 4(*a*) justifies the Squire and Trouncer assumption of a cosine profile, especially when it is remembered that previous work on many similar problems using the integral momentum

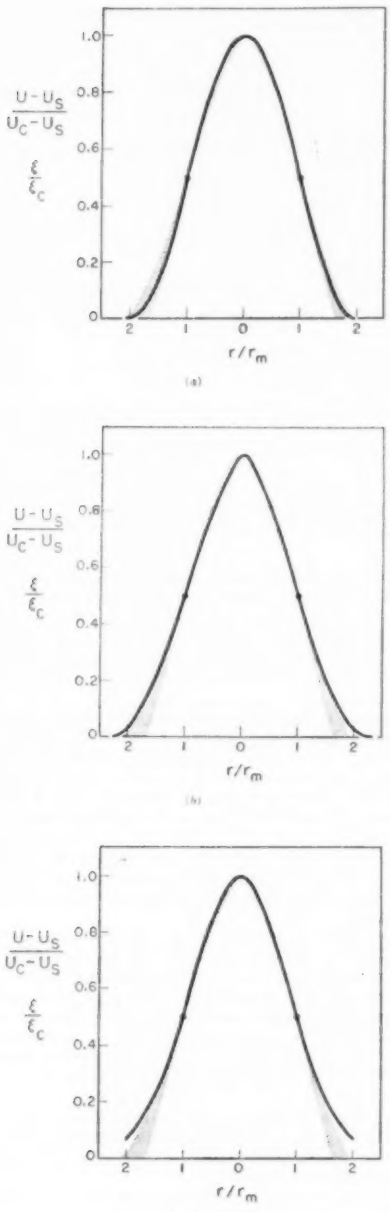

FIG. 4 NORMALIZED VELOCITY AND CONCENTRATION PROFILES

(Shaded band is identical for all three charts and includes all velocity and concentration data for series G, for values of x/D greater than 6. Heavy lines represent mathematical curves, as follows: *a*, cosine curve Equation [1]; *b*, three-halves power curve, Equation [2]; *c*, error curve, Equation [3].)

equations has shown that the results are insensitive to the shape of the assumed profile.

Slope Coefficients. Since the slope is a delicate test of shape, and since the Squire and Trouncer method uses the value of profile slope at the half-radius, it was thought desirable to examine the behavior of profile slopes at $r_v/2$. In terms of the radius, the equations for velocity and concentration are

$$\frac{U - U_s}{U_c - U_s} = f\left(\frac{r}{r_{v\sigma}}\right) \quad \ldots\ldots [4a]$$

$$\frac{\xi}{\xi_c} = f\left(\frac{r}{r_{\sigma\xi}}\right) \quad \ldots\ldots [4b]$$

where f is the profile shape function. We introduce the terminology

$$\text{Slope coefficient} = \sigma = -f'\left(\frac{1}{2}\right) \quad \ldots\ldots [5]$$

where the prime indicates differentiation of the function with respect to its argument, and the minus sign is brought in to keep σ positive, since $\partial U/\partial r$ and $\partial \xi/\partial r$ are negative.

Slope coefficients were obtained by measuring profile slopes at the half-radius for both velocity and concentration, and the results are shown in Fig. 5. The striking thing is that, despite the difficulty of measuring slopes from plotted data, the slope coefficients remain nearly constant, beginning a short distance down-

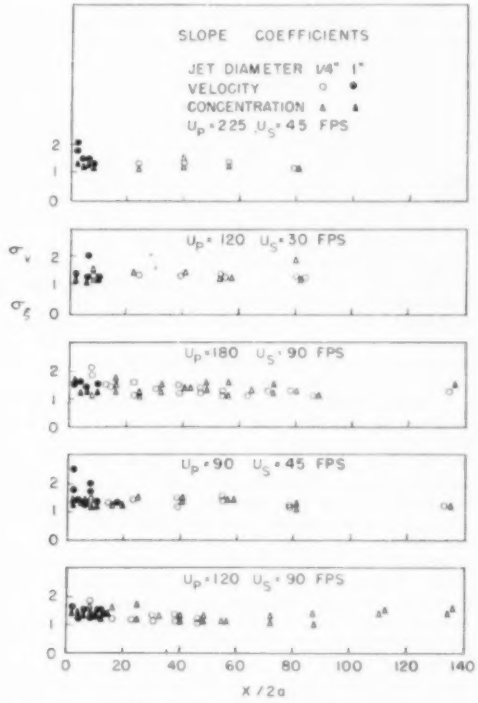

FIG. 5 SLOPE COEFFICIENTS

(Ordinates σ_v and σ_ξ are defined by Equations [4] and [5], and represent normalized slopes of velocity and concentration profiles at $r = r_{v\sigma}/2$ and $r = r_{\sigma\xi}/2$, respectively.)

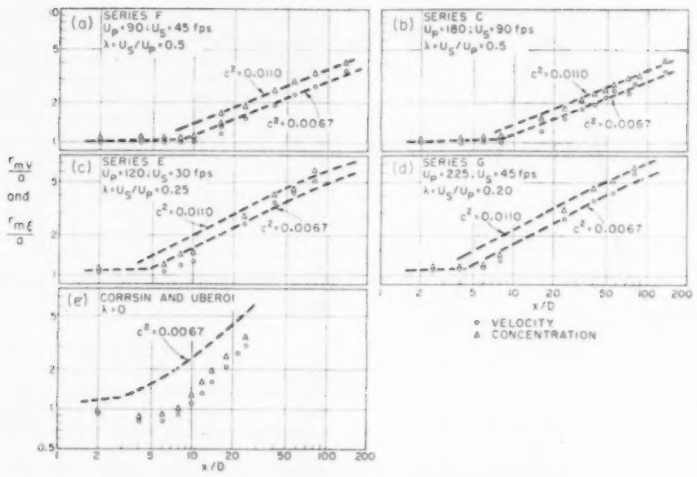

FIG. 6 HALF-BOUNDARIES OF MIXING

(Dashed lines are from analysis of Squire and Trouncer, for two values of mixing-length coefficient, c^2. Data in Fig. 6*e* are for a jet emerging in stationary air from a hole in a plane wall, and therefore refer to a geometry slightly different from that of Figs. 6(*a*), (*b*), (*c*), (*d*), and from that of the Squire and Trouncer analysis.)

stream from the end of the potential core. There is no systematic difference between the slope coefficients for velocity and concentration, and they appear to be entirely independent of velocity ratio. This is further confirmation of the conclusions of the previous section.

Spreading of Jet. Although the outer boundary of mixing is the obvious measure of the spreading of the jet, the determination of the point where a property just reaches zero involves far more difficulty than for the point where it reaches half its maximum value. Consequently it is common practice to employ the "half-boundaries" instead of the outer boundaries, and since similarity of profiles has been established, it is permissible to do so.

Fig. 6 shows half-boundaries for velocity and concentration plotted against x/D with logarithmic scales. In each chart the lines indicate the half-boundaries as computed by the method of Squire and Trouncer, using two values of their mixing length coefficient, c^2. It can be seen that material diffuses faster than momentum, just as other investigators have found that temperature spreads faster than momentum.

Reference to the list of experimental velocities given earlier will show that the velocities employed in series F and C, Figs. 6(*a*) and 6(*b*), respectively, are quite different, but that the velocity ratio is 0.50 for both series. The similarity of the results for these two series is an indication that the velocity ratio is the most important independent variable in determining the flow configuration.

The data for Fig. 6(*e*) are taken from Corrsin and Uberoi (17), and refer to a jet issuing from a round hole in an infinite wall into air at rest. Thus, while these data are for a velocity ratio, U_s/U_p, of zero, they do not represent the limiting case of the present tests because of the difference in geometry due to the wall. Since the Squire and Trouncer theory with $c^2 \cong 0.007$ fits the present velocity data, as shown in Figs. 6(*a*) to (*d*), it is reasonable to suppose that it is valid for that same geometry in the limiting case where $U_s/U_p = 0$. Therefore, comparing the line for $c^2 = 0.0067$ in Fig. 6(*e*) with the data of Corrsin and Uberoi, we see that when the jet issues from a hole in a wall, the mixing is less rapid than when the jet issues from a pipe.

Figs. 6(*a*) to (*d*) show that the Squire and Trouncer analysis is, for most practical purposes, adequate for predicting the half-boundaries of mixing, with $c^2 \cong 0.007$ for velocity, and $c^2 \cong 0.010$ for concentration. It is of considerable theoretical interest that the most suitable value of c^2 is independent of the velocity ratio, U_s/U_p, for this means that the factor of proportionality between the turbulent shear stress and $(U_s - U_s)^2$ is independent of velocity ratio.

Decay Along Axis. Fig. 7 shows values of the properties on the center line plotted against x/D with logarithmic scales. The dotted lines result from calculations according to the method of Squire and Trouncer, using two values of the mixing-length coefficient. The data show that, beyond the end of the potential core, the value of either velocity or concentration on the axis varies inversely with x, irrespective of the velocity ratio. Again, the agreement of data for series F and C, Figs. 7(*a*) and (*b*), shows that property values in the mixing region are a function of the velocity ratio rather than the absolute velocities of the two streams.

Figs. 7(*b*) to (*d*) show that, in general, the dimensionless concentration on the center line is less than the dimensionless velocity on the center line. This confirms the evidence in Fig. 6 that concentration spreads more rapidly than momentum. The apparent inversion of the evidence in Fig. 7(*a*) is due to an extraneous influence. Low absolute velocities were employed in that series, and the relatively thick boundary layer formed on the outer wall of the nozzle had a significant effect on the velocity profile.

From Fig. 7 it is clear that the analysis of Squire and Trouncer predicts the general order of magnitude of the center-line properties, but presents a false picture of the way in which the center-line properties vary with distance.

Empirical Formulas. Examination of the data reveals that the mixing region can be well defined by simple empirical formulas. These are discussed in more detail in reference (86). We give here some rules which may be used as a rough guide to the designer for the "velocity field" downstream of the potential core.

Let L be the x/D value for the end of the potential core and λ

be the ratio of initial secondary velocity to initial primary velocity, $\lambda = U_s/U_p$; then

$$L = 4 + 12\lambda \quad [6]$$

and, downstream of the potential core ($x/D > L$)

$$\frac{U_c - U_s}{U_p - U_s} = \frac{L}{x/D} \quad [7]$$

$$\frac{r_{m\nu}}{a} = \left(\frac{x/D}{L}\right)^{(1-\lambda)} \quad [8]$$

$$\frac{U - U_s}{U_c - U_s} = \frac{1}{2}\left(1 + \cos\frac{\pi r}{2r_{m\nu}}\right) \quad [9]$$

Thus the law of spreading for the axial-symmetric case of two streams with equal densities seems to be

$$r_m \sim (x)^{(1-\lambda)} \quad [10a]$$

$$r_\nu \sim (x)^{(1-\lambda)} \quad [10b]$$

which is known to be correct for the often measured case of $\lambda = 0$ and fits also the theoretical case of $\lambda = 1$, where for no initial turbulence and negligible molecular diffusivity the streams may be presumed not to mix at all.

The lines marked "empirical" in Fig. 7 show how well the rules of Equations [6] and [7] fit the experimental data. Good agreement is obtained also when Equation [8] is compared with the experimental data in Fig. 6.

Comparison Between Turbulent Transfers of Momentum, Temperature, and Mass

It is widely felt that one of the clues which might lead to an understanding of turbulent mixing is the experimental determination of the relative magnitudes of momentum transfer, enthalpy transfer, and mass transfer.

For this purpose it is convenient to define "turbulent" coefficients of viscosity, heat conductivity, and mass diffusion which are analogous to the corresponding coefficients for laminar flow, as outlined in the following comparison

Property transferred	Laminar	Turbulent
Momentum	$\frac{\tau}{\rho} = \nu\frac{\partial U}{\partial y}$	$\frac{\tau}{\rho} = \nu_t\frac{\partial U}{\partial y}$ ..... [11]
Temperature	$\frac{Q_A}{c_p\rho} = \left(\frac{k}{c_p\rho}\right)\frac{\partial T}{\partial y}$	$\frac{Q_A}{c_p\rho} = \left(\frac{k_t}{c_p\rho}\right)\frac{\partial T}{\partial y}$ ..... [12]
Mass	$N_A = D\frac{\partial \xi}{\partial y}$	$N_A = D_t\frac{\partial \xi}{\partial y}$ ..... [13]

where the exchange coefficients, the coefficients of the gradients, are all in units of length squared, divided by time. The exchanges of momentum, temperature, and mass may then be compared by evaluating the ratios of the respective exchange coefficients. In the laminar case, the ratio of momentum-exchange coefficient to temperature-exchange coefficient is

$$\frac{\nu}{k/c_p\rho} = \frac{\mu c_p}{k}$$

and is known as the Prandtl number. Likewise, the ratio of momentum-exchange coefficient to mass-exchange coefficient is

$$\frac{\nu}{D} = \frac{\mu}{\rho D}$$

and is known as the Schmidt number. The corresponding ratios for turbulent exchange have become known as "turbulent Prandtl number," and "turbulent Schmidt number," respectively.

Now the laminar Prandtl and Schmidt numbers are fluid properties, and are independent of the flow pattern so long as the flow is laminar. The turbulent Prandtl and Schmidt numbers, however, must be determined in part by the nature of the turbulent process, and hence depend on the dynamics of the flow. A basic question which arises here is whether the turbulent indexes are somehow controlled by the laminar indexes, or whether they are controlled entirely by the dynamics of the turbulence.

By analyzing the case of mass transfer, according to the integral-equation method of Squire and Trouncer, with the additional premise (justified by the present data) that the normalized velocity and concentration profiles are identical, it may be shown that the ratio of the experimentally determined values of c^2 for velocity and for concentration is the turbulent Schmidt number. Thus, using mean values of $c^2 \cong 0.007$ for velocity, and $c^2 \cong 0.010$ for concentration, the average turbulent Schmidt number for the present tests is about 0.70, as compared with a laminar Schmidt number for the diffusion of helium in air of only 0.34. Within the accuracy of the measurements, the turbulent Schmidt number is independent of velocity ratio.

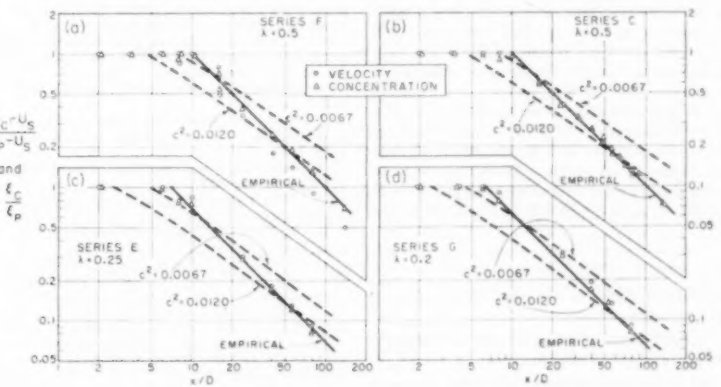

Fig. 7 Center-Line Values of Velocity and Concentration

(Dashed lines are from analysis of Squire and Trouncer, for two values of the mixing-length coefficient, c^2. Heavy line in each chart represents empirical formula, Equation [7].)

TABLE 3 SUMMARY OF EXPERIMENTAL DATA

Fluid	Tracer	Laminar[a] Prandtl number	Laminar[a] Schmidt number	Turbulent[b] Prandtl number	Turbulent[b] Schmidt number	Turbulent index investigated by	Reference
Air	Helium	....	0.34	....	0.70	Forstall[c]	(86)
Air	City gas	....	....	....	0.74	Hinze[d]	(31)
Air	Warm air	0.74	....	0.76	....	Lin[d]	(39)
Air	Warm air	0.74	....	0.70	....	Corrsin[d]	(17)
Air	Warm air	0.74	....	0.77	....	Cleeves[d]	(14)
Air	Water vapor	....	0.71	....	0.63	Woertz[e]	(87)
Helium	Water vapor	....	1.96	....	0.63	Woertz[e]	(87)
Carbon dioxide	Water vapor	....	0.45	....	0.63	Woertz[e]	(87)
Water	Salt water	....	785	....	0.64	Bicknell[f]	(85)

[a] Laminar Prandtl and Schmidt numbers are fluid properties, independent of flow pattern, and are found from density, specific heat, and molecular coefficients of viscosity, thermal conductivity, and mass diffusion.
[b] Turbulent Prandtl and Schmidt numbers are based on measured spread of velocity, temperature, and mass in turbulent mixing process. Values reported here represent average experimental values for turbulent zone of mixing in each set of experiments.
[c] Round jet discharging into moving air stream, with ratio of secondary velocity to primary velocity ranging from 0.2 to 0.5.
[d] Round jet discharging into stationary air.
[e] Turbulent core of a two-dimensional duct in which water vapor was transferred through various gases from one wall to opposite wall.
[f] Plane jet of saline water discharging into stationary water.

To shed further light on the question, a great deal of experimental data of various observers on turbulent exchange, including the data reported here, have been reduced to this form and summarized in the form of Table 3. For purposes of comparison, the table shows the laminar Prandtl and Schmidt numbers as well as the experimentally determined values of turbulent Prandtl and Schmidt numbers.

Several general conclusions may be reached from Table 3:

(*a*) Although the laminar indexes vary over a range of some 2000-fold, the turbulent indexes vary by only ±10 per cent from a value of 0.70, thus indicating that the turbulent-exchange processes are substantially independent of the laminar coefficients.

(*b*) The turbulent Prandtl and Schmidt numbers are substantially independent of the nature of the experiment.

(*c*) The turbulent Prandtl and Schmidt numbers are approximately equal, thus indicating that in turbulent flow, mass and temperature diffuse at equal rates, and that this rate is greater than the rate of turbulent diffusion of momentum.

(*d*) Speaking in speculative terms, the foregoing comments imply that in practical problems of turbulence, the ratio of momentum transport to either mass or temperature transport has a constant value of about 0.7.

One of the puzzling questions not yet clearly resolved is why momentum should transfer less rapidly than mass or temperature, even though, in all qualitative aspects there are remarkable similarities among the turbulent transports of the three properties. Part of the answer must lie in the fact that momentum is a vector quantity, whereas mass and temperature are both scalar properties, which means that the averaging procedures in a turbulent flow are somewhat different in nature. For example, if one considers the large-scale eddies at the edges of a jet, it is clear that the velocity boundary of the jet is near the center of the eddies, whereas the temperature and concentration boundaries are near the outer edges of the eddies. Much remains to be done, however, before this question is answered adequately, and it is hoped that the data presented here will be a stimulus in this direction.

Conclusions

1 The fully normalized shapes of the velocity and concentration profiles are substantially alike.

2 The fully normalized shapes of the profiles are substantially independent of velocity ratio and of axial distance.

3 Beyond the end of the potential core, center-line values of velocity and concentration decrease in inverse proportion to increase in axial distance.

4 The width of the jet depends on the velocity ratio and axial distance according to the empirical relation, $r_c \backsim (x)^{(1-\lambda)}$.

5 Mass transport is more rapid than momentum transport.

6 The method of Squire and Trouncer, like the integral method in general, gives an over-all picture of the mixing process which is in the main correct, but is inaccurate in some of the details. Their analysis predicts the width of the jet more reliably than the center-line values of velocity and concentration. For velocity, a satisfactory value of their mixing length coefficient is $c^1 \leqq 0.007$, while for concentration the best value is $c^1 \leqq 0.010$. These experimentally determined constants are independent of velocity ratio, within the accuracy of the method.

7 The turbulent Prandtl and Schmidt numbers collected from diverse experiments of several investigators were all within ±10 per cent of 0.70, despite a 2000-fold variation in the laminar Prandtl and Schmidt numbers among these same experiments.

Bibliography

1 "Investigation of the Flow in the Open Jet of a Wind Tunnel," by G. N. Abramovich, Central Aero-Hydrodynamical Institute of Moscow, USSR, Reports 223, 236, 1935.

2 "On the Theory of a Free Jet and Its Application," by G. N. Abramovich, Central Aero-Hydrodynamical Institute of Moscow, USSR, Report 293, 1936.

3 "The Theory of a Free Jet of a Compressible Gas," by G. N. Abramovich, Central Aero-Hydrodynamical Institute of Moscow, USSR, Report 377, 1939. Translated as NACA TM 1058.

4 "Diffusion of Submerged Jets," by M. L. Albertson, Y. B. Dai, R. A. Jensen, and Hunter Rouse, Proceedings of the ASCE, vol. 74, December, 1948, pp. 1571–1596.

5 "Studies in Diffusion, I—Estimation of Diffusivities in Gaseous Systems," by J. H. Arnold, *Industrial and Engineering Chemistry*, vol. 22, 1930, p. 1091.

6 "Mechanics of Turbulent Flow," by B. A. Bakhmeteff, Princeton Press, 1936.

7 "Velocity Distribution Across a Turbulent Jet," by A. Betz, Ergebnisse der Aerodynamische Versuchsanstalt zu Göttingen II, 1923, p. 69.

8 "The Plane Jet," by W. G. Bickley, *Philosophical Magazine*, vol. 23, 1937, pp. 727–731.

9 "The Turbulent Spreading of a Water Jet," by A. M. Binnie, *Engineering*, vol. 153, 1942, pp. 503–504.

10 "Laminar Mixing of a Compressible Fluid," by D. R. Chapman, NACA TN 1800, February, 1949.

11 "On an Extension of Reynolds' Method of Finding Apparent Stress and the Nature of Turbulence," by P. Y. Chou, *Chinese Journal of Physics*, Peiping, China, vol. 4, 1940, pp. 1–33.

12 "The Laminar Mixing Motion of Two Incompressible Gases," by P. Y. Chou, *Chinese Journal of Physics*, China, vol. 7, 1947, p. 96.

13 "New Investigations on the Spread of a Liquid Jet in a Stationary Liquid," by D. Citrini, *Energia Elettrica*, Milano, Italy, vol. 24, 1947, pp. 177–192.

14 "Isothermal and Non-Isothermal Air Jet Investigations," by V. Cleeves and L. M. K. Boelter, *Chemical Engineering Progress*, vol. 43, 1947, pp. 123–134.

15 "Investigation of the Behavior of Parallel Two-Dimensional Jets," by S. Corrsin, NACA Wartime Report W-90 (ACR 4H24, November, 1944).

16 "Investigation of Flow in an Axially Symmetrical Heated Jet of Air," by S. Corrsin, NACA Wartime Report W-94 (ACR 3L23, December, 1943).

17 "Further Experiments on the Flow and Heat Transfer in a Heated Turbulent Air Jet," by S. Corrsin and M. S. Uberoi, NACA TN 1865, April, 1949.

18 "An Investigation of the Round Jet in a Moving Air Stream," by J. B. Deodati and E. B. Monteath, California Institute of Technology, Jet Propulsion Laboratory, Memorandum No. 3-8, June 30, 1947.

19 "Aerodynamic Theory," edited by W. F. Durand, 1935.

20 "The Transfer of Heat From a Hot Plate to an Air Stream," by Franz Elias, Abhandlungen aus dem Aerodynamischen Institut an der Technischen Hochschule Aachen, no. 9, 1930, pp. 10–39. Translated as NACA TM 614.

21 "The Behavior of Fluids in Turbulent Motion," by A. Fage, *Journal of the Royal Aeronautical Society of London*, England, vol. 37, 1933, p. 573.

22 "Note on Experiments of the Temperature and Velocity in the Wake of a Heated Cylindrical Obstacle," by A. Fage and V. M. Falkner, Proceedings of the Royal Society of London, series A, vol. 135, 1932, p. 702.

23 "An Examination of Turbulent Flow With an Ultramicroscope," by A. Fage and H. C. H. Townend, Proceedings of the Royal Society of London, series A, vol. 135, 1932, p. 656.

24 "Sulla Teoria della Turbolenza," by C. Ferrari, Rendiconti della Reale Accademia Nazionale dei Lincei, Rome, Italy, 1934, p. 100.

25 "The Transport of Vorticity Through Fluids in Turbulent Motion," by C. Ferrari, L'Aerotecnica, vol. 15, 1935, pp. 1037–1056. Translated as NACA TM 799.

26 "Jet Mixing of Two Liquids," by R. G. Folsom and C. K. Ferguson, Trans. ASME, vol. 71, 1949, pp. 73–77.

27 "Über turbulente Strahlausbreitung," by E. Förthmann, *Ingenieur-Archiv.*, vol. 5, 1934, pp. 42–54. Translated as NACA TM 789.

28 "Some Two-Dimensional Aspects of the Ejector Problem," by J. A. Goff and C. H. Coogan, JOURNAL OF APPLIED MECHANICS, Trans. ASME, vol. 64, 1942, p. A-151.

29 "Modern Developments in Fluid Dynamics," by Sidney Goldstein, Clarendon Press, Oxford, England, 1938.

30 "A New Approximate Method for the Numerical Evaluation of the Free Turbulence Problem," by H. Görtler, *Zeitschrift für angewandte Mathematik und Mechanik*, vol. 22, 1942, pp. 244–254. Translated as ARC 7947, FM 718, RTP Translation no. 2234.

31 "Heat and Mass Transfer in the Turbulent Mixing Zone of an Axially Symmetrical Jet," by J. O. Hinze and B. G. van der Hegge Zijnen, Seventh International Congress for Applied Mechanics, London, England, 1948. (From "Delft" Laboratory, Royal Dutch Shell.)

32 "Concerning the Velocity and Temperature Distributions in Plane and Axially Symmetrical Jets," by L. Howarth, Proceedings of the Cambridge Philosophical Society, London, England, vol. 34, part 2, 1938, pp. 185–203.

33 "Diffusion in Turbulent Flow Between Parallel Planes," by J. C. Jaeger, *Quarterly of Applied Mathematics*, vol. 3, 1945, p. 210.

34 "Eddy Diffusion," by A. A. Kalinske and C. C. Pien, *Industrial and Engineering Chemistry*, vol. 36, 1944, pp. 220–223.

35 "Investigation of the Turbulent Region Formed by Jets," by by A. M. Kuethe, JOURNAL OF APPLIED MECHANICS, Trans. ASME, vol. 57, 1935, p. A-87.

36 "Shadowgraph Investigations of Gas Mixing and Flames," by Lenhart and Wohl, University of Delaware, Newark, Del., Report UD-83, Oct. 2, 1946.

37 "Some Measurements in Free Turbulent Shear Flow," by H. W. Liepmann, S. Corrsin, and J. Laufer, Sixth International Congress for Applied Mechanics, Paris, France, 1946.

38 "Investigations on Free Turbulent Mixing," by H. W. Liepmann and J. Laufer, NACA TN 1257, August, 1947.

39 "Velocity and Temperature Distributions in Turbulent Jets," by C. C. Lin, The Science Reports of National Tsing Hua University, series A, vol. 4, October, 1947.

40 "Teoria della Turbolenza," by G. D. Mattioli, Rendiconti della Reale Accademia Nazionale dei Lincei, Rome, Italy, vol. 17, 1933, p. 217.

41 "Dissipazione Vorticosa nei Regimi Turbolenti," by G. D. Mattioli, Rendiconti della Reale Accademia Nazionale dei Lincei, Rome, Italy, 1935, p. 87.

42 "Sopra l'Influenza della Viscosita del Fluido nei Regimi Turbolenti," by G. D. Mattioli, Atti della Reale Accademia della Scienze de Torino, Turin, Italy, 1935, p. 220.

43 "Effect of Size and Shape of Pipe and of Adjacent Walls on Velocity and Entrainment Ratio, Part II—Air Flow at Discharge of Fan Pipe Lines in Mines," by G. E. McElroy, U. S. Department of Interior, Bureau of Mines, Report of Investigations no. 3730, November, 1943.

44 "Schlieren Photographs of Two-Dimensional Flames and Flow Patterns," by H. L. Olsen, A. Ingersoll, and H. Rubin, University of Wisconsin Naval Research Laboratory, Madison, Wis., CM-484, Aug. 11, 1948.

45 "Geschwindigkeits—und Temperaturverteilung hinter einem Gitter bei turbulenter Strömung," by R. G. Olsson, *Zeitschrift für angewandte Mathematik und Mechanik*, vol. 16, 1936, pp. 257–274.

46 "Die Ausbreitung Heisser Gasstrahlen in Bewegter Luft, I Teil–Versuche im Kerngebiet," by O. Pabst, *Deutsche Luftfahrtforschung* U.u.M. 8004, August, 1944.

47 "Mischungsvorgang eines Luechtgasstrahles mit Ruhender Luft," by O. Pabst and J. G. von Bohl, Focke-Wulf Hausbericht 09 021 I.

48 "Bericht über Untersuchungen zur ausgebildeten Turbulenz," by L. Prandtl, *Zeitschrift für angewandte Mathematik und Mechanik*, vol. 5, 1925, pp. 136–139.

49 "Bermerkung zur Theorie der freien Turbulenz," by L. Prandtl, *Zeitschrift für angewandte Mathematik und Mechanik*, vol. 22, 1942, p. 241.

50 "A Contribution to the Problem of the Decay of a Gas Jet Discharging From a Pipe," by A. Predvoditelev and E. Stupotshenko, Moscow Thermo-Technical Institute, USSR.

51 "Heat Transfer Through Turbulent Friction Layers," by H. Reichardt, *Zeitschrift für angewandte Mathematik und Mechanik*, vol. 20, 1940, pp. 297–328. Translated as NACA TM 1047.

52 "A New Theory of Free Turbulence," by H. Reichardt, *Zeitschrift für angewandte Mathematik und Mechanik*, vol. 21, 1941, pp. 257–264. Translated in *Journal of the Royal Aeronautical Society*, vol. 47, 1943, pp. 167–176.

53 "Gesetzmassigkeiten der freien Turbulenz," by H. Reichardt, VDI Forschungsheft 414, May-June, 1942; reproduced as ARC 6670, FM 586.

54 "Field of Flow About a Jet and Effect of Jets on Stability of Jet Propelled Airplanes," by H. S. Ribner, NACA Wartime Report L-213 (ARC L6C13, 1946).

55 "Modern Conceptions of the Mechanics of Fluid Turbulence," by H. Rouse, Proceedings of the ASCE, vol. 62, 1936, p. 21.

56 "Turbulente Ausbreitungsvorgänge im Freistrahl," by P. Ruden, *Die Naturwissenschaften*, vol. 21, 1933, pp. 375–378.

57 "Apparatus for the Determination of the Concentration of Helium in Air by the Thermal Conductivity Method," by D. Rush and W. Forstall, Jr., Massachusetts Institute of Technology, Gas Turbine Laboratory Internal Report no. 4, January, 1947.

58 "Über das ebene Windschattenproblem," by H. Schlichting, *Ingenieur-Archiv.*, December, 1930, p. 533.

59 "Laminare Strahlausbreitung," by H. Schlichting, *Zeitschrift für angewandte Mathematik und Mechanik*, vol. 13, 1933, p. 260.

60 "Der Massenaustausch in freier Atmosphäre und verwandte Erscheinungen," by Wilhelm Schmidt, Hamburg, Germany, 1925.

61 "Turbulente Ausbreitung eines Stromes erhitzter Luft," by Wilhelm Schmidt, *Zeitschrift für angewandte Mathematik und Mechanik*, vol. 21, 1941, pp. 265–278.

62 "Absorption and Extraction," by T. K. Sherwood, McGraw-Hill Book Company, Inc., New York, N. Y., 1937.

63 "Mass Transfer and Friction in Turbulent Flow," by T. K. Sherwood, Trans. AIChE, vol. 36, 1940, p. 817.

64 "The Role of Eddy Diffusion in Mass Transfer Between Phases," by T. K. Sherwood and B. B. Woertz, Trans. AIChE, vol. 35, 1939, p. 517.

65 "Reconsideration of the Theory of Free Turbulence," by H. B. Squire, RAE Farnborough, Report No. Aero 2023, March, 1945. Abstract in *Philosophical Magazine*, vol. 39, January, 1948, pp. 1–20.

66 "Round Jets in a General Stream," by H. B. Squire and J. Trouncer, ARC Technical Report R&M No. 1974, 1944.

67 "Mass Transfer in Turbulent Flow," by L. F. Stutsman doctoral dissertation, University of Pittsburgh, Pittsburgh, Pa., 1946.

68 "On the Turbulent Wake Behind a Body of Revolution," by L. M. Swain, Proceedings of the Royal Society of London, series A, vol. 125, 1929, pp. 647–659.

69 "Zur Theorie der Ausbreitung eines aus einer Düse austretenden freien Strahls. I Teil—des Strömungsfeld im Kernbereich," by Szablewski, *Deutsche Luftfahrtforschung* U.u.M. 8003, November, 1944.

70 "Diffusion by Continuous Movements," by G. I. Taylor, Proceedings of the London Mathematical Society, London, England, vol. 20, 1921, p. 196.

71 "The Transport of Vorticity and Heat Through Fluids in Tur-

bulent Motion," by G. I. Taylor, Proceedings of the Royal Society of London, series A, vol. 135, 1932, pp. 685–702.

72 "Statistical Theory of Turbulence," by G. I. Taylor, Proceedings of the Royal Society of London, series A, vol. 151, 1935, pp. 421–478.

73 "Calculation of Turbulent Expansion Processes," by W. Tollmien, *Zeitschrift für angewandte Mathematik und Mechanik*, vol. 6, 1926, pp. 468–478. Translated as NACA TM 1085.

74 "Application of the Modified Vorticity Transport Theory to the Turbulent Spreading of a Jet of Air," by S. Tomotika, Proceedings of the Royal Society of London, series A, vol. 165, 1938, pp. 65–72.

75 "Mixing of Gases in Turbulent Flow," by W. L. Towle, Sc.D. thesis, Course X, Massachusetts Institute of Technology, 1937.

76 "Eddy Diffusion. Mass Transfer in the Central Portion of a Turbulent Air Stream," by W. L. Towle and T. K. Sherwood, *Industrial and Engineering Chemistry*, vol. 31, 1939, p. 457.

77 "The Control of Air Streams in Large Spaces," by G. L. Tuve and G. B. Priester, Trans. ASHVE, vol. 50, 1944, p. 153.

78 "Untersuchung turbulenter Mischvorgänge," by K. Victorin, *Forschungsarbeiten auf dem Gebiete des Ingenieurwesens*, vol. 12, 1941, p. 16.

79 "Some Aspects of the Turbulence Problem," by Th. von Kármán, Proceedings of the Fourth International Congress for Applied Mechanics, Cambridge, England, 1934, pp. 54–91.

80 "Entrainment of Air by Axially Symmetrical Gas Jets," by T. S. Voorhees, MS thesis in Mechanical Engineering, University of California, Berkeley, Calif., 1939.

81 "The Behavior of a Pitot Tube in a Transverse Total Pressure Gradient," by A. D. Young and J. N. Maas, ARC Technical Report R&M no. 1770, 1937.

82 "Über die Strömungsvorgänge im freien Luftstrahl," by W. Zimm, *Forschungsarbeiten auf dem Gebiete des Ingenieurwesens*, no. 234, 1921.

83 "The Velocity Field in an Isothermal Turbulent Free Jet Adjacent to the Source," by L. G. Alexander, University of Illinois Engineering Experiment Station, Urbana, Ill., Technical Report no. 3, Nov. 20, 1948, Contract N6-ori-71, Task Order no. XI, Office of Naval Research, Navy Department.

84 "Dynamics of Free Turbulence," by Thomas Baron, University of Illinois Engineering Experiment Station, Urbana, Ill., Technical Report no. 1, Nov. 1, 1948, Contract N6-ori-71, Task Order no. XI, Office of Naval Research, Navy Department.

85 "A Study of Turbulent Mixing Between a Plane Jet of Fluid of Various Densities and Still Fluid," by Joseph Bicknell, Massachusetts Institute of Technology, Course XVI, MS thesis, 1937.

86 "Material and Momentum Transfer in Coaxial Gas Streams," by Walton Forstall, Jr., Massachusetts Institute of Technology, Course II, Sc.D. thesis, 1949.

87 "Mass Transfer Between Phases. Role of Eddy Diffusion," by T. K. Sherwood and B. B. Woertz, *Industrial and Engineering Chemistry*, vol. 31, 1939, pp. 1034–1041.

88 "Turbulent Mixing in an Isothermal Free Jet," by J. F. Taylor, H. L. Grimmett, and E. W. Comings, University of Illinois Engineering Experiment Station, Urbana, Ill., Technical Report no. 2, Nov. 15, 1948, Contract N6-ori-71, Task Order no. XI, Office of Naval Research, Navy Department.

89 "On Vortex Motion in Gaseous Jets and the Origin of Their Sensitivity to Sound," by G. B. Brown, Proceedings of the Physical Society of London, England, vol. 47, 1935, pp. 703–732.

Impact on a Multispan Beam

By W. H. HOPPMANN, 2ND,[1] BALTIMORE, MD.

In this paper a study is made of impact on a continuous beam on four supports. The impact is produced by collision of a solid sphere with the beam at the mid-point of the center span. The spans are of equal length and of constant cross section. Formulas are obtained for the deflections and strains. A numerical example illustrating the theory is worked out in detail.

Nomenclature

The following nomenclature is used in the paper:

m = mass of body which strikes beam
v = velocity of body which strikes beam
e = coefficient of restitution
E = Young's modulus of elasticity
ρ = mass per unit volume
ν = Poisson's ratio
l = length of each span
A = area of cross section of each span
I = moment of inertia of cross section of each span about neutral axis
M = a reduced mass (one half of total mass of each span)
$a = \sqrt{\frac{EI}{\rho A}}$
n = number of nth mode
k_n = quantity such that $k_n l$ is a root of the frequency equation
p_n = circular frequency of the nth mode
t = time
$F(x, t)$ = driving force assumed to be acting at any point x along beam at time t
$f(t)$ = driving or contact force at center of middle span during impact
T_L = length of time sinusoidal pulse is assumed to act on beam
E_{pk} = sum of potential and kinetic energy in entire beam at end of contact between sphere and beam ($t = T_L$)
Φ_n = dimensionless factor in the expression for E_{pk}
ψ_n = dimensionless function of $k_n l$
θ_n = dimensionless function of $k_n l$
G_n = dimensionless function of $k_n l$
$Q_n = \frac{P_n T_L}{2\pi}$
$w(x, t)$ = deflection of beam

Introduction

It is technically important to know the strains and deflections in a continuous beam subjected to an impulsive load at a point in one of the spans. This knowledge is particularly useful in studying the motion to which light equipment mounted on the beam at some point may be subjected. Such a situation arises in problems of mechanical shock.

In the present paper a study is made of a three-span beam with simply supported ends subjected to an impulsive load at the center of the middle span. The impulse load is assumed to be produced by the collision of a solid sphere with the beam. The method can be generalized for a beam of any number of spans and struck at any point. Plans are under way to investigate the problem experimentally.

Statement of Problem

The continuous beam on four supports is shown in Fig. 1 on page 3. The ends of the beam are hinged.

A solid sphere of mass m and Young's modulus E strikes the beam at normal incidence with the velocity v as shown. The cross-sectional area of the beam throughout its length is A. The moment of inertia I, is also constant. The density is designated by ρ and is assumed to be the same for both sphere and beam.

Differential Equation of Motion

The Bernoulli-Euler beam theory will be assumed. The cross-sectional dimensions of the beam will be considered small in comparison with the length of the span, and the effects of shearing force and of rotatory inertia will be neglected. The differential equation then is

$$EI\frac{\partial^4 w}{\partial x^4} + \rho A\frac{\partial^2 w}{\partial t^2} = F(x, t) \quad \ldots\ldots\ldots\ldots [1]$$

in which $F(x, t) \equiv 0$ in the side spans, and $= f(t)$ at the mid-point of the center span.

The boundary, continuity, and initial conditions are

$$\left.\begin{aligned}
&w_1 = 0, \quad EI\frac{\partial^2 w_1}{\partial x_1^2} = 0, \quad \text{at } x_1 = 0\\
&w_3 = 0, \quad EI\frac{\partial^2 w_3}{\partial x_3^2} = 0, \quad \text{at } x_3 = 0\\
&w_1 = w_2 = 0, \quad \frac{\partial^2 w_1}{\partial x_1^2} = \frac{\partial^2 w_2}{\partial x_2^2}, \quad \frac{\partial w_1}{\partial x_1} = \frac{\partial w_2}{\partial x_2} \text{ at } x_2 = -\frac{l}{2}\\
&w_3 = w_2 = 0, \quad \frac{\partial^2 w_3}{\partial x_3^2} = \frac{\partial^2 w_2}{\partial x_2^2}, \quad \frac{\partial w_3}{\partial x_3} = -\frac{\partial w_2}{\partial x_2} \text{ at } x_3 = \frac{l}{2}\\
&w\Big]_{t=0} = 0, \quad \frac{\partial w}{\partial t}\Big]_{t=0} = 0
\end{aligned}\right\} \quad \ldots [2]$$

and

the solution of Equation [1] may be obtained by separation of variables so that

$$w = \Sigma q_n(t) \cdot X_n(x) \quad \ldots\ldots\ldots\ldots [3]$$

where

$$X_n = A_n \sin k_n x + B_n \cos k_n x + C_n \sinh k_n x + D_n \cosh k_n x \quad \ldots [4]$$

---

[1] Associate Professor, Mechanical Engineering, School of Engineering, The Johns Hopkins University. Mem. ASME.

Presented at the Annual Conference of the Applied Mechanics Division, Purdue University, Lafayette, Ind., June 22–24, 1950, of The American Society of Mechanical Engineers.

Discussion of this paper should be addressed to the Secretary, ASME, 29 West 39th Street, New York, N. Y., and will be accepted until January 10, 1951, for publication at a later date. Discussion received after the closing date will be returned.

Note: Statements and opinions advanced in papers are to be understood as individual expressions of their authors and not those of the Society. Manuscript received by the Applied Mechanics Division September 29, 1949. Paper No. 50—APM-15.

$i = 1, 2, 3$ depending on the span under consideration. For all values of the time t, X_n must satisfy the twelve conditions given by Equations [2].

This fact leads to the following frequency equations

$$\cos\frac{k_n l}{2}\sin k_n l\left(\cot k_n l - \coth k_n l - \tan\frac{k_n l}{2} - \tanh\frac{k_n l}{2}\right) = 0$$

for the symmetrical modes of vibration, and ... [5]

$$\sin\frac{k_n l}{2}\sin k_n l\left(\cot k_n l - \coth k_n l + \cot\frac{k_n l}{2} - \coth\frac{k_n l}{2}\right) = 0$$

for the unsymmetrical modes of vibration.

For the case of symmetrical vibrations, the deflection of each side span is

$$w_1 = w_3 = \Sigma q_n(t)\cdot\left(\sin k_n x - \frac{\sin k_n l}{\sinh k_n l}\sinh k_n x\right)$$

and the deflection of the center span is

$$w_2 = 2\Sigma q_n(t)\cdot\sin\frac{k_n l}{2}\left(\cos k_n x - \frac{\cos\frac{k_n l}{2}}{\cosh\frac{k_n l}{2}}\cosh k_n x\right) \quad \ldots [6]$$

for the roots of the frequency equation that are not multiples of π.

The deflection of each side span is

$$w_1 = w_3 = \Sigma q_n(t)\cdot\sin k_n x$$

and the deflection of the center span is

$$w_2 = \Sigma -(-1)^{\frac{s-1}{2}} q_n(t)\cdot\cos k_n x \quad \ldots [7]$$

for roots of the frequency equation that are multiples of π $s = 1, 3, 5, 7$, etc.

For the class of unsymmetrical vibrations

$$w_1 = -w_3 = \Sigma q_n(t)\cdot\left(\sin k_n x - \frac{\sin k_n l}{\sinh k_n l}\sinh k_n x\right)$$

and

$$w_2 = -2\Sigma q_n(t)\cdot\cos\frac{k_n l}{2}\left(\sin k_n x - \frac{\sin\frac{k_n l}{2}}{\sinh\frac{k_n l}{2}}\sinh k_n x\right) \quad \ldots [8]$$

for roots of the frequency equation that are not multiples of π; while

$$w_1 = -w_3 = \Sigma q_n(t)\cdot\sin k_n x$$

and

$$w_2 = \Sigma(-1)^{\frac{s}{2}} q_n(t)\cdot\sin k_n x \quad \ldots [9]$$

for the roots of the frequency equation that are multiples of π; $s = 2, 4, 6, 8$, etc.

The roots of the frequency Equations [5] for the symmetrical case are

$$k_n l = 4.30, 6.71, 4.3 + 2\pi, 6.71 + 2\pi, 4.3 + 4\pi, \ldots$$

and

$$k_n l = \pi, 3\pi, 5\pi, 7\pi \quad \ldots [10]$$

For the unsymmetrical case, the roots are

$$k_n l = 3.56, 7.43, 3.56 + 2\pi, 7.43 + 2\pi, 3.56 + 4\pi \ldots$$

and

$$k_n l = 2\pi, 4\pi, 6\pi, 8\pi \quad \ldots [11]$$

These frequencies have been presented elsewhere in the literature as part of studies of frequencies of continuous beams (1, 2).[2] It may be noted, however, that Kaufmann (1) erroneously omits multiples of π for a three-span beam.

The Lagrangian equations of motion (3) are used to obtain the solution corresponding to impact loading on the beam. For this purpose we use the potential-energy function

$$V = \Sigma\frac{EI}{2}\int\left(\frac{\partial^2 w}{\partial x^2}\right)^2 dx \quad \ldots [12]$$

and the kinetic-energy function

$$T = \Sigma\frac{\rho A}{2}\int\dot{w}^2 dx \quad \ldots [13]$$

The Lagrangian equations of motion are then

$$\frac{d}{dt}\left(\frac{\partial T}{\partial\dot{q}_n}\right) + \frac{\partial V}{\partial q_n} = R_n \quad \ldots [14]$$

in which R_n is the generalized force.

Equations [14] with the aid of Equations [6], [7], [12], and [13] become

$$\ddot{q}_n + p_n^2 q_n = \frac{R_n}{G_n M} \quad \ldots [15]$$

where p_n are the circular frequencies, M is the half-mass of a single span

$$G_n = \frac{1}{k_n l}\left[2k_n l\left(1 + 2\sin^2\frac{k_n l}{2}\right) + \sin^2 k_n l\left(\frac{k_n l}{\cosh^2\frac{k_n l}{2}} - \frac{2k_n l}{\sinh^2 k_n l}\right)\right] \quad \ldots [16]$$

for roots $k_n l$ which are not multiples of π, and

$$G_n = 3$$

for roots $k_n l$ which are multiples of π. The values of G_n are given in Table 1.

The solutions of Equations [15] may now be readily obtained (3). They are

$$q_n = \frac{1}{p_n G_n M}\int_0^t R_n(\tau)\sin p_n(t-\tau)d\tau \quad \ldots [17]$$

[2] Numbers in parentheses refer to the Bibliography at the end of the paper.

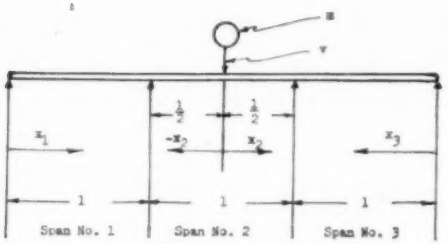

FIG. 1 GENERAL ARRANGEMENT

The complete deflection equation may be obtained if we can determine an explicit expression for R_n. This may be accomplished readily if first an expression for the impact force can be derived in terms of known physical quantities.

THE FORCE OF IMPACT

The method of obtaining the force of impact with the aid of the Hertz contact theory (4) was explained in a previous paper (5). It may be written as a sinusoidal pulse as follows

$$\left.\begin{aligned} f(t) &= mv(1+e)\frac{\pi}{2T_L}\sin\frac{\pi t}{T_L} \quad 0 \le t < T_L \\ f(t) &= 0 \qquad\qquad t \ge T_L \end{aligned}\right\} \quad [18]$$

where

e = coefficient of restitution
$T_L = 0.855\ T_H$
T_H = Hertz time of contact during impact

Force of impact $f(t)$, then depends on the coefficient e, which may be determined in terms of known parameters with reasonable accuracy. For this purpose it is necessary to use an expression for the sum of the potential and kinetic energies in the continuous beam at the end of the time of contact. Using Equations [12] and [13] it can be shown that the expression is

$$E_{pk} = \frac{1}{2}\,mv^2(1+e)^2\,\frac{m}{M}\,\Sigma\psi_n \cdot \frac{1+\cos 2\pi Q_n}{2(1-4Q_n^2)^2} \quad [19]$$

where

$$Q_n = \frac{p_n T_L}{2\pi}$$

M = half the mass of one span
m = mass of sphere
v = velocity of sphere

$$\psi_n = \frac{4\sin^2\dfrac{k_n l}{2}\left(1-\dfrac{\cos\dfrac{k_n l}{2}}{\cosh\dfrac{k_n l}{2}}\right)^2}{2\left(1+2\sin^2\dfrac{k_n l}{2}\right)+\sin^2 k_n l\left(\dfrac{1}{\cosh^2\dfrac{k_n l}{2}}-\dfrac{2}{\sinh^2 k_n l}\right)}$$

for roots $k_n l$ which are not multiples of π and

$$\psi_n = \frac{1}{3} \quad [20]$$

for roots $k_n l$ which are multiples of π. The values of ψ_n are given in Table 1.

TABLE 1 FUNCTIONS USED IN COMPUTING COEFFICIENT OF RESTITUTION AND DEFLECTION

n	$k_n l$	G_n	ψ_n	θ_n
1	3.14	3.00	0.333	0.333
2	4.30	4.84	0.733	0.163
3	6.71	2.18	0.094	0.022
4	9.42	3.00	0.333	0.333
5	10.58	4.80	0.577	0.145
6	12.99	2.18	0.082	0.021
7	15.70	3.00	0.333	0.333
8	16.86	4.80	0.584	0.146
9	19.27	2.18	0.082	0.021

NOTE: This table is for symmetrical vibrations only; vibrations excitable by central impact. For convenience n is given as 1, 2, 3, 4, 5, etc. In a set containing both the symmetrical and unsymmetrical vibrations a different method of enumeration would be required.

Then the coefficient of restitution can be written as follows (5)

$$e = \frac{1-\dfrac{m}{M}\,\Sigma\psi_n \cdot \Phi_n}{1+\dfrac{m}{M}\,\Sigma\psi_n \cdot \Phi_n} \quad [21]$$

where

$$\Phi_n = \frac{1+\cos 2\pi Q_n}{2(1-4Q_n^2)^2}$$

The function Φ_n is plotted in Fig. 2.

BENDING DEFLECTIONS AND STRAINS

Returning now to Equations [17] for q_n, we may determine R_n explicitly and integrate. The condition for determining R_n is (3)

$$R_n \delta q_n = f(t) \cdot \delta q_n \cdot X_n\big|_{x_1=0}$$

whence

$$R_n = f(t) \cdot X_n\big|_{x_1=0}$$

$f(t)$ is given by Equations [18], X_n is given by Equations [6] and [7]. Hence

$$q_n = \frac{X_n\big|_{x_1=0}}{p_n G_n M}\int_0^t f(\tau)\sin p_n(t-\tau)\,d\tau \quad [22]$$

This integral is readily evaluated so that q_n can then be explicitly obtained for the time of contact and for the time after contact as explained elsewhere (5).

Hence we may write the equation for the deflection at any point in the continuous beam at any time, using Equations [22] in Equations [6] and [7].

In particular, the deflection of the center span at any time after the contact ceases is

$$w = 4\,\frac{m}{M}\,v(1+e)\Sigma\,\frac{\theta_n}{p_n}\,\frac{\cos\pi Q_n}{(1-4Q_n^2)}\sin p_n\left(t-\frac{T_L}{2}\right)\left(\cos k_n x - \frac{\cos\dfrac{k_n l}{2}}{\cosh\dfrac{k_n l}{2}}\cosh k_n x\right) \quad [23]$$

where

$$\theta_n = \sin^2\frac{k_n l}{2}\left(1-\frac{\cos\dfrac{k_n l}{2}}{\cosh\dfrac{k_n l}{2}}\right)^2\frac{1}{G_n}$$

for roots $k_n l$ which are not multiples of π and

$$w = \frac{m}{M} v(1+e)\Sigma \frac{\theta_n}{p_n} \cdot \frac{\cos \pi Q_n}{(1-4Q_n^2)} \sin p_n \left(t - \frac{T_L}{2}\right) \cos k_n x \quad [24]$$

where

$$\theta_n = \frac{1}{G_n}$$

for roots $k_n l$ which are multiples of π.

As previously noted, the required values of G_n and ψ_n are given in Table 1. The circular frequencies p_n are obtained from

$$p_n = \frac{(k_n l)^2}{l^2} \cdot \sqrt{\frac{EI}{\rho A}} \quad [25]$$

The values of $k_n l$ are also given in Table 1 for convenience.

The bending strains may be computed from the deflections by differentiating with respect to x twice in the usual manner. Because of the presence of damping in any real beam the first few terms in the series are usually sufficient. For any particular problem, however, a sufficient number of terms in the series should be investigated to determine the rate of convergence or, what is the same thing, the number of modes appreciably excited.

Numerical Example

In order to illustrate the theory, the details of determining the deflections and strains for a beam on four supports struck at the mid-point of the center span will now be considered. The dimensions are so chosen that comparison of the results can be made with those for a single-span beam investigated in a previous paper (6).

Each span is 59 in. long with a square cross-sectional area of 10 sq in. The sphere weighs 50 lb and strikes with a velocity of 5 fps. For both beam and sphere, Young's modulus is 30×10^6 psi, Poisson's ratio is 0.3, and the weight per cubic inch is 0.284 lb.

The circular frequencies of the symmetrically vibrating beam are in radians per second

$$p_n = \frac{(k_n l)^2}{l^2} \sqrt{\frac{EI}{\rho A}}$$

and then using the values of $k_n l$ from Table 1, in radians per second

$p_1 = 522$	$p_6 = 8900$
$p_2 = 980$	$p_7 = 13100$
$p_3 = 2380$	$p_8 = 15000$
$p_4 = 4699$	$p_9 = 19700$
$p_5 = 5930$	

The effective contact time of the impact is (5)

$$T_L = 3.28 \left[\frac{m^2}{tr} \frac{(1-\nu^2)^2}{E^2}\right]^{1/5} = 4.83 \times 10^{-4} \text{ sec}$$

Recalling the expression for Q_n

$$Q_n = \frac{p_n T_L}{2\pi}$$

and using the values just computed for p_n and T_L

$\sqrt{Q_1} = 0.200$, $\sqrt{Q_2} = 0.275$, $\sqrt{Q_3} = 0.428$, $\sqrt{Q_4} = 0.601$

$\sqrt{Q_5} = 0.676$, $\sqrt{Q_6} = 0.828$, $\sqrt{Q_7} = 1.002$, $\sqrt{Q_8} = 1.075$

$\sqrt{Q_9} = 1.23$

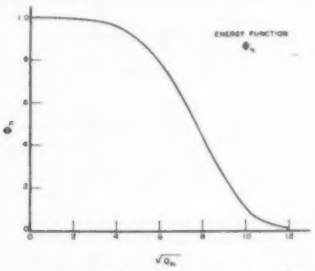

Fig. 2 Energy Function Φ_n

From Fig. 2 it is found that $\Phi_1 = 0.99$, $\Phi_2 = 0.98$, $\Phi_3 = 0.93$, $\Phi_4 = 0.78$, $\Phi_5 = 0.67$, $\Phi_6 = 0.38$, $\Phi_7 = 0.10$, $\Phi_8 = 0.04$, $\Phi_9 = 0.00$

and from Table 1 the corresponding values of ψ_n are

$\psi_1 = 0.333$, $\psi_2 = 0.733$, $\psi_3 = 0.094$, $\psi_4 = 0.333$, $\psi_5 = 0.577$, $\psi_6 = 0.082$, $\psi_7 = 0.333$, $\psi_8 = 0.584$, $\psi_9 = 0.082$

Hence, using Equation [21], the coefficient of restitution is

$$e = \frac{1 - \frac{m}{M}\Sigma\psi_n\Phi_n}{1 + \frac{m}{M}\Sigma\psi_n\Phi_n} = -0.05$$

Now all of the quantities in Equation [23] and in Equation [24] for the deflection can be calculated. The deflections at the center of the mid-span corresponding to each mode excited by the impact are plotted in Fig. 3.

The corresponding bending strains at the top and bottom surfaces of the beam have been computed and are plotted in Fig. 4.

Because the impact is at the center of the mid-span only, the symmetric modes of the beam are excited. For convenience these are referred to as the 1st mode, 2nd mode, 3rd mode, etc.

The deflection and strain for a single-span beam, having all

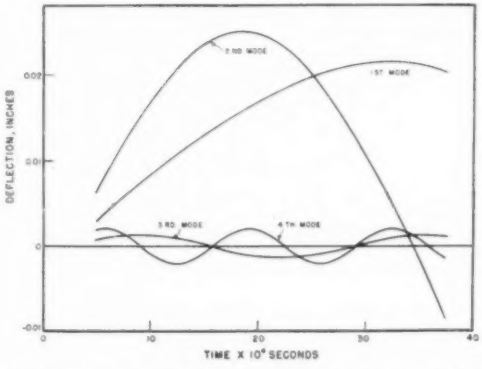

Fig. 3 Variation of Displacement at Center of Mid-Span in 3-Span Beam

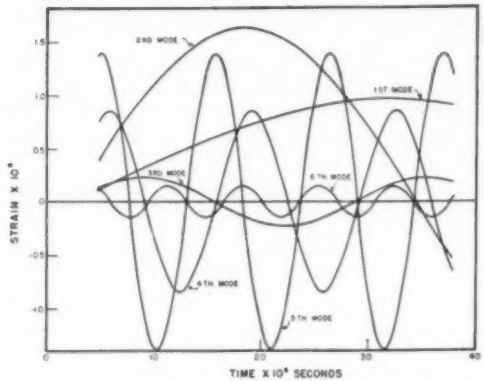

FIG. 4 VARIATION OF STRAIN AT CENTER OF MID-SPAN IN 3-SPAN BEAM

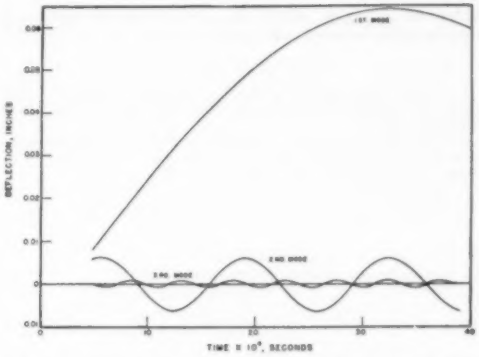

FIG. 5 VARIATION OF DISPLACEMENT CENTER OF SINGLE-SPAN BEAM

of its dimensions the same as those for a single span of the three-span beam just considered, are given in Fig. 5 and Fig. 6, respectively. The striking sphere is the same in both cases and strikes with the same velocity.

The shapes of the entire beam for the first four symmetric modes have been determined and they are shown for an arbitrary displacement scale in Fig. 7.

DISCUSSION

It may be of interest to compare the maximum deflection and strain obtained in the numerical example of the three-span beam with those obtained elsewhere (6) for the single-span beam. In the former case the maximum deflection is approximately 0.043 in. and the maximum strain approximately 3.68×10^{-4}. In the latter case, the maximum deflection is approximately 0.070 in. and the maximum strain approximately 6.5×10^{-4}. There is, therefore, a reduction of somewhat over one third in both deflection and strain in the three-span beam as compared with the single-span beam.

It is the opinion of the author that slow convergence of the series representing strain or its actual divergence is not serious because of the presence of damping in a real beam. Of course each case must be examined on its own merits but if the strain amplitude decreases as rapidly as it does in the numerical example just given, it would seem that the higher modes may be ignored. Experiments appear to confirm this belief.

It is of interest to note that two sets of frequencies arise in the problem of a beam on four supports. One set corresponds to frequency roots which are not multiples of π, and the other set corresponds to frequency numbers which are multiples of π. In the paper of Kaufmann (1) the second set is apparently overlooked and therefore omitted.

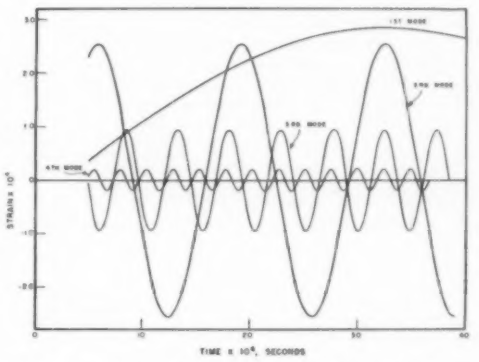

FIG. 6 VARIATIONS OF STRAIN AT CENTER OF SINGLE-SPAN BEAM

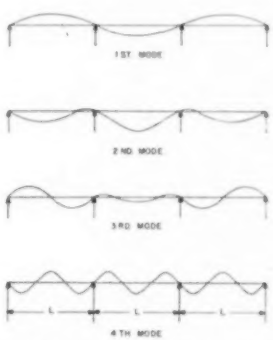

FIG. 7 SHAPES OF SEVERAL MODES OF VIBRATION OF 3-SPAN BEAM

CONCLUSION

The deflection equation has been developed for central impact on a three-span beam. The bending strains may be obtained readily from it by differentiating twice with respect to the position co-ordinate. The question of convergence of the strain equation is actually obviated by the observation that damping is always present in a real beam.

The method used for developing the deflection equation can readily be extended to the case of a beam on any number of supports simply by deriving the frequency equations and other necessary functions in a manner similar to that in this paper.

ACKNOWLEDGMENTS

The author wishes to acknowledge the sponsorship of the Office of Naval Research, Navy Department, Washington, D. C. He also wishes to express appreciation to Mr. P. D. Flynn, a graduate

student in mechanical engineering, for considerable assistance with the calculations and curve drawing.

BIBLIOGRAPHY

1 "Über Biegungsschwingungen stabförmiger Träger," by W. Kaufmann, *Zeitschrift für angewandte Mathematik und Mechanik*, vol. 2, 1922, pp. 34–45.

2 "Natural Frequencies of Continuous Beams of Uniform Span Length," by L. S. Jacobsen and R. S. Ayre, Technical Report No. 5, Navy Contract N6-OR1-154, Task Order I, March, 1949.

3 "Vibration Problems in Engineering," by S. Timoshenko, second edition, D. van Nostrand Company, Inc., New York, N. Y., 1937, pp. 348–349.

4 "Über die Berührung fester elastischer Körper," by H. Hertz, *Journal für Mathematik* (Crelle), vol. 92, 1881, p. 155.

5 "Impact of a Mass on a Damped Elastically Supported Beam," by W. H. Hoppmann, 2nd, JOURNAL OF APPLIED MECHANICS, Trans. ASME, vol. 70, 1948, p. 125.

6 "Impact of a Mass on a Column," by W. H. Hoppmann, 2nd, JOURNAL OF APPLIED MECHANICS, Trans. ASME, vol. 71, 1949, p. 370.

The Theory of Spring-Loaded Valves for Reciprocating Compressors[1]

By MICHAEL COSTAGLIOLA,[2] GREAT NECK, N. Y.

The inlet and discharge processes of a reciprocating compressor equipped with spring-loaded valves of the automatic type have been analyzed to determine the effects of the main design variables on performance. The most important criterion is found to be a parameter involving effective flow area through the valves and piston speed. Valve dynamics is a secondary consideration. For optimum valve dynamics, the valve would have no weight and a very small spring constant, giving an infinite natural frequency of the valve system. If certain valve characteristics are known (or measured by static-flow test), the performance of a compressor using these valves can be predicted with fair accuracy.

Nomenclature

The following nomenclature is used in this paper:

A_0 = maximum area for flow (either inlet or discharge valves) with valves fully open
A = area for flow at any time (valves partly open)
x_0 = maximum possible lift of valve
x = lift of valve at any time
W_v = weight of one valve
A_v = face area of one valve
ω_n = natural frequency of valve and spring
K_s = discharge coefficient associated with A
C_D = drag coefficient associated with Av
p = absolute pressure in cylinder at any time
p_i = inlet receiver pressure (const)
p_1, p_2, p_3, p_4 = pressures at points 1, 2, 3, 4 of p-v diagram (Fig. 2)
T = absolute temperature of air in cylinder at any time
T_1, T_2, T_3, T_4 = absolute temperature of air in cylinder at points 1, 2, 3, 4 of p-v diagram
T_i = absolute temperature of air in inlet receiver
m = weight of air in cylinder at any time, lb
m_1, m_2, m_3, m_4 = weight of air in cylinder at points 1, 2, 3, 4 in p-v diagram
v = specific volume of air in cylinder at any time
w = mass flow of air in or out of cylinder, lb per sec
v_i = specific volume of air in inlet receiver
C_2 = velocity of sound in air, at temperature T_2
C_i = velocity of sound in air, at temperature T_i
k = ratio of specific heats for air
K_1 = valve-spring constant
z = piston position from end of cylinder
s = stroke of piston
A_p = cross-sectional area of piston
Ω = angular speed of crank
θ = crank angle measured from top dead center
t = time, measured from top dead center
R = gas constant in equation, $pv = RT$
ΔE = change in internal energy of a system during a process
ΔQ = heat added to a system in a process
ΔW = work done by a system in a process
g = gravitational acceleration
c_v = specific heat at constant volume
η_v = volumetric efficiency
η_T = thermal efficiency

Dimensionless Ratios:

$$\frac{x}{x_0} = \frac{A}{A_0} = \alpha$$

$$\frac{p}{p_2} = \phi$$

$$\frac{p}{p_4} = \psi$$

$$\sqrt{\frac{8}{k-1}}\,\frac{A_0 K_s C_2}{s A_p \Omega} = B_4$$

$$\frac{C_D A_v p_1}{\frac{W_v}{g}\omega_n^2 x_0} = J_4$$

$$\sqrt{\frac{8}{k-1}}\,\frac{A_0 K_s C_i}{s A_p \Omega} = B_i$$

$$\frac{C_D A_v p_i}{\frac{W_v}{g}\omega_n^2 x_0} = J_i$$

$$\frac{\Omega}{\omega_n} = q$$

Introduction

Reciprocating air compressors are usually equipped with automatic spring-loaded valves, as shown schematically in Fig. 1. Valves of this type open automatically when subjected to a pressure difference. On the suction stroke, the inlet valves begin to open as soon as the cylinder pressure drops below the inlet-receiver pressure, and on the compression stroke, the discharge valves open when the cylinder pressure exceeds the discharge-receiver pressure. A typical p-v diagram for such a compressor

[1] This paper is based on a thesis by the author in partial fulfillment of the requirements for the degree of Doctor of Science in Mechanical Engineering at the Massachusetts Institute of Technology, June, 1949.

[2] Project Engineer, Sperry Gyroscope Company, Great Neck, N. Y. Jun. ASME.

Presented at the Annual Conference of the Applied Mechanics Division, Purdue University, Lafayette, Ind., June 22–24, 1950, of The American Society of Mechanical Engineers.

Discussion of this paper should be addressed to the Secretary, ASME, 29 West 39th Street, New York, N. Y., and will be accepted until January 10, 1951, for publication at a later date. Discussion received after the closing date will be returned.

Note: Statements and opinions advanced in papers are to be understood as individual expressions of their authors and not those of the Society. Manuscript received by the Applied Mechanics Division August 19, 1949. Paper No. 50—APM-12.

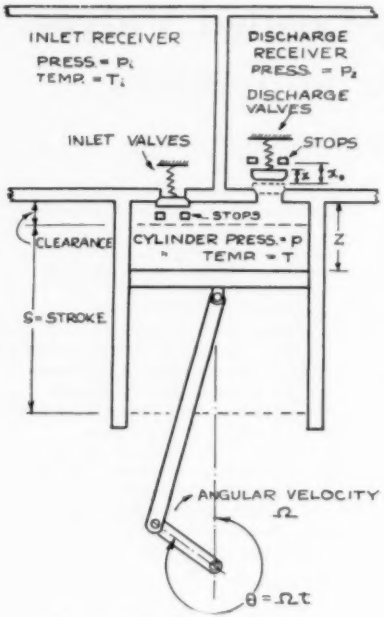

FIG. 1 COMPRESSOR ARRANGEMENT

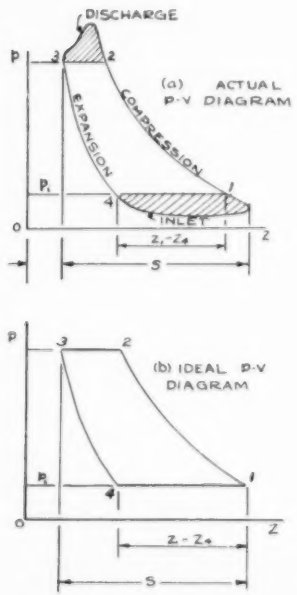

FIG. 2 P-V DIAGRAM

is given in Fig. 2(*a*). For comparison, the "ideal" *p-v* diagram is shown in Fig. 2(*b*). The shaded areas in Fig. 2(*a*) are the result of the pressure drops across the valves and, therefore, increase the work required to compress a given amount of air. These shaded areas, which we may term the "valve losses," should be made as small as possible to obtain good efficiency.

In order to determine the valve losses theoretically, one must be able to predict the inlet and discharge portions of the diagram. This can be achieved if a few simplifying assumptions are made. The purpose of the theoretical analysis is twofold:

1 To determine the parameters affecting performance and their relative importance.

2 To establish a basis for predicting the efficiency of a compressor when the major elements of the design have been selected.

The simplified system analyzed is that shown in Fig. 1. However, the analysis is applicable to any type of valve which approximates the single-degree-of-freedom system shown. Although the drawing shows only two valves, any number may be used. A valve is assumed to consist of an elastically restrained mass with stops to limit the lift to a definite amount. The valve-spring force is assumed linear, with zero spring force when the valve is closed. "Perfect gas" laws are used, with no heat transfer throughout the cycle. The piston speed is always low compared to the speed of sound in air so that the air in the cylinder is essentially at stagnation conditions. Flow through the valve ports is calculated by the formula for one-dimensional flow through an orifice, with a constant-discharge coefficient. It is also assumed that inlet and discharge receivers are infinitely large so that pressures in these spaces are constant over the entire cycle.

Discharge Process

Using the nomenclature given, we write the equation of state for the gas in the cylinder at any time

$$pA_p z = mRT \qquad [1]$$

For the condition at point 2 in Fig. 2 (*a*) (the start of discharge), the foregoing relation is

$$p_2 A_p z_2 = m_2 R T_2 \qquad [2]$$

Dividing Equations [1] and [2] gives

$$\frac{m}{m_2} = \left(\frac{z}{z_2}\right)\left(\frac{p}{p_2}\right)\left(\frac{T}{T_2}\right) \qquad [3]$$

During discharge, the process in the cylinder may be considered as adiabatic and isentropic, so we write

$$pv^k = \text{const} \qquad [4]$$

With this assumption we have

$$\frac{T}{T_2} = \left(\frac{p}{p_2}\right)^{\frac{k-1}{k}} = \phi^{\frac{k-1}{k}} \qquad [5]$$

where $\phi = p/p_2$

Substituting Equation [5] in [3] and simplifying

$$m = m_2 \frac{z}{z_2} \phi^{1/k} \qquad [6]$$

The mass flow out of the cylinder is given by the well-known formula for subcritical flow through an orifice

$$w = K_c A \sqrt{\frac{2gk}{R(k-1)T}}\, p \left(\frac{p_2}{p}\right)^{1/k} \sqrt{1 - \left(\frac{p_2}{p}\right)^{\frac{k-1}{k}}} \qquad [7]$$

where w = flow out of cylinder, lb per sec

Since the area for flow is proportional to the valve lift at any time we put

$$A = A_0 \frac{x}{x_0} = A_0 \alpha \quad [8]$$

where

$$\alpha = \frac{x}{x_0}$$

Substituting for T from Equation [5], in Equation [8], and using the formula for the velocity of sound in air

$$C_2 = \sqrt{kgRT_2} \quad [9]$$

Equation [7] becomes, after simplification

$$w = K_c A_0 \alpha \sqrt{\frac{2}{k-1}} g \frac{kp_2}{C_2} \sqrt{\phi^{\frac{k-1}{k}} - 1} \quad [10]$$

Now we can eliminate w by noting that, during discharge

$$w = -\frac{dm}{dt} \quad [11]$$

Therefore Equation [6] is differentiated with respect to time t, and combined with Equation [10] by using Equation [11]. As a further convenience, the crank angle θ is taken as the independent variable, and the time derivatives converted by the relation

$$\theta = \Omega t \quad [12]$$

$$\frac{d[\ldots]}{d\theta} = \frac{1}{\Omega} \frac{d[\ldots]}{dt} \quad [13]$$

Where Ω = angular speed of crank. The final equation can be expressed in the following form

$$\frac{d\phi}{d\theta} = -\frac{k}{z/(s/2)} \left(B_d \alpha \phi^{\frac{k-1}{k}} \sqrt{\phi^{\frac{k-1}{k}} - 1} + \frac{2\phi}{s} \frac{dz}{d\theta} \right) \quad [14]$$

where s = stroke of piston, and

$$B_d = \sqrt{\frac{8}{k-1}} \frac{C_2 K_c A_0}{A_p s \Omega} \quad [15]$$

This gives a differential equation for the dimensionless cylinder pressure ϕ, involving the piston position z, the valve lift α, the crank angle θ, and the dimensionless flow parameter B_d. The piston position is given as a function of the crank angle by

$$z = a - b \cos\theta - c \cos 2\theta \quad [16]$$

Where $a, b, c \ldots$, are constants for a given compressor.

We cannot yet solve Equation [14] as it contains two unknowns, ϕ and α, as functions of the independent variable θ.

To get another equation we consider the dynamics of the valve itself. During opening or closing of the valve, the forces on the valve body are as shown in Fig. 3. The force F is due to fluid drag of the gas flowing around the valve body. This force can be expressed as

$$F = C_D A_v (p - p_2) \quad [17]$$

This would be an exact statement of pressure drag for incompressible flow but is only approximate where compressibility is concerned. Writing the equation of motion of the valve

$$C_D A_v (p - p_2) - K_1 x = \frac{W_v}{g} \frac{d^2x}{dt^2} \quad [18]$$

As before, we convert to the dimensionless form by using

$$\alpha = \frac{x}{x_0}, \quad \phi = \frac{p}{p_2}, \quad \text{and} \quad \theta = \Omega t$$

We also introduce the natural frequency of the valve system by the equation

$$\omega_n = \sqrt{\frac{g K_1}{W_v}} \quad [19]$$

The resulting dimensionless equation is

$$q^2 \frac{d^2\alpha}{d\theta^2} + \alpha - J_d (\phi - 1) = 0 \quad [20]$$

where

$$q = \frac{\Omega}{\omega_n} \quad [21]$$

$$J_d = \frac{C_D A_v p_2}{K_1 x_0} = \frac{C_D A_v p_2}{W_v \omega_n^2 x_0 / g} \quad [22]$$

Thus, in Equation [16], we have another differential equation in ϕ and α, involving two dimensionless parameters J_d and q.

During opening or closing of the valve, Equations [14] and [20] must be solved simultaneously for ϕ and α in terms of θ.

The initial conditions for the opening process are

$$\alpha = 0, \ \phi = 1, \ \frac{d\alpha}{d\theta} = 0 \text{ at crank angle } \theta = \theta_2$$

The solution of Equation [20] during this process is given by "Duhamel's Integral"[3]

$$\alpha = J_d \int_{\theta' = \theta_2}^{\theta' = \theta} \left(\frac{d\phi}{d\theta'} \right) \left[1 - \cos\left(\frac{\theta - \theta'}{q} \right) \right] d\theta' \quad [23]$$

In this formula, θ' is a variable of integration, as distinguished from θ, which is constant in the integration. The solution for the valve lift α, and dimensionless cylinder pressure ϕ are given in the opening process by a point-to-point integration of Equations [14] and [23]. Fig. 4 shows a typical solution for the complete discharge process. The integration of Equations [14] and [23] is carried out until $\alpha = 1$ (point b in Fig. 4), where the valve strikes the stops. It is assumed thatt he valve remains against the stops and does not rebound. While the valve is held against the stops, the dynamic Equation [20] is not valid, and is of course not required. During this period the solution for ϕ is obtained from Equation [14] with $\alpha = 1$. The general solution of this part of the process is easily found by the method of isoclines,[4] since the equation is in the form

$$\frac{d\phi}{d\theta} = f(\phi, \theta)$$

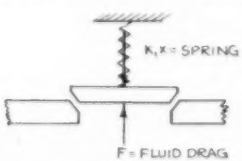

FIG. 3 FORCES ON VALVE

[3] "Mathematical Methods in Engineering," by Th. von Kármán and M. A. Biot, McGraw-Hill Book Company, Inc., New York, N. Y., 1940, pp. 397–405.

[4] Ibid., pp. 6–7.

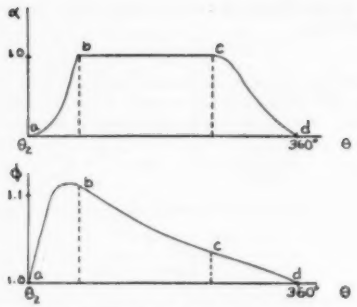

FIG. 4 TYPICAL CURVES FOR VALVE LIFT AND DIMENSIONLESS PRESSURE ϕ DURING DISCHARGE

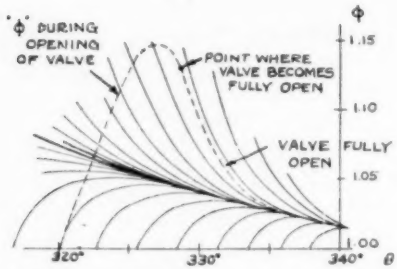

FIG. 5 PORTION OF ϕ CURVES FOR FULLY OPEN VALVES ($B_d = 6$) WITH TYPICAL SOLUTION SUPERIMPOSED

This is convenient where a large number of solutions are required, since a plot of ϕ versus θ for the valves fully opened can be constructed for any constant value of B_d.

Fig. 5 shows a part of such a plot as derived by the isocline method. Since the equation is of the first order, only one initial condition is required to locate a point on one of the integral curves. This point is found by plotting the curve of ϕ versus θ for the opening process on this diagram, as shown in Fig. 4. The point where the valve first becomes fully opened (point b), will lie on one of the integral curves of ϕ for the fully opened valve. Then one follows this curve (in the direction of increasing θ) until the pressure drops to such a value that it no longer will hold the valve against the stops, and the valve will start to close (point c in Fig. 4). This point is found from Equation [20], putting $\alpha = 1$ and $(d^2\alpha)/(d\theta^2) = 0$. This gives for point c

$$\phi = 1 + \frac{1}{J_d} \quad [24]$$

For the closing process, the initial conditions are

$$\alpha = 1, \quad \frac{d\alpha}{d\theta} = 0, \quad \text{and} \quad \phi = 1 + \frac{1}{J_d}$$

The solution for the valve motion is

$$\alpha = 1 + J_d \int_{\theta' = \theta_c}^{\theta' = \theta} \left(\frac{d\phi}{d\theta'}\right)\left[1 - \cos\left(\frac{\theta - \theta'}{q}\right)\right] d\theta' \quad [25]$$

The complete solution is obtained by a point-to-point integration of Equations [14] and [25], the numerical integration being carried out until $\phi = 1$, which occurs at, or soon after, top dead center ($\theta = 2\pi$).

Thus the cylinder pressure and valve lift (in dimensionless form) have been determined for the whole discharge process.

INLET PROCESS

The thermodynamic system considered in the inlet process is shown in Fig. 6. Instead of the adiabatic relation, Equation

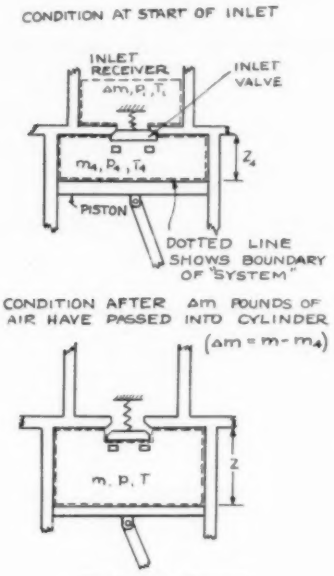

FIG. 6 INLET PROCESS

[4], used in the discharge, we used the statement of the first law of thermodynamics[5]

$$\Delta E = \Delta Q - \Delta W \quad [26]$$

For our system, putting $\Delta Q = 0$ (as we are neglecting heat transfer), Equation [26] becomes

$$C_v[mT - m_4T_4 - (m - m_4)T_s] = -\int_{z_4}^{z} pA_p dz + p_s v_s(m - m_4) \quad [27]$$

As before, we use the equation of state and the formula for flow through an orifice

$$p\,A_p z = mRT \quad [28]$$

$$p_s v_s = RT_s \quad [29]$$

$$w = K_e A \sqrt{\frac{2gk}{R(k-1)T_s}}\, p_s \left(\frac{p}{p_s}\right)^{1/k} \sqrt{1 - \left(\frac{p}{p_s}\right)^{\frac{k-1}{k}}} \quad [30]$$

(Here K_e and A are the values for the inlet valves.) To get the differential equation for the cylinder pressure, we first eliminate T from Equation [27] by using Equations [28] and [29], and differentiate with respect to time. Then solve for $(dm)/(dt)$ from this relation and equate it to Equation [30], since, for the inlet process

[5] "Thermodynamics," by J. H. Keenan, John Wiley & Sons, Inc., New York, N. Y., 1941, p. 12.

$$w = \frac{dm}{dt} \quad [31]$$

The resulting equation is simplified and made dimensionless as before by using the relations

$$\theta = \Omega t, \quad \frac{x}{x_0} = \alpha, \quad \frac{p}{p_s} = \psi \quad [32]$$

$$C_s = \sqrt{kgRT_s} \quad [33]$$

(Note that $p_s = p_1 = p_4$, and $C_v/R = 1/k - 1$.)

The final result is

$$\frac{d\psi}{d\theta} = \frac{k}{z/(s/2)}\left(B_i \alpha \psi^{1/k}\sqrt{1 - \psi^{\frac{k-1}{k}}} - 2\frac{\psi}{s}\frac{dz}{d\theta}\right) \quad [34]$$

where

$$B_i = \sqrt{\frac{8}{k-1}}\frac{K_v A_v C_s}{A_p s\Omega} \quad [35]$$

The equation of motion for the valve is derived in a similar manner to that for the discharge valves. The result is

$$q^2\frac{d^2\alpha}{d\theta^2} + \alpha - J_i(1 - \psi) = 0 \quad [36]$$

where

$$q = \frac{\Omega}{\omega_n} \quad [37]$$

$$J_i = \frac{C_D A_v p_s}{\frac{W_v}{g}\omega_n^2 x_0} = \frac{C_D A_v p_s}{K_1 x_0} \quad [38]$$

In these formulas, C_D A_v, ω_n, x_0, W_v, and K_1 are the values for the inlet valves. The general solution of Equation [36] for the opening process is

$$\alpha = -J_i\int_{\theta'=\theta_c}^{\theta'=\theta}\left(\frac{d\psi}{d\theta'}\right)\left[1 - \cos\left(\frac{\theta - \theta'}{q}\right)\right]d\theta' \quad [39]$$

For the closing of the valve, the solution is

$$\alpha = 1 - J_i\int_{\theta'=\theta_c}^{\theta'=\theta}\left(\frac{d\psi}{d\theta'}\right)\left[1 - \cos\left(\frac{\theta - \theta'}{q}\right)\right]d\theta' \quad [40]$$

Here θ_c is the value of θ when the inlet valve starts to close, and is determined from

$$\psi = 1 - \frac{1}{J_i} \quad [40a]$$

at point c where valve begins to close.

The complete solution is similar to that for the discharge process. First Equations [34] and [39] are numerically integrated until $\alpha = 1$. Then, while the valves are fully open, put $\alpha = 1$ in Equation [34] and use the isocline method for the general solution. Use Equation [40a] to find the value of ψ for which the valves will start to close. For the closing process, Equations [34] and [40] are numerically integrated.

Calculation of Valve Losses and Efficiency

A compressor in any given operating condition will have definite values of B, J, and q for both inlet and discharge valves, and a certain pressure ratio p_2/p_1. The curves of ϕ and ψ can be computed for this condition, and from them the inlet and discharge portions of the p-v diagram. The compression and expansion lines may be assumed as adiabatic with $pv^k = \text{const.}$ Thus the complete p-v diagram is obtained.

The theoretical cycle thermal efficiency will then be given by [referring to Fig. 2(*a*)]

$$\eta_T = \frac{\text{Total diagram area} - \text{loss areas}}{\text{Total diagram area}}$$

It is evident that the actual diagram, Fig. 2(*a*), differs from the ideal, Fig. 2(*b*), in two respects, as follows:

1 In the ideal diagram, inlet and discharge take place at constant pressure, while the actual diagram has additional areas, the shaded portions in Fig. 2(*a*), which increase the work per stroke.

2 In the ideal diagram, expansion and compression start at top and bottom dead center, respectively. Within the range of good design practice, the actual expansion line begins very close to top dead center. However, due to the inlet throttling, the cylinder pressure does not rise to the value of the inlet pressure until somewhat after bottom dead center, thereby delaying the start of compression.

This results in reducing the [illegible]th of the diagram, but also reduces the amount of air deliv[illegible] per stroke (and consequently lowers the volumetric efficiency), in the same proportion. The volumetric efficiency is defined as

$$\eta_v = \frac{\text{Volume of air at inlet conditions delivered per stroke}}{\text{Piston displacement}}$$

In the ideal case, the volumetric efficiency is readily found to be

$$\eta_{vi} = \frac{z_1 - z_4}{s} \quad [41]$$

where z_1 and z_4 are the piston positions as given on Fig. 2(*b*).

The volumetric efficiency of the actual case can be obtained from Equation [27] since the volume of air delivered per stroke (at inlet conditions) is simply $(m_1 - m_4)v_1$, if there is no leakage. One can solve for this quantity from Equation [27] with m_1 substituted for m, z_1, for z, etc.

After rearrangement, the final value of the volumetric efficiency is

$$\eta_v = \frac{z_1 - z_4}{s} - \frac{k-1}{k}\int_{z_4}^{z_1}(\psi - 1)\frac{dz}{s} \quad [42]$$

Thus the actual volumetric efficiency is lower than the ideal due to the following effects:

1 The value of $z_1 - z_4$ is lower since the start of compression is delayed after bottom dead center, making z_1 smaller.

2 The second term in Equation [42] also reduces volumetric efficiency, and is proportional to the inlet loss area in Fig. 2(*a*). The larger this term, the greater the degree of irreversibility in the inlet process, and, consequently, the greater the increase in entropy and specific volume of the air in the cylinder.

Thus, for all practical purposes, the volumetric efficiency is solely a function of the inlet process and independent of the discharge process.

Effect of Various Parameters on Valve Losses

The foregoing discussion describes how one can plot the theoretical p-v diagram for a compressor in any operating condition. From the theoretical diagram the valve losses, cycle efficiency, and volumetric efficiency can be computed.

In order to investigate the general problem of valve losses, however, it is best to treat the inlet and discharge processes

independently. There are three basic parameters B, J, and q (for each process) in the differential equations. There is a fourth parameter, the pressure ratio of the compressor p_2/p_1, which determines the crank angles at which discharge and inlet begin. Besides these quantities, one could also consider variations in the clearance ratio and crank-connecting rod ratio for the compressor, but we will consider them fixed, since they do not affect valve losses critically within the usual range of design practice.

A large number of separate cases were calculated, with various values of the parameters B, J, and q for both inlet and discharge processes, and for different values of the crank angles θ_2 and θ_4, where discharge and inlet begin, respectively. For each case, the valve loss was computed as a percentage of the theoretical cycle area. Also, the volumetric efficiency was obtained for each case of the inlet process.

Since there are so many variables, the results cannot be presented in any simple form. However, the main results of the investigation can be summarized as follows:

1 The flow parameter B is the most important factor in valve losses. The parameters J and q are of secondary effect. For low losses, B should be as large as possible.

2 Valve losses decrease with increase in pressure ratio.

3 For large values of B ($B > 6$), the losses vary inversely as the square of B, or, in other words, inversely as the square of valve flow area and directly as the square of the piston speed.[6] At low values of B ($B = 1$, approx.), the losses vary about as the inverse of B.

4 When the flow area is small, the effect of valve dynamics (as expressed by variations in J and q), has little influence on valve losses. When the flow area is large, valve dynamics is important. For example, with very stiff springs and a large flow area, the valves make several cycles of opening and closing during the inlet or discharge period, thereby increasing losses.

5 For dynamic considerations the valve would have no weight and an infinitesimal spring constant, giving an infinite natural frequency. To reach this goal, one must reduce valve weight and spring stiffness to a minimum, while keeping the natural frequency of the valve system very high.

6 The parameter B_1 is the most important consideration for volumetric efficiency (in so far as the valves are concerned). Valve dynamics has a much smaller effect. For a high volumetric efficiency, B_1 should be as large as possible.

Correlation of Theory With Experiments

Numerous tests were run on a small single-cylinder compressor, and the results compared with the theory. The type of valve actually used was that known as the "reed" or "feather" valve.[7] This type consists of a flat strip of steel covering a slot which forms the valve port. A pressure difference will lift the valve, causing it to flex against a curved stop plate.

If the reed is considered to move only in the first mode of vibration as a simply supported beam, the derived equations are the same as for the single-degree-of-freedom system analyzed previously.

[6] The piston speed is given by the product sl, or the stroke $\times$ rotational speed of crank.

[7] "Air Compressor Valves," by J. D. Watson, *Colliery Engineering*, vol. 16, April, 1939, pp. 130–136.

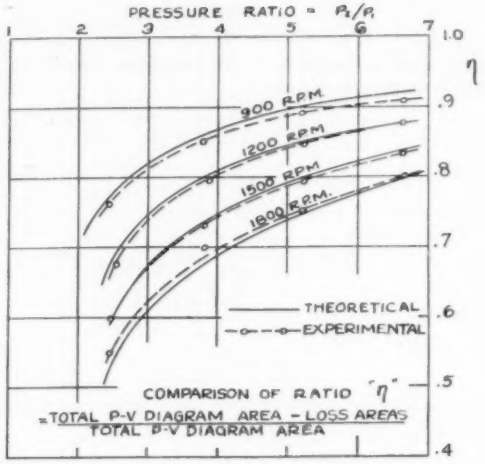

Fig. 7 Comparison of Theory With Experiments

One can predict the performance of a compressor if one knows the values of the parameters B, J, and q in any operating condition. These parameters are calculated from the known design dimensions and the empirical coefficients K_r and C_D which are found by means of a simple static test.

Fig. 7 shows the comparison of predicted cycle efficiency with that obtained from the actual indicator cards. This shows an agreement within 1 per cent. However, the actual cycle efficiency should not be calculated solely from the p-v diagram (as for the theoretical efficiency) but as a ratio of

$$\frac{\text{Ideal cycle work per lb of air} \times \text{actual air flow (lb/stroke)}}{\text{Actual cycle work per stroke}}$$

With this method of calculating efficiency the actual efficiency comes out from 3 to 7 per cent lower than the theoretical. The measured volumetric efficiencies are also about 1 to 5 per cent lower than the theoretical. It is felt that these discrepancies are largely due to leakage and heat transfer.

The dynamics of the valves was investigated also, using a mechanical device to record the valve lift as a function of time. The results showed that the theoretical curves of valve lift are essentially correct, with the exception of a small amount of rebound where the valves strike the stops. There was no observable rebound where the valves struck their seats.

Conclusion

The performance of reciprocating compressors with spring-loaded valves can be analyzed successfully, provided a few simplifying assumptions are made. Actual volumetric and thermal efficiencies will be slightly lower than the theoretical. The theory indicates that for a given pressure ratio the valve performance is principally a function of a parameter involving piston speed and valve flow area.

Characteristics of Irrotational Flow Through Axially Symmetric Orifices

By HUNTER ROUSE[1] and ABDEL-HADI ABUL-FETOUH[2]

Although an exact analytical solution of the orifice problem has not yet proved feasible, use of the method of relaxation has permitted a numerical determination of the flow characteristics to be made with sufficient precision for the problem to be considered solved. The coefficient of contraction is found to be practically identical with that evaluated by von Mises for two-dimensional flow from slots over the entire range of area ratio, and reasonable agreement is shown to exist between measurement and computation. Co-ordinates of the jet profiles are presented in tabular and graphical form, and are found to differ appreciably from those previously adapted from the two-dimensional case. A composite dimensionless chart is also provided showing the distribution of pressure along the boundary and center line and across the efflux section for the various area ratios.

Introduction

DESPITE the underlying similarity that exists between many patterns of two-dimensional and axially symmetric three-dimensional flow, there is a pronounced dissimilarity in the mathematical limitations to which problems in the two flow categories are subject. This situation results in large measure from the fact that no three-dimensional counterpart has yet been devised for the powerful two-dimensional tool of conformal transformation. There are, to be sure, various alternative methods of successive approximation which are applicable alike to boundary conditions of either category. However, these are seldom general in their applicability, and in no instance can they be said to yield an exact solution.

A case in point is the analysis of flow from slots and orifices. In 1869 Kirchhoff (1)[3] solved the problem of the slot in an infinite plane boundary, deriving an exact relationship for the jet profile and showing the linear contraction factor to have the magnitude $\pi/(\pi + 2) = 0.611$. The corresponding axially symmetric case—a circular orifice in an infinite plane boundary—was treated in 1913 by Trefftz (2), who found by successive approximation that the ratio of the cross-sectional area of the contracted jet to the area of the orifice likewise had a magnitude between 0.60 and 0.62. Despite the fact the jet profiles for the two cases were thus shown to be quite different, definition of the contraction coefficient C_c in terms of the area ratio nevertheless permitted the discharge equation for both cases to be written simply as

$$Q = C_c\, a \sqrt{2p/\rho} \qquad [1]$$

in which a is the area of the outlet and $C_c \approx 0.61$. This, however, marked the end of the parallel development; in fact, although the exact analysis of flow from slots in finite boundaries has been carried essentially to completion, no comparable analysis of orifice flow has yet proved possible.

Some fifty years after Kirchhoff's original solution, von Mises (3) published a very broad treatment of the two-dimensional efflux problem, determining by conformal methods the coefficients of contraction for jets from slots under a wide variety of boundary conditions. The series which is of particular interest in the present discussion involved a symmetric slot in a plane at right angles to parallel walls, as shown in Fig. 1, the coefficient of contraction (see Table 1) varying from 0.611 to 1.0 as the ratio of slot width b to wall spacing B varied from zero to unity. Although this investigation was restricted to the determination of the asymptotic limit of jet width, other analyses have yielded the corresponding co-ordinates of the jet profiles, at least for the case of a symmetric slot in a normal boundary. For example, in 1931 Betz and Petersohn (4) extended the analysis of Kirchhoff over the entire range of b/B by means of the hodograph method.

Since the limiting conditions of flow from slots and orifices may be expressed in terms of the same equation, the assumption is frequently made (5) that the discharge function for slots of various proportions may be adapted to orifices of similar proportions (compare Figs. 1 and 2), by utilizing the von Mises coefficient C_c corresponding to a given value of b/B for the same magnitude of the diameter ratio d/D. Under such circumstances both cases of flow would be described by the same efflux equation

$$Q = C_d\, a \sqrt{2p/\rho} \qquad [2]$$

in which p is the pressure intensity in the uniform zone of approach and C_d is a discharge coefficient depending, like C_c, upon the ratio of the outlet area a to the cross-sectional area A of the approach passage

$$C_d = \frac{C_c}{\sqrt{1 - (C_c a/A)^2}} \qquad [3]$$

This assumption formed the basis of a study published in 1936 by Kretzschmer (6), who further hypothesized that the jets from similar slots and orifices would have not only equal relative cross-sectional areas at the limit but also equal relative areas at the same relative distances from the efflux sections—in other words, that the jet profiles determined for slots by Betz and Petersohn

TABLE 1 COEFFICIENTS OF CONTRACTION FOR SLOTS, AFTER VON MISES

b/B	0.0	0.1	0.2	0.3	0.4	0.5	0.6	0.7	0.8	0.9	1.0
C_c	0.611	0.612	0.616	0.622	0.631	0.644	0.662	0.687	0.722	0.781	1.00

[1] Director, Iowa Institute of Hydraulic Research, State University of Iowa, Iowa City, Iowa. Mem. ASME.

[2] Lecturer, College of Engineering, Farouk El-Awal University, Alexandria, Egypt.

[3] Numbers in parentheses refer to Bibliography at end of paper.

Presented at the National Conference of the Applied Mechanics Division, Purdue University, Lafayette, Ind., June 22–24, 1950, of The American Society of Mechanical Engineers.

Discussion of this paper should be addressed to the Secretary, ASME, 29 West 39th Street, New York, N. Y., and will be accepted until January 10, 1951, for publication at a later date. Discussion received after the closing date will be returned.

Note: Statements and opinions advanced in papers are to be understood as individual expressions of their authors and not those of the Society. Manuscript received by the Applied Mechanics Division August 15, 1949. Paper No. 50—APM-11.

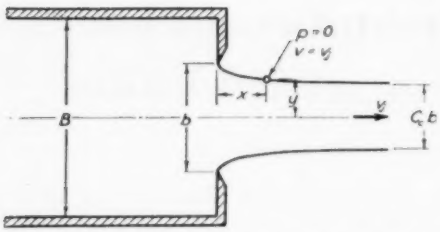

FIG. 1 DEFINITION SKETCH FOR FLOW FROM A SLOT

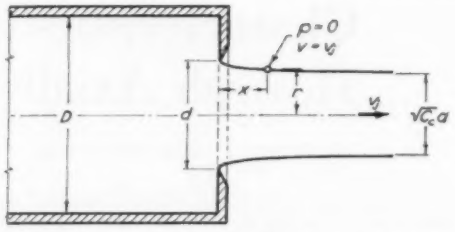

FIG. 2 DEFINITION SKETCH FOR FLOW FROM AN ORIFICE

could be used to predict the corresponding profiles for orifices, through the assumed relationship $2r/d = \sqrt{2y/b}$ for $d/D = b/B$ and $x/d = x/b$. The validity of this approximation was tested by Kretzschmer both by means of the electrical analogy and through comparison with measured profiles, without evidence of appreciable error.

The fact remains, nevertheless, that experimental measurements of jet profiles are in themselves rather inconsistent, due in large measure to the variable influence of gravity, viscosity, and capillarity upon the flow pattern; use of the electrical analogy is also subject to experimental inaccuracies unless extreme care is taken. For these reasons the Kretzschmer approximation cannot be regarded in any sense as an exact evaluation of the axially symmetric efflux problem. In view of this conclusion, it was decided by the authors to undertake a full investigation of the problem through use of two alternative procedures which had proved of considerable value in similar fields of study at the Iowa Institute of Hydraulic Research, namely, an improved electrical-analogy technique, and the Southwell process of relaxation.

METHODS OF INVESTIGATION

The electrical-analogy technique used by the Iowa Institute has been described elsewhere (7) in detail. It involves, in brief, (*a*) representation of a body of revolution by such a small segment that the boundary surface need curve in only one plane, and (*b*) replacement of the usual movable probe by a series of small electrodes precisely located along the boundary. The electrolyte is thus contained between a sheet of plate glass inclined at perhaps 5 deg to the horizontal, two vertical copper terminal plates in the approximate form of potential surfaces and well removed from the zone of measurement, and a strip of plastic at right angles to the glass and formed to represent the curved boundary. The center line, corresponding to the intersection of the free surface of the electrolyte and the glass plate, is further defined by a low wall of paraffin to eliminate capillary creep. A 0.01-molar solution of copper sulphate with a small admixture of sulphuric acid is used as the electrolyte. The electrodes are formed of 0.015-in. copper wire passing through holes in the plastic strip; the holes are drilled on a precision milling machine, the wires cemented in place, and the contact surfaces polished flush.

An electrical potential is applied between the terminal plates, and the resulting potential difference between each successive pair of boundary electrodes is measured by means of a bridge circuit containing a sensitive null indicator. The potential difference, divided by the electrode spacing, is assumed proportional to the velocity at the mid-point between the electrodes. For precise determinations the electrode spacing must be relatively small, the surfaces clean, the joints tight, and the electrolyte free from stratification. Noteworthy is the fact that errors in measurement will be compensative rather than cumulative, since a local discrepancy will merely affect two successive differences in opposite directions.

Application of this technique to the study of orifice flow involved the trial-and-error adjustment of the boundary strip in such a manner as to yield an essentially constant velocity (required by the boundary condition of constant pressure) at all points of the simulated free surface. Therefore, those portions of the boundary representing the pipe wall and the orifice plate were made of $^1/_8$-in. lucite plate sealed to the glass by means of melted paraffin, while that portion corresponding to the free surface consisted of $^1/_{16}$-in. pyraline sheet sealed with an external fillet of readily removable plasticine. For the chosen orifice radius of 5 in. the electrode spacing varied from $^1/_2$ in. near the edge of the orifice to 1 in. far upstream and downstream. The flexible free-surface strip was first given a reasonable shape and then adjusted in accordance with the electrical indications, gradually approaching the desired shape by the process of successive approximation. A point of diminishing returns appeared to have been reached when the maximum local variation in potential gradient was reduced to $\pm 1^1/_2$ per cent. The surface profile was thereafter transferred to co-ordinate paper by means of a wax mold.

The general method of relaxation has also been described elsewhere (8, 9); in fact, Southwell and Vaisey (10) have already applied it to orifice flow for a particular value of d/D. Suffice it to say that a longitudinal section through the given zone of flow is subdivided by a series of equally spaced horizontal and vertical lines, and reasonable values of the stream function ψ are assumed for all intersections of these lines with each other and with the boundary. By expressing the Laplacian equation in terms of finite differences, a relationship may be written between the values of ψ at any given intersection and at the four intersections which surround it. The correct values are then gradually approached by a systematic procedure of reducing the errors in the original assumptions in accordance with this relationship. Since no part of the flow pattern can be wholly rectified unless those parts in the immediate vicinity are also essentially correct, the procedure necessarily involves a gradual refining of the pattern as a whole in successive steps. On the other hand, once the pattern is as nearly correct as the original degree of subdivision will permit, greater local accuracy may be obtained by further subdivision and repetition of the relaxation process.

The foregoing method of determining the flow pattern for a given boundary configuration was adapted to the problem of flow with a free surface by assuming the free-surface profile, performing the relaxation, and evaluating the free-surface velocity from the resulting distribution of ψ. The profile was then adjusted in such manner as to make the velocity more nearly constant, and the relaxation process was repeated. Evaluation of the velocity at a given point on the free surface proceeded in accordance with the relationship

$$v = \frac{1}{r}\frac{\partial \psi}{\partial n} = \frac{1}{r \cos \alpha}\frac{\partial \psi}{\partial r} \qquad [4]$$

in which n refers to distance normal to the streamline in the

direction of curvature, and α is the angle of inclination of the streamline to the axis. In view of the fact that the values of ψ were at hand only at intermittent points and values of α only from graphical measurement of an assumed curve, application of Equation [4] required considerable refinement of technique (i.e., curvilinear rather than linear approximation), before the desired accuracy along the curved portion of the surface could be attained. Less difficulty was encountered at the asymptotic limit, where $\alpha \to 0$, the correspondingly more accurate value of v_j providing the reference magnitude toward which the velocity at other points was adjusted.

Unlike the electrical-analogy method, the accuracy of which is definitely limited by practical considerations of construction and instrumentation, the relaxation method is governed in accuracy only by the element of time. In other words, although the latter method cannot be classed as exact, the residual errors may be reduced to any desired extent commensurate with the labor which can be devoted to the solution. In the present case, once the necessary technique had been perfected, the electrical solution was carried to its practical limit for the boundary condition $d/D = 0$ in about 200 hr. The same degree of accuracy was obtained by relaxation in 100 hr, this process then being continued another 50 hr, and the maximum variation in the free-surface velocity thereby being reduced to ± 0.7 per cent. Therefore, use of the electrical method was restricted to the one boundary condition, and the relaxation method was extended to $(d/D)^2 = a/A$ ratios of 0.25, 0.5, and 0.75. The upper limit $a/A = 1.0$, of course, has a self-evident solution.

Once the jet profiles for the five systematically progressive cases had been determined, further use was made of the relaxation nets in evaluating the distribution of pressure along the fixed boundary and the center line and across the orifice opening. As in all cases of irrotational flow, the pressure intensity at any point with respect to that at a reference point may be expressed dimensionlessly in terms of the local velocity in its ratio to the velocity at the reference point. If a point on the free surface is taken as reference, the expression becomes

$$\frac{p}{\rho v_j^2/2} = 1 - \left(\frac{v}{v_j}\right)^2 \qquad [5]$$

Use of this expression evidently requires evaluation of the velocity ratio v/v_j at all points in question. Along the boundary and across the orifice opening this evaluation proceeded in the same manner as for the free surface. At the center line, however, both the reciprocal of the radius and the lateral gradient of the stream function become equal to zero, and the corresponding magnitude of v had to be determined as a limit from the second derivative of the function.

Discussion of Results

As may be seen from Table 2, the contraction coefficients determined by the relaxation method for axially symmetric flow were practically identical with those determined from the von Mises function for two-dimensional flow at equal values of $(b/B)^2$ and $(d/D)^2 = a/A$.

There is no reason to suspect, moreover, that the slight discrepancies (less than 0.3 per cent at the most) were anything but computational. In other words, the fact that almost exact agreement between the two functional relationships was found at evenly spaced points over the entire functional range would appear to indicate that the relationships are indeed identical. For all practical purposes, at any rate, the values of C_c in Table 1 may now be considered fully applicable through Equations [2] and [3] to the evaluation of discharge conditions for irrotational orifice flow. Fig. 3 shows a plot of the resulting discharge coefficient against the area ratio, the curve representing the adapted von Mises function and the encircled points the values determined at Iowa by the relaxation method.

TABLE 2 COMPARISON OF CONTRACTION COEFFICIENTS FOR SLOTS AND ORIFICES

$(b/B)^2 = (d/D)^2$	0	0.25	0.50	0.75	1.00
C_c for slot	0.611	0.644	0.689	0.757	1.000
C_c for orifice	0.612	0.644	0.691	0.757	1.000

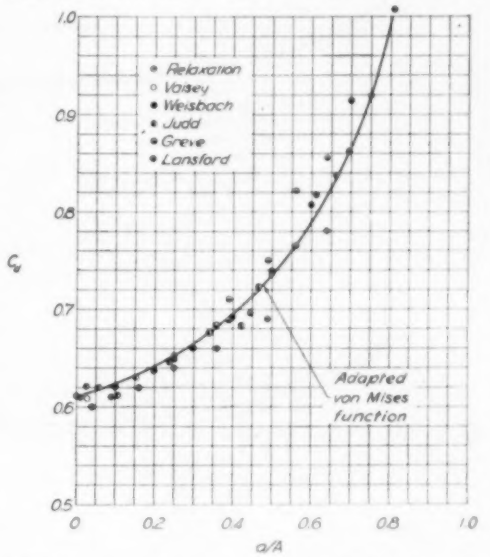

Fig. 3 Variation of Discharge Coefficient With Orifice Area Ratio

Passing mention should be made of the value given by Southwell and Vaisey for the ratio $a/A = 1/36$. As may be seen from the single open circle in Fig. 3, the corresponding point falls below the actual curve. Although the paper from which this value was taken did not provide sufficient information to permit a numerical check of the computations, it would appear from the text and from the foregoing discussion that the discrepancy could be reduced by increasing the number of successive approximations.

The remaining points shown in Fig. 3 were taken from actual measurements of orifice discharge by various investigators. Those shown as solid points stem from studies made by Weisbach (11) nearly one hundred years ago, and are included largely because of their frequent citation in hydraulics. Those shown as half-solid points were determined by Judd (12), and Greve (13), while the crossed points represent average values presented by Lansford (14) for both conduit orifices and end orifices.

Such experimental data, in general, include the effects of gravity, viscosity, and capillarity, which can be evaluated qualitatively but not quantitatively. Thus gravitational influence upon the discharge coefficient is negligible except at low Froude numbers. Capillary action, similarly, is of little consequence except at low Weber numbers. The effect of viscosity is twofold: namely, the effective head is reduced through boundary resistance in the orifice vicinity; and boundary resistance in the uniform zone of approach results in an increased velocity in the central region and hence a reduction in the degree of jet contraction. These two effects are opposite in nature, the former tending to decrease the discharge coefficient and the latter to increase it. At

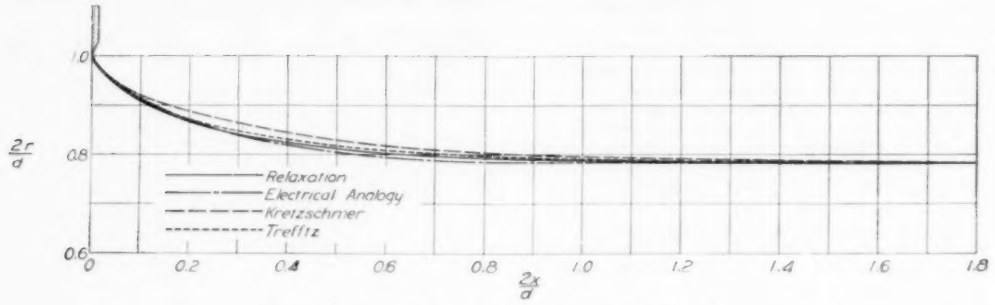

FIG. 4 COMPARISON OF JET-PROFILE EVALUATIONS FOR $a/A = 0$

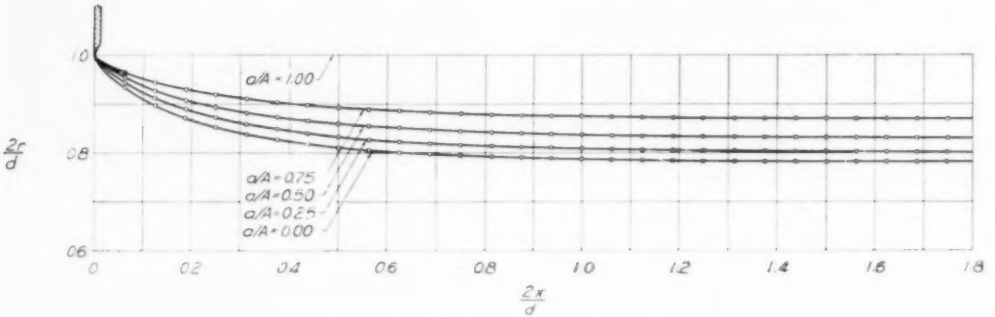

FIG. 5 JET PROFILES FOR SYSTEMATIC SERIES OF AREA RATIOS

moderate to high Reynolds numbers they appear to balance one another, since, as may be seen from all points in Fig. 3 except those of Lansford, the experimentally determined values of the coefficient scatter on both sides of the computed curve for irrotational flow. The fact that the Lansford values are consistently low is probably due to the effect of the eddies which form around the diffusing jet of an orifice located within rather than at the end of a pipe.

Fig. 4 permits a comparison to be made between the four methods of let-profile evaluation described herein. All four curves are for the limiting ratio $d/D = 0 = a/A$. The short-dash profile indicates the original Trefftz solution. The long-dash profile corresponds to the Kretzschmer approximation based upon the two-dimensional profile for $b/B = 0$. The dot-dash profile is that determined at Iowa by electrical analogy. Finally, the full profile represents the results obtained at Iowa by the method of relaxation. If the latter (for which the maximum error in r is estimated to be ± 0.2 per cent) is used as the basis of comparison, the Trefftz and the electrical solutions are seen to involve relative errors of approximately $+1$ per cent and -1 per cent, respectively, and the Kretzschmer two-dimensional adaptation a relative error nearly as great as $+3$ per cent. Although similar comparisons have not been made for other diameter ratios, the foregoing may be considered roughly indicative of the discrepancies to be expected.

All profile data determined by the relaxation method for net subdivisions of $d/32$ are plotted in Fig. 5. More convenient coordinate values obtained from these data by curvilinear interpolation are presented numerically in Table 3. Through use of the limiting dimensions indicated by the coefficients of contraction in Table 1, the profile co-ordinates for any value of $d/D = \sqrt{a/A}$ should be readily obtainable through further interpolation.

TABLE 3 PROFILE CO-ORDINATES FOR JETS FROM ORIFICES

a/A =	0.00	0.25	0.50	0.75
$2x/d$	$2r/d$	$2r/d$	$2r/d$	$2r/d$
0.00	1.000	1.000	1.000	1.000
0.05	0.945	0.955	0.963	0.971
0.10	0.911	0.923	0.937	0.954
0.20	0.867	0.887	0.906	0.928
0.30	0.841	0.862	0.884	0.912
0.40	0.824	0.845	0.871	0.901
0.50	0.812	0.833	0.860	0.893
0.70	0.797	0.819	0.847	0.883
1.00	0.788	0.809	0.838	0.876
1.40	0.783	0.804	0.833	0.871
2.00	0.782	0.802	0.831	0.870

Fig. 6 presents in a composite dimensionless diagram after Equation [5] the curves of pressure distribution along the boundary and center line and across the orifice opening for the four values of a/A investigated at Iowa and for the obvious limit of zero contraction. These curves show at a glance the relative magnitude of the acceleration in the various zones and for the various boundary proportions, since the component of acceleration in any direction is directly proportional to the negative pressure gradient in the corresponding direction. At once apparent is the fact that the major part of the acceleration is confined to the immediate vicinity of the efflux section. In fact, although the extent of the region of appreciable acceleration increases somewhat with decreasing values of a/A, even for the limiting ratio of $a/A = 0$ the pressure is within 1 per cent of its asymptotic values only one orifice diameter upstream and downstream from the efflux section.

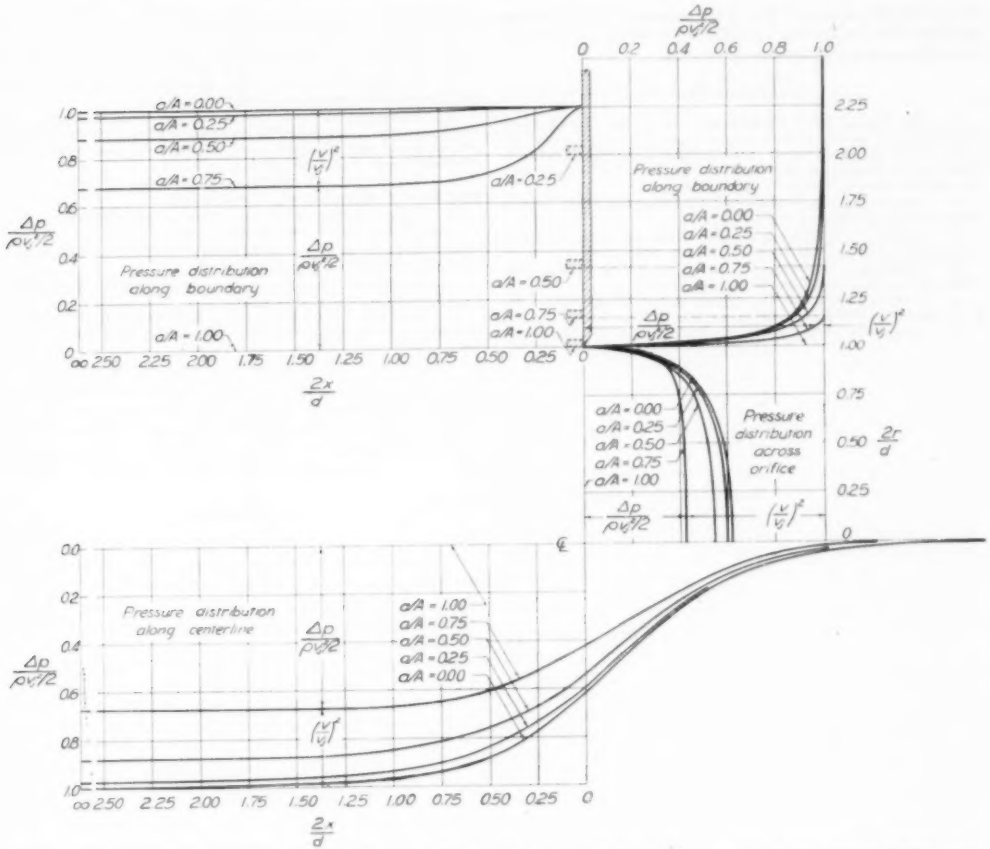

FIG. 6 DISTRIBUTION OF PRESSURE FOR AREA RATIOS OF FIG. 5: *Top*, ALONG CONDUIT WALL; *Right*, ACROSS ORIFICE PLATE AND OPENING; *Below*, ALONG CENTER LINE

Attention should be called, in connection with Fig. 6, to the one pronounced difference which necessarily exists between the irrotational and the actual patterns of flow. In the irrotational pattern the pressure attains its full stagnation value $\rho v_j^2/2$ at the juncture between pipe and orifice plate, whereas in the actual pattern separation occurs a short distance upstream. The eddies which form in such a zone of discontinuity not only result in a lowering of the local boundary pressure but also produce an appreciable disturbance of the jet. If the irrotational pattern is to be used as the basis of discharge measurement, the piezometer must be located at least one orifice diameter upstream, rather than at the juncture (15) as frequently encountered in meter construction. If the turbulence of the jet is to be minimized, on the other hand, a sizable fillet may be introduced at the boundary juncture; although this should change the flow pattern to some extent, the difference will probably be less than that due to the loss in energy which the eddies would otherwise produce.

In view of the general agreement which exists between the characteristics of the irrotational flow pattern and those of actual flow conditions, the information presented herewith should prove of practical value in a number of ways: (*a*) The discharge function provides at least an approximate relationship for fluid metering; in other words, although the calibration of precision meters is invariably a necessity, use of the curve plotted in Fig. 3 should insure a probable accuracy of perhaps ±2 per cent when calibration is not feasible or greater accuracy is not required; (*b*) the jet profiles and the corresponding pressure-distribution curves may be utilized in the design of nozzles or transitions for conditions under which local drops in pressure would lead to cavitation or separation; (*c*) with essentially exact information as to the characteristics of irrotational orifice flow now at hand, a basic reference at last exists for evaluating the effects of gravity, viscosity, and capillarity upon the discharge function.

ACKNOWLEDGMENTS

This paper is based upon a dissertation of the same title prepared by the junior author under the supervision of the senior author in partial fulfillment of the doctoral requirements of the Graduate College of the State University of Iowa. The relaxation and electrical-analogy techniques were applied at the Iowa Institute of Hydraulic Research under the general guidance of Dr. John S. McNown and Mr. Philip G. Hubbard, respectively.

Messrs. En-Yun Hsu and Wen Hsieh assisted in the relaxation analysis. The project was partially supported by the Office of Naval Research under Contract N8onr-500.

BIBLIOGRAPHY

1 "Zur Theorie freier Flüssigkeitsstrahlen," by G. Kirchhoff *Crelles Journal*, vol. 70, 1869, p. 289.

2 "Über die Kontraktion kreisförmiger Flüssigkeitsstrahlen," (Dissertation, Strassburg, Germany, 1913), by V. E. Treffts, *Zeitschrift für Mathematik und Physik*, vol. 64, 1917, p. 34.

3 "Berechnung von Ausfluss und Überfallzahlen," by R. von Mises, *Zeitschrift VDI*, vol. 61, 1917, p. 447.

4 "Anwendung der Theorie der freien Strahlen," by B. Bets and E. Petersohn, *Ingenieur-Archiv*, vol. 2, 1931, p. 190.

5 "Elementary Mechanics of Fluids," by Hunter Rouse, John Wiley & Sons, Inc., New York, N. Y., 1945, p. 59.

6 "Strömungsform und Durchflusszahl der Messdrosseln," by F. Kretzschmer, *VDI Forschungsheft* no. 381, 1936.

7 "Application of the Electrical Analogy in Fluid Mechanics Research," by P. G. Hubbard, *Review of Scientific Instruments*, vol. 20, no. 11, 1949, p. 802.

8 "Relaxation Methods in Engineering Science," by R. V. Southwell, Clarendon Press, Oxford, England, 1940.

9 "Relaxation Methods in Theoretical Physics," by R. V. Southwell, Clarendon Press, Oxford, England, 1946.

10 "Relaxation Methods Applied to Engineering Problems: XII Fluid Motions Characterized by Free Stream Lines," by R. V. Southwell and G. Vaisey, Philosophical Transactions of the Royal Society of London, series A, vol. 240, 1946, p. 117.

11 "Die Experimental-Hydraulik," by Julius Weisbach, J. S. Engelhardt, Freiberg, Germany, 1855, p. 116.

12 "Experiments on Water Flow Through Pipe Orifices," by Horace Judd, Trans. ASME, vol. 38, 1916, p. 331.

13 "Relation of Discharge to Pressure Head," by F. W. Greve, *Water Works*, vol. 67, 1928, p. 180.

14 "Discharge Coefficients for Pipe Orifices," by W. M. Lansford, *Civil Engineering*, vol. 4, 1934, p. 245.

15 "Modified I.S.A. Orifice With Free Discharge," by M. P. O'Brien and R. G. Folson, Trans. ASME, vol. 59, 1937, p. 61.

The Design of Resonant Quartz-Crystal Ultrasonic Transducers for Research Purposes

By G. W. SWANSON, JR.,[1] AND W. T. THOMSON,[2] MADISON, WIS.

Ultrasonic waves have become an important research technique in many fields, including chemistry, mechanics, and others. Piezoelectric crystals excited by a source of alternating voltage are commonly used as a method of producing ultrasonic mechanical vibrations for such purposes. Hence it is often necessary that crystal transducers be designed, and to those unfamiliar with the theory of piezoelectricity, such a design problem may entail time-consuming research. The present paper is intended to co-ordinate the several approaches to the design problem and to present a practical method for designing quartz-crystal transducers for ultrasonic frequencies.

Introduction

THE use of ultrasonic waves has become an important research technique in many different fields, including chemistry, mechanics, electrometallurgy, biology, and medicine. The most commonly used method of producing ultrasonic mechanical vibrations for such purposes is through the use of piezoelectric crystals excited by a source of alternating voltage of the proper magnitude and frequency, usually produced by electronic oscillators and amplifiers. It is frequently necessary, therefore, for a worker in one of these fields to design a crystal transducer to operate at the desired frequency and amplitude to accomplish his purposes. This paper, then, is an interpretation of the existing literature.

For one who is not already familiar with transducer-design techniques, and particularly with the theory of piezoelectricity, such a design problem may entail a good deal of time-consuming research in the literature and may result in a certain degree of frustration, inasmuch as there exist two somewhat different procedures for the derivation of the piezoelectric equations. It is the purpose of the present paper to co-ordinate the various approaches to the design problem and to present a practical method for designing quartz-crystal transducers for ultrasonic frequencies.

Piezoelectricity

Suppose that a quartz plate, cut with its major faces perpendicular to the x-axis of the crystal (an "x-cut" crystal), is plated on both sides with a metallic coating, as shown in Fig. 1. If a potential difference is now applied between the plated surfaces, a deformation of the crystal will occur in two dimensions, along the x-axis and along the y-axis. The two deformations are 180 deg out of time-phase, that is, if at any instant the plate undergoes a contraction in the x-direction, it will simultaneously undergo an expansion in the y-direction, and vice versa. Conversely, if such a plate is subjected to a force in either the x or the y-direction, an electrical potential difference will appear between the plated surfaces. It is these properties that make piezoelectric substances useful for transducers.

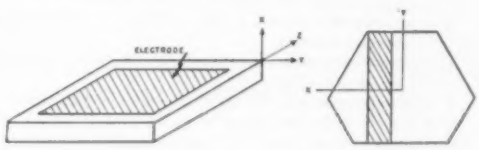

Fig. 1(*a*) (*left*) X-Cut Quartz Plate
Fig. 1(*b*) (*right*) Orientation of Plate in Natural Crystal

In an actual transducer, only the deformation along one of the crystal axes is utilized; for example, in an x-cut "thickness-mode" transducer the force is applied between the two plated faces, while, in an x-cut "longitudinal-mode" transducer, the force is applied between the faces perpendicular to the y-axes. Both types of transducers can be used equally well for producing or for detecting vibrations, the mode of operation being determined chiefly by the frequencies. Longitudinal-mode transducers are useful in the range between 2×10^4 and 10^6 cycles per second (cps), while the thickness mode is used for higher frequencies up to about 10^7 cps. In recent years little use has been made of quartz crystals operating in the longitudinal mode, because synthetic crystals and magnetostriction devices are more satisfactory for these frequencies. The present paper, therefore, will be concerned chiefly with thickness-mode applications.

The two more common theories of Voight and Mason can be summarized for thickness vibration by the following equations:

Electric-Field Theory, Voight (1)[3]

$$-X_x = C^E \frac{\partial \xi}{\partial x} - eE_x \quad \ldots\ldots [1]$$

$$P_x = e \frac{\partial \xi}{\partial x} + k\epsilon_0 E_x \quad \ldots\ldots [2]$$

Charge-Density Theory, Mason (2)

$$-X_x = C^q \frac{\partial \xi}{\partial x} + f\sigma \quad \ldots\ldots [3]$$

$$E_x = f \frac{\partial \xi}{\partial x} + \sigma / K\epsilon_0 \quad \ldots\ldots [4]$$

[3] Numbers in parentheses refer to Bibliography at end of paper.

[1] Instructor in Electrical Engineering, The University of Wisconsin.

[2] Associate Professor, Department of Mechanics, College of Engineering, The University of Wisconsin. Mem. ASME.

Contributed by the Applied Mechanics Division and presented at the Semi-Annual Meeting, St. Louis, Mo., June 19–23, 1950, of The American Society of Mechanical Engineers.

Discussion of this paper should be addressed to the Secretary, ASME, 29 West 39th Street, New York, N. Y., and will be accepted until January 10, 1951, for publication at a later date. Discussion received after the closing date will be returned.

Note: Statements and opinions advanced in papers are to be understood as individual expressions of their authors and not those of the Society. Manuscript received by the Applied Mechanics Division December 19, 1939. Paper No. 50—SA-12.

All units are in the rationalized MKS system and are defined as follows:

X_x = stress in x-direction (positive for compression)
ξ = particle displacement in x-direction
$\frac{\partial \xi}{\partial x}$ = strain in x-direction (positive for extension)
E_x = electric intensity in x-direction (applied voltage divided by crystal thickness)
σ = charge density on electrodes
P_x = polarization in x-direction
C^q = stress-to-strain ratio under constant charge
f = piezoelectric constant = ratio of stress to charge density at constant strain
e = piezoelectric constant = ratio of stress to electric intensity at constant strain
k = dielectric susceptibility of crystal under constant strain
$K = 1 + k$ = dielectric constant of quartz
C^E = stress-to-strain ratio under constant electric intensity
$\epsilon_0 = 8.854 \times 10^{-12}$ farads m^{-1} = permittivity of free space

The relationship between the coefficients of the two theories can be obtained by substituting the expression for the charge density

$$\sigma = K\epsilon_0 E_x + P_x \quad [5]$$

into Equations [3] and [4] and comparing with [1] and [2]. It now appears that

$$C^q = C^E\left(1 + \frac{e^2}{K\epsilon_0 C^E}\right) \quad [6]$$

$$f = -e/K\epsilon_0 \quad [7]$$

$$K = 1 + k \quad [8]$$

It is immaterial which theory is used provided the foregoing relationships are adhered to.

Using the electric-field theory of Voight, the steps leading to the three final equations are as follows: Substituting P_x from Equation [5] into Equation [2] one obtains

$$\sigma = K\epsilon_0 E_x + e\frac{\partial \xi}{\partial x} \quad [9]$$

Because σ is zero within the dielectric and appears only on the electrodes, $(\partial\sigma)/(\partial x) = 0$, and

$$\frac{\partial E_x}{\partial x} = -\frac{e}{K\epsilon_0}\frac{\partial^2 \xi}{\partial x^2} \quad [10]$$

Taking an element of thickness dx and applying Newton's equation of motion, the unbalanced force on the element, per unit area, is

$$\frac{-\partial X_x}{\partial x} = C^E\frac{\partial^2 \xi}{\partial x^2} - e\frac{\partial E_x}{\partial x} = C^E\left(1 + \frac{e^2}{K\epsilon_0 C^E}\right)\frac{\partial^2 \xi}{\partial x^2} \quad [11]$$

and

$$\frac{\partial^2 \xi}{\partial t^2} = \frac{C^E}{\rho}\left(1 + \frac{e^2}{K\epsilon_0 C^E}\right)\frac{\partial^2 \xi}{\partial x^2} \quad [12]$$

The latter equation is recognized as the wave equation in one space co-ordinate, representing a plane wave of displacement propagated with a velocity of

$$v = \left[\frac{C^E}{\rho}\left(1 + \frac{e^2}{K\epsilon_0 C^E}\right)\right]^{1/2} \quad [13]$$

meters per second. Accepted values of the constants appearing in Equation [13] are (from Cady, but converted into MKS units):

$C^E = 8.51 \times 10^{10}$ newton meter^{-2}
$\rho = 2.65 \times 10^{3}$ kilogram meter^{-3}
$e = 1.73 \times 10^{-1}$ coulomb meter^{-2}
$K = 4.46$
$k^2 = \frac{e^2}{\epsilon_0 K C^E} = 9.0 \times 10^{-2}$

It is evident from these figures that k^2 is negligible compared with unity, so that, from Equation [6], C^q is equal to C^E for practical purposes.

Assuming simple harmonic motion, a solution to Equation [12] can be written as

$$\xi = \left[C_1 \cos\frac{\omega x}{v} + C_2 \sin\frac{\omega x}{v}\right]e^{j\omega t} \quad [14]$$

C_1 and C_2 are evaluated at the face $x = 0$, where the velocity and force are $\dot{\xi}_1$ and $F_1 = AX_x$, respectively. Letting $\dot{\xi}_2$ and F_2 be the corresponding quantities at the other face $x = l_t$ it follows that

$$\dot{\xi}_2 = \dot{\xi}_1 \cos\frac{\omega l_t}{v} - j\frac{(F_1 - \phi E)}{Z_0}\sin\frac{\omega l_t}{v} \quad [15]$$

$$F_2 - \phi E = (F_1 - \phi E)\cos\frac{\omega l_t}{v} - j\dot{\xi}_1 Z_0 \sin\frac{\omega l_t}{v} \quad [16]$$

where

A = plated area of crystal face
l_t = thickness of crystal
$\phi = \frac{Ae}{l_t}$
ρ = density of crystal
$Z_0 = A\rho v$ = characteristic mechanical impedance of crystal
$E = l_t E_x$ = applied voltage

The current in the crystal is

$$i = \int \frac{\partial \sigma}{\partial t}\, dA \quad [17]$$

Differentiating Equation [9] with respect to t

$$\frac{\partial \sigma}{\partial t} = j\epsilon_0 K\omega E_x + e\frac{\partial \dot{\xi}}{\partial x} \quad [18]$$

and substituting into Equation [17] yields

$$i = j\omega\frac{AK\epsilon_0}{l_t}E + \frac{eA}{l_t}\int \frac{\partial \dot{\xi}}{\partial x}\frac{l_t dA}{A} \quad [19]$$

The surface integration can be changed to integration in the x-direction by noting that $l_t\, dA = dV = A\,dx$. Then

$$\frac{\partial \dot{\xi}}{\partial x}\frac{l_t dA}{A} = \frac{\partial \dot{\xi}}{\partial x}dx = d\dot{\xi}$$

and

$$i = j\omega C_0 E + \phi(\dot{\xi}_2 - \dot{\xi}_1) \quad [20]$$

C_0 is thus defined as the capacitance between the two plated surfaces of the crystal $AK\epsilon_0/l_t$.

Equations [15], [16], and [20] can be rearranged into the form

$$F_1 - F_2 = (\dot{\xi}_1 + \dot{\xi}_2)jZ_0 \tan\frac{\omega l_t}{2v} \quad [21]$$

$$F_1 - \phi E = jZ_0\left(\tan\frac{\omega l_t}{2v}\right)\dot{\xi}_1 + j\frac{Z_0}{\sin\dfrac{\omega l_t}{v}}(\dot{\xi}_2 - \dot{\xi}_1) \quad [22]$$

$$F_2 - \phi E = -jZ_0\left(\tan\frac{\omega l_t}{2v}\right)\dot{\xi}_2 + j\frac{Z_0}{\sin\dfrac{\omega l_t}{v}}(\dot{\xi}_2 - \dot{\xi}_1) \quad [23]$$

If forces are considered analogous to voltages and velocities to currents, these equations represent a six-terminal electrical network as shown in Fig. 2.

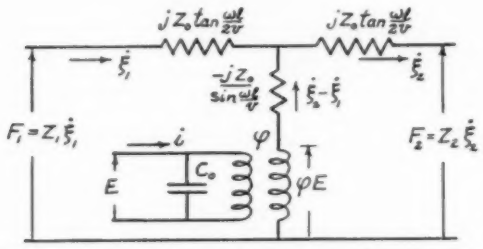

Fig. 2 Six-Terminal Network Representing Crystal System

Fig. 2 represents a crystal with an electrical input voltage driving two mechanical loads, one on each plated surface. In practice this scheme is seldom, if ever, used; the more common situation is the one in which all the energy is radiated from one of the faces of the crystal. In the latter case the nonradiating face must be treated in such a way that no energy can be radiated in this direction; in other words, a nonabsorbing backing material must be used. If one considers the propagation of compressional waves through the crystal to be analogous to the propagation of voltage waves along an electrical transmission line, then it is apparent that the mechanical impedance of the backing material must be much greater or much less than the characteristic impedance of the quartz, in order that the energy transfer be negligible.

Air is commonly used as a backing material, because its characteristic impedance is extremely small in comparison with that of quartz. Furthermore, the energy dissipation in air at ultrasonic frequencies is high enough so that the input acoustical impedance to a thickness of several wave lengths is nearly equal to the characteristic impedance, regardless of the material at the far side. Should an infinite terminating impedance be desired for the crystal, it is necessary merely to place against it a quarter-wave-length plate of metal, which, in turn, is backed by air. The metal plate then acts as a "transformer" to produce an infinite impedance at the surface of the crystal.

Returning again to Fig. 2, it is apparent that if one side of the crystal is exposed to air, Z_1 must be a short circuit. The resulting equivalent circuit, after simplification, is shown in Fig. 3(*a*). At the resonant frequency of the crystal, the thickness is $^1/_2$ wave length, or $l_t = \lambda/2 = v/(2f)$ m; therefore the circuit reduces to the simple form shown in Fig. 3(*b*).

If one side of the crystal is backed by an infinite impedance, the terminals at F_1 are open-circuited and the circuit diagram is given by Fig. 4(*a*), in which

$$\cot\frac{\omega l_t}{v} = \sin^{-1}\left(\frac{\omega l_t}{v}\right) - \tan\frac{\omega l_t}{2v}$$

At resonance, for this type of backing, the thickness is only $^1/_4$

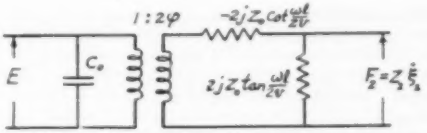

Fig. 3(*a*) Equivalent Circuit for Air-Backed Crystal

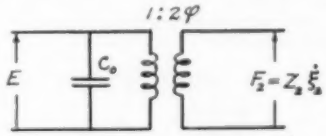

Fig. 3(*b*) Air Backing With $l_t = \frac{\lambda}{2}$

wave length because the crystal surface next to the backing material cannot move. For this condition, the equivalent circuit is given in Fig. 4(*b*).

For either type of backing, it is clear that at resonance the only impedances in the circuit are Z_2, the input impedance of the load, and C_0, the capacitance between the plated surfaces of the crystal.

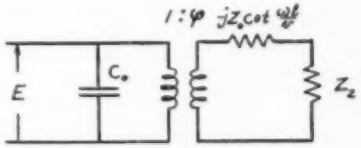

Fig. 4(*a*) Crystal Backed by Infinite Impedance

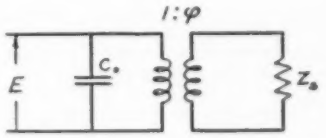

Fig. 4(*b*) Infinite Impedance Backing With $l_t = \frac{\lambda}{4}$

Characteristics of Load Media

Load media can be liquid, solid, or gaseous. In the case of a gas, however, the impedance presented to the transducer is so low that it is usually difficult to accomplish a significant power transfer without the use of a large diaphragm or cone (as in the case of a loud-speaker). The successful operation of the system depends upon the proper impedance match between the alternating-voltage source and the mechanical load. If the load is assumed to be purely resistive, it is clearly impossible to match the conventionally resistive output impedance of a vacuum-tube amplifier without the addition of an inductance to the transducer circuit. The inductance can be connected in parallel with C_0, or it can be connected in series with the entire circuit. In either case its value should be calculated to make the input impedance to the transducer purely resistive. The output impedance of the electronic amplifier, of course, should equal the input impedance to the crystal, which in turn is determined by the load medium.

In most applications, very little of the radiated energy will be

reflected back into the transducer; therefore the impedance Z_3 seen by the crystal will be nearly a pure mechanical resistance. The value of this resistance is found by multiplying the characteristic impedance of the load medium by the plated area of the crystal. Division of the resulting number by ϕ^2 (or $4\phi^2$ as the case may be) gives the equivalent electrical resistance in ohms, provided all quantities are stated in MKS units. Table 1 gives the characteristic impedances of a number of typical media (3). The velocities given for solid media are the velocities of longitudinal waves. All values are approximately correct for atmospheric pressure and 20 C.

TABLE 1 CHARACTERISTIC IMPEDANCES OF TYPICAL MEDIA

Medium	Velocity of propagation (v), m/sec	Density (ρ) kg/m^3	Characteristic impedance (ρv), MKS unit
Cast iron	3400	7800	26.5×10^6
Lead	4800	11300	54.2×10^6
Mercury	1400	13500	18.9×10^6
Brass	3400	8400	28.6×10^6
Steel (mild)	5000	7700	38.5×10^6
Concrete	3100	2600	8.06×10^6
Limestone	3300	2600	8.57×10^6
Fresh water	1440	1000	1.44×10^6
Sea water	1500	1030	1.54×10^6
Air	344	1.29	444

Example Calculation

Air-Backed Crystal, 1mc. An air-backed crystal must be $\frac{1}{2}$ wave length thick. For quartz, from Equation [13], the velocity is 5670 m per sec. The wave length at 1 mc is, therefore, 5.67×10^{-3} m, so that the crystal should be ground to a thickness of 0.283 cm. Assume that the plated area of the crystal is 4 cm^2. Then C_0, the shunt capacitance across the crystal, is $AK\epsilon_0/l_4 = 5.58 \times 10^{-13}$ farad. The value of $\phi = Ae/l_4$ is 2.46×10^{-4} coloumb-meter^{-1}. If the load on the radiating face of the crystal is water, the mechanical impedance on the crystal face is $1.44 \times 10^6 \times 4 \times 10^{-4} = 576$ MKS mechanical ohms. Dividing by $4\phi^2$, the electrical impedance due to the mechanical load is 2.38×10^9 ohms. If an inductive reactance equal to the reactance of C_0 is connected in parallel with the crystal, the input resistance of the crystal is 2.38×10^9 ohms, and the output impedance of the driving amplifier should also have this value. It can be shown that if the compensating inductance is connected in "series" with the crystal, any desired input impedance much lower than the load impedance can be obtained by making

$$\frac{1}{\omega C_0} = \omega L = \sqrt{R_{in} R_{load}}$$

Usually an additional capacitance must be connected in parallel with C_0 to bring about this condition.

A typical method of mounting an air-backed crystal is shown in Fig. 5. The particular application illustrated is the projection of a beam of ultrasonic energy into a tank of liquid. If the liquid is a nonconductor, a light flexible wire must be soldered to each plated surface of the crystal to provide an electrical connection. It is worthy of mention that actually plating the crystal is unnecessary; thin sheets of aluminum foil carefully cemented to the surfaces have given excellent results.

The directional properties of crystal transducers must be considered in connection with most applications. In the megacycle range a practical crystal plate has surface dimensions large with respect to a wave length in any medium; therefore the energy is radiated in a narrow beam. A commonly used formula for determining the beam width of a circular plate (4)

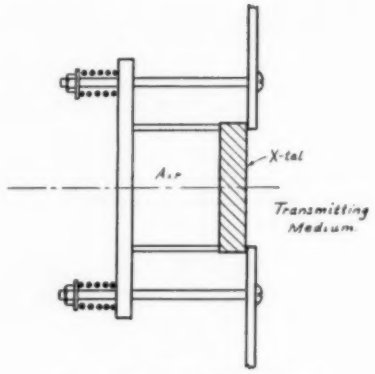

Fig. 5 Air-Backed Crystal Mounting

$$\alpha = 2 \tan^{-1} (0.45 \lambda/a)$$

where α is the angle between the directions in which the radiated power is 0.1 that radiated normal to the plate, λ is the wave length in the external medium, and a is the radius of the plate.

For practical purposes the energy dissipated within the crystal can be neglected. The radiated power therefore can be calculated from the relationship E^2/R, where E is the effective value of the applied voltage, and R is the input electrical resistance of the crystal at the frequency in question. It must be remembered, however, that quartz has a breakdown potential gradient of 6.7 $\times 10^6$ volts per meter, which must not be exceeded. Furthermore, the maximum permissible voltage is often limited by the formation of an arc in the medium in which the crystal is immersed.

BIBLIOGRAPHY

1 "Piezoelectricity," by W. G. Cady, McGraw-Hill Book Company, New York, N. Y., 1946.

2 "Electromechanical Transducers and Wave Filters," by W. P. Mason, second edition, D. Van Nostrand Company, New York, N. Y., 1948.

3 "Elements of Acoustical Engineering," by H. F. Olson, second edition, D. Van Nostrand Company, New York, N. Y., 1947.

4 "Acoustics," by G. W. Stewart and R. B. Lindsay, D. Van Nostrand Company, New York, N. Y., 1930.

5 "Piezoelectric Crystals in Their Relation to Ultrasonics," by W. P. Mason, D. Van Nostrand Company, New York, N. Y., 1949.

6 "Design of Crystal Vibrating Systems," by W. J. Fry, J. M. Taylor, and B. W. Henvis, Dover Publications, 1948.

7 "Piezoelectric Transducers," by W. Roth, Proceedings of the IRE, vol. 37, July, 1949, p. 750.

8 "Standards on Piezoelectric Crystals, 1949," Proceedings of the IRE, vol. 37, December, 1949, p. 1378.

The Uniform Distribution of a Fluid Flowing Through a Perforated Pipe

By WILLARD M. DOW,[1] SHREVEPORT, LA.

A theoretical analysis is made of the flow through a perforated pipe with a closed end for the special case of a constant linear rate of discharge along the length of the pipe. The results of the fluid-flow considerations are applicable to many practical manifold systems. The practical significance of the results with respect to pipe burners for gaseous fuels is emphasized as the results make possible the design of simple high-capacity and extended-range pipe burners of industrial importance. The capacity of commercially available pipe burners may be increased several hundred per cent. The validity of the theoretical results was verified by experiment.

Nomenclature

The following nomenclature is used in the paper:

A = cross-sectional area of manifold pipe at any point, sq ft
A_0 = cross-sectional area of manifold pipe at inlet end, sq ft
A_p = total port area, sq ft
b = numerical constant
D = diameter of manifold pipe at any point, ft
D_0 = diameter of manifold pipe at inlet end, ft
f = Fanning friction factor, dimensionless, defined by relation, $dF = \frac{2v^2 f}{D}\,dx$, where dF is the friction in foot-pounds per unit mass of fluid flowing for a differential length of pipe, dx
L = active length of manifold pipe, ft
L_t = length of pipe in which fluid flow is in turbulent-flow region, ft
m = hydraulic radius, defined as cross-sectional area divided by wetted perimeter, ft
m_0 = hydraulic radius at inlet end, ft
n = numerical constant
p = pressure, psf
Δp = pressure difference, psf
Q = volume rate of flow at any point, cu ft per hr
Q_0 = volume rate of flow at inlet end, cu ft per hr
v = average velocity of fluid in manifold, ft per hr
x = distance along manifold pipe from inlet end, ft
y = distance along manifold pipe from dead end, ft
α = constant (approximately 1 for turbulent flow and $^1/_2$ for streamline flow), dimensionless
$\delta = 4\alpha\nu L/Q_0$, dimensionless
$\gamma = \alpha b \Big/ \left(\frac{4Q_0}{\pi\nu L}\right)^n$, dimensionless
μ = absolute viscosity, lb sec/ft^2
ν = kinematic viscosity, ft^2/sec
ρ = density, slugs/ft^3

Introduction

The problem of uniform distribution of a fluid flowing through a manifold with spaced outlets arises in many practical systems. Familiar examples are liquid-distribution systems, steam and feedwater-distribution systems in boilers, sewage-disposal systems, multitube air heaters, and pipe burners for gaseous fuels. It is a problem of particular interest in the case of pipe burners because the potential industrial utility of this simple type of gas burner appears to be great.

The pipe burner is one of the many types of burners which use gas as a fuel and, in its simplest form, consists of a closed length of pipe having a row of ports drilled along its length. The gas is introduced through the open end inspirating primary air. The air-gas mixture flows toward the closed or dead end, escaping through the burner ports where the gas is ignited to provide the flame. In spite of its physical simplicity and potential utility, it has not been widely used in industry, apparently because the dynamics of its gas flow has not been well understood.

Accepted burner design[2] stipulates that pipe burners should not be designed for lengths greater than 6 ft and that the cross-sectional area of the pipe should not be less than $1^1/_2$ times the total port area. These conditions impose serious limitations on the capacity and utility of the burner. A drilled-port pipe burner which could have a high capacity and unlimited length, as well as uniform flame height and heating characteristics, would be desirable and applicable in many industrial heating installations. It would have the obvious advantages of simple and cheap construction, and it would obviate the usual hazards of fire and damage due to overheating by a concentrated gas flame. It could be adapted to many heating installations where direct gas-flame heating is normally precluded owing to high cost and impracticability of a large number of conventional burners.

The limitations and necessary conditions for satisfactory burner performance of drilled-port pipe burners were disclosed by a mathematical consideration of the more general problem of the uniform distribution of a fluid flowing through a perforated pipe with a closed end. A system of ordinary differential equations was set up and solved for the special case of a constant linear rate of discharge along the length of the pipe. Theoretically, this solution should be the design basis for a pipe burner which would give a uniform flame height and uniform heating along its length. The validity of the theoretical design equation was checked by experimentation with conventional and modified pipe burners. The agreement between the theory and experiment was excellent.

Theoretical Considerations

Briefly, the mathematical treatment consists of the development of the necessary conditions to insure that the pressure drop

[1] Assistant to Director of Research, United Gas Company. Jun. ASME.

Contributed by the Applied Mechanics Division and presented at the Semi-Annual Meeting, St. Louis, Mo., June 19–23, 1950, of The American Society of Mechanical Engineers.

Discussion of this paper should be addressed to the Secretary, ASME, 29 West 39th Street, New York, N. Y., and will be accepted until January 10, 1951, for publication at a later date. Discussion received after the closing date will be returned.

Note: Statements and opinions advanced in papers are to be understood as individual expressions of their authors and not those of the Society. Manuscript received by the Applied Mechanics Division February 8, 1950. Paper No. 50—SA-14.

[2] "Combustion," American Gas Association, Mack Printing Company, Easton, Pa., third edition, 1932, pp. 122, 132–134.

due to friction losses in the flow through the pipe is exactly balanced by the pressure increase due to the deceleration of the flow in the pipe which necessarily occurs when part of the gas escapes through the ports. When these two pressure trends are exactly balanced, the static pressure remains constant along the entire length of the burner, which insures a uniform flame height and uniform heating.

In general, the pressure loss due to friction is related to the surface area of the pipe, while the pressure gain due to deceleration is related to the cross-sectional area of the pipe. Therefore it is possible to control the pressure by adjusting the ratio of these two areas. This can be accomplished by several means, such as inserting a tapered plug in the pipe, actually changing the diameter of the pipe, or constructing the burner manifold according to a geometric design.

For mathematical purposes the discharge of the fluid through the ports may be considered as a continuous function of the distance along the pipe. An energy balance for a differential length dx of the perforated pipe

$$\frac{u\,du}{\alpha} + \frac{dp}{\rho} + \frac{2fu^2}{D}\,dx = 0 \qquad [1]$$

If the ports are the same size and their distribution along the length of the pipe is constant, uniform fluid distribution requires that the rate of flow through the pipe must vary linearly from a maximum at the inlet to zero at the dead end, or

$$uA = Q = Q_0\left(\frac{y}{L}\right) \qquad [2]$$

The fluid velocities through the ports must be equal to give a uniform distribution. Therefore, $(dp)/(dx)$ must equal zero for a discharge into a constant-pressure atmosphere. Equation [1] may now be reduced to

$$\frac{du}{u} = -\frac{2\alpha f}{D}\,dx = \frac{2\alpha f}{D}\,dy \qquad [3]$$

Differentiation of Equation [2] and substitution into Equation [3] gives

$$\frac{dD}{dy} = \frac{D}{2y} - \alpha f \qquad [4]$$

This is the fundamental differential equation to be solved to give the physical dimensions of a pipe burner which will have uniform flame height and heating characteristics. The friction factor f is a function of the Reynolds number, Du/ν, which varies from a maximum at the inlet end of the pipe to zero at the dead end.

Case 1, Laminar Flow. If the Reynolds number is less than about 2100, the flow through the pipe will be in the laminar region, and the friction factor will vary inversely as the Reynolds number

$$f = \frac{16\,\nu}{Du} \qquad [5]$$

This relationship may be introduced into Equation [4] to give

$$\frac{dD}{dy} = \frac{D}{y}\left[\frac{1}{2} - \frac{4\alpha\nu\pi L}{Q_0}\right] \qquad [6]$$

which may be integrated for the boundary condition of $D = D_0$ when $y = L$, to yield

$$D = D_0\left(\frac{y}{L}\right)^{1/2-\beta} \qquad [7]$$

where

$$\beta = \frac{4\alpha\nu\pi L}{Q_0}$$

Equation [7] relates the diameter of the pipe to the distance from the dead end for laminar flow through the pipe. If $\beta = 1/2$, the diameter of the pipe remains constant. If $\beta < 1/2$, the diameter decreases with the distance x. If $\beta > 1/2$, the diameter increases with the distance x.

Equation [7] holds only if the cross-sectional shape of the pipe is circular. For other shapes, a satisfactory approximation should be obtained by substituting the hydraulic radius for the diameter

$$m = m_0\left(\frac{y}{L}\right)^{1/2-\beta} \qquad [7a]$$

Equation [7a] may be verified mathematically for certain elementary shapes, such as a square or rectangle whose length ratio of sides remains constant. However, the differential equation becomes intractable for other shapes. Fig. 1 is a plot of Equation [7a] which shows how the hydraulic radius varies with distance along the pipe manifold for various values of the parameter $Q_0/(\nu L)$.

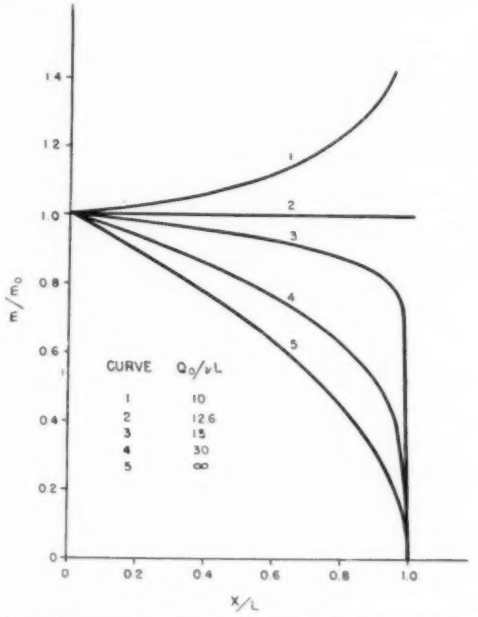

FIG. 1 VARIATION OF HYDRAULIC RADIUS WITH DISTANCE ALONG MANIFOLD FOR LAMINAR FLOW

Case 2, Turbulent Flow. In the turbulent-flow region, Fanning's friction factor may be expressed empirically as a function of the Reynolds number by the following type of equation which represents the relationship exceptionally well over a wide range of Reynolds numbers

$$f = \frac{b}{(N_{Re})^a} \qquad [8]$$

where b and n = numerical constants. This is a form of the familiar Blasius relationship

$$f = \frac{0.3164}{4(N_{Re})^{1/4}} \quad [8a]$$

Equation [8] may be combined with Equation [4] to give the differential equation

$$\frac{dD}{dy} = \frac{D}{2y} - \gamma \left(\frac{D}{y}\right)^n \quad [9]$$

where

$$\gamma = \frac{ab}{(4Q_0/\pi\nu L)^n}$$

This is a homogeneous first-order differential equation which may be integrated after a suitable change of variables has been made. However, it is also the so-called Bernoulli type of differential equation which may be reduced to a first-order linear equation whose integration is somewhat easier than the homogeneous form. Therefore the following substitution of variables

$$v = D^{1-n}$$

reduces the equation to the linear equation

$$\frac{dv}{dy} = \frac{(1-n)v}{2y} - \frac{(1-n)\gamma}{y^n} \quad [9a]$$

which may be integrated for the boundary conditions of $D = D_0$ when $y = L$, and expressed in terms of the original variables to yield

$$\left(\frac{D}{L}\right)^{1-n} = \left[\left(\frac{D_0}{L}\right)^{1-n} + 2\gamma\right]\left(\frac{y}{L}\right)^{\frac{1-n}{2}} - 2\gamma\left(\frac{y}{L}\right)^{1-n} \quad [10]$$

For noncircular cross-sectional manifold shapes, the diameter may be replaced by 4 times the hydraulic radius to give the design equation

$$\left(\frac{4m}{L}\right)^{1-n} = \left[\left(\frac{4m_0}{L}\right)^{1-n} + 2\gamma\right]\left(\frac{y}{L}\right)^{\frac{1-n}{2}} - 2\gamma\left(\frac{y}{L}\right)^{1-n} \quad [10a]$$

Fig. 2 is a plot of Equation [10a], showing the variation of the hydraulic radius with distance along the pipe manifold for various values of the parameters $Q_0/(\nu L)$ and $4m_0/L$.

Case 3, Negligible Friction. For this case Equation [1] reduces to

$$du = 0 \quad [11]$$

which combined with Equation [2] gives

$$du = \frac{Q_0}{L}\left[\frac{dy}{A} - y\frac{dA}{A^2}\right] = 0 \quad [12]$$

or

$$\frac{dy}{y} = \frac{dA}{A} \quad [12a]$$

When this last equation is integrated for the boundary condition of $A = A_0$ when $y = L$, one gets

$$A = A_0\left(\frac{y}{L}\right) \quad [13]$$

which represents a true linear taper of the cross-sectional area of the manifold with distance along the pipe.

Case 4, Manifold Serves as Infinite Reservoir. If the pressure changes accompanying the flow of the fluid through the manifold due to frictional and kinetic-energy forces are negligible in comparison to the pressure drop across the discharge ports, then the flow will be distributed uniformly through the ports. In effect, this is the case where the manifold is so large that it is equivalent to an infinite reservoir.

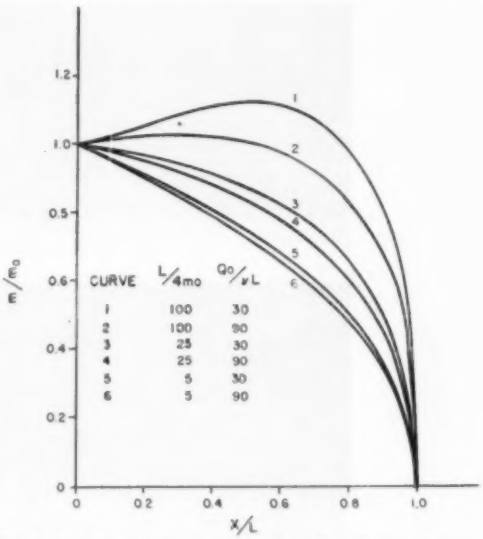

FIG. 2 VARIATION OF HYDRAULIC RADIUS WITH DISTANCE ALONG MANIFOLD FOR TURBULENT FLOW

To obtain design criteria for this condition, one may assume that the pressure changes are negligible, so that uniform distribution of the fluid through the ports exists, and then calculate the pressure change due to friction alone and due to kinetic-energy effects alone, and compare these values with the pressure drop through the ports.

For drilled-port pipe manifolds the pressure drop across the ports may be approximated by assuming the ports behave as sharp-edge orifices with discharge coefficients equal to 0.60. Using Poiseuille's relationship for laminar flow and Blasius' empirical relationship for turbulent flow, one may then develop the design criteria for the case of negligible pressure change along the constant diameter manifold

$$\frac{(\Delta p)_{ports}}{(\Delta p)_{KE}} = 2.8\left(\frac{A}{A_p}\right)^2 >> 1 \quad [14]$$

$$\frac{(\Delta p)_{ports}}{(\Delta p)_{laminar}} = 0.10\left(\frac{Q_0}{\nu L}\right)\left(\frac{A}{A_p}\right)^2 >> 1 \quad [15]$$

$$\frac{(\Delta p)_{ports}}{(\Delta p)_{turbulent}} = 26\left(\frac{Q_0}{\nu L}\right)^{0.25}\left(\frac{A}{A_p}\right)^2\left(\frac{D}{L_1}\right)^{0.75} >> 1 \quad [16]$$

EXPERIMENTAL VERIFICATION

Equation [7] shows that there is a single optimum delivery rate for the uniform distribution of the fluid when the flow is in the laminar region and the manifold does not behave as an infinite reservoir. A pipe burner operating at this optimum rate would produce a uniform flame height and uniform heating. At higher flow rates, the flame height and heating would tend to increase toward the dead end, while at lower flow rates they would tend

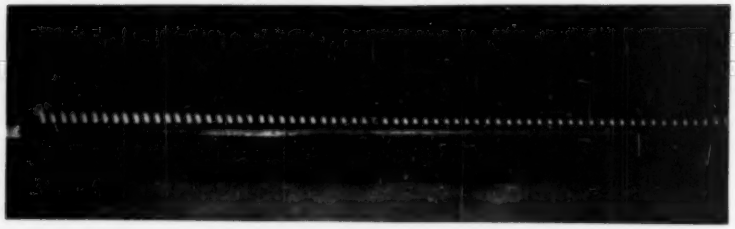

FIG. 3(*a*) CONSTANT-DIAMETER PIPE BURNER, HIGH DELIVERY RATE

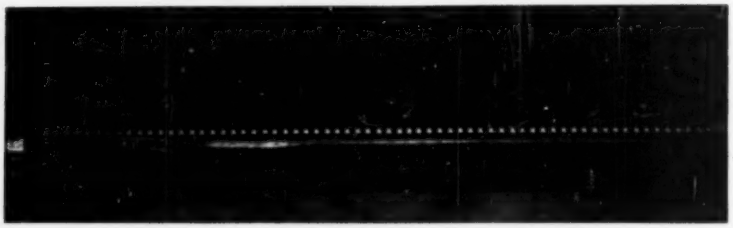

FIG. 3(*b*) CONSTANT-DIAMETER PIPE BURNER, OPTIMUM DELIVERY RATE

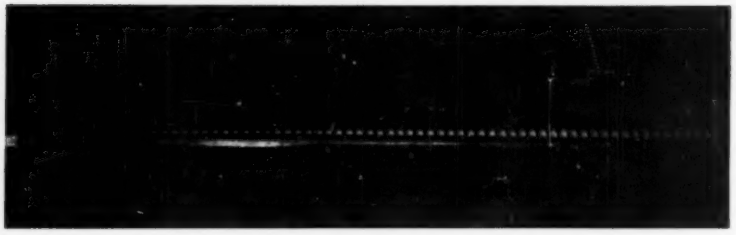

FIG. 3(*c*) CONSTANT-DIAMETER PIPE BURNER, LOW DELIVERY RATE

to decrease toward the dead end. Theoretically, this optimum flow rate of primary air-gas mixture is

$$Q_0 = 4\pi\nu L \quad \ldots\ldots\ldots\ldots\ldots\ldots\ldots\ldots \quad [17]$$

Figs. 3(*b*) and 6(*c*) show two different pipe burners each operating at the optimum flow rate and producing exceptionally uniform flames in agreement with the theory. Figs. 3(*a*) and (*c*) show the first burner operating at rates above the optimum and below the optimum, respectively. Fig. 6(*a*) shows the second burner operating at a rate above its optimum. These results are in agreement with the theoretical predictions.

Fig. 4(*a*) shows a simple pipe burner operating at a flow rate approximately 4 times the optimum rate, and its flame distribution obviously is unsatisfactory. Fig. 4(*b*) shows the same burner under the same conditions but with a tapered plug designed in accordance with Equation [7*a*] inserted in the pipe. The flame height is now remarkably uniform along the length of the burner. The flow through the manifolds of all the burners mentioned was in the laminar region.

Figs. 5(*a*) and (*b*) show a simple commercial pipe burner operating at low and high flow rates. This burner represents the maximum-capacity 2-in-diam pipe burner commercially available. For a reasonable range of flow rates the physical dimensions of this burner satisfy the criteria developed in the foregoing for the case of the manifold behaving as an infinite reservoir. There are two rows of ports along the manifold of this burner. The slight irregularities of the flames are caused by burrs formed when the ports were drilled.

Figs. 6(*a*), (*b*), and (*c*) show the same burner as in Figs. 5 (*a*) and (*b*) with the ports enlarged from $^1/_8$ in. to $^3/_{16}$ in. in order to increase its capacity. The conditions necessary for the manifold to behave as an infinite reservoir were no longer satisfied, and the simple constant-diameter burner did not produce a uniform distribution of the gas as one can see from Fig. 6(*a*). Fig. 6(*b*) shows the modified burner with a tapered plug inserted in its manifold producing a uniform flame. The tapered insert was designed in accordance with Equations [7*a*] and [10*a*] as the flow through the manifold was in both the turbulent- and laminar-flow regions. Fig. 6(*c*) shows the simple pipe burner operating at the optimum rate of flow as specified by Equation [17].

Figs. 7(*a*) and (*b*) show the same burner as in the two previous series of illustrations but with the ports enlarged to $^1/_4$ in., which enabled the burner to operate at 400 per cent of the capacity of the original commercial burner. Fig. 7(*a*) shows the modified burner operating without an insert and producing a very nonuniform flame. Fig. 7(*b*) shows the modified burner with an insert, producing a uniform flame.

Figs. 8 (*a*) and (*b*) show the same burner further modified by

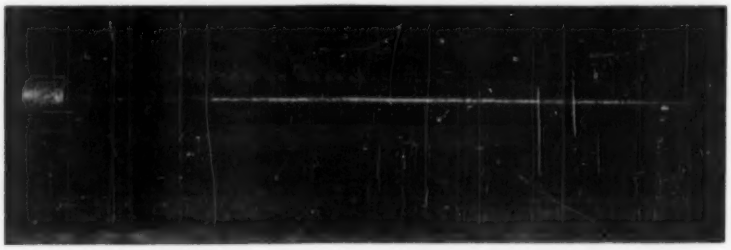

FIG. 4(a) CONSTANT-DIAMETER PIPE BURNER

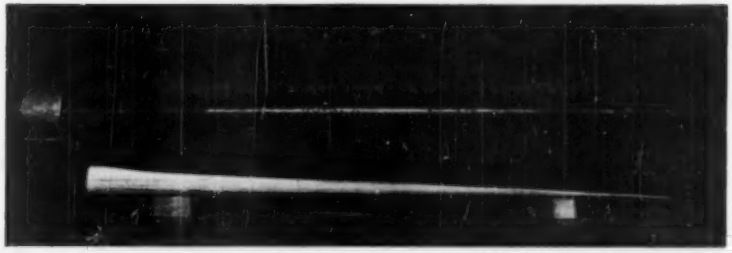

FIG. 4(b) PIPE BURNER WITH INSERT

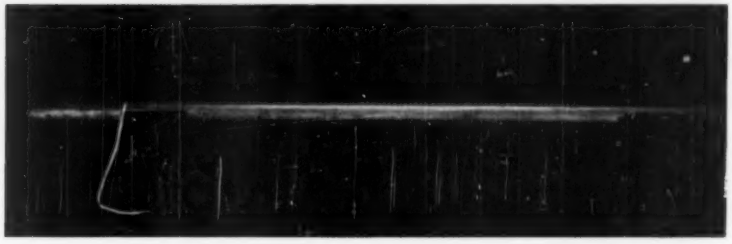

FIG. 5(a) COMMERCIAL CONSTANT-DIAMETER PIPE BURNER, LOW DELIVERY RATE

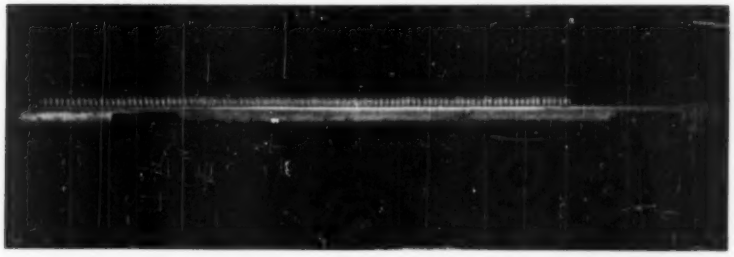

FIG. 5(b) COMMERCIAL CONSTANT-DIAMETER PIPE BURNER, HIGH DELIVERY RATE

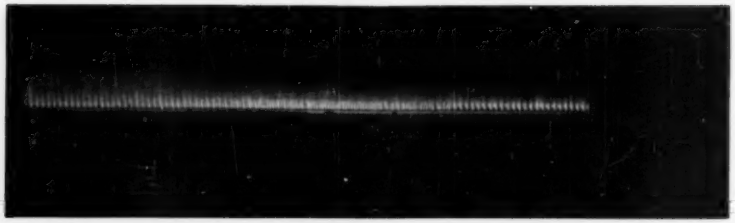

FIG. 6(*a*) MODIFIED COMMERCIAL BURNER WITHOUT INSERT

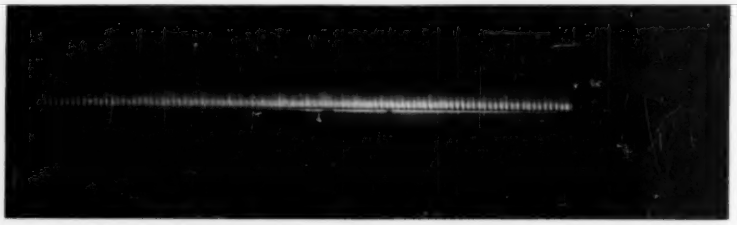

FIG. 6(*b*) MODIFIED COMMERCIAL BURNER WITH INSERT

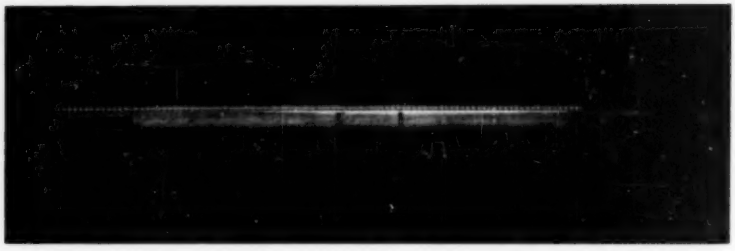

FIG. 6(*c*) MODIFIED COMMERCIAL BURNER WITHOUT INSERT, OPTIMUM DELIVERY RATE

the addition of a third row of $\frac{1}{4}$-in. ports which permitted an operating rate equal to 600 per cent of the capacity of the original commercial burner. They show the burner operating without and with a tapered insert under a yellow-flame condition of low primary air - gas ratio. Although such a flame condition is unsatisfactory for an actual heating application, it clearly shows the difference in the distribution of the gas in the two cases. This burner was successfully operated under blue-flame conditions.

Table 1 gives the pertinent data for the experimental tests conducted with the pipe burners.

DISCUSSION OF RESULTS AND PREVIOUS WORK

The theoretical and experimental investigation has resulted in a rational guide for the design of a simple high-capacity and extended-range pipe burner which should have considerable industrial importance. The investigation has demonstrated that the conventional low-capacity pipe burner may be converted into a high-capacity and more useful gas burner. The theoretical results are also applicable to other fluids and devices such as liquid-distribution systems, headers of multitube air heaters, steam and feedwater-distribution systems in boilers, sewage-disposal systems, and many others. However, the application of the results

TABLE 1 EXPERIMENTAL DATA

Burner, Fig. no.	Flow rates, cfh — Natural gas	Primary air	Total	Active length, in.	Pipe diam., in.	Total port area, sq in.
3(*a*)	7.8	38.1	45.9	36	0.622	0.903
3(*b*)	5.0	20.0	25.0	36	0.622	0.903
3(*c*)	3.5	15.0	18.5	36	0.622	0.903
4(*a*)	4.2	30.0	34.2	12	0.622	0.601
4(*b*)	4.5	30.0	34.5	12	0.622	0.601
5(*a*)	10.2	44.1	54.3	48	2.067	2.42
5(*b*)	40.8	164	205	48	2.067	2.42
6(*a*)	106	410	516	48	2.067	5.44
6(*b*)	100	380	480	48	2.067	5.44
6(*c*)	9	32	41	48	2.067	5.44
7(*a*)	120	481	601	48	2.067	9.68
7(*b*)	164	670	834	48	2.067	9.68
8(*a*)	570	625	1195	48	2.067	14.52
8(*b*)	580	640	1220	48	2.067	14.52

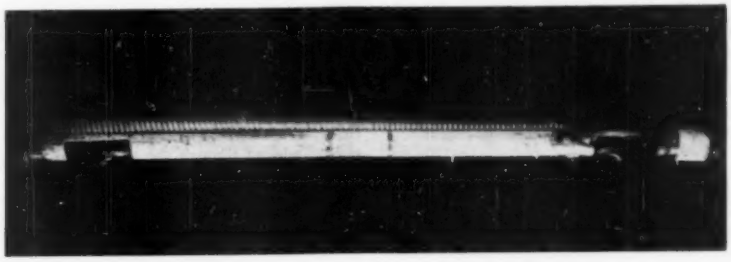

FIG. 7(*a*) MODIFIED COMMERCIAL BURNER WITHOUT INSERT

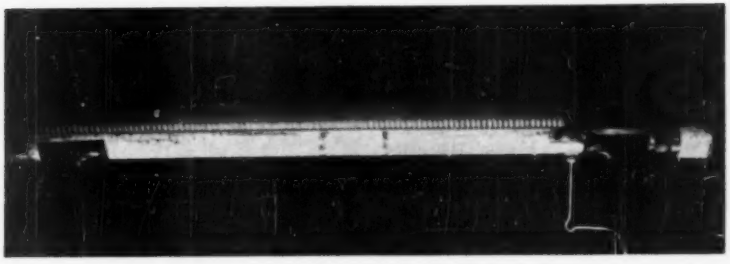

FIG. 7(*b*) MODIFIED COMMERCIAL BURNER WITH INSERT

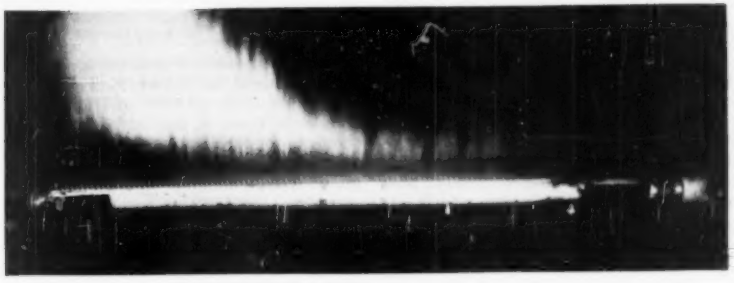

FIG. 8(*a*) MODIFIED COMMERCIAL BURNER WITHOUT INSERT

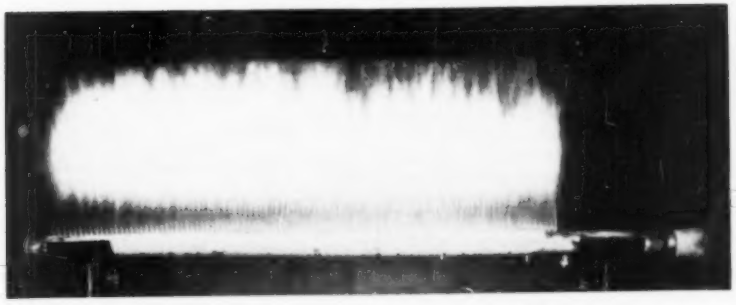

FIG. 8(*b*) MODIFIED COMMERCIAL BURNER WITH INSERT

to pipe burners was emphasized due to the industrial importance of a high-capacity pipe burner and the convenience of experimental verification of the theory with such a device.

The theoretical solutions can be extended readily to numerous other problems, such as a definite but nonuniform distribution of fluid from the manifold. Thus a pipe burner could be designed for a controlled distribution of heat over an extended length.

It was tacitly assumed in the theoretical solutions that the discharge ports were so small and closely spaced that the laminar and turbulent velocity profiles normally found in tubes would exist in the manifolds, and also that the discharge could be treated as a continuous function of distance along the manifold. It was also assumed that a fully developed flow pattern would exist at the first port of the inlet end, and that the flow through the pipe changed abruptly from turbulent to laminar. As the experiments have demonstrated, these assumptions are acceptable for standard-size pipe burners with conventional port openings and likewise should be acceptable for other physically similar systems. Obviously, the present results could not be applied to any manifold system regardless of size and number of discharge ports.

Keller[3] made a mathematical analysis of the flow of a fluid through a manifold having a uniform cross section and uniformly spaced discharge ports along its length. This is the case of the ordinary pipe burner. He concluded that there are two dimensionless ratios which define the operating characteristics of such a manifold, namely, the ratio of active length to diameter L/D, and the area ratio A_p/A. His theoretical reasoning led him to conclude that the variation of discharge is uniquely defined by these two ratios, and that only for the conditions of $L/D \cong 70$ and $A_p/A \leq 1$ is the distribution sufficiently uniform to meet practical requirements. He stated that for higher or lower values of L/D or higher values of A_p/A, it would be impossible to obtain a uniform flame height. Figs. 3(*b*), 5(*a*), (*b*), and 6(*d*) are graphic proof of the fallacy of Keller's conclusion. The variation of the discharge is not a unique function of these factors but also depends on the rate of total gas flow. The variation of the discharge may be altered for any constant-diameter pipe burner as shown by Equations [7] and [10], and Figs. 3(*a*), (*b*), and (*c*). Keller failed to recognize the variation of the Reynolds number and the corresponding variation of the friction factor with distance along the manifold even though a constant fluid-flow rate exists at the inlet end. He assumed that the friction factor was constant along the entire length of the manifold for any given inlet-flow rate. Keller also considered manifold problems which were variations of the pipe-burner problem; however, these solutions also involved the erroneous assumption of a constant friction factor.

Olson[4] has given a theoretical solution for the flow through a pipe with a porous wall when the flow is in the laminar region. However, his solution is valid only for the limiting case of negligible discharge through the porous wall because he neglected the kinetic-energy term.

Wills[5] made a theoretical investigation of gas flow through burner manifolds. However, he ignored friction losses in the manifold. He concluded that the cross-sectional area of the manifold should be about 3 times the port area in order to obtain a uniform flame. This conclusion corresponds to one of the criteria for the case of the manifold acting as an infinite reservoir.

Summary and Conclusions

Theoretical considerations of the flow through a perforated pipe have resulted in a clarification of the operating characteristics of pipe burners and physically similar manifold systems. It has been demonstrated that drilled-port pipe burners for gaseous fuels, which have a far greater utility and capacity than now realized, may be designed readily. The capacity of commercially available pipe burners may be increased several hundred per cent.

Design equations have been developed for the construction of manifold systems which would have a uniform distribution of fluid along their length. Likewise, a manifold which would have a desired but nonuniform distribution of fluid along its length could be designed. The validity of the theoretical considerations has been verified by experiment for manifold systems which are physically similar to ordinary pipe burners.

Acknowledgments

The author wishes to acknowledge his appreciation to Mr. Burnie Porter of the United Gas Pipe Line Company, for the formulation of the problem, and to Mr. D. T. MacRoberts, Director of Research, and the management of United Gas, for permission to publish this work. The assistance of William F. Cummer who conducted all phases of the photographic work is gratefully acknowledged.

[3] "The Manifold Problem," by J. D. Keller, Trans. ASME, vol. 71, 1949, pp. 77–85.

[4] "Flow Through a Pipe With a Porous Wall," by F. C. W. Olson, Trans. ASME, vol. 71, 1949, pp. 53–54.

[5] "Design of Gas Burners by the Use of Fundamental Flow Formulae," by F. Wills, *Western Gas*, vol. 7, 1931, pp. 87–89.

Measurements of Diffraction of Shock Waves and Resulting Loading of Structures[1]

By WALKER BLEAKNEY,[2] D. R. WHITE,[3] AND W. C. GRIFFITH,[3] PRINCETON, N. J.

Although the idea of using a shock tube to generate waves of large amplitude and to study their properties is not new,[4] nevertheless this technique has been improved greatly in recent years. This circumstance, taken together with good optical methods of measurement, has provided a powerful tool for the investigation of a great variety of problems in transient interactions of shocks and fluid flows with solid objects and with each other. This paper is concerned with the evolution in time of a flow pattern about an obstacle initially in still air, passed over by a sudden front of high-speed flow induced by a shock wave, the stream approaching a steady configuration. Such information is not only of interest in the theory of fluid dynamics but it also is of considerable practical importance, since the principal forces on the obstacle can be measured as a function of time, and the character of the loading determined. The main objective of this paper is to elucidate the method by giving examples of a great variety of experiments and at the same time to provide a large amount of basic data which may be used by others in various types of analyses.

Description of Method

THE apparatus employed in these investigations has already been described.[5] Suffice it to say that the plane shock wave is generated in a rectangular tube of 4 in. × 18 in. cross section. The observation windows are 5 in. in diam and through them photographs are made by the shadow, schlieren, or interferometric methods, usually the last. In order to interpret the data about to be described, it is important to realize that a uniform free-stream velocity and constant pressure extend over a considerable region behind the incident shock, and all of the results given in this paper were obtained in this region. The Mach number of this flow relative to the laboratory may be anything from zero to 1.7 in practice, depending upon the strength of the shock which may be adjusted at will within this range. Quantitative interpretations of the optical data are readily made if the phenomena are two-dimensional in character; otherwise the computations are difficult if not impossible. One other circumstance should be borne in mind, and that concerns the boundary layers which are negligibly thin on the walls of the tube, apparently because of the short duration of the flow.

In the experiments described in this paper, interferograms are made both in still air and in the disturbed flow, and from these, contours of equal fringe shift are plotted throughout the fields of interest. Since the density change in the air integrated over the optical path is directly proportional to the fringe shift, these curves are also density contours. In many cases, if the shocks are not too strong, it is sufficiently accurate to assume isentropic flow behind the incident shock, and to this approximation the density contours are identical with the pressure contours.

There is no adequate theory for the diffraction of a shock wave around simple objects. Even the case of propagation along a wall which makes a sudden change in direction has not been treated except in the case where this change is small.[6] In an effort to determine the actual facts in simple cases a number of experiments were performed, each designed to measure the density pattern at different times after the shock wave collided with the obstacle. There are two distinct ways of using the interferometer to obtain the density contours. In the first, the adjustment is such that in the undisturbed state of the gas the order of interference is the same all over the field of view, and hence no fringes are visible. In the disturbed state, any fringes that appear represent lines of constant fringe shift and, therefore, contours of constant density directly. This method displays the phenomena in dramatic fashion, but it is not always possible to identify the quantitative values of the contours. In the second method closely spaced parallel fringes represent the undisturbed state and any changes in the field will shift this pattern. Contours of constant fringe shift may be plotted and the density field determined.

An example of the first method is shown in Fig. 1 which depicts the density field about a rectangular block after being struck by a shock wave of pressure ratio 2 across its front. The shock has passed out of view on the right. This photograph may be compared with Fig. 6 which was evaluated by the other method for the same conditions of pressure and time. Fig. 2 illustrates an interferogram obtained by the second method, the one used for all the other experiments described in this paper.

The following notation applies to the figures included in this report:

1 The incident shock wave travels toward the right.

2 Subscript 0 refers to conditions in the undisturbed medium ahead of the shock.

3 Subscript 1 refers to conditions behind the incident shock in regions not disturbed by the obstacle.

4 Quantities without a subscript refer to a general field point behind the incident shock.

5 ΔT is the time elapsed in microseconds after the incident shock first touches the obstacle.

[1] This research was supported by the Office of Naval Research of the Navy Department. Reproduction, translation, publication, use and disposal in whole or in part by or for the United States Government is permitted.

[2] Palmer Physical Laboratory, Princeton University.

[3] AEC Postdoctoral Fellow, Princeton University.

[4] "Interaction of Shock Waves," by W. Bleakney and A. H. Taub, *Reviews of Modern Physics*, vol. 21, 1949, pp. 584–605.

[5] "The Shock Tube: Facility for Investigations in Fluid Dynamics," by W. Bleakney, D. K. Weimer, and C. H. Fletcher, *Review of Scientific Instruments*, vol. 20, 1949, pp. 807–815.

Presented at the Los Angeles 1950 Meeting of the Heat Transfer and Fluid Mechanics Institute.

Discussion of this paper should be addressed to the Secretary, ASME, 29 West 39th Street, New York, N. Y., and will be accepted until January 10, 1951, for publication at a later date. Discussion received after the closing date will be returned.

NOTE: Statements and opinions advanced in papers are to be understood as individual expressions of their authors and not those of the Society. Manuscript received by ASME Applied Mechanics Division on Sept. 11, 1950.

[6] "Pressure Behind a Shock Wave Diffracted Through a Small Angle," by C. H. Fletcher, D. K. Weimer, and W. Bleakney, *Physical Review*, vol. 78, 1950, pp. 634–635.

FIG. 1 CONTOUR FRINGES OF DIFFRACTION OF A SHOCK WAVE OVER A RECTANGULAR BLOCK
(With this adjustment of interferometer, points of equal gas density lie on the same fringe.)

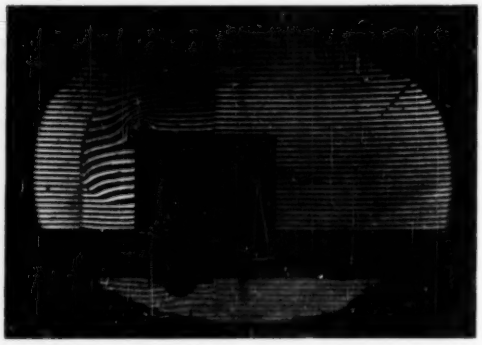

FIG. 2 ILLUSTRATING DISTORTION OF PARALLEL FRINGES PRODUCED BY DIFFRACTION OF SHOCK WHICH APPEARS MIDWAY ACROSS THE BLOCK
(A discontinuous jump of about eight fringes occurs across the incident shock front.)

6 The number N associated with each contour in the figure, represents the total fringe shift with reference to the undisturbed air ahead of the incident shock. Therefore the curves represent contours of equal fringe shift or contours of constant density change.

7 P denotes pressure, ρ density, and γ the ratio of specific heats taken as 7/5 for air.

8 The incident shock when visible is denoted by a heavy continuous line ——————.

9 All other shocks are denoted by a dashed line – – – – –.

10 Density contours are denoted by continuous lines ————.

11 Slip streams are denoted by crossed dashes + + + +. A slip stream may result from the interaction of shock waves. It represents a discontinuity in density but not in pressure.[7]

12 The leading edge of a rarefaction is denoted by alternate dots and dashes · — · — · — ·.

Since $N = k(\rho - \rho_0)$ and $N_1 = k(\rho_1 - \rho_0)$, where k is a constant, it follows that

$$(\rho - \rho_0)/N\rho_0 = (\rho_1 - \rho_0)/N_1\rho_0 \quad [1]$$

or

$$\rho/\rho_0 = 1 + N(\rho_1 - \rho_0)/N_1\rho_0 \quad [2]$$

It is not easy to calculate P/P_0 precisely from Equation [2] and the diffraction pattern, but fortunately, the assumption that all changes are isentropic and adiabatic after the incident shock has passed leads to an approximation which in the work discussed here is never in error by more than a few per cent and usually is considerably better than this. Making use of this assumption

$$P/\rho^\gamma = P_1/\rho_1^\gamma$$

and

$$P/P_0 = (P_1/P_0)(\rho_0/\rho_1)^\gamma(\rho/\rho_0)^\gamma \quad [3]$$

The first two factors on the right side of Equation [3] are related to each other by the Rankine-Hugoniot equations[7]

$$\rho_1/\rho_0 = [\gamma + 1 + (\gamma - 1)P_0/P_1]/[(\gamma - 1) + (\gamma + 1)P_0/P_1] \quad [4]$$

This expression substituted in Equation [3] gives a relation for P/P_0 in terms of ρ/ρ_0, which in turn is obtained from the fringe shift by the relation for ρ/ρ_0 given on each figure.

A somewhat cruder approximation is to neglect the entropy change across the incident shock in which case

$$P_1/P_0 = (\rho_1/\rho_0)^\gamma$$

and Equation [3] becomes simply

$$P/P_0 = (\rho/\rho_0)^\gamma \quad [5]$$

or in the case of Figs. 3 to 24, inclusive, where the initial conditions are nearly the same

$$P/P_0 = (1 + 0.074\,N)^{7/5} \quad [6]$$

This relation will never be in error by more than 2 per cent when applied to these cases, and usually will be more accurate than this limit.

APPARATUS AND PROCEDURE

To adapt the apparatus described by Bleakney, Weimer, and Fletcher[5] to this experiment, a horizontal plate with a sharp edge was installed just below the center of the window. The plate was about 2 ft long, the edge pointing upstream. On this plate in the middle of the field of view the various objects whose outlines appear in the figures were bolted. The blocks were made of steel or aluminum and extend the full width of the tube from one window to the other.

After the lines of constant fringe shift are plotted, there remains the problem of numbering the contours correctly. Usually this is solved when the absolute fringe shift is determined for one point. One method of finding the fringe shift across a discontinuity, such as a shock, makes use of white-light fringes. If the shift is not too great, one can identify the central or zero order of numbering. In the work described in this report a piece of plane glass was inserted at 45 deg in the light beam just before the light enters the filter in the camera. A few per cent of the light was reflected in this way to a second plate, the intensity being sufficient to record the white-light fringes, while the main beam, after passing the filter records the usual monochromatic interferogram. Hence the determination of the absolute shift was made on the same event as that from which the other contours were drawn.

It will be noted that each figure represents a different experiment, the time delay being the adjusted parameter. However, other conditions were not reproduced exactly so that small variations in pressures and shock strengths occur. All necessary

[7] "Introduction to Aerodynamics of a Compressible Fluid," by H. W. Liepmann and A. E. Puckett, John Wiley & Sons, Inc., New York, N. Y., 1947.

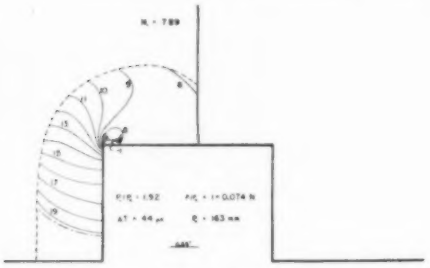

FIG. 3 PLOT OF FRINGE SHIFTS AS MEASURED ON INTERFEROGRAM IN FIG. 2

(Number attached to each curve may be substituted for N in formula to obtain value of density contour.)

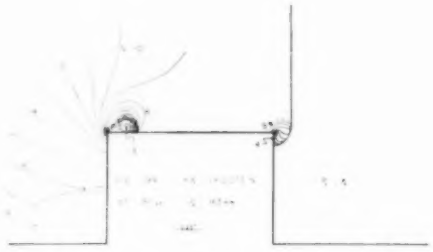

FIG. 4

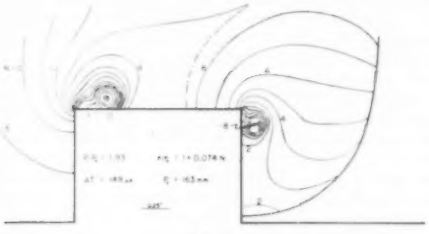

FIG. 5

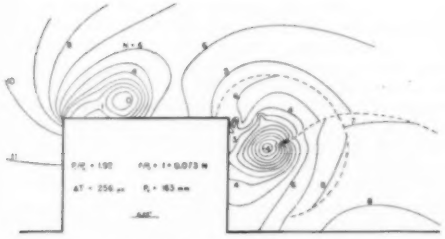

FIG. 6 SITUATION IN THIS FIGURE CORRESPONDS WITH THAT IN FIG. 1

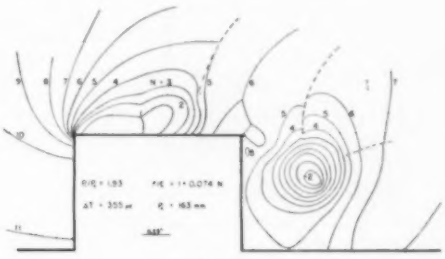

FIG. 7

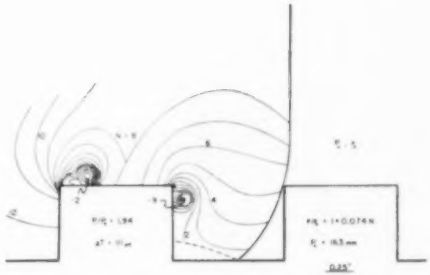

FIG. 8 DIFFRACTION OVER TWO RECTANGULAR BLOCKS

(These blocks are somewhat smaller than the one in first series.)

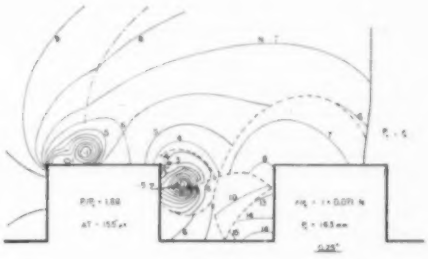

FIG. 9

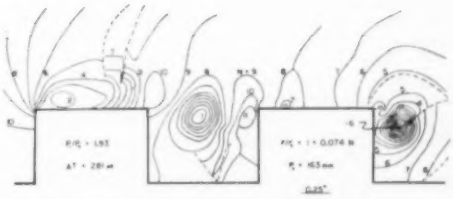

FIG. 10

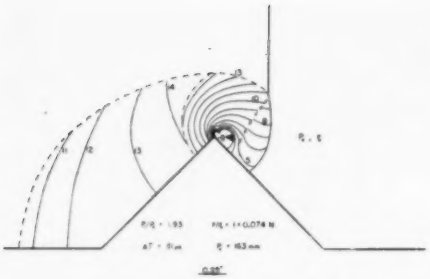

FIG. 11 DIFFRACTION OVER TRIANGULAR BLOCK

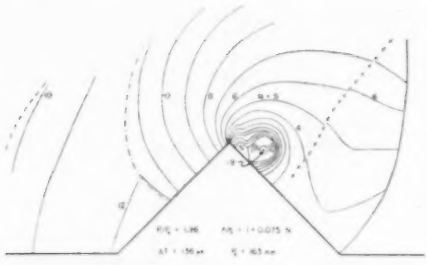

FIG. 12

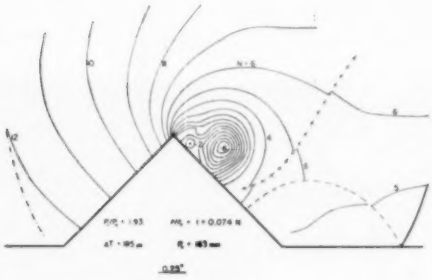

FIG. 13

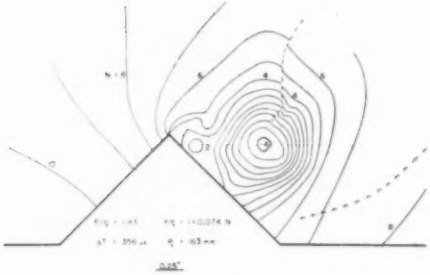

FIG. 14

data are given in each figure. As yet, no experiment has been performed where the scale or Reynolds number was a variable. There is reason to believe that scale effects will not be large, especially on those surfaces of the objects where the velocity of flow is small. This point, however, needs further investigation.

RESULTS

The diffraction of a shock wave of pressure ratio about 2 around a two-dimensional rectangular block is portrayed in Figs. 3 to 7. In Figs. 8 to 10 the same initial conditions are applied to two blocks in series so that one may determine the amount of shielding of one block by another. Note that these blocks are smaller in size than the first series. The third series, Figs. 11 to 14, is concerned with a triangular block, and the fourth series, Figs. 15 to 18, with a "loaf," that is, a rectangular block with rounded corners. The results for a semicylinder will be found in Figs. 19 to 24. The absence of sharp corners in the last two shapes results in smoother flow with reduced gradients, except for the disturbance which seems to be caused by the reflection of the incident shock after passing over the block. This effect is illustrated in Fig. 23.

To illustrate the method by which the transient forces may be evaluated, the rectangular block has been investigated in some detail. Using the methods described, the pressure distributions on the front, top, and back faces are plotted in Fig. 25. Here the number attached to each curve is the time on a scale such that the length of the top face divided by the velocity of the incident shock is unity. The pressure in "atmospheres" (given by $(P - P_0)/P_0$) is plotted perpendicular to each face. The area between each curve and the corresponding face is a measure of the total force on that face at the designated time. These loads, obtained from Figs. 3 to 7, and some others not included here, are plotted as a function of time in Fig. 26, where the load on the back side is taken as negative. Obviously, a similar variation of force with time could be made for any small segment of the surface. Let it not be forgotten that this is a two-dimensional phenomenon and one must speak of loads per unit distance perpendicular to the plane of the figure.

The density field surrounding a typical airfoil[9] when struck by a shock wave is shown in Figs. 27 to 31. This foil, a modification of NACA $65_2 - 015$, is in still air until struck by the wave at an angle of attack of 4.5 deg. It remains to be seen what theoretical and practical value can be made of these measurements, but it is obvious that a large amount of data can be secured by this technique. It is also possible that a combination of two shock waves may be devised such that the first sets up a quasi-steady flow over the foil, while the second is used to study the transient perturbation resembling gust loading.

In mounting instruments such as pressure gages and other devices in the path of shock waves to measure their properties, care must be taken that the instruments themselves do not distort the pressure field unduly. Usually this precaution involves some kind of baffling system. Interferograms of shocks passing over wedges serve to determine the regions where the free-flow variables are least affected for this type of baffle. The density field around such two-dimensional wedges at various times is shown in Figs. 32 to 36. For the indicated shock strength, little variation in density occurs on the parallel sides if the point of observation is 5 or more thicknesses behind the shoulder. When the incident shock is strong enough to set up supersonic flow in its wake, the situation may become quite complicated as indicated

[9] We are indebted to Lawrence Levy and H. G. Stever of M.I.T. for the model of the airfoil and for suggestions regarding the experiment.

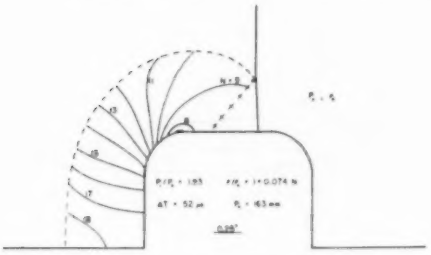

FIG. 15 DIFFRACTION OVER BLOCK WITH ROUNDED CORNERS

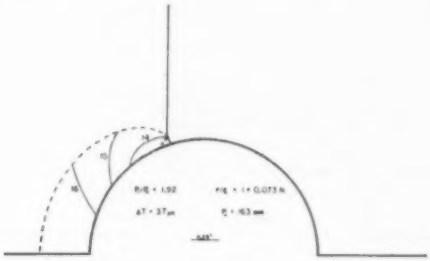

FIG. 19 DIFFRACTION OVER A SEMICYLINDER

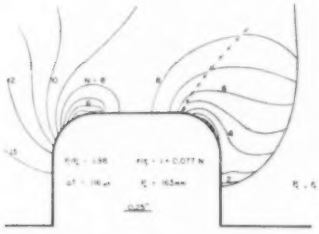

FIG. 16

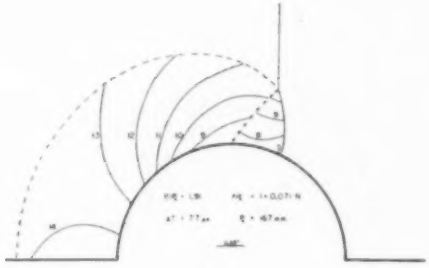

FIG. 20

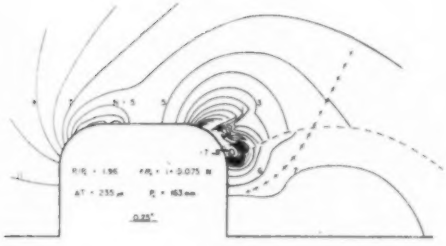

FIG. 17

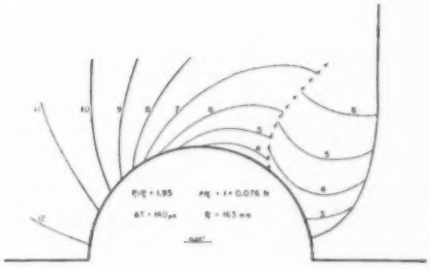

FIG. 21

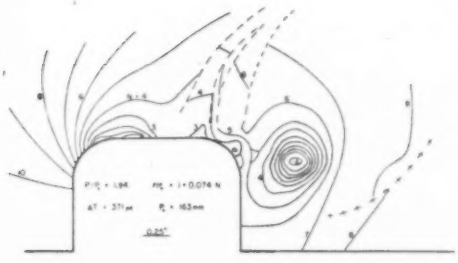

FIG. 18

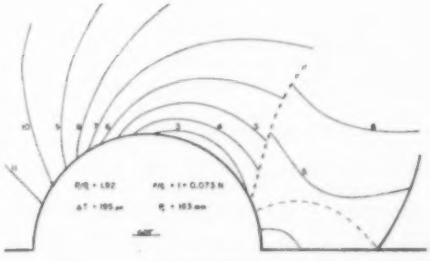

FIG. 22

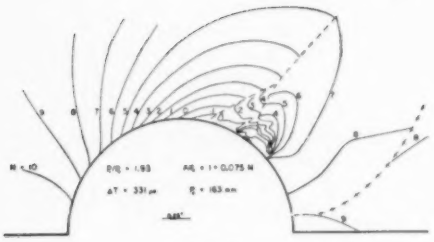

FIG. 23

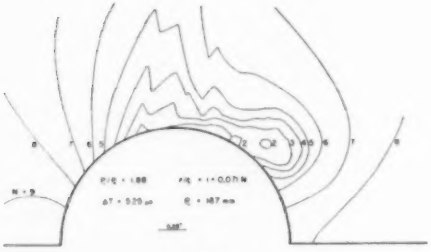

FIG. 24

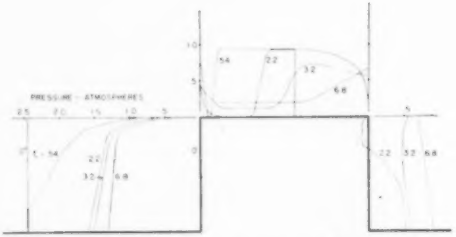

FIG. 25 PRESSURES ON FACES OF RECTANGULAR BLOCK AT VARIOUS TIMES, PLOTTED PERPENDICULAR TO CORRESPONDING FACE
(Time attached to each curve is in units of transit time across block.)

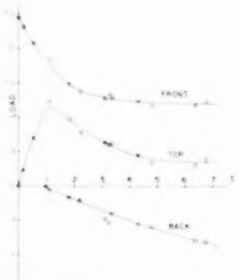

FIG. 26 TOTAL LOAD ON EACH FACE AS FUNCTION OF TIME
(Each point represents area under a curve such as those appearing in Fig. 25, the length of corresponding face being taken as unity.)

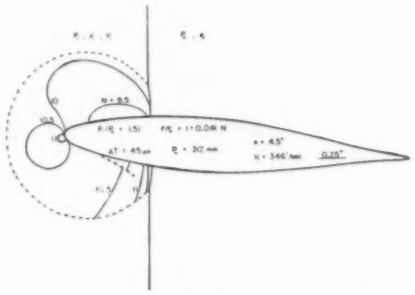

FIG. 27 DIFFRACTION OF A SHOCK WAVE OVER A SYMMETRICAL AIRFOIL AT AN ANGLE OF ATTACK OF 4.5 DEG

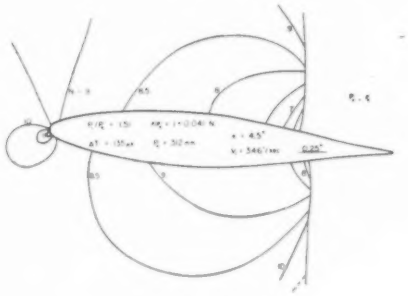

FIG. 28

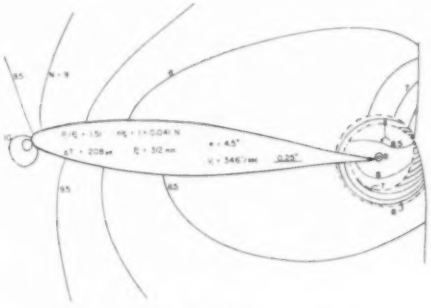

FIG. 29

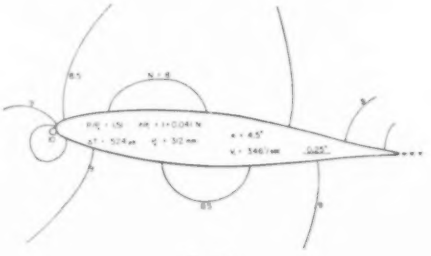

FIG. 30

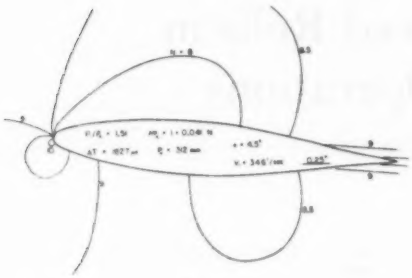

FIG. 31

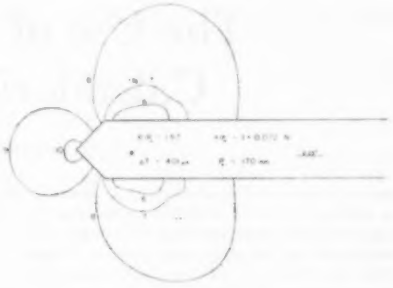

FIG. 35

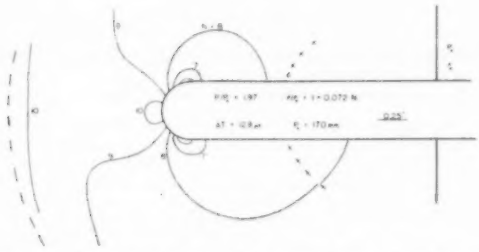

FIG. 32 DIFFRACTION OF SHOCK WAVE OVER ROUND-NOSED WEDGE
(Inadvertently this occurred at a small angle of attack.)

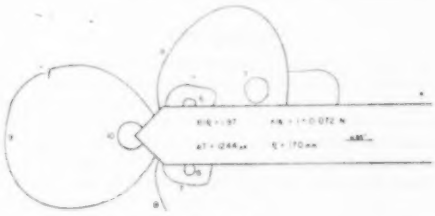

FIG. 36

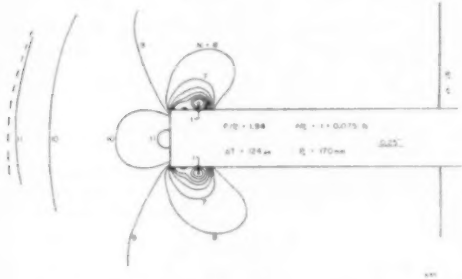

FIG. 33 DIFFRACTION OVER SQUARE-ENDED WEDGE

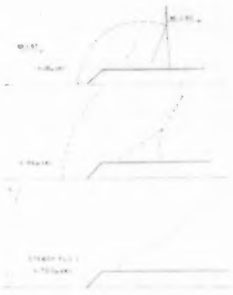

FIG. 37 SHOCK CONFIGURATION AROUND A 90-DEG WEDGE ARISING FROM DIFFRACTION OF A STRONG SHOCK
(Pressure ratio of incident shock here is $P_1/P_0 = 9.05$ giving a free-stream Mach number of 1.33.)

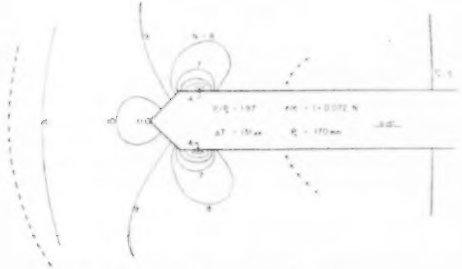

FIG. 34 DIFFRACTION OVER 90-DEG WEDGE

in Fig. 37, where the configuration of shocks only is shown at three different times. When the flow becomes steady, a shock radiates from a point near the shoulder, but in the earlier phases a secondary transient shock sweeps along the parallel sides of the plate.

ACKNOWLEDGMENT

The authors appreciate the great assistance of D. K. Weimer and C. H. Fletcher throughout the course of this work. They also wish to thank C. W. Lampson for his many suggestions.

The Use of Skewed Rolls in Calendering Operations

By G. F. CARRIER,[1] PROVIDENCE, R. I.

In many commercial operations it is desirable to produce a uniform sheet of material by passing the viscous raw ingredients through rotating cylindrical rolls. With rolls supported at the ends only there is danger of wide variations in thickness of the finished product. This may be overcome by "skewing" the rolls the amount necessary for any given thickness and material properties. This paper presents an analytical approach to determining the optimum operating position of the rolls.

Introduction

In many commercial operations (such as in the manufacture of linoleum), it is desired to produce a uniform sheet of material by passing a viscous raw material between a pair of rotating cylindrical rolls. However, when the rolls are supported only at the ends, the uniformity in the sheet thickness frequently is lost when large deflections of the roll occur. These deflections arise, of course, because of the large force exerted by the viscous material on the roll. In view of the fact that the magnitude of the deflection depends upon the thickness of the sheet being manufactured, it is desirable to find an adjustable "cure" for this situation. Such a cure can be found by skewing the rolls by an amount depending upon the sheet thickness and material properties. The present paper is an analysis which predicts the optimum operating position of the rolls.

Analysis of Skewed Rolls

Consider the rolls, Fig. 1, whose axes are inclined at an angle α. If the deflection of the rolls is denoted by y, the undeflected roll clearance at $x = 0$ by $2t_0$, and the roll radius by R, then we may write

$$O_1' O' = 2(R + t_0 + y \cos \beta)$$

$$O_2' O' = x \tan \alpha + 2y \sin \beta$$

and

$$(O_1' O_2')^2 = 4(R + t)^2 = 4(R + t_0 + y \cos \beta)^2 + (x \tan \alpha + 4y \sin \beta)^2$$

or

$$R + t = \sqrt{(R + t_0 + y)^2 + \frac{x^2 \tan^2 \alpha}{4} + 2xy \tan \alpha \sin \beta - 2(R + t_0)y(1 - \cos \beta)} \quad \ldots [1]$$

We may, however, anticipate that α, β, y/R as well as t_0/R are very small so that Equation [1] becomes

$$t = t_0 + y + \frac{\alpha^2}{8R} x^2 + \ldots$$

where the omitted terms are of higher order in the quantities taken as small.

If we observe that the rolls are essentially pin-supported beams, we may write

$$(d^4y)/(dx^4) = p$$

where p is the force per unit length normal to the beam. The boundary conditions require that $y'(0) = y''(0) = 0$, $y(l) = y''(l) = 0$. It is an experimental fact that the pressure p exerted

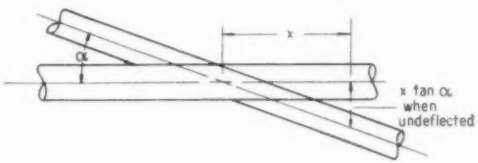

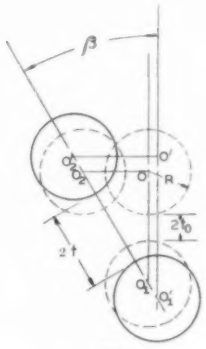

Fig. 1

by a material such as we are discussing is closely given by k/t for a given roll diameter, speed of rolling, and the like. The value of k must, in general, be determined from known properties of the material or experimentally. Using this formula (i.e., $p = k/t$) we obtain

$$(EI\, d^4y)/(dx^4) = k/(t_0 + cx^2 + y) \quad \ldots [2]$$

For convenience we introduce the dimensionless parameters

$$\xi = x/l, \quad u = y/t_0, \quad s = t/t_0$$

$$a = (kl^4)/(EIt_0), \quad \lambda = (\alpha^2 l^2)/(8Rt_0)$$

[1] Professor, Brown University. Jun. ASME.

Presented at the National Conference of the Applied Mechanics Division, Purdue University, Lafayette, Ind., June 22–24, 1950, of The American Society of Mechanical Engineers.

Discussion of this paper should be addressed to the Secretary, ASME, 29 West 39th Street, New York, N.Y., and will be accepted until January 10, 1951, for publication at a later date. Discussion received after the closing date will be returned.

Note: Statements and opinions advanced in papers are to be understood as individual expressions of their authors and not those of the Society. Manuscript received by Applied Mechanics Division August 30, 1949. Paper No. 50—APM-10.

and obtain in place of Equation [2]

$$(d^4u)/(d\xi^4) = a/s = a/(1 + \lambda\xi^2 + u) \quad [3]$$

where $u'(0) = u''(0) = u(1) = u''(1) = 0$.

We wish, of course, a solution u such that s is constant. This (rigorously) is impossible, however, since, when we write $s = \text{const} = s_0$, the solution of Equation [3] is

$$u = \frac{a}{24\,s_0}(\xi^4 - 6\xi^2 + 5) \quad [4]$$

which leads to

$$s = 1 + \lambda\xi^2 + \frac{a}{24\,s_0}(\xi^4 - 6\xi^2 + 5) \quad [5]$$

which cannot be constant for any values of λ and s_0 other than $\lambda = 1/s_0 = 0$ (this solution is, of course, meaningless).

Let us, then, try the following procedure: Assume that λ can be chosen so that s varies only a little about some average value

$$s_0 = \int_0^1 s(\xi)d\xi$$

Replace s by this value s_0 in Equation [3] and obtain the approximate solution as given in Equations [4] and [5]. To find the "best" value of λ we write

$$\frac{\partial}{\partial\lambda}\int_0^1 (s - s_0)^2 d\xi = \frac{\partial}{\partial\lambda}\left(\int_0^1 s^2 d\xi - s_0^2\right) = 0 \quad [6]$$

We also have the condition that

$$\int_0^1 1 + \lambda\xi^2 + \frac{a}{24\,s_0}(\xi^4 - 6\xi^2 + 5)\,d\xi = s_0 \quad [7]$$

in order that the function s of Equation [5] have the average value s_0. Equations [6] and [7] lead successively to the results

$$a/s_0 = 14\,\lambda/3$$

$$\lambda = (45/86)\left[\sqrt{1 + \frac{86}{105}a} - 1\right] \quad [8]$$

Now, if one knows a, the "skew angle" α is determined for any sheet thickness. The average of the sheet thickness as given by the foregoing formulas is

$$s_0 = 1 + \frac{43}{45}\lambda$$

and the maximum and minimum values are

$$1 + \lambda, \quad 1 + \frac{413}{441}\lambda$$

Numerical Example

According to information at our disposal, a typical situation is associated with the following values of the parameters:

$t_0 = 0.020$ in., $a = 1.92$, $R = 14$ in., $l = 54$ in., sheet thickness = 0.050 in.

Using the foregoing formulas, these values lead to the following results

$$\lambda = 0.314, \quad t_{max} = 1.314, \quad t_{min} = 1.294, \quad t_{avg} = 1.300$$

Thus the deviation in the sheet thickness is less than 2 per cent. Without skewed rolls it would be 20 per cent. The skew angle for this case is given by

$$\alpha = \sqrt{8\,R\,t_0\,\lambda/l} = 0.022 \text{ radians}$$

Accuracy of Solution

The solutions obtained in the foregoing (Equations [4], [5], [8]) are valid only if Equation [4] is very nearly the correct solution of Equation [3]. To show that this is the case we may write (where u^* is the exact solution of Equation [3])

$$\partial^4 u^*/\partial\xi^4 = \frac{a}{1 + \lambda\xi^2 + u^*}$$

$$\partial^4 u/\partial\xi^4 = \frac{a}{s_0}$$

or

$$\frac{\partial^4}{\partial\xi^4}(u^* - u) = \frac{\partial^4\varphi}{\partial\xi^4} = \frac{a(s_0 - 1 - \lambda\xi^2 - u^*)}{s_0(1 + \lambda\xi^2 + u^*)}$$

$$= \frac{a}{s_0}\,\frac{-\epsilon(\xi) - \varphi}{s_0 + \epsilon(\xi) + \varphi}$$

where $\epsilon(\xi) = 1 + \lambda\xi^2 + u - s_0$, is never greater in magnitude than $2\lambda/45$.

We may now introduce a successive-approximation scheme wherein we set

$$\varphi_0 = 0$$

$$\varphi_1 = \text{solution of } \varphi_1^{IV} = \frac{a}{s_0}\,\frac{-\epsilon(\xi) - \varphi_0}{s_0 + \epsilon(\xi) + \varphi_0}$$

$$\varphi_n^{IV} = \frac{a}{s_0}\,\frac{-\epsilon - \varphi_{n-1}}{s_0 + \epsilon + \varphi_{n-1}}$$

The exact solution of Equation [3] is then given by

$$u^* = u + \lim_{n\to\infty} \varphi_n$$

and this differs so little from u that the variations in t still remain within 2 per cent of t_{avg} for values of a in the range discussed.

Acknowledgment

The suggestion that this problem be investigated, certain of the information used, and permission to publish the paper are through the courtesy of the Armstrong Cork Company.

Vibration of Rectangular Plates by the Ritz Method

By DANA YOUNG,[1] AUSTIN, TEXAS

Ritz's method is one of several possible procedures for obtaining approximate solutions for the frequencies and modes of vibration of thin elastic plates. The accuracy of the results and the practicability of the computations depend to a great extent upon the set of functions that is chosen to represent the plate deflection. In this investigation, use is made of the functions which define the normal modes of vibration of a uniform beam. Tables of values of these functions have been computed as well as values of different integrals of the functions and their derivatives. With the aid of these data, the necessary equations can be set up and solved with reasonable effort. Solutions are obtained for three specific plate problems, namely, (*a*) square plate clamped at all four edges, (*b*) square plate clamped along two adjacent edges and free along the other two edges, and (*c*) square plate clamped along one edge and free along the other three edges.

Nomenclature

THE following nomenclature is used in the paper. Any consistent set of units can be used for the physical quantities. For reference purposes the units are given in terms of the engineering inch-pound-second system:

V = elastic strain energy of bending of a plate, in-lb
E = modulus of elasticity, psi
μ = Poisson's ratio
h = thickness of plate, in.
$D = Eh^3/12(1 - \mu^2)$ = bending stiffness of a plate, lb-in.
w = lateral deflection of plate, in.
x, y = rectangular co-ordinates
ρ = mass density of plate material (lb sec^2/in.^{4})
f = frequency, cycles per sec (cps)
$\omega = 2\pi f$ = angular frequency, radians/sec
$\lambda = \omega^2\rho h a^2 b/D$ = characteristic value
a, b = lateral dimensions of plate, in.: see Fig. 1
l = length of beam, in.
m, n; i, k; p, q; r, s = positive integers
A_{mn} = coefficient used in series representation of deflection
X_m = a function of x alone
Y_n = a function of y alone
φ_r = characteristic function of a vibrating beam, as defined by Equations [5], [6], [7]
α_r = parameter in expressions for φ_r: values given in Table 1
ϵ_r = parameter in expressions for φ_r: values given in Table 1
E_{ni}, F_{ks}; H_{im}, K_{ks} = definite integrals defined by Equations [10], [11], [12]
$C_{mn}^{(ik)}$ = coefficients defined by Equations [15] and [16]
δ_{mn} = Kronecker delta, defined by Equation [14]

Introduction

An exact solution of the differential equation of a vibrating plate is known for the case of a rectangular plate which is simply supported at all four edges (1, 2),[2] and also for a rectangular plate which is simply supported along one pair of opposite edges with any conditions at the other two edges (3). For other combinations of edge conditions the solutions are more complicated, and it has been necessary to resort to various approximate methods. The procedure developed by Ritz (4) has been found to be useful in such problems and, in fact, was used by Ritz himself (5) to calculate in great detail the frequencies and nodal patterns of a square plate with all four edges free.

The convergence and accuracy of Ritz's method have been discussed by various authors including E. Trefftz (6), R. Courant (7), and L. Collatz (8). It is known that this method gives upper bounds for the frequencies, that is, the frequencies calculated by Ritz's procedure are always higher than the exact values. Also, the accuracy of the results cannot be estimated with certainty in most cases. In spite of these limitations, the method has yielded satisfactory solutions for numerous problems in equilibrium, buckling, and vibration.

While Ritz's method is well known, it has not been used as much as might be expected for plate-vibration problems. There appears to be little published data for the vibration of rectangular plates by Ritz's method except for a square plate with free edges (5). This is probably due, at least in part, to the great amount of computational labor which is required both to set up and to solve the necessary equations. The amount of computation involved depends to a large extent upon the set of functions that is used to represent the plate deflection. For these functions some investigators have taken a series of polynomials while others have used combinations of the characteristic functions which define the normal modes of a vibration of a uniform beam. For example, an application of the polynomial functions to a plate equilibrium problem has been given by G. Pickett (9), while the use of the beam-vibration functions is illustrated by Ritz's solution (5). It is these latter types of functions that have been selected for use in this study.

In order to simplify the computations, values of different integrals of the functions and their derivatives have been calculated, and the results are given herein. In addition, tables of

[1] Professor of Applied Mechanics, University of Texas. Mem. ASME.

Presented at the Annual Conference of the Applied Mechanics Division, Purdue University, Lafayette, Ind., June 22-24, 1950, of The American Society of Mechanical Engineers.

Discussion of this paper should be addressed to the Secretary, ASME, 29 West 39th Street, New York, N. Y., and will be accepted until January 10, 1951, for publication at a later date. Discussion received after the closing date will be returned.

Note: Statements and opinions advanced in papers are to be understood as individual expressions of their authors and not those of the Society. Manuscript received by the Applied Mechanics Division March 27, 1950. Paper No. 50—APM-18.

[2] Numbers in parentheses refer to the Bibliography at the end of the paper.

values for the functions are now available (10). With the aid of these data the work required to set up the necessary equations is considerably reduced. A simple iteration procedure can be used to solve the equations.

It is to be observed that the analysis herein is for a homogeneous plate of uniform thickness and is based upon the ordinary theory of thin plates.

Ritz's Method

For a uniform plate which is vibrating harmonically with amplitude $w(x, y)$ and angular frequency ω, the maximum potential energy is given by

$$V = \frac{D}{2}\int\int\left[\left(\frac{\partial^2 w}{dx^2}\right)^2 + \left(\frac{\partial^2 w}{\partial y^2}\right)^2 + 2\mu\frac{\partial^2 w}{\partial x^2}\frac{\partial^2 w}{\partial y^2} + 2(1-\mu)\left(\frac{\partial^2 w}{\partial x \partial y}\right)^2\right]dx\,dy \quad [1]$$

and the maximum kinetic energy is

$$\frac{1}{2}\rho h\omega^2\int\int w^2\,dx\,dy$$

where the integrations are to be taken over the domain of the plate surface. Equating these two expressions, we have

$$\omega^2 = \frac{2}{\rho h}\frac{V}{\int\int w^2 dx dy} \quad [2]$$

It is known, see (2), (5), or (11), that the natural frequencies are determined by finding expressions for w that satisfy the boundary conditions and minimize the expression, Equation [2]. The direct application of the calculus of variations to minimize Equation [2] leads to the partial differential equation for a vibrating plate. Instead of following such a procedure, Ritz's method consists of assuming the deflection $w(x, y)$ as a linear series of "admissible" functions and adjusting the coefficients in the series so as to minimize Equation [2].

For rectangular plates, with the edges parallel to the x- and y-axes, it is expedient to take the series approximation for w in the form

$$w(x, y) = \sum_{m=1}^{p}\sum_{n=1}^{q} A_{mn}X_m(x)\cdot Y_n(y) \quad [3]$$

Each function X_mY_n must be "admissible," that is, it must satisfy the so-called "artificial boundary conditions," but need not satisfy any "natural boundary conditions;" see (8) or (11). In the case of plates, prescribed values for the deflection and also for the slope constitute artificial boundary conditions, while the requirement that second or third derivatives or combinations thereof vanish at the boundary is a natural condition. From a practical consideration of the rate of convergence, it is desirable to satisfy natural boundary conditions if possible.

When $w(x, y)$ as given by Equation [3] is substituted in Equation [2], the right-hand side becomes a function of the coefficients A_{mn}. This is minimized by taking the partial derivative with respect to each coefficient and equating to zero. Thus we arrive at a set of equations each of which has the form

$$\frac{\partial V}{\partial A_{ik}} - \frac{\omega^2\rho h}{2}\frac{\partial}{\partial A_{ik}}\int\int w^2 dx dy = 0 \quad [4]$$

where A_{ik} is any one of the coefficients A_{mn}. Equation [4] represents a system of linear homogeneous equations in the unknowns A_{mn}. The natural frequencies $\omega_1, \omega_2, \ldots$ are determined from the condition that the determinant of the system must vanish.

As discussed in the introduction, the appropriate characteristic functions for vibrating beams will be used for X_m and Y_n. A summary of the properties of these functions is given in the next section.

Characteristic Functions for Vibrating Beam

The different types of beams will be identified by a compound adjective which describes the end conditions. Thus a "clamped-clamped" beam is one which is rigidly clamped at both ends; a "clamped-free" beam is clamped at the end $x = 0$ and free at the end $x = l$; a "free-free" beam is free at both ends.

For each type of beam there is an infinite number of normal modes in which the beam can vibrate laterally. The method of determining the set of characteristic functions which define the normal modes for any type of beam is given in standard references such as (1) and (2). The characteristic functions for the three types of beams used in this paper are as follows

Clamped-Clamped Beam

$$\varphi_r = \cosh\frac{\epsilon_r x}{l} - \cos\frac{\epsilon_r x}{l} - \alpha_r\left(\sinh\frac{\epsilon_r x}{l} - \sin\frac{\epsilon_r x}{l}\right) \quad [5]$$

Clamped-Free Beam

$$\varphi_r = \cosh\frac{\epsilon_r x}{l} - \cos\frac{\epsilon_r x}{l} - \alpha_r\left(\sinh\frac{\epsilon_r x}{l} - \sin\frac{\epsilon_r x}{l}\right) \quad [6]$$

Free-Free Beam

$$\varphi_1 = 1 \quad [7a]$$

$$\varphi_2 = \sqrt{3}\,(1 - 2x/l) \quad [7b]$$

$$\varphi_r = \cosh\frac{\epsilon_r x}{l} + \cos\frac{\epsilon_r x}{l} - \alpha_r\left(\sinh\frac{\epsilon_r x}{l} + \sin\frac{\epsilon_r x}{l}\right), \quad (r = 3, 4, 5, \ldots) \quad [7c]$$

In each of the foregoing expressions $r = 1, 2, 3, \ldots$; hence each expression defines an infinite set of functions. The numerical values of α_r and ϵ_r for each set of functions are given in Table 1. It should be noted that, while Equations [5] and [6] have the same general form, the values of α_r and ϵ_r are different. The functions have significance only in the interval $0 \le x \le l$.

Tables of values of these functions are given in (10) to five decimal places and at intervals of the argument-$x/l = 0.02$.

Equation [7c] is the usual expression for the characteristic functions of a free-free beam; when $r = 3$ we have the first mode of free vibration. The functions φ_1 and φ_2 represent a rigid-body translation and rotation and are included in order to obtain a complete orthogonal set.

The boundary conditions satisfied by the functions in each set are the same as the end conditions of the corresponding beam. That is, for the clamped-clamped functions $\varphi_r = d\varphi_r/dx = 0$ at $x = 0$ and $x = l$; for the clamped-free functions $\varphi_r = d\varphi_r/dx = 0$ at $x = 0$ and $d^2\varphi_r/dx^2 = d^3\varphi_r/dx^3 = 0$ at $x = l$; for the free-free functions

$$d^2\varphi_r/dx^2 = d^3\varphi_r/dx^3 = 0 \text{ at } x = 0 \text{ and } x = l$$

Each of the characteristic functions except Equations [7a] and [7b] satisfies the differential equation $d^4\varphi_r/dx^4 = \epsilon_r^4\varphi_r/l^4$. Each set of the functions is orthogonal in the interval 0 to l, that is, for any two functions φ_r and φ_s in the same set, the following relations hold

TABLE 2 INTEGRALS OF CHARACTERISTIC FUNCTIONS OF CLAMPED-CLAMPED BEAM

Values of $I = \int_0^1 \frac{d\phi_r}{dx}\frac{d\phi_s}{dx}\,dx$

r \ s	1	2	3	4	5	6
1	12.30962	0	- 9.75079	0	- 7.61544	0
2	0	46.05012	0	- 17.12892	0	- 15.19457
3	- 9.75079	0	98.90480	0	- 24.54987	0
4	0	- 17.12892	0	171.58566	0	- 51.27645
5	- 7.61544	0	- 24.54987	0	265.99798	0
6	0	- 15.19457	0	- 51.27645	0	376.15008

Note: $\int_0^1 \phi_r \frac{d^2\phi_s}{dx^2}\,dx = -\int_0^1 \frac{d\phi_r}{dx}\frac{d\phi_s}{dx}\,dx$

TABLE 1 VALUES OF α_r AND ϵ_r

Type of Beam	r	α_r	ϵ_r^2	ϵ_r^3
Clamped-Clamped	1	0.9825 0222	4.7300 408	500.564
	2	1.0007 7731	7.8532 046	3 803.537
	3	0.9999 6645	10.9956 078	14 617.630
	4	1.0000 0145	14.1371 655	39 945.799
	5	0.9999 9994	17.2787 596	80 135.407
	6	1.0000 0000	20.4203 522	173 881.316
	r>6	1.0	(2r + 1)π/2	
Clamped-Free	1	0.7340 955	1.8751 041	12.362
	2	1.0185 6041	4.6940 911	485.519
	3	0.9999 2450	7.8547 774	3 806.546
	4	1.0000 3355	10.9955 407	14 617.273
	5	0.9999 9855	14.1371 684	39 945.852
	r>5	1.0	(2r - 1)π/2	
Free-Free	1		0	0
	2		0	0
	3	0.9825 0222	4.7300 408	500.564
	4	1.0007 7731	7.8532 046	3 803.537
	5	0.9999 6645	10.9956 078	14 617.630
	6	1.0000 0145	14.1371 655	39 945.799
	7	0.9999 9994	17.2787 596	80 135.407
	r>7	1.0	(2r - 3)π/2	

$$\int_0^l \varphi_r\,\varphi_s\,dx = l \quad (\text{for } r = s); \qquad = 0 \quad (\text{for } r \neq s) \qquad \ldots\ldots\ldots\ldots [8]$$

The second derivatives of the function in each set are also orthogonal and satisfy the relations

$$\int_0^l \frac{d^2\varphi_r}{dx^2}\frac{d^2\varphi_s}{dx^2}\,dx = \frac{\epsilon_r^4}{l^3} \quad (\text{for } r = s); \qquad = 0 \quad (\text{for } r \neq s) \qquad \ldots\ldots\ldots [9]$$

with the exception of φ_1 and φ_2 for the free-free functions, Equations [7(a), (b)], for which

$$\int_0^l \left(\frac{d^2\varphi_1}{dx^2}\right)^2 dx = \int_0^l \left(\frac{d^2\varphi_2}{dx^2}\right)^2 dx = 0$$

For convenience in handling these exceptions, it is expedient to define $\epsilon_1 = \epsilon_2 = 0$ arbitrarily for the free-free functions; with this notation the relations, Equations [9], are valid for all functions in each set. Numerical values of ϵ_r^4 are given in Table 1.

In addition to the integrals defined by Equations [8] and [9], it is necessary to evaluate

$$\int_0^l \varphi_r \frac{d^2\varphi_s}{dx^2}\,dx, \text{ and } \int_0^l \frac{d\varphi_r}{dx}\frac{d\varphi_s}{dx}\,dx$$

TABLE 3 INTEGRALS OF CHARACTERISTIC FUNCTIONS OF CLAMPED-FREE BEAM

Values of $I = \int_0^1 \frac{d\phi_r}{dx}\frac{d\phi_s}{dx}\,dx$

r \ s	1	2	3	4	5
1	1.84778	- 7.37587	5.94153	- 6.59339	6.59196
2	- 7.37587	32.41739	- 22.35845	13.58245	- 22.83952
3	5.94153	- 22.35845	77.29889	- 35.64827	20.16203
4	- 6.59339	13.58245	- 35.64827	167.90185	- 48.71964
5	6.59196	- 22.83952	20.16203	- 48.71964	228.13525

Values of $I = \int_0^1 \phi_r \frac{d^2\phi_s}{dx^2}\,dx$

r \ s	1	2	3	4	5
1	0.85824	- 11.74322	27.45515	- 37.39025	51.95662
2	1.87385	- 15.39429	- 9.04202	30.40139	- 33.70907
3	1.56451	5.28933	- 45.90423	- 8.33537	36.38656
4	1.08737	5.54060	6.25360	- 98.91821	- 7.82895
5	0.91404	5.71642	11.23264	4.73605	-171.58466

TABLE 4 INTEGRALS OF CHARACTERISTIC FUNCTIONS OF FREE-FREE BEAM

Values of $I = \int_0^1 \frac{d\phi_r}{dx}\frac{d\phi_s}{dx}\,dx$

r \ s	1	2	3	4	5	6	7
1	0	0	0	0	0	0	0
2	0	12.00000	0	13.85641	0	13.85641	0
3	0	0	49.48088	0	35.57751	0	36.60732
4	0	13.85641	0	108.92459	0	97.58881	0
5	0	0	35.57751	0	186.86671	0	78.10116
6	0	13.85641	0	97.58881	0	284.68314	0
7	0	0	36.60732	0	78.10116	0	402.89805

Values of $I = \int_0^1 \phi_r \frac{d^2\phi_s}{dx^2}\,dx$

r \ s	1	2	3	4	5	6	7
1	0	0	18.59010	0	43.98096	0	69.11504
2	0	0	0	40.59446	0	84.08889	0
3	0	0	- 12.90062	0	32.58440	0	101.62755
4	0	0	0	- 46.05012	0	95.50860	0
5	0	0	1.00009	0	- 98.90480	0	60.12891
6	0	0	0	5.28566	0	-171.58566	0
7	0	0	0.57069	0	9.86075	0	-265.99798

when using these functions in Ritz's method. Values of these integrals have been computed and are given in Tables 2, 3, and 4, for the clamped-clamped, clamped-free, and free-free functions, respectively.

Application of Ritz's Method

The characteristic functions discussed previously are the functions that will be used for X_m and Y_n in Equation [3]. The particular sets to be used in any problem will depend upon the boundary conditions of the plate. Consider a rectangular plate, Fig. 1, bounded by the lines $x = 0, x = a, y = 0, y = b$. Assume, for example, that the plate is clamped along the edge $x = 0$ and free along the other three edges. In this case the clamped-free functions, Equation [6], should be used for X_m, and the free-free functions, Equation [7], should be used for Y_n. We observe that when any one of the sets of functions, Equation [5], [6], or [7], is used for X_m, we take $l = a$; if used for Y_n, we take $l = b$ and replace x by y. Appropriate changes of the subscripts r and s to either m and i or to n and k are to be made in each case. With the three sets of functions given herein, solutions can be obtained for rectangular plates having any combination of free and clamped edges.

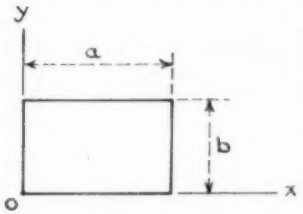

Fig. 1 Co-Ordinate System for Plate

It is convenient to introduce the following notation

$$E_{im} = a\int_0^a X_i \frac{d^2X_m}{dx^2}\,dx \qquad E_{mi} = a\int_0^a X_m \frac{d^2X_i}{dx^2}\,dx \quad [10]$$

$$F_{kn} = b\int_0^b Y_k \frac{d^2Y_n}{dy^2}\,dy \qquad F_{nk} = b\int_0^b Y_n \frac{d^2Y_k}{dy^2}\,dy \quad [11]$$

$$H_{im} = a\int_0^b \frac{dX_i}{dx}\frac{dX_m}{dx}\,dx \qquad K_{kn} = b\int_0^b \frac{dY_k}{dy}\frac{dY_n}{dy}\,dy \quad [12]$$

Since the appropriate φ-functions are to be used for X_m and Y_n the numerical values of the foregoing integrals can be taken directly from the data given in Tables 2, 3, and 4.

Using Equations [3] and [1], and taking into account the orthogonality relations, Equations [8] and [9], the set of Equations [4] can be reduced to the form

$$\sum_{m=1}^{p}\sum_{n=1}^{q}\left[C_{mn}^{(ik)} - \lambda\delta_{mn}\right] A_{mn} = 0 \quad [13]$$

where

$$\lambda = \omega^2 \rho h a^2 b/D \quad [14]$$

$$\delta_{mn} = 1 \text{ for } mn = ik$$
$$= 0 \text{ for } mn \neq ik$$

and

$$C_{mn}^{(ik)} = \mu\frac{a}{b}\left[E_{mi}F_{kn} + E_{im}F_{nk}\right] + 2(1-\mu)\frac{a}{b}H_{im}K_{kn} \quad [15]$$

which is valid for $mn \neq ik$. For $mn = ik$, the coefficient is

$$C_{ik}^{(ik)} = \frac{b}{a}\epsilon_i^4 + \frac{a^3}{b^3}\epsilon_k^4 + 2\mu\frac{a}{b}E_{ii}F_{kk} + 2(1-\mu)\frac{a}{b}H_{ii}K_{kk} \quad [16]$$

In Equation [16], ϵ_i is to be taken from the data in Table 1 corresponding to the φ-function that represents X_m, while ϵ_k is to be taken from data for the φ function that represents Y_n.

There will be one equation of the type [13] for each of the $p \cdot q$ combinations of ik. The characteristic values λ are found from the condition that determinant of this system of equations must vanish. If there are more than three or four equations in the system, the mathematical labor of expanding the determinant and solving for roots of the polynomial in λ is prohibitive. In such cases it is expedient to solve for λ by one of the known iterative procedures. One of the advantages of using the φ-functions for X_m and Y_n is that the diagonal terms in the determinant are large compared to the others, and as a result the characteristic values and modes can be found by the simple iteration procedure used by Ritz (5).

Square Cantilever Plate

Consider the case of a square plate which is clamped along one edge and free along the other three edges. Using the co-ordinate system in Fig. 1, let us take $x = 0$ as the clamped edge. For X_m we use the clamped-free functions, Equation [6], and for Y_n we use the free-free functions, Equation [7]. Taking $a = b$ and assuming Poisson's ratio $\mu = 0.3$, the coefficients $C_{mn}^{(ik)}$ as defined by Equations [15] and [16] have been computed for an 18-term series based on taking $m = 1, 2, 3$ and $n = 1, 2, 3, 4, 5, 6$. It is found that the corresponding system of 18 Equations [13] divides into two independent groups of 9 equations each. One of these groups includes only $n = 1, 3, 5$ and represents deflections which are symmetrical about the line $y = b/2$. The other group includes only $n = 2, 4, 6$, and represents deflections which are antisymmetrical with respect to the line $y = b/2$.

The coefficients for the symmetrical group are given in Table 5. The coefficients along the principal diagonal are large compared to the others and, consequently, the system can be solved quite simply by the iteration procedure which was used by Ritz (5). A brief explanation of this procedure will now be given. The equations corresponding to the coefficients in Table 5 are

$$(12.36 - \lambda)A_{11} + 4.79\,A_{13} + 11.33\,A_{15} + \ldots\ldots\ldots = 0$$
$$4.79\,A_{11} + (828.51 - \lambda)A_{13} + 244.21\,A_{15} + \ldots\ldots\ldots = 0$$
$$11.33\,A_{11} + 244.21\,A_{13} + (15794.99 - \lambda)A_{15} + \ldots\ldots = 0$$

Only the first three equations have been indicated here in order to save space; the six other equations are to be understood as following these.

Assume that we wish to find the lowest frequency. It may be inferred from examination of the equations that A_{11} is the predominant amplitude coefficient. For convenience, take $A_{11} = 1.0$. The first equation can be written as

$$\lambda = 12.36 + 4.79\,A_{13} + 11.33\,A_{15} + \ldots\ldots\ldots\ldots [a]$$

and the others can be put in the form

$$A_{13} = -(4.79 + 244.21\,A_{15} + \ldots)/(828.51 - \lambda) \ldots [b]$$

$$A_{15} = -(11.33 + 244.21\,A_{13} + \ldots)/(15794.99 - \lambda) \ldots [c]$$

and similarly for the other six equations. For the first trial, assume values for $A_{13}, A_{15}, \ldots$; these may be taken as zero if no better guess is apparent. Using these first trial values, calculate λ from Equation [a] and then calculate A_{13} from Equation [b]. Using this improved value for A_{13} and the first trial values for the other A_{mn}, calculate A_{15} from Equation [c]. Continue the procedure for the remaining equations.

After these improved values for A_{mn} are calculated, they are substituted back into Equation [a] and a second trial value for λ is calculated. Following the same steps as before, we now re-

calculate A_{13}, A_{15}, ... The procedure is repeated until the values of λ and A_{mn} in successive iterations are close enough to give the desired accuracy.

The same procedure can be used for the higher frequencies. For example, examination of Table 5 indicates that A_{31} is the predominant amplitude coefficient for the next higher frequency. Accordingly, we take $A_{31} = 1.0$ and start by rewriting the equation corresponding to the fourth row of coefficients in Table 5 in the form

$$\lambda = 485.52 - 65.49\,A_{13} - 154.94\,A_{15} + \ldots .$$

The other equations are written in a form similar to Equations [*b*] and [*c*], and then the equations are solved in the same manner as before.

The first three frequencies of the symmetrical modes and the first two frequencies of the antisymmetrical modes have been calculated and the results are given in Table 6. The relative magnitudes of the amplitude coefficients A_{mn} corresponding to each frequency are also given in the table. In each case the magnitude of the predominant amplitude coefficient is taken equal to unity.

Knowing the relative values of A_{mn} and the values of the φ-functions, the shape of each mode of vibration can be calculated from Equation [3]. In this particular example, the predominant amplitude coefficient is so large compared to the others that the shape of each mode is practically determined by the term in Equation [3] corresponding to that one coefficient. Thus it is seen that the lowest symmetrical mode is primarily a cantilever beam deflection in the x-direction and practically a constant in the y-direction. In the lowest antisymmetrical mode, each section x = const rotates essentially as a straight line about the axis $y = b/2$. The nodal lines for each mode of vibration are shown by the sketches in Table 6.

TABLE 5 COEFFICIENTS FOR VIBRATION OF SQUARE CANTILEVER PLATE SYMMETRIC MODES

i	k	$c_{11}^{(ik)}$	$c_{13}^{(ik)}$	$c_{15}^{(ik)}$	$c_{31}^{(ik)}$	$c_{33}^{(ik)}$	$c_{35}^{(ik)}$	$c_{51}^{(ik)}$	$c_{53}^{(ik)}$	$c_{55}^{(ik)}$
1	1	12.36	4.79	11.33	0	10.95	24.72	0	8.72	20.64
1	3	4.79	808.51	244.21	-65.49	-476.86	-342.30	155.10	165.95	259.73
1	5	11.33	244.21	13798.99	-154.94	-969.75	-1677.87	362.87	689.15	170.16
3	1	0	-65.49	-154.94	485.52	-76.14	-175.41	0	18.01	42.61
3	3	10.95	-476.86	-969.75	-76.14	5389.87	1588.69	-50.43	-1526.98	-1061.08
3	5	24.72	-342.30	-1677.87	-175.41	1588.69	26272.88	-119.51	-1247.98	-5675.25
5	1	0	155.10	362.25	0	-50.43	-119.51	3806.79	-256.00	-605.67
5	3	8.72	165.95	689.15	18.01	-1526.98	-1247.98	-256.00	10000.69	5079.54
5	5	20.64	259.73	170.16	42.61	-1061.08	-5675.25	-605.67	5079.54	41370.70

TABLE 6 FREQUENCIES AND MODES OF VIBRATION OF SQUARE CANTILEVER PLATE

	1st Mode	2nd Mode	3rd Mode	4th Mode	5th Mode
$\frac{\omega}{\sqrt{D/\rho h^4}}$	3.496	8.547	22.46	29.46	31.19
Amplitude coefficients	$A_{11} = 1.0000$ $A_{13} = -0.0037$ $A_{15} = -0.0008$ $A_{31} = -0.0026$ $A_{33} = -0.0050$ $A_{35} = -0.0011$ $A_{51} = 0.0001$ $A_{53} = -0.0014$ $A_{55} = -0.0006$	$A_{12} = 1.0000$ $A_{14} = -0.0134$ $A_{16} = -0.0011$ $A_{32} = 0.1252$ $A_{34} = 0.0044$ $A_{36} = -0.0006$ $A_{52} = -0.0020$ $A_{54} = -0.0011$ $A_{56} = -0.0006$	$A_{11} = 0.0054$ $A_{13} = 0.2731$ $A_{15} = 0.0092$ $A_{31} = 1.0000$ $A_{33} = 0.0713$ $A_{35} = 0.0079$ $A_{51} = -0.0118$ $A_{53} = 0.0050$ $A_{55} = 0.0063$	$A_{11} = 0.0090$ $A_{13} = 1.0000$ $A_{15} = 0.0120$ $A_{31} = -0.2866$ $A_{33} = -0.1796$ $A_{35} = 0.0009$ $A_{51} = -0.0452$ $A_{53} = 0.0125$ $A_{55} = 0.0023$	$A_{12} = -0.1261$ $A_{14} = -0.0627$ $A_{16} = -0.0080$ $A_{32} = 1.0000$ $A_{34} = -0.0188$ $A_{36} = -0.0013$ $A_{52} = 0.0776$ $A_{54} = -0.0086$ $A_{56} = -0.0024$
Nodal lines					

Clamped Square Plate

Consider a square plate which is clamped along all four edges. For this case we use the clamped-clamped functions Equation [5] for both X_m and Y_n. The calculations for this problem have been carried out for a 36-term series based on taking both m and n equal to 1, 2, 3, 4, 5, 6. The 36 equations of the type [13] divide in four independent groups of 9 equations each. If we denote by x' and y' the co-ordinates referred to a set of axes through the middle point of the plate, then one group contains only functions which are even in both x' and y'; the second group contains only functions which are odd in both x' and y'; the third group contains functions which are even in x' and odd in y'; the fourth group contains functions which are odd in x' and even in y'. The last two groups are essentially the same if we interchange x and y, and lead to identical frequencies; hence there are only 3 groups to solve. Further, each of the first two groups can be rearranged to form two independent subgroups, one of which has 6 equations and the other 3 equations; the first subgroup includes solutions for which $A_{mn} = A_{nm}$ while the second subgroup includes solutions for which $A_{mn} = -A_{nm}$.

The frequencies and relative amplitudes have been calculated for the first 6 modes and the results are presented in Table 7. The magnitude of the predominant amplitude coefficient is taken as unity for each mode.

The fundamental frequency of a vibrating clamped square plate under a uniform tension in both the x and y-directions has been computed by A. Weinstein and W. Z. Chien (12). The calculations are based upon a variational method developed by A. Weinstein. This method gives a "lower" bound for the frequency as contrasted to Ritz's method which gives an "upper" bound. As a check, the Ritz method calculations for a clamped square plate were extended to include the effect of a uniform tension T per unit length. In order to obtain a direct comparison with the results in (12), the calculations were carried through for two different values of T, namely, $T_1 = 10\pi^2 D/a^2$ and $T_2 = 100\,\pi^2 D/a^2$. A 9-term series, corresponding to taking both m and n equal to 1, 3, 5 was used; this leads to a system of only 6 equations since $A_{mn} = A_{nm}$ for the fundamental frequency. The fundamental frequency calculated on this basis was found to be higher than the lower bound given in (12) by only 0.1 per cent for the tension T_1 and by 2.5 per cent for the tension T_2. Results are given in (12) for a Ritz method solution based upon the two-term series

$$w = A\cos^2\frac{\pi x'}{a}\cos^2\frac{\pi y'}{b} + B\cos^2\frac{\pi x'}{a}\cos^2\frac{\pi y'}{b}$$

The upper bound for the frequency in this case is higher than the lower bound by 0.8 per cent for the tension T_1, and by 4.5 per cent for the tension T_2.

TABLE 7 FREQUENCIES AND MODES OF VIBRATION OF CLAMPED SQUARE PLATE

	1st Mode	2nd Mode	3rd Mode	4th Mode	5th Mode	6th Mode
$\omega\sqrt{\rho/Eh^2}$	35.99	73.41	108.27	131.64	159.05	169.15
Amplitude coefficients	$A_{11} = 1.0000$ $A_{12} = 0.6182$ $A_{13} = 0.0030$ $A_{21} = 0.6182$ $A_{22} = 0.3824$ $A_{23} = -0.0031$ $A_{31} = 0.0030$ $A_{32} = -0.0031$ $A_{33} = -0.0009$	$A_{12} = 1.0000$ $A_{14} = 0.6181$ $A_{15} = 0.0020$ $A_{24} = 0.3826$ $A_{25} = 0.0036$ $A_{26} = -0.0032$ $A_{35} = -0.0007$ $A_{36} = -0.0007$ $A_{45} = 0.0079$ $A_{56} = -0.0011$ $A_{66} = -0.0005$	$A_{22} = 1.0000$ $A_{24} = 0.6326$ $A_{26} = 0.0073$ $A_{42} = 0.6326$ $A_{44} = -0.0019$ $A_{46} = -0.0010$ $A_{62} = 0.0073$ $A_{64} = -0.0010$ $A_{66} = -0.0006$	$A_{13} = 1.0000$ $A_{15} = 0.0085$ $A_{31} = -1.0000$ $A_{33} = -0.0181$ $A_{51} = -0.0085$ $A_{53} = 0.0181$	$A_{11} = -0.0850$ $A_{13} = 1.0000$ $A_{15} = 0.0055$ $A_{31} = 1.0000$ $A_{33} = 0.1247$ $A_{35} = 0.0118$ $A_{51} = 0.0055$ $A_{53} = 0.0118$ $A_{55} = -0.0018$	$A_{12} = -0.0806$ $A_{14} = -0.0805$ $A_{16} = -0.0017$ $A_{32} = 1.0000$ $A_{34} = 0.0566$ $A_{36} = 0.0181$ $A_{52} = 0.0850$ $A_{54} = -0.0011$ $A_{56} = -0.0009$
Nodal lines						

Square Plate Clamped at Two Adjacent Edges and Free at the Other Edges

For this case assume that the plate is clamped along the two edges $x = 0$ and $y = 0$, and free along the other two edges. The clamped-free functions, Equation [6], are used for both X_m and Y_n. Calculations for this problem have been carried out for a 9-term series based on taking both m and n equal to 1, 2, 3. The set of 9 equations can be divided in two independent groups. One group which contains 6 equations represents modes which are symmetrical about the diagonal line $x = y$, while the other which contains 3 equations represents modes which are antisymmetrical about the line $x = y$.

The frequencies, relative amplitudes, and nodal patterns for the first 5 modes are presented in Table 8. As before, the magnitude of the predominant amplitude coefficient is taken as unity for each mode.

TABLE 8 FREQUENCIES AND MODES OF VIBRATION OF SQUARE PLATE HAVING TWO ADJACENT EDGES CLAMPED AND OTHER TWO EDGES FREE

	1st Mode	2nd Mode	3rd Mode	4th Mode	5th Mode
$\omega\sqrt{\rho/Eh^2}$	6.958	20.68	26.80	48.05	62.14
Amplitude coefficients	$A_{11} = 1.0000$ $A_{12} = 0.6604$ $A_{13} = -0.3030$ $A_{21} = 0.6604$ $A_{22} = -0.0101$ $A_{23} = -0.0063$ $A_{31} = -0.3030$ $A_{32} = -0.0063$ $A_{33} = -0.0017$	$A_{11} = 0$ $A_{12} = 1.0000$ $A_{13} = 0.00005$ $A_{21} = -1.0000$ $A_{22} = 0$ $A_{23} = -0.0221$ $A_{31} = -0.00005$ $A_{32} = 0.0221$ $A_{33} = 0$	$A_{11} = -0.1172$ $A_{12} = 1.0000$ $A_{13} = 0.0555$ $A_{21} = 1.0000$ $A_{22} = 0.2825$ $A_{23} = 0.0111$ $A_{31} = 0.0555$ $A_{32} = 0.0111$ $A_{33} = 0.0029$	$A_{11} = 0.0956$ $A_{12} = -0.1566$ $A_{13} = -0.0825$ $A_{21} = -0.1566$ $A_{22} = 1.0000$ $A_{23} = 0.1456$ $A_{31} = -0.0825$ $A_{32} = 0.1456$ $A_{33} = -0.0010$	$A_{11} = 0$ $A_{12} = 0.0650$ $A_{13} = 1.0000$ $A_{21} = -0.0830$ $A_{22} = 0$ $A_{23} = 0.1250$ $A_{31} = -1.0000$ $A_{32} = -0.1250$ $A_{33} = 0$
Nodal lines					

Acknowledgment

A portion of this work was carried out as a part of the program of the Defense Research Laboratory of the University of Texas and was sponsored by the Navy Department, Bureau of Ordnance.

BIBLIOGRAPHY

1 "Theory of Sound," by Lord Rayleigh, second American edition, Dover Publications, New York, N. Y., 1945.

2 "Vibration Problems in Engineering," by S. Timoshenko, second edition, D. Van Nostrand Company, Inc., New York, N. Y., 1937.

3 "Bermerkung zu dem Problem der transversalen Swingungen rechtteckiger Platten," by W. Voight, *Göttingen Nachrichten*, 1893, pp. 225–230.

4 "Über eine neue Method zur Losung gewisser Variationsprobleme der Mathematische Physik," by W. Ritz, *Journal für reine and angewandte Mathematik*, vol. 135, 1909, pp. 1–61.

5 "Theorie der Transversalschwingungen einer quadratischen Platten mit freien Randern," by W. Ritz, *Annalen der Physik*, Vierte Folge, vol. 28, 1909, pp. 737–786.

6 "Konvergenz und Fehlerschätzung beim Ritzchen Verfahren," by E. Treffts, *Mathematische Annalen*, vol. 100, 1928, p. 503.

7 "Variational Methods for the Solution of Problems of Equilibrium and Vibration," by R. Courant, *Bulletin of the American Mathematical Society*, New York, N. Y., vol. 49, 1939, pp. 1–23.

8 "Eigenwertprobleme," by Lothar Collatz, Chelsea Publishing Company, New York, N. Y., 1948.

9 "Solution of Rectangular Clamped Plate With Lateral Lead by Generalized Energy Method," by Gerald Pickett, Journal of Applied Mechanics, Trans. ASME, vol. 61, 1931, p. A-178.

10 "Table of Characteristic Functions Representing the Normal Modes of Vibration of a Beam," by D. Young and R. P. Felgar, Engineering Research Series, No. 44, University of Texas, Austin, Texas, July 1, 1949.

11 "Advanced Methods in Applied Mathematics," by R. Courant, New York University, New York, N. Y., 1941.

12 "On the Vibrations of a Clamped Plate Under Tension," by A. Weinstein and W. Z. Chien, *Quarterly of Applied Mathematics*, vol. 1, April, 1943, pp. 61–68.

13 "The Solution of Small Displacement Stability or Vibration Problems Concerning a Flat Rectangular Panel When the Edges Are Either Clamped or Simply Supported," by H. G. Hopkins, Reports and Memoranda, Aeronautical Research Council, London, England, no. 2234, June, 1945.

Discussion

Gaskets and Bolted Joints[1]

H. G. Koch.[2] The author has given us a simple and logical relation between the significant properties of a gasket and the performance of an assembled flanged joint. Some of this theory will require verification by test. For example, the assumption that the hydrostatic pressure works only to the inside diameter of the gasket (Equation [9] of the paper), the use of an averaged recovery modulus (Equation [15]), and the assumption that elastic and plastic effects occur independently in the gasket material (Equation [22]) are approximations which should be evaluated by experiment.

To the gasket manufacturer, the paper is valuable as a listing of the gasket properties which are of specific interest to the designer and on which data eventually should be made available. Accumulation of such data will be a formidable task, as the author points out. It is not generally recognized that gasket characteristics such as m values are not a fixed property of the gasket material, but depend to a great extent on the service conditions. Thus values of m, differing as widely as $m = 50$ and $m = 3$, have been observed on the same gasket material when sealing against nitrogen and water, respectively, under the same conditions of load and temperature. Other service variables which will have an appreciable effect on this property are temperature, thickness and width of gasket, roughness of flange and gasket surfaces, etc. We hope, therefore, that the flange designer will not be surprised to find that gasket data corresponding to his particular service conditions are not immediately available from the manufacturer; it is probable that it will take many years to gather reasonably complete information. Certainly this paper will help to stimulate interest in the accumulation of such data.

A. R. C. Markl.[3] The writer is in wholehearted sympathy with the author's desire to see flange design established on a fully rational basis and welcomes the contributions offered toward attaining this goal in the present paper, which may be considered as covering the following two phases of the wider problem:

1 The determination of the gasket loading required to maintain a tight joint between rigid flanges.

2 The determination of the optimum gasket type and size and the corresponding maximum bolt spacing for a ring flange with full-face gasket.

In so far as gasket loading constants are concerned, the German[4] and British[5] papers referred to by the author, together with less comprehensive American[6] contributions to the subject, were not entirely unknown or unconsidered when the Rules for Bolted Flanged Connections in the ASME Code were formulated. But, considering that the constants were obtained under idealized conditions, it was felt that they should not be accepted directly as a design basis, but should be modified on the basis of service experience. While no claim is made that the values so derived are scientifically correct, their application has generally led to satisfactory designs. The basis, moreover, is more in accord with logic and experimental results than the author has perhaps realized, as will be shown.

As a result of his study of the conditions for tightness, the author has concluded that the tests can be interpreted in terms of a gasket factor which decreases from infinity toward unity as a limit as the initial gasket stress is increased. They can be evaluated thus but the question arises whether the assumption of a continuous mathematical law, which appears implicit in this approach, however attractive, does not tend to misdirect future efforts. Also, the author's disregard of the repeat measurements taken in the German tests is open to criticism. It is suggested that the curve visualized by the author strictly consists of two distinct branches and that the Code procedure, with its dual check for gasket seating and tightness under pressure, gives a more adequate qualitative interpretation of the two stages involved, (1) of producing, and (2) of maintaining, a tight joint.

The first stage involves the application of a sufficient bolt load to bring the mating surfaces of the gasket and flange into conformity through "plastic" deformation. The effort required is a function of the contact area and the yield strength (or, where yield strength is not recognized, its equivalent, for which the term "design seating stress" is used in the Code). As an illustration of an instance where this controls up to high pressures, the data on initial tightening of flat copper gaskets given in the German paper[4] have been redrawn in Fig. 1, herewith. Note

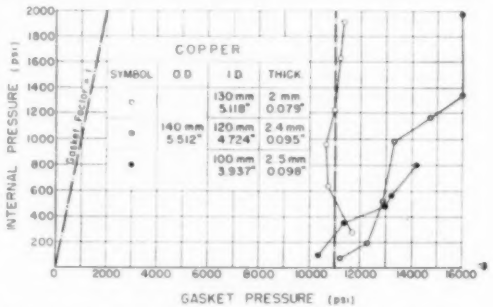

Fig. 1 Leakage Test Data for Copper Gasket on Initial Tightening

that the unit gasket compression is practically constant for the narrowest width tested, varying by no more than about 500 psi from a mean of 11,000 psi. Observe further that the author's logical deduction that gasket factors should decrease with increasing width because of reduced chances of the fluid finding a leakage channel is contradicted by the test data; the probable cause of this unexpected trend, in the German authors' opinion, is to be found in the increased probability, with increased gasket width, of encountering thickness differences of sufficient magni-

[1] By Irving Roberts, published in the June, 1950, issue of the Journal of Applied Mechanics, Trans. ASME, vol. 72, pp. 169–179.

[2] In charge of Packing Research, Johns Manville Research Center, Manville, N. J. Jun. ASME.

[3] Chief Research Engineer, Product Engineering and Research, Tube Turns, Inc., Louisville, Ky.

[4] Author's Bibliography, ref. (1).

[5] Author's Bibliography, ref. (2).

[6] "The Ring Joint," by E. C. Petrie, *Heating, Piping & Air Conditioning*, vol. 9, 1937, pp. 213–220, among others.

tude to impede sealing. The order of magnitude of the stresses required to effect a tight joint corresponds to about 5 per cent strain in fully annealed copper, which may be considered to support the concept of yield or seating stress postulated herein.

In the second stage, a reduced loading is generally adequate to keep the joint tight; once the gasket has been made to conform in the first stage, more or less "elastic" action is sufficient to maintain the intimacy of contact necessary to avoid leakage. The ratio of gasket pressure to leakage pressure is substantially constant, i.e., the gasket factor controls. In a final analysis, the latter can probably be related to short-time and creep data of the type presented by the author for Cranite. As an illustration of the dual control of yield strength and gasket factor over the joint behavior, data on lead abstracted from the German paper are given in Fig. 2. The vertical line drawn through the approxi-

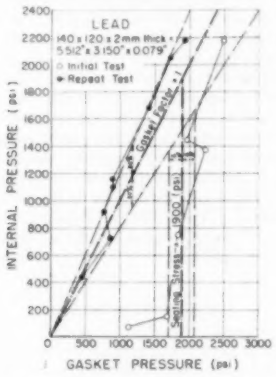

FIG. 2 LEAKAGE TEST DATA ON LEAD, BOTH UNDER INITIAL AND REPEAT LOADING

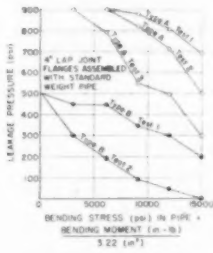
4" LAP JOINT FLANGES ASSEMBLED WITH STANDARD WEIGHT PIPE
Type A Test 1
Type A Test 2
Type B Test 1
Type B Test 2
LEAKAGE PRESSURE (psi)
BENDING STRESS (psi) IN PIPE = BENDING MOMENT (in.-lb) / 5.22 (in³)

FIG.[4] 3 TYPICAL LEAKAGE TEST DATA ON FLANGED JOINTS SUBJECTED TO BENDING MOMENTS
(Bending moment plotted in terms of extreme fiber stress in attached pipe.)

mate mean of the initial test values indicates a seating stress of approximately 1900 psi,[7] while the sloping lines radiating from the origin and bracketing the repeat-test values reflect a gasket factor of unity with about 20 per cent scatter.

While the Code approach accordingly appears basically sound from a qualitative standpoint, much work needs to be done to improve the adequacy of the quantitative values given. It is greatly to be hoped that the experimental program mentioned in the introduction to the paper will come to pass and that it will receive generous support from all interested parties. To be fully useful, the following program would appear necessary:

1 Stress-strain determinations on strips of preferably at least three standard widths, both under short-time and creep conditions. (Strips of as great as practicable a length-to-width ratio are suggested in preference to the author's 1-in. squares, so as more closely to simulate actual conditions.)

2 Gasket compression versus leakage pressure determinations between rigid platens, similar to the German tests.

3 Similar determinations between pairs of actual flanges of one or more sets of standard dimensions so selected as to permit evaluation of the effect of flange stiffness and bolt spacing.

4 Additional investigations as in item (2), but with eccentric load attack to simulate combined pressure and bending moment.

5 Additional investigations as in item (3), with the addition of a bending moment. Fig. 3 of this discussion illustrates to what extent even relatively moderate[8] bending moments influence leakage pressure.

6 Duplication of all the foregoing tests at different temperatures, subzero and elevated.

7 Supplementary tests under pulsating pressure, cyclic bending, thermal-shock, or quench conditions.

The development of an approach to the determination of the maximum permissible bolt spacing by means of the theory of elastic foundations given in the latter part of the paper is interesting and useful, although its application would appear limited to extremely light flanges, such as used as examples by the author. For ordinary flanges, tests have indicated that variations in bolt spacing within reasonable limits, which are intuitively understood by the average designer, have no effect on leakage pressure.

The author makes a good point in calling attention to the necessity of considering the interaction of all component parts of a flanged assembly if a truly rational analysis is to be achieved. All who have given thought to this problem will agree that this is so, but, considering the complexity of present flange calculations, despite simplified assumptions and precalculation of constants, the question arises how much refinement can be justified, weighing increased engineering time against possible savings in materials.

R. W. NOLAN.[9] Another factor, which complicates the problem of gasket design, is temperature differential. A high-temperature steam line may be shifted suddenly to saturated steam, or may suddenly receive a slug of water because of boiler priming. In either case, the flange will cool considerably faster than the bolts, and the differential may, in some cases, be several hundred degrees. Since the flange is cooler than the bolts, it will contract more and thus cause a reduction in gasket pressure. In one case, which the writer has in mind, with high-temperature steam and high gasket modulus, there is a possibility of entirely removing the gasket pressure and causing leakage.

D. B. ROSSHEIM[10] AND J. J. MURPHY.[11] The author is to be congratulated on his basic approach and presentation of the gasketed-joint problem. As he has pointed out, no co-ordinated attack on the essential factors has been made, and reliable basic data on gasket properties are lacking, particularly in the case of soft nonmetallic gaskets. The paper should reawaken interest

[7] Throughout the present discussion, yield strength and seating stress are referred to the full contact area, in distinction from the Code, which applies them to one half the area only.

[8] The present rules of the Code for Pressure Piping, Section 6, Expansion and Flexibility, permit extreme fiber stresses up to 24,000 psi in seamless Grade B pipe.

[9] Newport News Shipbuilding and Dry Dock Company, Newport News, Va. Mem. ASME.

[10] Chief Engineer, The M. W. Kellogg Company, New York, N. Y. Mem. ASME.

[11] The M. W. Kellogg Company, Jersey City, N. J.

in the problem to the point that work will be done to get the desired data and improve present methods of handling the problem.

The author has criticized certain features in the ASME Boiler Code's method of dealing with this problem and suggests a new approach for establishing gasket and bolting. Therefore a discussion on the Code approach and the suggestions made should be in order.

The ASME Boiler Code Rules for Bolted Flange Connections have come into wide usage because of their adoption by the Code Committee. In formulating these rules the Committee was concerned primarily with flange strength. However, tightness cannot be divorced from flange design, being of prime importance to users, and involving safety to a varying degree. Hence gasket factors were included, but the Committee was hampered by the same lack of gasket data the author experienced, and further felt that the rules must be kept as simple as possible. For these reasons the use of these gasket factors has never been mandatory and no attempt has been made to bring in the effect of gasket thickness, variations in surface finish, creep, or the variation of gasket properties with temperature. The author has referred to the paper by the writer and Mr. Markl (reference 8) proposing revisions to the Code. Most of these suggested changes have now been incorporated in the Code and include recognition of a width effect as shown by the tests of reference (1). The Code now reduces the effective seating width of a wide gasket for calculation purposes leaving m unchanged. An equivalent effect could be obtained by leaving the width unchanged and reducing m.

While the Code method of establishing minimum bolting and gasket factors has been kept simple, the general success of flanges so designed for all types of service is a tribute to the approach used. An important factor in the successful usage of such flanges undoubtedly has been the relatively low allowable bolt stress used in design calculations, which never exceeds one quarter the yield point. Code allowable bolt stresses are intended to reflect the value to which the bolt stress can relax in service with the expectancy that a tight joint will be maintained rather than the initial stress on tightening. Those who formulate these rules are fully aware that bolted joints are commonly made up by pipe fitters without any special instructions and that the initial stress in the bolts is generally much higher, approaching the yield point in the case of carbon-steel bolts. This factor provides a desirable margin for variations and imperfections in surface finish, for uncertainties of gasket properties and variations between manufactured products for: relaxation due to properties of the gasket, flange materials, flange rotation or temperature differentials, and for loadings other than internal pressure which may be experienced in service, such as piping thermal-expansion moments. Code-designed flanges have demonstrated a practical capacity to absorb the usual handling and service loadings. In some cases such flanges may appear overdesigned. These are likely to be joints using soft gaskets for relatively mild pressure and temperature conditions. More precise test data and knowledge of the behavior of such gaskets can improve this situation but modification of gasket factors would have relatively little effect on the design of flanges for the more severe services.

While the Code Committee will be found quite receptive to proposals for changes substantiated by good theory and test data, such proposals will be closely scrutinized from the practical angle. The writers' present reaction to some of the proposals made in this paper is to doubt their practicability.

In deriving Equation [12], the author predicts an increase in bolt stress and draws some qualitative observations. To our knowledge no increase in bolt stress has ever been observed with gaskets located inside the bolts, even with very soft gaskets. On the contrary, the bolt stress has been observed to reduce as internal pressure is applied both with solid metal and soft gaskets until the gasket precompression is lost and leakage begins, after which the bolt stress begins to rise again if higher internal pressure can be applied. This effect is due to rotation of the ring flanges under the applied moments and far outweighs the effect formulated by the author which was based on the assumption of rigid flanges. In recent tests of light plate flanges using cloth-inserted rubber gaskets under simple hydrostatic test, the initial bolt stress was observed to fall off as much as 25 per cent as internal pressure was applied before leakage was experienced. Any precise treatment of bolt and gasket stress relations with changing pressure would have to include the effect of flange rotation, whereas the effect cited by the author would be negligible for most services. It would also have to include the effect of temperature differentials between bolts, flanges, and gaskets under operating and transient conditions, an impractical problem for general design purposes.

The author includes a proposal for bolt spacing to insure tightness. The refinements of including the effect of boltheads in distributing the load and for the stiffening effect of the hub certainly cannot be ignored for most applications and would add to the complexity of the approach. Any such approach would have to be proved by experience also. The Code makes no recommendation on bolt spacing nor on the materials or facing for a given service. Taylor Forge Company, in its manual "Modern Flange Design," recommends an empirical formula for maximum bolt spacing of

$$2d + \frac{6t}{m + 0.5}$$

where

d = bolt diameter
t = flange thickness
m = Code gasket factor

This has been generally used by designers for many years with good results.

In discussing Code m-values, the author states the Code uses one half the gasket area as a design basis. A more complete statement is desirable on this point. The Code establishes an effective gasket seating width for applying the y-factor, and this is varied with the type gasket and facing. In the case of a flat gasket on a smooth facing it is one half the gasket bearing width. In applying the m-factor, however, it is applied to twice this width, which in the case of the same gasket and facing becomes the full width. By working in terms of an effective width, the Code has endeavored to take some account that the gasket may not seal over its full width due to nonuniform bearing stress caused by the gasket or facing detail or flange rotation. The author suggests use of a variable m-factor depending on initial stress with no minimum seating load and with a lower limit of $m = 1$. This would leave no margin for uncertainties and operating variables, and present test data are wholly inadequate to support it to the extent that it could be used in design. Experience and observation of the behavior of flanges in service and on test indicates to us that for all practical purposes there is a minimum initial gasket stress which must be applied before a particular joint will hold any pressure to speak of, but it is subject to variation, and the minimum value undoubtedly cannot be tied down as definitely as the table of Code values might seem to indicate. Looking on code practice as one designed to insure a low m-value is an acceptable viewpoint.

Experience also shows that much more care and attention must be given to surface finish and the manner of making up flanges with metal gaskets, than with soft gaskets, the difficulty increas-

ing with the hardness of the gasket and its tendency to work-harden. A design basis requiring a progressively higher minimum m-factor for such cases is felt to be better than one which goes down to a common minimum of $m = 1$, depending on initial gasket stress.

The use of torque wrenches has been recommended. This undoubtedly represents the best practice, but it is not commonly used, by any means, and apparently has not been found necessary by users except in relatively few instances for severe service, particularly at elevated temperatures. The superiority of such practice in the latter instances has been adequately demonstrated in service, but users are not likely to be receptive to it as general practice.

It is hoped that this paper will spur work to obtain the needed gasket data. Such data will be invaluable for final evaluation of this paper relative to modification of the present Code design basis or the gasket factors or both. Tests on gasketed joints should not be confined to tests in a tensile machine which maintains uniform gasket compression but must include tests with bolted flanges so that the effect of nonuniform gasket stress both radially and circumferentially due to flange rotation and bolt-load concentration may be better evaluated. More accurate design information is also desirable on maximum permissible loading to avoid gasket crushing or marring of contact facing and gasket proportions to avoid blowout.

R. A. Strub.[12] Besides the uneven distribution of gasket stress due to the concentrated bolt load, the deflection of the flanges due to bending stresses also contribute toward an uneven distribution of the gasket stress. As shown by tests[13] this effect may be, in certain cases, sufficiently large to justify a study similar to the one carried out for concentrated bolt loads.

The theory of the paper giving the stress variations in th assembly is based on a relation assuming that the elastic deformation of the bolt is compensated by an equal amount of gasket expansion when the assembly is submitted to the working load $A_i p_i$. This assumption is only an approximation which, in some cases, will lead to erroneous calculations. In so far as the writer is aware, previous works on bolted assemblies by T. J. Dolan,[14] A. Thum, and others are based on relations similar to those, Equations [12] to [14], introduced into the paper. It can, however, be shown that these relations correspond only to an extreme case in which the working load $A_i p_i$ is assumed to have no direct influence on the elastic deformation of the assembly.

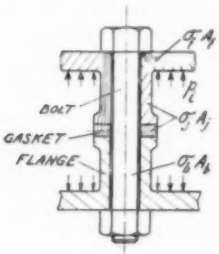

FIG. 4

Referring to the accompanying illustrations, it can be seen at once that in Fig. 6 the stress in the gasket will be relieved by the application of pressure more than in assembly Fig. 4 though the elasticities of the bolt and the joint are the same. The joint is defined here as being the gasket and the zone of the structure transmitting the gasket load to the bolts. As shown in the illustrations, the load due to the pressure itself is also supported by the bolts (flange stress field), and the corresponding stress field is different from the one produced by the gasket load (joint stress field). These two stress fields can never be combined in a single one for the computation.

The variation of the joint length δ when the internal load is applied, must compensate the deformation of the bolt and the deformation of the flanges due to the effect of the working load $A_i p_i$ alone. Therefore we have to consider three elastic characteristics which will be called: the flange characteristic giving the law of deformation at the gasket when the assembly is submitted to internal pressure only, the bolt characteristic, and the joint characteristic.

This general way of studying the load distribution in a bolted assembly leads to a better understanding of the mechanism of deformation and load distribution. The condition of compatibility can be established readily by referring to Fig. 5 represent-

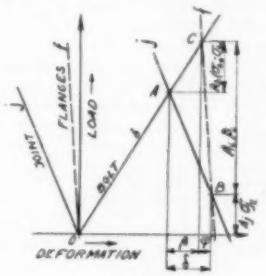

FIG. 5

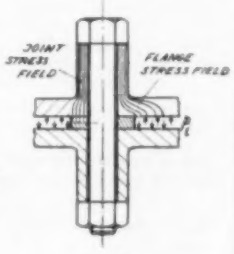

FIG. 6

ing the graphical computation of a bolted joint within the elastic range. The joint deformation δ must be compensated by the bolt deformation β and the flange deformation φ due to the working load alone

$$\delta = \beta + \varphi$$

This relation, together with the equilibrium condition of loads

$$A_b(\sigma_{b(2)} - \sigma_{b(1)}) - A_j(\sigma_{j(2)} - \sigma_{j(1)}) = A_i p_i$$

will lead to the general relations giving the load variation in the bolts

$$(\sigma_{b(2)} - \sigma_{b(1)})A_b = A_i p_i \frac{1 - \dfrac{A_j E_j f}{A_f E_f t}}{1 + \dfrac{A_j E_j l}{A_b E_b t}} \qquad [1]$$

and in the joint

$$(\sigma_{j(1)} - \sigma_{j(2)})A_j = A_i p_i \frac{1 + \dfrac{A_b E_b f}{A_f E_f l}}{1 + \dfrac{\sigma_{j(2)}}{\sigma_{b(1)}} \dfrac{E_b t}{E_j l}} \qquad [2]$$

Relations [12] and [14] of the paper under discussion can be obtained from relations, Equations [1] and [2], herewith, if we assume that the flanges are infinitely rigid $f/(A_f E_f) = 0$, when submitted to the working load $A_i p_i$. In this case the flange characteristic f will be a vertical line. However, if the deflection at the gasket of both flanges and joint are equal, when submitted to unit loads $A_i p_i$ and $A_j \sigma_j$, respectively, the corresponding elastic characteristics symbolized by the factors $f/(A_f E_f)$ and $t/(A_j E_j)$ will be equal, and no variation of stress will take place in the bolt. A pure exchange of load occurs between the joint

[12] E. I. du Pont de Nemours and Company, Inc., Belle Works, W. Va.

[13] "The Influence of Bolt Tension and Eccentric Tensile Loads on the Behavior of a Bolted Joint," by T. J. Dolan and J. H. McSlow, presented to The Society for Experimental Stress Analysis, Detroit, Mich., May 20, 1949.

[14] "Load Relations in Bolted Joints," by T. J. Dolan, *Mechanical Engineering*, vol. 64, 1942, pp. 607–611 and 688.

load $A_f\sigma_f$ and the working load $A_i p_i$. In Fig. 7, herewith, the load $A_f\sigma_{f(2)}$ is the final load in the joint which is almost ready to open whereas in Fig. 5 a much larger working load $A_i p_i$ can still be applied before opening occurs.

If the joint characteristic j is not a linear function of the gasket load, relations (a) and (b) will no longer be linear. These types of relations can, however, be used if the secant modulus E_f is introduced. The graphical representation can still be used after drawing the curve of the experimental law of deformation of the

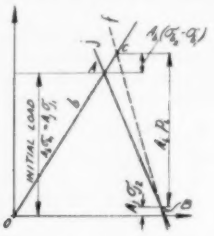

FIG. 7

joint in place of the straight line j. In this case the variation of the joint load after time has been allowed for creeping is

$$(\sigma_{f(1)} - \sigma_{f(2)})A_f = A_i p_i \left(1 + \frac{A_b}{A_f}\frac{E_b f}{E_f l}\right) - \frac{E_b}{l} A_b f(\sigma_{f(1)}; \sigma_{f(2)}; T)$$

the joint deformation $\delta = f(\sigma_{f(1)}; \sigma_{f(2)}; T)$ being a function of the stress range and of the working temperature T.

For superpressure equipment in which sealing is often made by lapped faces, it is important to consider the third characteristic f if good correlation between tests and calculation is expected. It is also important to consider it in the design of bolted assemblies using relatively hard metallic gaskets. However, in cases dealing with lower pressures and soft gaskets the approximate formula may be sufficiently accurate.

F. C. THORN.[18] The author has performed an excellent service in pointing out four fundamental errors in the present ASME Code formulas. These are as follows:

1 The m-value is not a constant but is a function of initial gasket load, flange finish, and probably also gasket width and thickness, temperature, time, and the intrinsic tendency of the gasket to adhere, which may be modified by surface coatings such as graphite.

When the subject is fully explored, it will be found also that the m-value is influenced by the medium being packed. Perhaps technically all fluids are alike in that they penetrate any clearance however small. Practically, the more viscous fluids, such as liquids, take a long time to get through, so that a joint may be called leakless when it is not really leakless as is shown promptly when the same joint is tested with gas. Also, some liquids are self-sealing in that they tend to swell the gasket material as they pass.

2 There is no such thing as a y-value for any gasketing material in the sense that $y/2$ is a constant unit initial load necessary to prevent leakage at all fluid pressures below a fixed minimum. Actually, the transfer from a high m-value to a low m-value takes place over a rather broad band of initial loads.

3 The introduced fluid load does not simply subtract itself from the original gasket load—as assumed in the formulas—neither does it add itself to the bolt load, leaving the gasket load unimpaired. The truth lies in between. The added fluid load is distributed, in part as a subtraction from the gasket load, and in part as an addition to the bolt load, the manner of distribution depending upon the dimensions and elastic constants of the opposing members. In an earlier article[19] the writer called attention to this in the form of a graph (Fig. 8, herewith).

The procedure was to take any point on the gross load line, and plot in opposite directions from this point, the gasket retraction curve, and extension curve of the bolt circle, all to the same scale. The point of intersection C represents the initial equilibrium between gasket and bolts. This equilibrium is disturbed by the introduction of fluid pressure times the inside area of the

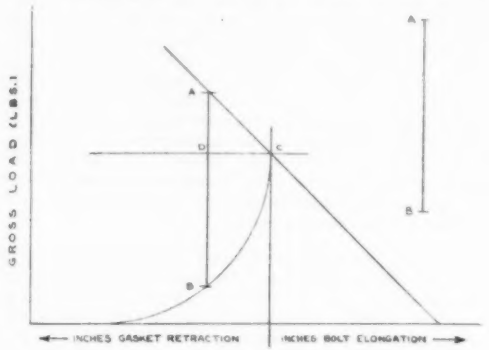

FIG. 8

joint, which is represented by line AB. The new equilibrium is found by tucking line AB into the angle formed by the bolt and gasket curves. The part AD is an addition to the bolt load; the part BD is a subtraction from the gasket load. Referring to Equation [10] of the paper, it will be seen that the first term is line DB; the second term is line AB, and the third term is line AD. This equation is, therefore, the mathematical expression of the graph and of course is much more satisfactory to use providing we know DC as a function of DB; in other words, we know $f(\sigma_g, \sigma)_{\frac{1}{2}g}$. It seems probable that the author's assumption of a straight-line retraction curve down to 50 per cent retraction is a sufficiently good approximation for compressed asbestos sheet, and his more elaborate parabolic formula is not really needed.

4 The fourth error in the formulas to which the author calls attention is the absence of any provision for gasket creep in the interval between bolt tightenings. Most of the packing failures which occur in joints designed in accordance with ASME formulas, occur at gasket loads which are far below either the gasket load called for in the formula or the gasket load actually developed in installation. These low gasket loads are the consequence of creep. We have data in our laboratory indicating declines in gross gasket loads of ordinary $^1/_{16}$-in. compressed-asbestos gaskets between 400 lb ASA flanges of the order of 68 per cent in 20 hr at a temperature corresponding to 350 psi steam. The decline in the residual gasket load, after correcting for fluid relief, is even worse, of the order of 82 per cent. An initial m-value of 2.5 as prescribed by the ASME tables would have been quite inadequate to have prevented a blowout under these conditions. The higher m-value of the ASA joint—about 6.3—was barely sufficient to prevent a blowout at the end of 20 hr operation.

[18] Research Director, The Garlock Packing Company, Palmyra, N. Y. Mem. ASME.

[19] "Gaskets," by F. C. Thorn, *Industrial and Engineering Chemistry*, vol. 28, 1936, pp. 164–174.

In view of the seriousness of gasket creep as a factor in joint design, the writer regrets that the author did not see fit to make provision for it in his formulas. His reason is that no formula exists for computing the creep. This may be true at the present time, but, pending such time as a formula may be developed, the designer would do well to incorporate empirical corrections for creep, based on observations of actual decreases in bolt length with exposure time of similar gaskets mounted in standard steam joints.

D. B. Wesstrom.[17] In this well-conceived and well-written paper the author presents a number of concepts in flanged-joint design that appear for the first time in print. These are concepts that must be understood and appreciated by designers if there is to be any progress in thinking on the subject. Therefore the author is to be congratulated on having made a valuable contribution to the art.

The author brings out the highly significant fact that the decompression modulus of the gasket material, obtained on release of the load, is an important factor in determining the amount of gasket loading that remains after application of the internal pressure. Many gaskets and gasket materials have a certain amount of "slack" that must be taken up in the initial tightening of the bolts, and the elastic property that really counts is that which exists after the slack has been eliminated. It is the "springback" or elastic recovery, therefore, that is important in keeping a gasket tight, and this is the physical property that should receive most attention from gasket manufacturers in their research programs.

In view of this, it is not so apparent why the modulus during initial compression should be used in calculating the permissible spacing of the bolts. The bolt-tightening operation is usually a slow-loading effect, especially for large-diameter joints, and the effective modulus at final pull-up can be expected to be comparable with that existing thereafter. The final "once around" on the bolts also may eliminate a large part of the time effect shown in the author's Fig. 10.

The importance of the time effect obviously depends on the type of gasket material, as well as the time taken to tighten the bolts, which in turn depends on the size of joint, number of bolts, and general procedure in tightening. It is sometimes necessary to retighten joints after a short period of service, and this may be due partly, although not entirely, to relaxation of the gasket that follows too rapid a make-up of the joint.

The time effect also may be important when there are rapid pressure fluctuations. The creep or hysteresis, or call it what you will, of the gasket material should result in a temporary reduction of the gasket force below its expected value when the internal pressure is applied quickly; and, conversely, in a temporary increase above the expected value when the pressure is suddenly decreased, followed by relaxation to the value previously existing at the decreased pressure. This would indicate that a joint that would remain tight with slow application and variation of pressure might not do so if the changes in pressure are very rapid. The time effect should receive further study by gasket manufacturers, as well as designers, in general, as it may have an important bearing on the successful functioning of designs in some services.

There is one essential point in which the type of joint covered by the paper differs from that covered by the rules of the ASME Unfired Pressure Vessel Code, and, therefore, makes the theory developed by the author inadequate for the design of the latter type of joint. The author, it will be noted, takes account of the elasticity of the bolts and the elastic characteristics of the gasket, but neglects the flexibility of the flanges. This is entirely correct for the type of joint shown in Fig. 7 of the paper, where the gasket is centered about the line of the bolts and the flanges cannot be deflected, regardless of how severely the bolts may be tightened. However, this is the type of joint to which the rules in the ASME Code specifically do not apply. The ASME rules apply only to joints having gaskets entirely inside the bolt circle, in which the moment of the bolt force can deflect the flanges toward each other. This is the usual type of bolted-flanged connection, and to cover it adequately, the author's theory should be extended to include the deflection of the flanges.

If this is done, it will be found that in an actual joint the total bolt load is not constant but varies with the internal pressure in such a way that changes in the bolt load are proportional to the pressure. In many cases, the bolt load will decrease appreciably as the internal pressure increases so that even less gasket force will be available than otherwise might be expected.

One such case was clearly demonstrated in tests made on heat-exchanger joints and reported by Rossheim, Gebhardt, and Oliver.[18] From the actual strain measurements shown in Fig. 7 of that paper, it can be determined that the reduction in bolt stress upon applying 650 psi hydrostatic pressure amounted to about 12,000 psi. Mathematical analysis will show that this is exactly what should be expected and, in fact, will check the actual results with reasonable accuracy. Assuming a design pressure of one half the test pressure, the initial bolt stress in this case had to be at least 2.75 times the stress assumed under the Code rules, for the joint to be tight at test pressure.

The author's reference in his suggested design procedure to "the allowable working stress of the bolts" and "the design stress" seems to overlook the important consideration that the initial bolt stress upon tightening must be sufficient to provide a tight joint, not at the design pressure, but at the hydrostatic test pressure of $1^1/_2$ or 2 times the design pressure, according to the appropriate Code rule for testing. Among the elements that make up a pressure vessel, the bolted-flanged joint is unique in that it is a prestressed structure in which high stress is deliberately generated and exists before any internal pressure is applied. The point at which m-values as low as unity might be tolerated, therefore, is at the test pressure. At the design pressure, the bolt load is somewhere between the initial load and the load at test pressure, with the result that the actual gasket force at the design pressure may represent an m-value of many times unity.

Unless the elastic action of the flanges is included in the analysis and unless the necessity of tightness in the hydrostatic test is taken into account, joints designed by the author's procedure might be inadequate, especially if a low value of m, approaching unity, is used. The actual initial bolt stress required might be 2 or more times the design stress on which the Code calculation is based. Two recent experiences in the writer's knowledge attest to this. In one case it was impossible to obtain a tight joint at the test pressure until a softer gasket was substituted. Analysis showed that the initial bolt stress required for the harder gasket was greater than could be developed by the usual means in bolts as large as were used ($3^1/_4$ in. diam). In another case, the joint was tight at test but leaked at the operating pressure. This was believed to be due to differential expansion between the flanges and the bolts that overstressed the flange and caused it to yield and thereby relax the force on the gasket. Both of the designs men-

[17] Design Division, Engineering Department, E. I. du Pont de Nemours & Company, Wilmington, Del. Mem. ASME, and Past-Chairman, ASME Boiler Code Subcommittee on Bolted-Flanged Connections.

[18] "Tests of Heat-Exchanger Flanges," by D. B. Rossheim, E. H. Gebhardt, and H. G. Oliver, Trans. ASME, vol. 60, 1938, pp. 305–314.

tioned were large-diameter joints for moderately high pressure and met all the requirements given in the ASME Code.

It would be rather premature, therefore, to adopt the author's suggested design procedure before the subject has been developed further, and other factors as just described are taken into account. The author's paper, however, is a very necessary first step leading to the ultimate development of a satisfactory theory. For the time being, the rules of the ASME Code should be followed, as tending to lead to more trouble-free designs. The writer looks upon the m-factors given in the Code as weighted constants that compensate in most cases for the changes in bolt load and gasket force which take place between the design pressure and the test pressure.

The author's equations, which do not include the flexibility of the flanges, should be correct for an experimental setup for determining gasket properties, such as shown in his Fig. 7, or any similar arrangement using a testing machine, provided the applied forces are not affected by deflection of the parts.

The values of m derived from the British and German tests seem to present some anomalies. However, the lower m-values for the wider gaskets can be interpreted by saying that statistically there is less probability of a complete leakage channel with a wider gasket. It should be pointed out, also, that the effective width for the arrangement in Fig. 7 is probably the shortest distance from the inside edge of the gasket to the bolthole.

The writer considers it significant that the effect of gasket width becomes less important with higher initial gasket stress. This is most clearly indicated in Fig. 1 of the paper, where, if the initial stress is high enough, a value of unity for m can be used regardless of width. Although the data indicate that there may be no unique value of initial stress which can be called a "yield value," it does appear that if the initial stress is made high enough, the gasket width can be neglected as a complicating factor in the choice of initial stress. Where the data indicate that the gasket width is a factor, it suggests that the initial stress is not high enough to seat the gasket properly.

The term yield value is not a happy one and the latest revision of the rules has changed it to "design seating stress." Since the actual initial bolt stress must be on the order of 2 times the design stress, in order to pass the hydrostatic test, the actual seating stress will be on the order of 2 times the values given in the Code. These doubled values, therefore, should be the real measure of what is actually required to make the gasket seat itself properly.

The author's theory for maximum permissible bolt spacing and his experience data on actual designs apparently have to do with the arrangement of his Fig. 7 where the gasket width is centered about the line of bolts. If so, it would not necessarily be applicable to the type of joint covered by the Code rules. This is not only because the bolt force depends on the flexibility of the flanges, but also because the flange deflection tends to pinch the gasket at its outer edge.

With regard to the actual examples cited by the author, there is a question whether tightness could not have been obtained by further loading of the bolts. In other words, would a value of q/q_0 less than 0.95 be suitable if q_0 were great enough to provide an adequate value of q? This should be possible if alloy-steel bolts are used instead of carbon-steel bolts, provided the yield strength of the flange is not exceeded. The author's theory seems to be based only on deflection, without any check of the stresses that may exist.

It is the writer's opinion that further development of the theories presented by the author is needed, and that the paper is a welcome and timely contribution toward reaching the ultimate answers.

Author's Closure

The author is gratified by the volume of discussion which has followed this paper, and believes that this reflects the general desire to establish the design of bolted joints on a rational basis.

Mr. Markl, in his discussion, has attempted to find some justification for the Code concept of "yield value" or "design seating stress" on the basis of the data in the Siebel, Hering, and Raible paper. If this concept were correct, there would be found, for a given gasket material, a unique value of gasket stress which would seal a wide range of pressures, and below which no sealing would occur. In Fig. 1 of the discussion Mr. Markl finds such a constant gasket stress value for the narrowest of three copper gaskets, while the two wider gaskets do not give this effect. A similar constant stress value is shown in Fig. 2 of the discussion for a lead gasket, but this is the widest of three lead gaskets studied by the German authors, and the other two do not show a constant value. Finally, none of the other five gasket materials studied in the German paper yields a curve which can reasonably be interpreted to show a constant stress value for any of the gasket widths. It seems likely, then, that the two examples of apparent constancy in the curves found by Mr. Markl are explained by the large amount of scatter in the data. Even if a yield value does exist for the cases quoted, the effect is apparently the exception rather than the rule, and cannot reasonably be used as a general basis of design.

Mr. Markl also argues that the conclusion of the paper that wider gaskets should give lower m values is contradicted by the fact that the curves for the 10 and 20-mm width gaskets fall to the right of the 5 mm curve in Fig. 1 of the discussion. This figure plots the gasket stress at the point of leakage only, and gives no indication of the *initial* gasket stress to which each gasket was subjected. In actual fact, the 10-mm and 20-mm gaskets had lower initial stresses than did the 5-mm gasket, which is probably the major reason for their poorer sealing properties. As may be seen from Fig. 7 of the paper, at the same value of initial stress, the wider gaskets show as good sealing properties as the 5-mm gasket. It may be concluded that plots such as Figs. 1 and 2 of the discussion do not adequately represent the data since they do not show the effect of initial gasket stress, and it is for this reason that the author prefers to plot the data as in Figs. 1 through 7 of this paper.

Mr. Nolan and other discussers bring up the question of thermal shock as a complicating factor. It is known that the design of simple bolted joints to take up the amount of thermal shock mentioned by Mr. Nolan requires the introduction of so much elastic effect as to make the joints impractical. A more promising approach is the development of other types of closures which do not depend upon the elastic properties of bolts for tightness. The author knows of one program for the development of such closures which is in progress.

Messrs. Rossheim and Murphy, and Mr. Wesstrom emphasize the complicating effect of the rotation of the flanges when the gasket is located inside the bolts. Such rotation is usually a factor in high-pressure joints of small diameter, in which the stiffness of the vessel walls adjacent to the flanges restricts the flange rotation to a reasonable value. For such joints, advantage can be taken of the increased flange stiffness to make use of small-gasket widths in order to decrease bolt load and weight of flanges. There is, however, a large class of bolted joints for which the stiffening effect of the vessel wall is minor. This includes large rectangular joints such as in gas-turbine power plants, and large-diameter circular joints such as in low-pressure process vessels. For such joints, unless additional flange stiffening is provided, the use of a gasket inside the line of the bolts results in such severe rotation that it is impossible to achieve tightness. Therefore in this class

of joints, it is common practice to prevent rotation by the use of a full-face gasket or equivalent means, such as two narrow gaskets one inside and one outside the line of the bolts. For these joints, and others in which the gasket is centered around the line of the bolts, the treatment given in the paper should be adequate. It will also apply to joints in which the flange rotation is a negligible factor because of the stiffness of the closure.

For joints in which flange rotation is important, its effect on the gasket and bolt stresses must, of course, be included in the design procedure. The effect may be large or small, depending primarily upon the diameter of the joint, the thickness of the vessel wall, the thickness of the flanges, the elastic modulus of the gasket and flange material, and the operating pressure. It is to be hoped that a theory will be developed for flange rotation, so that the gasket loading in such joints may be computed for at least the standard pipe flanges with the more common gasket materials. Mr. Wesstrom mentions that he has calculated with reasonable accuracy the rotation effects for one group of tests; the publication of the method used, even if it gives only approximate results, would be of interest.

Mr. Strub, in his discussion, has extended the theory of gasket and bolt loading given in the paper to include the elasticity of the flanges. The theory does not consider flange rotation, but it does take in two effects, namely, the elastic follow-up of the flanges with stretching of the bolts, and the elastic compression of the flanges under internal pressure. As pointed out by Mr. Strub, these corrections will be important in cases in which the flanges are highly stressed, as in superpressure equipment using hard metallic gaskets or using lapped faces for sealing.

The author is in complete agreement with Mr. Wesstrom's comment on design for the hydrostatic-test pressure rather than for the operating pressure. The author did not make this differentiation in the paper, and welcomes Mr. Wesstrom's clear statement on this point. In answer to Mr. Wesstrom's question regarding further tightening of the bolts in the examples cited in the paper, no amount of further tightening would seal the joints. In some cases, the provision of alloy-steel bolts might have sealed the joints by increasing q_0 to the point that an adequate value of q were obtained. However, in most cases, the gaskets were so severely crushed or hardened in the region beneath the bolts as to make them useless as elastic sealing members.

The author is pleased to take this opportunity to state that, under the auspices of the Subgroup on Gaskets of the ASME Boiler Code Special Committee on Rules for Bolted Flange Connections, a limited experimental program for the measurement of m values, gasket modulus, and gasket creep is already under way. It is realized that a considerable amount of work, both theoretical and experimental, remains to be done in this field, and the suggestions made by all the discussers are greatly appreciated.

Some Experiments on the Interaction of Shock Waves With Boundary Layers on a Flat Plate[1]

LESTER LEES.[2] Although one can disagree sharply with certain conclusions stated in this paper, the authors are to be commended for their approach to the experimental investigation of the boundary layer - shock wave interaction problem. They have attempted to eliminate as many extraneous variables as possible in order to deal with fundamental problems, such as the shock-wave reflection from a plane surface, where some theoretical results are also available.

The writer cannot agree with the statement, "the effect of the boundary-layer regime noted here, and the other effects found by previous investigators, may be in part illusory." It seems that the experimental results here presented, and others, show quite clearly that the difference in behavior between the laminar and turbulent boundary layers can be traced essentially to the different response of these two flows to pressure increases in the flow direction. In the case of the laminar boundary layer, the effect is felt far upstream, of the order of 100–150 boundary-layer displacement thicknesses from the point of incidence of the oblique shock. For the turbulent boundary layer, it is known that a much larger pressure gradient is required to cause a given rate of thickening, and the shock-wave interaction effects do not spread upstream nearly as far as for the laminar layer.

One important fact that is revealed by the present experiments is the difference in boundary-layer behavior for strong and weak incident shocks, particularly in the case of the laminar boundary layer. For the weak incident shock, the boundary layer appears to separate upstream as predicted theoretically, but the flow downstream appears to remain laminar. The incident shock is reflected as an expansion, followed by rapid compression as described by the authors. In the case of the strong incident shock, however, separation occurs so far upstream that the laminar "jet" becomes turbulent, and a very rapid thickening of the "boundary layer" occurs in the immediate vicinity of the incident shock. With such thick viscous regions, the incident shock is apparently refracted through the viscous layer and reflected, followed by an expansion region, and then a gradual compression as the flow turns parallel to the wall again. In the case of a strong shock, then, one might expect a rapid pressure rise followed by pressure drop on the wall in the immediate vicinity of the point of incidence of the shock. This phenomenon might also occur for weak shocks but would be confined to a very narrow region. This fact might account for the result found by Liepmann, Ackeret, and others, that the pressure distribution on an airfoil in transonic flow with shock wave in the flow is "smooth" for a laminar boundary layer.

It will be interesting to see whether the approximations for upstream influence found in Princeton University Aeronautical Engineering Laboratory Report No. 143 are borne out by these measurements. It seems clear that any theoretical approach based on the older Prandtl boundary-layer theory might be successful in predicting the extent of upstream influence of the incident shock, but could not describe the phenomena in the immediate vicinity of the incident shock where there must be very large pressure and density gradients normal to the flow.

H. W. LIEPMANN[3] AND S. DHAWAN.[3] The authors' work represents a worth-while attempt to extend the investigations of the interaction of shock waves and boundary layer to higher Mach numbers. The investigation is of specific interest to the writers since research on the interaction problem in transonic and supersonic flow has been pursued for some time at the California Institute of Technology.[4] In particular, measurements of the reflection of shock waves from boundary layers at Mach numbers of about $M = 1.3$ to 1.4 made at the Institute are closely related to the

[1] By F. W. Barry, A. H. Shapiro, and E. P. Neumann, published in the June, 1950, issue of the JOURNAL OF APPLIED MECHANICS, Trans. ASME, vol. 72, pp. 126–131.

[2] Aero Engineering Laboratory, Princeton, N. J.

[3] California Institute of Technology, Pasadena, Calif.

[4] "Experiments in Transonic Flow," by H. W. Liepmann, H. Ashkenas, and J. D. Cole, USAF Technical Report No. 5667, February, 1948.

"On the Reflection of Shock Waves From Boundary Layers," by H. W. Liepmann, A. Roshko, and S. Dhawan, NACA Contract NAw5631, July, 1949. In press.

work of the authors at higher Mach numbers, and the results can be compared.

1 In investigating the reflection characteristics of shock waves from boundary layers we have found that the case of a shock wave of a "step type" must be distinguished from that of an "impulse-type" wave. The pressure in the former, the ordinary type, rises from one constant level to another higher level. In the impulse-type wave the initial compression is followed immediately by a rapid expansion. The reflection patterns in these two cases differ. For example, we believe that the shock wave in Fig. 8 of the paper is definitely of the impulse type; the shock waves in Figs. 3 to 7 are probably step waves, but the expansion zone from the shoulder of the wedge which produces the shock waves does not appear to be far enough downstream to leave the reflection pattern completely unaffected. It seems to us that for quantitative data more clearly defined experimental conditions are needed.

2 The velocity profile in the boundary layer at the point of impingement is clearly of importance. This statement in itself is too broad and insufficient to lead to any definite conclusions. More important appears the question whether or not the reflection phenomenon is essentially nonlinear, i.e., the extent to which the shock itself influences the boundary-layer velocity profile ahead of it and vice versa. The degree of influence of the shock upon the development of the boundary layer differs for laminar and turbulent layers, and the reflection patterns in these two cases differ accordingly.

3 We agree with the authors that parameters such as surface curvature, origin of the shock wave, etc., are important. But we are actually more impressed with the general similarity of the results between the early measurements in transonic flow and the recent investigations in supersonic flow, e.g., the reflection characteristics of a shock wave from a laminar boundary layer are strikingly similar to the phenomena observed in transonic flow, etc.

There is no doubt that the limitations imposed by the small tunnel used render the experimental technique more difficult and the results less clear than similar investigations in a larger tunnel. It is greatly hoped, therefore, that the authors' investigations will be continued and if possible carried out in a larger tunnel.

W. A. Loeb.[5] The authors have ably discussed this extremely complicated problem with an eye to both generality and detail. There are, however, a few points that may be worthy of further expansion and emphasis.

In the early work on this subject it was generally concluded that the boundary-layer regime (turbulent or laminar) was of the utmost importance in determining the nature of the shock wave-boundary layer interaction. In disputing such a conclusion, this paper mentions the results of the injection of a high-speed air stream into a thick turbulent boundary layer in order to alter the velocity profile of the boundary layer. This experiment was carried out in much the same manner as those described in the present paper. By increasing the injected air flow it was at times possible to alter the character of the reflected shock from the original no injection configuration, to no apparent reflection, and, thence to an entirely new configuration. This indicates that the turbulence of the boundary layer does not, of itself, determine the shock wave-boundary layer interaction, and that the boundary-layer velocity profile may play a large part in this complicated relationship.

The manner of shock generation is another variable mentioned. In this paper and in the work discussed previously the incident shock was generated by turning the stream toward the wall on which the interaction was observed. Had the shock been generated by some other method, the observed interaction might have been altered considerably. This seems logical since the configuration is determined not only by pressure, inertia, and viscosity requirements, but by directional bounding conditions imposed by the solid wall.

In the injection work mentioned, the wedge used to generate the initial shock slanted back to the passage wall some distance downstream. Thus an oblique compression shock was generated at this point by turning the air stream into a direction parallel to the passage walls. The observed boundary-layer interaction differed considerably from that observed in the case of the primary upstream shock even when this primary shock was moved downstream to a corresponding position in the passage. This may be due of course to the many upstream disturbances preceding this second compression shock, but the possible effect of the method of shock generation cannot be ignored.

This paper points up the generally increasing interest in boundary-layer effects. Today, as we move toward higher-performance aerodynamic machinery, the necessity for such knowledge is becoming more and more evident. Soon the designer of such machinery must seek to incorporate in his designs the newer advances in boundary-layer knowledge. Further extensions of such knowledge are to be heartily welcomed and applauded.

[5] De Laval Steam Turbine Company, Trenton, N. J.

Authors' Closure

The authors wish to thank the reviewers, all of whom have made original contributions to this problem, for their interesting and relevant discussions.

It is clear from the disagreement in interpretation of some of the measurements that there are still many unsolved questions relating to the complex problem of the interaction between shock waves and boundary layers.

The authors have completed a further investigation in an 8 × 8-in. tunnel, incorporating considerable quantitative data, which sheds additional light on these questions, and which is soon to be published.

Longitudinal and Torsional Impact in a Uniform Bar With a Rigid Body at One End[1]

E. H. Lee.[2] It may be of interest to mention the application of the Laplace transform to this type of problem, since it can be used to give expressions for stress and velocity for all values of the time in terms of the Heaviside step function. This automatically contains the results of the recurrence formulas, which are in this case obtained from the single expression for the associated Laplace transform. Expansion by the binomial theorem in powers of e^{-p} gives the successively reflected wave fronts, the delay in their appearance in the equation being determined by the step-function multiplier. This method is described by Carslaw and Jaeger.[3] The writer has found it to be a most convenient way of dealing with successive reflections in both the types of problems dealt with, namely, "striking" and "force" impact.

Alexander Yorgiadis.[4] The author has applied the mathe-

[1] By A. H. Burr, published in the June, 1950, issue of the Journal of Applied Mechanics, Trans. ASME, vol. 72, pp. 209–217.

[2] Associate Professor of Applied Mathematics, Brown University, Providence, R. I. Mem. ASME.

[3] "Operational Methods in Applied Mathematics," by Carlsaw and Jaeger, Oxford 1941.

[4] Chief Engineer, Sonntag Scientific Corporation, Greenwich, Conn. Mem. ASME.

matical method of analysis to the solution of the problem of elastic impact in a certain linear mechanical system. The results, summarized in dimensionless charts in Figs. 5, 6, and 7 of the paper, form a valuable addition to the data in this field of mechanics.

While this mathematical analysis is exact and rigorous, it can be time-consuming, difficult, and often beyond the ability of the practicing engineer who is confronted with these problems. During the last two decades, graphical methods were developed which are relatively simpler, and enable better visualization of the phenomena involved. The general derivation of the graphical analysis as applied to impact in elastic bars, was presented by DeJuhasz[5] in one of his many publications on graphical methods.[6]

In the discussion to follow, the graphical method will be applied to obtain results similar to those in Figs. 3 and 4 of the paper.

The author's mathematical analysis considers finite elasticity and finite velocity of stress propagation in the bar, but assumes infinite rigidity and infinite velocity of propagation of stress waves in masses W and W'. The graphical method considers finite velocity of propagation in all members, the bar, as well as masses W and W'. When the time interval for the traversal of the stress waves in one member of the system is considerably smaller than the time needed for traversal of another member, the smaller time intervals can be "lumped," thereby simplifying the problem without substantial loss in accuracy.[7] In this particular case, the time interval for traversal of W (also W') was taken as $^1/_5$ of that needed for the traversal of the bar. If all three members are of the same material, the velocity of wave propagation c is the same for all three; weights W and W' have the same length ($^1/_5$ the length of the bar), and their areas are 20 times and 200 times, respectively, as large as the bar. These values correspond to a bar ratio of 4, and body ratio of 10 as in the main paper.

The graphical analysis is carried by the aid of two diagrams as follows:

1 *The time location or t-x diagram*, Fig. 1 herewith, in which a point denotes a certain cross section x and a certain instant of time t. In this diagram, the progress of the stress waves are represented by straight lines having the slope

$$\frac{\Delta x}{\Delta t} = \pm C = \tan (\pm \phi)$$

These lines divide the diagram in areas marked 1, 2, 3, . . . 1′, 2′ 3′ . . . . . .

2 *The velocity-force diagram* in which a point denotes the velocity and force existing at x and t in similarly numbered regions. The force and velocity changes due to a stress wave are always proportional

$$\frac{\text{Change of force}}{\text{Change of velocity}} = \pm \frac{AE}{c} = \tan (\pm \theta)$$

Using subscripts 1 for the bar, 2 for mass W, and 3 for mass W', then, since E and c are material constants for all three members

$$\tan \theta_1 : \tan \theta_2 : \tan \theta_3 = 1 : 20 : 200$$

Values in the velocity-force diagram were plotted in terms of velocity ratios V, V' and dimensionless total stresses R, R' in order to conform to the author's notation. The "velocities" and "stresses" to be mentioned, refer to V, V' and R, R', respectively. The unit of time in the t-x diagram is the value T, the time required for the stress wave to travel twice the length of the bar.

Initially the bar and weight W are at rest under zero stress so that their state is defined by point 0 on the velocity-stress diagram in Fig. 2 of this discussion. At the instant of impact, both the velocity and stress in the bar increase from that point, along a line making an angle of plus θ_1 with the V-axis. Initially, weight W' has a velocity $V' = 1$ and stress $R' = 0$, so that its state is represented by point 0′ in Fig. 2. Upon impact, its velocity is decreased in proportion to the impacting stress. The new values are represented by a point on the line starting from 0′ making an angle of minus θ_3 on the velocity-stress diagram (for convenience such a line is called the minus θ_3-line). Point 1′, the point of intersection of these two lines therefore defines the force and velocity immediately after impact.

The disturbance thus produced travels in both directions and with velocity c, as shown in the t-x diagram in Fig. 1. New disturbances are created every time the waves reach an end or junction of the three members. When the wave defined by point 1′ reaches the free end of W', the stress becomes zero, causing a reduction of velocity along the plus θ_3-line. Upon reflection back to the impact point, the force and velocity change along the minus θ_3-line to point 2′.

In the meantime stress wave 1′ is transmitted to the other end of the bar ($x = 0$), and reaches weight W which is still at rest, under zero stress. The changes in W and in the bar take place along the plus θ_2 and minus θ_1-lines, respectively, so that the resulting conditions are shown by point 3. This wave is transmitted to the free end of W where it is changed along the minus θ_2-line and reflected back along the plus θ_2-line at zero stress so as to meet the minus θ_1-line from point 2 at point 4. The wave from region 3, reflected back through the bar, meets the reverberations of the wave in mass W' at 6′ causing a substantial increase in the stress at that point.

Successive points 7′, 8′, 9′, and so on, are obtained in a similar manner, each point defining the velocity and stress in similarly numbered t-x zones in the t-x diagram.

The values thus obtained were used to plot the velocity-time and stress-time diagrams in Figs. 3 and 4. The former represents the conditions at the striking end, $x = l$, while the latter shows the conditions at the other end of the bar, ($x = 0$). These diagrams are in the form of steps, due to consideration of the finite velocity of propagation of the stress waves in masses W and W'. The duration of a given step is equal to the period for propagation of a wave through W (or W') and return. Using a smaller such interval in this analysis would result in smaller steps, and when this interval approaches zero as a limit, the resulting step diagram becomes a gradual curve such as those in Figs. 3 and 4 of the main paper. Another method of obtaining these curves is by joining the middle points of the stepped diagrams for any given T-interval, as shown by the curves in Figs. 3 and 4 herewith. These are for all practical purposes, identical with those in Figs. 3 and 4 of the paper.

Fig. 5 of this discussion is a plot of the stress and velocity at $t/T = 1.5$. Point a on the velocity-stress diagram was obtained at the intersection of lines 7–10′ and 6–8′ since a is at the intersection of these two zones in the t-x diagram. Point b was determined at the intersection of 6–9′ and 7′–9. The stress and velocity at any other instant and location can be determined in a similar manner.

[5] "Graphical Analysis of Impact of Elastic Bars," by K. J. DeJuhasz, JOURNAL OF APPLIED MECHANICS, Trans. ASME, vol. 64, 1942, p. A-122.

[6] "Graphical Analysis of Transient Phenomena in Linear Flow," by K. J. DeJuhasz, Journal of The Franklin Institute, vol. 223, April, 1937, pp. 463–493; May, 1937, pp. 643–654; June, 1937, pp. 751–778.
"Graphical Analysis of Vibrations in Mechanical Springs," by K. J. DeJuhasz, Journal of The Franklin Institute, vol. 226, October, 1938, pp. 505–526; November, 1938, pp. 631–644.

[7] "Graphical Analysis of Free Vibrations in Helical Springs," by K. J. DeJuhasz, Journal of The Franklin Institute, vol. 227, May, 1939, pp. 647–672, Appendix III of this report analyzes the effect of assuming finite time intervals when these are infinitely small.

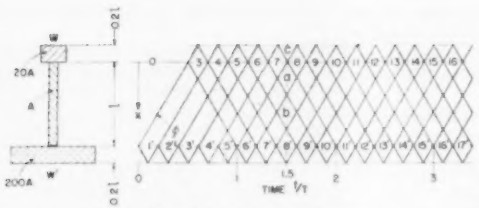

FIG. 1 TIME-LOCATION OR t-x DIAGRAM

(Unit of time T is $\frac{2l}{c}$. Lines of slope tan ($\pm \phi$) = $\pm c$, divide plane in various zones.)

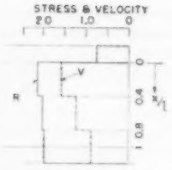

FIG. 5 VARIATION OF DIMENSIONLESS TOTAL STRESS R AND VELOCITY V ALONG BAR AND WEIGHTS W, W' AT INSTANT $t/T = 1.5$

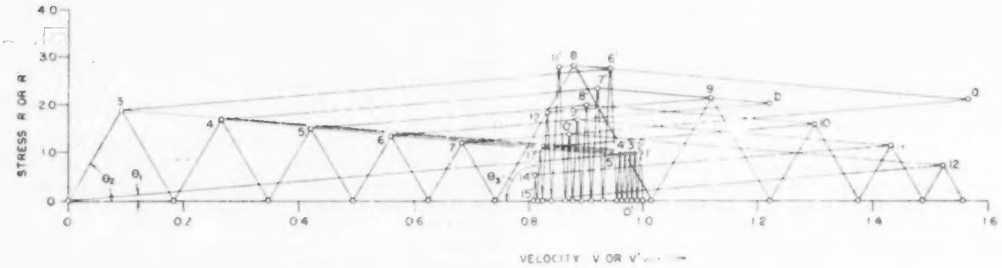

FIG. 2 VELOCITY-FORCE OR VELOCITY-STRESS DIAGRAM

(Co-ordinates of any given point represent velocity and stress correspondingly marked zones in t-x diagram.)

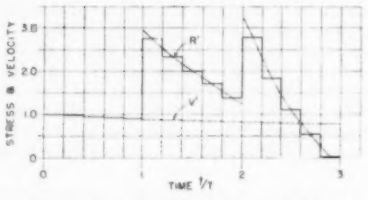

FIG. 3 TIME-VARIATION OF DIMENSIONLESS TOTAL STRESS R', AND VELOCITY V' AT STRIKING END, $x = l$

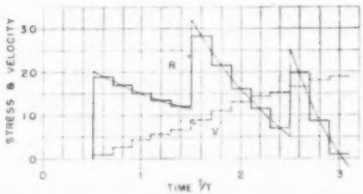

FIG. 4 TIME-VARIATION OF DIMENSIONLESS TOTAL STRESS R AND VELOCITY V AT END $x = 0$

The foregoing discussion is only intended as an indication that impact problems can be solved by graphical as well as by mathematical methods. This in no way reduces the very significant value of this paper.

AUTHOR'S CLOSURE

The author wishes to thank Messrs. Lee and Yorgiadis for the interest and contributions contained in their discussions.

Mr. Lee mentions the applicability of the Laplace transform method to the solution of force-impact and striking-impact problems. The book by Carslaw and Jaeger to which reference is made applies this method to the solution of numerous problems where the boundary conditions are definitely prescribed as a function of time. This is not the case for the striking-impact problem principally treated by the author; hence he would anticipate considerable difficulty in application of the transform method to it.

By the assumption of a certain time for propagation in the bodies W and W', Mr. Yorgiadis has extended DeJuhasz's graphical method to the solution of problems involving finite rigid bodies. This is a valuable addition to the literature of impact. For one example, Mr. Yorgiadis demonstrates that sufficient accuracy is obtained. If the inherent inaccuracies of any graphical construction and of the necessary assumption of time can be avoided, particularly cumulative errors, the graphical method should be considered for an extension of the maximum-stress chart, Fig. 7 of the author's paper, to higher values of bar ratio $1/\alpha$, for which the maximum stress is not reached until the fourth or higher time intervals. This is because with the graphical method the number of construction steps per interval is apparently constant, whereas with the mathematical method, the number of terms in the stress equations and hence the difficulties of solution increase with each succeeding interval. Another interesting application for the graphical method would be for those mechanical systems where an assumption of infinite rigidity for the end bodies would be very much in error.

Because of Mr. Yorgiadis' comments, it seems appropriate to point out that the author developed two methods to decrease the labor in application of the mathematical method. The main paper gives in detail one method, the A-operations useful in determining the stress equations of each interval. The paper mentions the second method, a rearrangement of the stress equations to utilize during computation the duplications of numerical values occurring in the equations of successive intervals. Details are

available elsewhere, in Reference 10 of the paper. Both methods are applicable to impact studies of other mechanical systems.

Whether mathematical or graphical methods are taken as the basis, the author believes that the degree of complexity in the calculation of an impact problem is such that maximum-stress charts should be prepared for design purposes. There should be no difficulty in the use of such charts.

Stresses and Deflections of Cylindrical Bodies in Contact With Application to Contact of Gears and of Locomotive Wheels[1]

E. E. Bisson.[2] The author has developed some interesting ideas, particularly so in the presentation of the tractive stress distribution which he illustrated graphically as well as checks mathematically.

Even though the problem is already complex, one additional complication should be added. It is appreciated that, for the sake of simplicity, the friction coefficient is assumed constant for slipping contact. While this assumption is undoubtedly correct at any one value of slip velocity, the NACA research on friction over a broad range of sliding velocities has shown[3] that the friction coefficient, under both dry and boundary-lubricated conditions, is a function of sliding velocity. The friction coefficient generally shows a downward trend with increase in sliding velocity. In certain applications, the change in friction coefficient may be negligible; as a general case, however, some correction for this variation must be made.

B. S. Cain.[4] The author considers one cylinder rolling on another with tangential traction between them. He shows that the area of contact may include a locked area, in which no relative slipping takes place and that areas of relative slip may occur ahead of and behind the locked area. He remarks that it is not clear what determines physically the location of the locked area with relation to the total area of contact.

It may, in fact, be shown that the locked area must extend to the edge of the area of contact where material is rolling into contact, and that relative slip can only occur after material has passed through the locked area. In the notation of the paper, $c = a - b$ for a driving wheel.

This follows if we examine the requirement that the frictional force due to relative slip must be opposite in direction to the slip itself. The direction of slip may be obtained by considering the rate of change of strain as the material passes through the contact area. From Equation [91] of the paper

$$\frac{de_{xx}}{dx} = \frac{d^2u}{dx^2} = -\frac{2(1-\sigma)}{G}$$

so that the part due to the tangential traction $\sqrt{a^2 - x^2}$ is negative over the entire contact area. Inspection of Fig. 8 of the paper shows that the part due to the traction $-\sqrt{b^2 - x^2}$, outside its area of application must have the same negative sign. Therefore $(de_{xx})/(dx)$ is negative over the whole of the areas of slip.

Now, referring to Fig. 14(*b*) of the paper, if the material is assumed to pass from right to left through the contact area, the material in the upper half-plane will extend as it passes through the slip areas and, therefore, will slip away from the locked area. Ahead of the locked area this will produce a frictional force opposite in direction to that assumed and this slip area, therefore, cannot exist. As the material leaves the locked area, its direction of slip, away from the area, produces a friction force in the direction assumed and this slip area is, therefore, possible.

Alexander Hammer.[5] While it is appreciated that the surface areas which develop to resist the pressure between cylindrical bodies in contact are due chiefly to elastic deformation of the material, one should not neglect the cushioning effect of the lubricant as a contributing factor. The oil is virtually entrapped on the approaching sides of the gear teeth as they roll and slide into contact, and the lubricating medium, due to the pressure that is developed in it, affects the shape of the area of contact and the induced stresses considerably.

Consequently, the question arises: Is it correct to apply the classical Hertzian theory based on metal-to-metal contact between elastic bodies to problems of contact stresses in lubricated gears, neglecting the effect of the oil wedge developed between the mating teeth?

The author of course is familiar with E. K. Gatcombe's theoretical investigations concerning the pressure between two rotating cylinders which are separated by an oil wedge.[6] In addition, according to the bibliography of the paper, he also wrote an unpublished report about the subject matter.[7]

Therefore it seemed to the writer that it would be of interest to mention the fact that, though Professor Gatcombe did not consider the elastic distortion of the cylinders, and did not attempt to obtain an exact analytical solution, his final results could be transformed, leading to a simple and practical formula to determine the load-carrying capacities of helical gears.

The conventional "*K*-factor," now widely used as a basis for design, K being equal to $(F/D) \times (R + 1/R)$, where F denotes tooth pressure per inch face, D the pitch diameter of the pinion, and R the reduction ratio, can be transformed into K equals const $\times \sqrt[3]{\frac{R+1}{R}}\, n$, where n is the pinion speed.

If we assume a reasonable temperature in the wedge, i.e., 150 F for a light oil or 200 F for a heavy one, for a pressure within the wedge not exceeding the surface compressive stress of the materials used, the constant in the foregoing equation remains the same. This would indicate that the load-carrying capacity of the oil wedge of the light oil at 150 F is about the same as that of the heavy oil at 200 F.

This could be expected, since we know that the difference in temperature between that of the entering oil and that of the oil wedge between the teeth is considered as indicative of the amount of work done within the oil film during the period of tooth contact. This temperature difference is considered proportional or nearly proportional to the resistance of the oil film, as the internal work done in the film can be dissipated only by heating the oil to its final temperature. Considering the same loading as the basis of comparison, the temperature differences gradually increase for the

[1] By H. Poritsky, published in the June, 1950, issue of the Journal of Applied Mechanics, Trans. ASME, vol. 72, pp. 191–201.

[2] Technical Staff, Lewis Flight Propulsion Laboratory, National Advisory Committee for Aeronautics, Cleveland, Ohio.

[3] "Friction at High Sliding Velocities," by R. L. Johnson, M. A. Swikert, and E. E. Bisson, NACA TN 1442, 1947.

[4] Assistant Engineer, Locomotive Engineering Division, Locomotive & Car Equipment Divisions, General Electric Company, Erie, Pa. Fellow ASME.

[5] Analytical Engineer, Gas Turbine Department, DeLaval Steam Turbine Company, Trenton, N. J. Mem. ASME.

[6] "Lubrication Characteristics of Involute Spur Gears," by E. K. Gatcombe, Trans. ASME, vol. 67, 1945, pp. 177–185.

[7] "Lubrication of Gears," by H. Poritsky unpublished General Electric Company report.

oils with increasing viscosities; hence the assumption of a higher temperature for the heavier oil seems reasonable.

Further analysis of the results shows that, for the same pressure in the wedge, a high-speed gear has a distinctly higher permissible K-factor than a low-speed gear. This would indicate that, for instance, in the case of a double-reduction gear, the first reduction can be designed for a substantially higher K-factor than the second reduction, permitting an increase of the transmitted horsepower or a decrease of the face width, thus, in the latter case, achieving a decrease in cutting time and manufacturing cost.

Furthermore, experience has shown that wear and pitting are more prevalent in the second reduction gears than in the first reduction when designed to approximately the same K-values, and the tendency has been, purely on an empirical basis, to allow higher K-factors in the high-speed element of a gear train. The modified stress figures differ substantially from the ones which are calculated with the help of the Hertz formula. They are consistently smaller in the high-speed element and larger in the low-speed element.

Pending the accumulation of greater knowledge resulting from service experience and research, one can only make certain assumptions as to the temperature in the oil wedge. Nevertheless, the results obtained at the assumed temperatures do facilitate a quantitative comparison and are apparently in step with our concept of load-carrying capacities.

It would be extremely interesting to know to what conclusions the author came at the end of his investigation of the effect of the oil wedge between the meshing gear teeth. Practical application of the correlated results of similar studies would benefit the art of gear design, in general, and the designer in particular.

H. G. Hopkins.[8] The writer has been working recently on some closely related problems, and feels that a brief summary of this work (which will be published shortly) will interest those who have read the author's paper.

The writer has used complex variables to solve some plane strain, isotropic, static, elastic problems for (*a*) a plane with a single straight cut along which there is zero shear stress and an arbitrarily prescribed distribution (symmetrical about the cut) of either normal stress or displacement, and (*b*) a half-plane with zero shear stress along its straight boundary over a part of which there is an arbitrarily prescribed distribution of normal displacement, with zero shear stresses at infinity. These two-dimensional problems referring to cracks and indentations are more general, and the solutions that have been found are simpler, than those previously published. The solution of these problems is possible through the use of either Airy stress (together with the allied displacement) functions or complex variables.

In the first method, Fourier integral transforms are used, and the basic mathematical problem is to solve single or dual (for mixed boundary conditions) integral equations; however, the final results, although laborious to obtain, are simple and independent of Fourier integrals.

The writer has found that in the second method, hitherto little used in the present connection, the solutions are obtained much more simply. It has been proved that, following a Joukowski transformation, the basic mathematical problem is to solve the plane harmonic equation, subject to different sets of boundary conditions, throughout the interior of the unit circle, which is accomplished through the use of Poisson's integral. There is no doubt that, for the problems considered, the use of complex variables is superior to the use of Airy stress (together with the allied displacement) functions.

[8] The Department of Mathematics, The University of Manchester, Manchester, England.

The foregoing work of the writer has included some discussion of that of Paras (2, 4) and he would like to commend the author for the neat solution of his problems. The writer would like to bring to the attention of the author the fact that the general solution of the plane stress or strain problem has also been given by A. C. Stevenson.[9] The general solutions given by the author and Stevenson are easily verified to be equivalent, but in making the comparison the writer noticed an error in Equation [9] of the present paper, where a factor 2 has been omitted from the left-hand-side, and this necessitates some minor changes in subsequent formulas, e.g., Equation [11] (cf. the result given by M. Sadowsky).[10]

F. K. G. Odqvist.[11] In 1932 the writer, together with G. Lundberg, published an investigation,[12] in which, where starting from Hertz' theory, formulas for the stress distribution in the interior of the solids in contact, accessible for numerical work, were derived in a series of important cases, including the one covered by Fig. 10 in the present paper. We also used, to some extent, methods of the theory of functions of a complex variable.

Somewhat earlier H. Thomas and V. Hoersch had entered upon the same lines of thought, though their publication[13] was unknown to us at the time of our publication. Later, Mr. Lundberg published an important paper,[14] taking up the questions of exact fulfillment of the boundary conditions within the contact surface and general direction of acting forces there. He also treated the contact problem of conical surfaces. As all these papers are closely related to the paper under discussion, though not mentioned in the author's Bibliography, the writer has ventured to mention them here.

Author's Closure

The author wishes to thank the discussers for their interesting and valuable comments, and their references to many published articles which he failed to include in the paper.

Mr. Bisson points out the variability of the friction coefficient μ and its dependence on sliding velocity. Only if the friction coefficient varies over the contact area does this variability of μ add a serious complication to the theory. While $\mu = 0.3$ was used in Fig. 12 of the paper, a similar figure can be plotted for any other value of μ. It is especially in rolling, when the traction-stress distribution varies, say, as in Fig. 14 of the paper, that the variability of μ, if significant, will contribute serious difficulties to the analysis and calculations; however, over the portions outside the inner semicircle, the slip velocity, though variable, is exceedingly small.

The author is indebted to B. S. Cain for the physical reasons which determine for a driving wheel the location of the area of no slipping, or the "locked" area, over the area of contact. Briefly stated, Mr. Cain shows that as rolling proceeds, unless the locked area extends to the forward edge of the contact area, the wheel

[9] "Complex Potentials in Two-Dimensional Elasticity," by A. C. Stevenson, Proceedings of the Royal Society of London, series A, vol. 184, 1945, pp. 129, 218.

[10] "Zwei Dimensionale probleme der Elastizitäte Theorie," by M. Sadowsky, *Zeitschrift für Angewandte Mathematik und Mechanik*, vol. 8, 1928, p. 107.

[11] Professor, Royal Institution of Technology, Stockholm, Sweden.

[12] "Researches Into the Stress Distribution in the Neighborhood of the Contact of Solids With Applications," by F. K. G. Odqvist and G. Lundberg, Proceedings of The Royal Swedish Institute for Engineering Research, vol. 116, 1932, pp. 1–64.

[13] "Stresses Due to the Pressure of One Elastic Solid Upon Another," by H. Thomas and V. Hoersch, University of Illinois, Bulletin No. 212, 1930.

[14] "Elastische Berührung zweier Halbräume," by G. Lundberg, *Forschung auf dem Gebiete des Ingenieurwesens*, vol. 10, 1939, pp. 201–211.

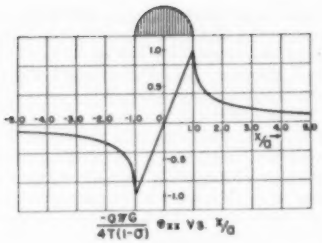

FIG. 15(*a*)

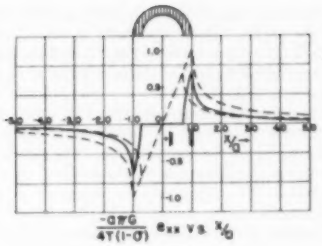

FIG. 15(*b*)

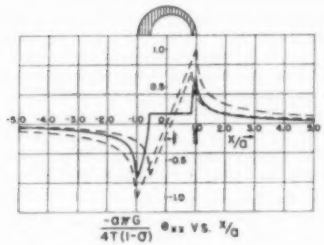

FIG. 15(*c*)

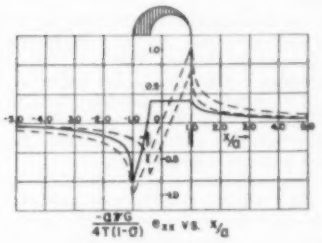

FIG. 15(*d*)

will slip relative to the track over the area between the locked area and the forward edge in the direction of the friction force, rather than in the direction opposite to it. The importance of these considerations warrants a more complete exposition.

The curve in Fig. 8 of the paper shows the normal deflection due to a Hertzian normal load. However, it can be used equally well to describe the tangential displacement due to a similar tangential tractive load, in view of the analogy between normal and tangential tractions and displacements, outlined in Table 1 of the paper. The slope of this curve then becomes a measure of the local strain $e_{xx} = \partial u/\partial x$. This strain is given for $|x| < a$ by Equation [63], and for $|x| > a$ by

$$\left.\begin{aligned} e_{xx} &= \frac{\partial u}{\partial x} = \frac{T(1-\sigma)}{\pi G}\frac{\partial}{\partial \xi}\left[e^{-2\xi} + 2\xi\right]\Big/\frac{\partial x}{\partial \xi} \\ &= \frac{2T(1-\sigma)}{\pi G a}\,[1 - e^{-2\xi}]/\sinh\,\xi \\ &= -\frac{4T(1-\sigma)}{\pi G a}\,e^{-\xi} \end{aligned}\right\} \quad [108]$$

(see Equations [61], [22]).

A plot of the strain is shown in Fig. 15(*a*) of this closure; it is odd in x and consists of a rising linear portion over $|x| < a$, and a falling curve over $x > a$.

In Figs. 15(*b*), (*c*), (*d*) are shown the strains corresponding to the tractive distributions described by Equations [96] and represented, respectively, by Figs. 14(*a*), (*b*), (*c*) for $c = 0$, for $c = b - a$ and for $0 < c < b - a$. In all three cases the strain is constant over the locked area, as indeed it must be, since otherwise slipping will take place as the rolling proceeds.

In Fig. 15(*d*), when the locked area is at the right-hand edge of the contact area, the strain decreases numerically as one proceeds from the locked area to the left-hand edge of the contact area. In Figs. 15(*b*), (*c*), when one proceeds over the contact area away from the locked area, the strain increases numerically to the right, decreases to the left.

Consider now a driving wheel rolling to the right, in the direction of positive x, over a stationary track, and exerting on the track a tractive force in the direction of negative x; the reaction of the track acts on the wheel is in the direction of positive x. When applied to the wheel the ordinates of Figs. 15(*a*) to (*d*), when positive, represent compressions, but, when applied to the track, the ordinates represent similar extensions. Relative to the track the curves in Fig. 15 move to the right, but if a system of axes moving with the wheel center be used, a fixed point of the track or of the wheel will pass through the fixed curves of Figs. 15(*a*), (*b*), (*c*), (*d*) to the left.

Consider a strip of the wheel material, shown shaded in Figs. 15, proceeding to the left over the contact band. In Fig. 15(*b*), the area under the strain curve decreases as the strip is moved to the left. Since the left-hand edge of the strip is in the locked area, slip must occur over the right edge, requiring a displacement or slip of that wheel point toward the right over to the track, that is in the same direction as the friction force; this, however, is physically impossible. The same argument applies to Fig. 15(*c*), but not for Fig. 15(*d*), where slipping can only occur at the left edge of the shaded area, involving a relative displacement to the left. Hence only the case shown in Fig. 15(*d*) can be realized by a rolling wheel.

When there is complete slippage of the contacting cylinders, there is no locked area, the large slipping velocity predominates over the minute slippage just considered, due to variations of e_{xx}, and the tractive force is as shown in Fig. 15(*a*).

If the cylindrical contact is not that of a steady rolling, then the tractive-stress distribution may be of the type shown in Figs. 15(*b*) or (*c*). Thus, if a purely compressive load be applied first, then a tangential load be added, the case shown in Fig. 15(*b*) may obtain. This situation is likely to arise in a photoelastic attempt to check these contact stresses, where steady rolling cannot be realized conveniently.

A photoelastic attempt to check the curves in Fig. 12 of the paper was made by R. D. Mindlin and was displayed during the oral discussion following the presentation of this paper; the

author regrets that it has not been included in the published discussions of the paper. The photoelastic curves of constant p-q differed considerably from those in Fig. 12, and the author is inclined to ascribe the difference to the fact that Fig. 12 pertains to the case shown in Fig. 15(a), while the photoelastic test would probably come closer to the cases shown in Figs. 14(b), (c).

In gear contact away from the pitch point, there is always complete slippage over the contact area. The direction of slipping reverses as contact proceeds from one side of the pitch point to the other side. The direction of the tangential force, and the direction of progress of the contact point relative to either tooth remain unchanged, however, as contact passes through the pitch point. Near the pitch point the cases shown in Figs. 15(b), (c) obtain; away from the pitch point the case of Fig. 15(a), and Fig. 12 applies.

In addition to the tangential displacements due to the shearing forces along the contact area, there are also tangential displacements due to the normal stresses. They have been omitted in the foregoing discussion. The reason is that, unless the elastic constants $G/(1-\sigma)$ for the two cylinders differ, these displacements are of the same sign for the two cylinders, and cause no relative slip; in this respect they differ completely from the tangential displacements due to the shearing forces.

For a steel wheel rolling on a steel rail the elastic constants are the same. For contacting cylinders with materials of different elastic constants, a modified theory applies to the tangential tractive distribution, similar to the one outlined in Equation [84] for the normal forces.

As pointed out by Alexander Hammer, in studying contact phenomena between lubricated gear teeth one must not neglect the cushioning effect of the oil. The treatment of the oil pressure by E. K. Gatcombe, s[illegible] to the author's own unpublished study referred to in the p[illegible], does not take into account the elastic deflection of the contacting bodies. While observed load-carrying ability can be accounted for on this basis, the required approach of the gear teeth often turns out to be far too small, indeed much smaller than the root-mean-square roughness of the surface finish.

It is difficult to justify the use of such close approaches in the equations. Closest approach distances equal to the surface roughness when substituted into the oil-pressure equations which do not include the elastic flattening of the contacting areas, yield load-carrying abilities far below the maximum loads which are actually observed under conditions implying oil-film lubrication.

Preliminary studies carried out by the author and his colleague, Dr. H. Weil, show that the difficulty can be overcome to some extent even by a very rough inclusion of the Hertz deflection. Publication of the results of these and further studies must await their completion and comparison with tests.

Extensive endurance tests of gears at different loads and different speeds have been carried out by D. W. Dudley of the Gear Division of the author's company at Lynn, Mass. To quote from a communication of Mr. Dudley:

"These tests show that for each set there is a certain "critical speed." Below this speed conditions of "boundary lubrication" prevail. The coefficient of friction is high, and there is measurable wear on the tooth surfaces. Above this speed, conditions of film lubrication obtain, the coefficient of friction is low, and there is no wear—provided the oil is clean—and no reduction of tooth thickness. However, pitting may occur if the set is run long enough to exceed the endurance limit of the material on the tooth surface. When the set is operated below the critical speed, pitting may occur prematurely as a secondary result of tooth-surface wear and destruction of the involute profiles.

"These tests to date indicate that Hammer's formula for the "K-factor" would give high-speed sets more advantage than they deserve. For instance, a pinion running at 16,000 rpm would have twice the capacity of a 2000 rpm set according to Hammer. If 2000 rpm was enough to get above the critical speed there would not be a 2 to 1 difference. If 2000 rpm was below the critical speed there could be much more than a 2 to 1 difference in capacity between 2000 and 4000 rpm."

According to Mr. Hammer's equation the allowable load could be doubled each time the speed is increased 8-fold. It would also imply that a high ratio gear could carry about 25 per cent more load than a low ratio. Mr. Dudley finds high-ratio gears to work better than low-ratio gears in some instances, but all in all it is hard to claim that he has any conclusive evidence on that point.

The publication of the results of the basic lubrication and contact analysis must await completion of the tests and comparison of the results of the analytical studies with the test results.

The author is pleased to learn of the results recently obtained by H. G. Hopkins in his study of two-dimensional-stress problems, utilizing conformal transformations and analytic functions. The transformation of a slit plane into a circle mentioned by Dr. Hopkins is closely related to the transformation, Equation [22] of the paper; in fact, by putting $\zeta' = \ln \zeta_1$ one maps the semi-infinite strip of double width 2π in Fig. 7, into a circle. This mapping was not used by the author because the half-plane was the basic region of interest, rather than the complete, but slit, plane.

In the author's opinion the use of the complex variables complements rather than interferes with the use of Airy's stress functions. However, as shown in reference (2), stress problems lead to much more difficult and unfamiliar analytic functions and functional equations than the analytic functions encountered in familiar potential-theory problems.

The author is grateful to Mr. Hopkins for calling attention to the factor 2 which was inadvertently omitted from the left-hand member of Equation [9] of the paper; in the cited reference (2), Equation [2.30], the correct form of the equation is given. As pointed out by Mr. Hopkins, this necessitates proper corrections in some of the subsequent equations; all displacements should be haived.

The author is pleased to learn of the work of F. K. G. Odquist and G. Lundberg. The work by Thomas and Hoersch is, of course, well known in English-speaking countries; it covers contact between general solids, but does not include tangential loading. The latter has been studied for finite, elliptical area contact by Mindlin.[15] Mr. Mindlin studied only the case analogous to that of Fig. 15(b), where the nonslip area is symmetrically situated relative to the contact area. The nonsymmetric orientation of these areas (this is of interest, say, for ball-bearing contacts) still remains to be investigated.

Acceleration of the Instant Center[1]

A. S. Hall.[2] One of the pleasing aspects of kinematics problems, especially velocity and acceleration analyses, is the fact that there are so many ways to "skin the cat." The author has admirably demonstrated one more technique for determining accelerations.

The writer would raise a mild objection to the statement: "The acceleration of the members of a mechanism having a floating link, such as that in Fig. 2, are not obtainable by the method of relative accelerations." A relative acceleration pro-

[15] "Compliance of Elastic Bodies in Contact," by R. D. Mindlin, Trans. ASME, vol. 71, 1949, pp. 259–268.

[1] By W. J. Carter, published in the June, 1950, issue of the Journal of Applied Mechanics, Trans. ASME, vol. 72, pp. 142–144.

[2] School of Mechanical Engineering, Purdue University, Lafayette, Ind.

cedure for handling the same type of problem considered by the author in his first example, is given in a paper by Hall and Ault.[5]

P. G. Jones.[6] The author has presented an interesting analysis of a "floating-link" mechanism by making use of the acceleration of the instant center of zero velocity. However, the statement, "if the motions of link 6 are the given data, an acceleration analysis is impossible by means of relative accelerations alone," would be difficult to justify. It is true that the author's Equation [2] alone is not sufficient to determine the acceleration of point C but a simultaneous solution of three equations consisting of Equation [2], a vector equation relating the accelerations of points C and A, and a vector equation relating the acceleration of points C and B, will enable one to determine the acceleration of C. This method, which has probably occurred to others, is as follows

$$a_c = a_D{}^n + \rightarrow a_D{}^t + \rightarrow a_{CD}{}^n + \rightarrow a_{CD}{}^t$$
$$a_c = a_A{}^n + \rightarrow a_A{}^t + \rightarrow a_{CA}{}^n + \rightarrow a_{CA}{}^t$$
$$a_c = a_B{}^n + \rightarrow a_B{}^t + \rightarrow a_{CB}{}^n + \rightarrow a_{CB}{}^t$$

The magnitudes of the acceleration components may be expressed by making use of the author's analysis for the velocities and assuming

$$\overline{Q_2A} = 1.5 \text{ ft}, \quad \overline{BC} = 1 \text{ ft}, \text{ and } \overline{Q_4B} = 1.75 \text{ ft}$$

(These values were not given in the author's paper)

$$a_D{}^n = 63.3 \text{ fps}^2, \quad a_D{}^t = 75 \text{ fps}^2$$
$$a_{CD}{}^n = 18.3 \text{ fps}^2, \quad a_{CD}{}^t = \overline{CD}\,\alpha_3 = 3\,\alpha_3$$
$$a_A{}^n = \frac{(V_A)^2}{\overline{Q_2A}} = \frac{(6.78)^2}{1.5} = 30.7 \text{ fps}^2$$
$$a_A{}^t = \overline{Q_2A} \times \alpha_2 = 1.5\,\alpha_2$$
$$a_{CA}{}^n = \overline{AC} \times \omega_3{}^2 = 2.5 \times (1.92)^2 = 9.23 \text{ fps}^2$$
$$a_{CA}{}^t = \overline{AC}\,\alpha_3 = 2.5\,\alpha_3$$
$$a_B{}^n = \frac{(V_B)^2}{Q_4B} = \frac{(7.68)^2}{1.75} = 33.7 \text{ fps}^2$$
$$a_B{}^t = Q_4B\,\alpha_4 = 1.75\,\alpha_4$$
$$a_{CB}{}^n = \overline{BC}\,\omega_4{}^2 = 1 \times (1.92)^2 = 3.69 \text{ fps}^2$$
$$a_{CB}{}^t = \overline{BC}\,\alpha_3 = 1 \times \alpha_3$$

Thus there are six unknown quantities in the three vector equations. These are α_2, α_3, α_4, a_c, the magnitude of a_c, and the direction of a_c. If the slopes of the links are given, an algebraic solution may be obtained conveniently by equating the algebraic sum of the horizontal components of each side of the respective equations and by equating the algebraic sum of the vertical components of each side of the respective equations. This will give six algebraic equations which may then be solved simultaneously for the six unknowns. The solution may also be obtained by an acceleration polygon as shown in Fig. 1 of this discussion. This polygon is constructed by laying off all of the vectors except those whose magnitudes are dependent on the unknown angular accelerations. However, the directions of these vectors are known, and further it is known that $a_{CA}{}^t = 2.5\,a_{CB}{}^t$. Thus the problem becomes one of drawing a line parallel to a known direction (perpendicular to link 3) so that its intercept with two nonparallel lines ($a_A{}^t$ and $a_B{}^t$) is divided by a third line ($a_{CD}{}^t$) into segments having a known ratio (2.5). This

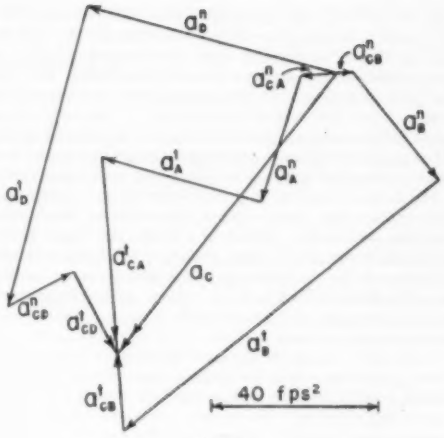

Fig. 1

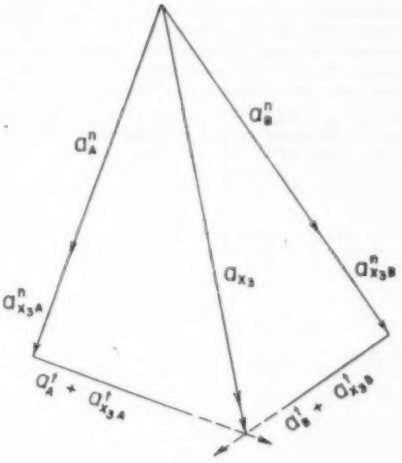

Fig. 2

is a simple problem in geometry for which a graphical solution may be readily made and the details need not be given in this discussion. From the polygon in Fig. 1 the acceleration of C is found to be 86 fps² which is approximately in agreement with the author's answer.

The author has determined a useful expression for the acceleration of the instant center. It may be noted that the acceleration of the instant center X_3, a point on link 3 extended, may also be found from two relative-motion equations by relating the acceleration of X_3 to A and to B. Thus

$$a_{X(3)} = a_A + \rightarrow a_{X(3)A}$$
$$a_{X(3)} = a_B + \rightarrow a_{X(3)B}$$

The acceleration polygon is shown in Fig. 2 herewith, and it is seen that the acceleration of $X_{(3)}$ is independent of the magnitudes of α_2, α_3, and α_4.

[5] "Auxiliary Points Aid Acceleration Analysis," by A. S. Hall and E. S. Ault, *Machine Design*, vol. 15, November, 1943, pp. 120–123 and 234.

[6] Associate Professor in Theoretical and Applied Mechanics, University of Illinois, Urbana, Ill.

L. R. Koenig.[5] In the writer's view, the central point of this paper is important to the science of kinematics, and even more so than would appear from the applications which the author makes of the results at the end of his paper. The essential theoretical point is that the relative linear acceleration of one with respect to the other of the paired body points at the instant center (which the writer prefers to call the rotopole) is independent of the relative angular acceleration of one with respect to the other of the paired links having the rotopole under consideration.

The author's proof of the general equation $a = v\omega$ is rigorous and sound. The writer makes the following observations: The inflection circle is defined as a circle (drawn on the body which has the relative angular velocity ω in question) on which all points are at the inflection points of their paths, as determined by the motion of the body. There can be no acceleration of any such point normal to its path, since each point is at the inflection of curvature of its path.

In the plane of motion, the acceleration vector represented by letter a (consistent with the author's nomenclature) lies on the inflection-circle diameter, being directed toward the opposite end of this diameter. The diameter is normal to the velocity vector v, and, therefore, vector a is also normal to vector v. A second point at the opposite end of the inflection-circle diameter (toward which vector a points) is also an inflection point but moves on a path, the tangent to which (at the second point) is normal to the diameter. Therefore the acceleration vector of this second point must be normal to the diameter, having zero component along it. Hence, assigning d to the diameter of the inflection circle, the condition for a rotation of the inflection-circle diameter in the plane of motion is that $a = \omega^2 d$. Since $\omega^2 d = \omega d \times \omega$, and $\omega d = v$ by simple substitution, the author's result of $a = v\omega$ is confirmed.

The writer has disclosed a direct procedure for determining the angular acceleration of any driven link in any mechanism where the angular velocity and angular acceleration of any driving link is known.[6] A simple procedure can be adduced for determining the center of acceleration of such a driven link when the angular acceleration of the driven link is known (as found by the writer's method), and the linear acceleration of the rotopole of the driven link is known (as found by the author's method). A knowledge of the position of the center of acceleration leads to extremely simple solutions for accelerations of all other points on a link. Publication of this procedure will be given by the writer in a later paper. Since the author's equation is of substantial use in such fundamental considerations, it is for this reason that the writer believes that the author's contribution to our knowledge of accelerations in linkages is of importance to kinematic theory, which should be cultivated if the science of mechanisms is to be kept vitalized.

[5] Member Firm, Haynes and Koenig, St. Louis, Mo.: Associate Professor of Mechanical Engineering, Washington University, St. Louis, Mo. Mem. ASME.

Authors' Closure

The author is willing to admit that he was on unsafe ground in asserting that the solution for accelerations was unobtainable by means of relative acceleration methods alone.

Professor Koenig's comment regarding the use of the center of acceleration is of great value.

[6] See the writer's paper entitled, "A Uniform Method for Determining Angular Accelerations in Mechanisms," Journal of Applied Mechanics, Trans. ASME, vol. 68, 1946, p. A-41; and discussion, p. A-309.

Book Reviews

Automatic Controls

DIE SELBSTTÄTIGE REGELUNG. By A. Leonhard. Springer-Verlag, Berlin, Germany, 1949. Paper, 6½ × 9½ in., ix and 284 pp., 254 figs., Dm 24; bound Dm 27.

REVIEWED BY R. H. MACMILLAN[1]

A BOOK on automatic control in the electrical field by Professor Leonhard was published in 1940 in Germany. This was reprinted in 1944 in the U.S.A. The present work is written from a general engineering, rather than a specifically electrical standpoint. In many respects it is the most comprehensive and readable text, dealing with the fundamental theory of control, which has yet appeared. Perhaps the easiest way to indicate the scope of this book is to list some of the major subjects which are either not treated at all or only in passing: nonlinear or discontinuous systems, distributed delays, the logarithmic form of the response locus, rms error criterion of performance, input noise or disturbance. But, within the limits suggested by these topics, the book deals with the theory of regulation in considerable detail and is illustrated profusely with line diagrams. The arrangement is clear and systematic. The mathematics used is no more advanced than necessary: the Laplace transformation is employed in its simplest form, as a tool rather than as a means to dazzle the reader with the author's mathematical prowess. There are many practical worked examples of all grades of difficulty, but no problems are provided for the reader. The bibliography is somewhat limited; of the forty-nine works mentioned, only one, Nyquist's original paper, is in English; the remainder are exclusively German publications. Certainly every scientific and engineering library should have a copy of this book and it is to be hoped that an English translation will become available.

Applied Elasticity

NEUERE FESTIGKEITSPROBLEME DES INGENIEURES—AUSGEWÄHLTE KAPITEL AUS DER ELASTOMECHANIK. By W. Flügge, R. Grammel, K. Klotter, K. Marguerre, and G. Mesmer. Edited by K. Marguerre. Springer-Verlag, Berlin, Germany, 1950. Cloth, 6 × 9 in., 120 figs., vii and 253 pp., Dm 25.50.

REVIEWED BY A. M. WAHL[2]

THIS book consists of a number of chapters by a group of authorities on selected subjects in the fields of applied elasticity and vibrations. As indicated in the preface the book is based on a series of lectures given in the greater Berlin area during 1941 and covering subjects which, although well known to scientific workers, are not so generally known to engineers. The various subjects treated include the following: experimental determination of stresses by Prof. G. Mesmer, fundamentals of the theory of elasticity and buckling phenomena by Prof. K. Marguerre, shell theory by Prof. W. Flügge, vibration problems in structures and machinery by Prof. K. Klotter, and methods of solution of technical eigenvalue problems by Prof. R. Grammel. In general, the subjects are treated from the viewpoint of value in engineering work. Throughout the text reference is frequently made to the more comprehensive books of the various writers, particularly *Technische Dynamik* by Biezeno-Grammel, *Statik und Dynamik der Schalen* by Flügge, and *Einführung in die technische Schwingungslehre* by Klotter.

Coming now to the various chapters, the first one on experimental stress determination (Mesmer) deals mainly with mechanical methods of strain measurement and the fundamentals of photoelasticity. However, this chapter appears to be somewhat out of date since the widely used wire resistance (SR-4) strain-gage method is not treated while the brittle-lacquer (Stresscoat) method is barely mentioned. However, the treatment of strain measuring instruments is of considerable interest.

In chapter 2 on fundamentals of elasticity theory (Marguerre), extensive use is made of vectorial methods and the subject is presented in a very readable manner, particularly for engineers having some knowledge of vector analysis. Energy methods (principle of virtual work) are also discussed and the application of such methods to problems in elasticity is indicated.

Besides a discussion of the damped single-degree system, the chapter on vibration phenomena (Klotter) includes a brief treatment of forced vibration of certain nonlinear systems, systems with many degrees of freedom, and vibration of elastic bodies (beams, shafts, plates). The section on eigenvalue problems (Grammel) deals with such important engineering subjects as natural torsional frequencies of in-line engines, critical speeds of steam-turbine rotors, frequencies of rotating disks, vibration of turbine blades, etc. The fundamentals of elastic stability, including the buckling of columns and plates, are dealt with in the concluding chapter by Marguerre.

Engineers and research workers interested in applied elasticity, stress analysis, or vibration problems should find much useful material in this volume.

Classical Mechanics

CLASSICAL MECHANICS. By Herbert Goldstein. Addison-Wesley Press, Inc., Cambridge, Mass., 1950. Cloth, 6 × 9 in., xii and 399 pp., illustrated, $6.50.

REVIEWED BY MORTON FINSTON[3]

THIS volume results from lectures in an advanced course for physics students at Harvard University and has obviously been prepared with an eye to companion courses in modern physics. When a choice is available, a problem is formulated with the aid of techniques useful in newer fields. For example, rigid body rotations are studied from the standpoint of matrix transformations thus allowing a unified mathematical treatment of the inertia tensor, Lorentz transformations in Minkowski space, and resonant frequencies of small oscillations.

Although a book on this subject can hold few surprises in the way of subject matter, the chapter titles are worth listing here to indicate its scope: (1) Survey of the Elementary Principles, (2) Variational Principles and Lagrange's Equations, (3) The Two-Body Central Force Problem, (4) The Kinematics of Rigid Body Motion, (5) The Rigid Body Equations of Motion, (6) Special Relativity in Classical Mechanics, (7) The Hamilton Equations of Motion, (8) Canonical Transformations, (9) Hamilton-Jacobi Theory, (10) Small Oscillations, (11) Introduction to the

[1] Visiting Assistant Professor of Mechanical Engineering, Massachusetts Institute of Technology, Cambridge, Mass.

[2] Advisory Engineer, Westinghouse Research Laboratories, East Pittsburgh, Pa. Mem. ASME.

[3] Naval Supersonic Laboratory, Massachusetts Institute of Technology, Cambridge, Mass.

Lagrangian and Hamiltonian Formulations for Continuous Systems and Fields.

One could easily list many other changes in treatment, from those given in older books, such as mentioned above. Since readers of this journal may have only a secondary interest in preparation for study in modern physics, and since Dr. Goldstein's preface describes accurately the features of his work, however, we may omit such comments. On the other hand, students of applied mechanics will be interested in the unusually clear discussions of basic physical principles which they often employ. They will also appreciate the care with which unfamiliar mathematical techniques (those beyond the scope of advanced calculus) are introduced and complemented by physical arguments. Also, chapter 11 provides an account such as the reviewer has not seen before, of the foundations of a topic increasingly important in applications.

Aside from its obvious value to physics students this work may be highly recommended to mathematicians and engineers, familiar with advanced calculus and intermediate mechanics, who wish to study further in classical mechanics with a minimum of discouragement and with considerable pleasure. In a field which has been covered by many masters, Dr. Goldstein's book is still a definitely worth-while addition.

The Creep of Metals and Alloys

THE CREEP OF METALS AND ALLOYS. By E. G. Stanford. Temple Press, Ltd., London, England, 1949. Cloth, 5½ × 8½ in., xvi and 162 pp., 32 figs., 15s.

REVIEWED BY E. OROWAN[4]

OUR knowledge of creep has only recently emerged from a state of rarefied chaos, and it will be years before the final stage of consolidated clarity is reached. It is in this period of the development of a scientific subject that the writing of a book is the most difficult; this point ought to be kept in mind in judging the present work which is a brief review of creep testing and of the physics of creep. Its 127 text pages are subdivided into five chapters: The Conditions Required for the Measurement of Creep (pp. 1–40); The Creep Curve (pp. 41–53); The Factors Which Influence the Creep of Metals (pp. 54–63); The Presentation of Creep Results (pp. 64–80); and The Physical Study of the Mechanism of Creep (pp. 81–127).

The first chapter reflects the attitude of the experienced practitioner. Creep-testing machines are not discussed at all, because they represent "the easiest part of the testing technique." Only four text figures show extensometers, two of these a design that, in the author's opinion (with which the reviewer agrees), is to be rejected. On the other hand, nine pages are devoted to the important matter of the calibration of thermocouples. Of the devices for measuring their emf, only the Diesselhorst potentiometer is described; its principle is not explained in detail, but the operating instructions occupy five pages.

Very understandably, in view of the limited size of the book, numerical creep data are not given, except as curves illustrating general points. This, however, is carried too far in Figs. 12 and 13 which show experimentally measured curves without mentioning the metal to which they refer.

In the discussion of creep curves, a remarkable dualism of the book becomes apparent. Several points that can be understood satisfactorily on the basis of the physical considerations reviewed in the last chapter are treated as unsolved problems in the second and third chapters. Thus the report on the role of grain boundaries is dominated by cautionary remarks against any general rule while, in fact, the matter has been elucidated to a great extent by R. Becker's work in 1925–1926 which is quoted in the list of references.

The fourth chapter is a very brief sketch of various methods for utilizing creep measurements in engineering design. Here also more precision in the elaboration of the subject matter would have been desirable. Thus, it is stated on p. 64 that "in most applications . . . . . a creep rate of 0.1 per cent in a life of from 10 to 20 years is an outside figure"; on the following page, however, we read "Tapsell has stated that if the applied stress is such that a stage of constant rate of strain of the order of 10^{-6} in. per in. per day is maintained, ... then such a rate of strain can be associated with a long life of many years under conditions similar to those of the test." The author accepts this statement although a simple calculation based on the number of the days in a year shows that, in this case, the "outside figure" of 0.1 per cent strain for the lifetime of a structural part would be reached in less then 3 years.

The last, very long, chapter is a compilation of recent theoretical physical work on transient creep. There is little doubt that this work does contain the basic elements for the understanding of the creep process; most of it, however, is still in a rough, unpolished, workshop stage, with many cul-de-sacs intersecting the passable roads. It is a question whether a textbook presentation at this stage is in the interest of anybody; however, this is a tactical question on which different opinions may be held.

[4] Professor of Mechanical Engineering, Massachusetts Institute of Technology, Cambridge, Mass.

Heat Transfer and Insulation

ELEMENTS OF HEAT TRANSFER AND INSULATION. By Max Jakob and George A. Hawkins. Second edition. John Wiley & Sons, Inc., New York, N. Y. 1950. Cloth, 6 × 9 in., xvi and 230 pp. illustrated, $4.

REVIEWED BY WARREN M. ROHSENOW[5]

THIS book constitutes an extension of its original version without change of structure or scope. Many new elements have been inserted to broaden the coverage of each section.

The steady-state conduction section includes, in addition to the usual treatment of plates, cylinders, and spheres, the solution of the edge and corner problems, and the solution of problems of complicated shapes by the methods of field mapping and relaxation. The solutions of a number of unsteady-state conduction problems, including flat plates with periodic change of surface temperature, are presented in equation and graphical form without proof. Also included is the Dusinberre method of numerical solution of unsteady-state conduction. A few pages are devoted to steady-state heat conduction in a flat plate carrying a uniformly distributed electric current.

The subject of heat transfer from solid surfaces to fluids is opened by a discussion of dimensional analysis followed by short chapters on free convection, forced convection, and condensation and boiling. In each of these, a brief discussion of the peculiarities associated with each phenomenon is followed by a summary of recommended correlation equations.

Following this discussion of surface heat-transfer coefficients, conduction problems with associated convection are treated. This comprises a steady-state study of fins and of heat exchangers (including multipass exchangers) and an unsteady-state study of the numerical solution of problems involving conduction in solids with heat transfer to a fluid at the surface.

The study of radiation is limited to the exchange of energy through transparent space between solid surfaces, black or grey.

[5] Assistant Professor of Mechanical Engineering, Massachusetts Institute of Technology, Cambridge, Mass. Mem. ASME.

Gaseous radiation is omitted. There follows a series of short chapters on miscellaneous subjects—combined effect of conduction, convection and radiation, experimental determination of thermal conductivity and emissivity, and thermal errors associated with temperature measurement. The last chapter is a presentation of the analogy between heat transfer and momentum transfer as stated by Reynolds (1874) and later modified by C. M. White (1932).

In the presentation of unsteady conduction the authors employ the term "heat storage" and, in the treatment of the temperature distribution in solids carrying an electric current, they employ the term "heat production." These are generally "frowned" upon in the study of thermodynamics. On page 205 in the last sentence of the first paragraph the word "increase" should be "decrease." On page 4 the discussion of units of density applies only to values at sea level. This is not stated.

The arrangement of material and the writing style are very good, making the reading enjoyable. The treatment of the various phases of the subject is brief, but the coverage is probably quite adequate for an elementary heat-transfer course.

Strength of Materials

EINFÜHRUNG IN DIE FESTIGKEITSLEHRE. By F. Schultz-Grunow. Werner-Verlag, Dusseldorf, Germany, 1949. Paper, 6¾ × 9½ in., 239 figs., index, 244 pp., Dm 15.

REVIEWED BY J. P. DEN HARTOG[6]

A REFRESHINGLY new textbook on Strength of Materials, published in Germany by a professor of mechanics of the Technical "Hochschule" at Aachen. It covers a much broader field than is usual for elementary texts in the United States, treating not only the usual topics of compression, bending, torsion, column buckling, and thin-walled vessels, but going as well into thick cylinders, curved bars, flat plates, beams on elastic foundations, Saint Venant torsion, and the principle of minimum energy. The chapters on buckling are particularly interesting, treating in an elementary manner several cases usually found only in advanced textbooks.

The book is very clearly written and the many illustrations are aptly chosen to show at a glance the intrinsic meaning of a formula or a stress distribution. As practically all other German or continental textbooks, it contains no problems.

The sections on thin-walled structures are particularly interesting, showing in pictures how the load is transmitted by shear through the skin to tension and compression in the edge fastenings.

Introduction to the Transfer of Heat and Mass

INTRODUCTION TO THE TRANSFER OF HEAT AND MASS. By E. R. G. Eckert. With an Appendix on Property Values, by Robert M. Drake, Jr. McGraw-Hill Book Company, Inc., New York, N. Y., 1950. Cloth, 6 × 9 in., 18 tables, index, xiii and 284 pp., illustrated. $4.

REVIEWED BY JOSEPH KAYE[7]

THIS book is a translation of the author's German text with the corresponding title. The translation has been modified to include some of the recent advances made in the field of heat transfer in the last decade.

The first 227 pages of the book cover the conventional material on heat transfer. Only 30 pages of the book are devoted to material on mass transfer. Some 17 pages, in the Appendix, present values of properties of various substances.

Chapter 1 introduces the basic definitions and concepts used. Chapter 2 considers both steady-state and transient-heat-conduction problems. Chapter 3 treats convective heat transfer, placing much emphasis on the nature of the flow in the boundary layer; this chapter includes also discussions of recent improvements in the theory of turbulent heat transfer and of heat transfer in gases at high velocities. Chapter 4 presents the basic concepts of thermal radiation together with heat transfer by radiation. Finally, chapter 5 presents some elementary concepts of mass transfer together with an exposition of the close relationship between heat and mass transfers.

Numerous examples, included throughout the book, are worked out in detail as an aid to the student. The index is excellent.

It is regrettable that the author did not attempt to achieve a better balance of the distribution of material between the fields of heat transfer and mass transfer. Although the important analogy between heat and mass transfer is stressed in the last chapter, many useful correlations in mass transfer are omitted completely. It is difficult to justify the omission of the Sherwood-Gilliland correlation of mass transfer between phases in view of the emphasis placed on the corresponding correlation in heat transfer. As a text in heat transfer, however, the book is commendable.

Mechanics of Deformable Bodies

MECHANICS OF DEFORMABLE BODIES. Lectures on Theoretical Physics, Vol. II. By Arnold Sommerfeld. Translated from the second German edition by G. Kuerti. Academic Press, Inc., New York, N. Y., 1950. Cloth, 6 × 9 in., 74 figs., problems, appendixes, index, xi and 396 pp., $6.60.

REVIEWED BY E. REISSNER[8]

ADVANCED students and workers in the fields of fluid mechanics and elasticity will find this second volume of Professor Sommerfeld's lectures on theoretical physics of considerable interest. While much of the factual contents of this book may of course be found also in other texts, the author's point of view and manner of presentation is bound to widen the reader's horizon and increase his understanding of the physical significance of important methods and results.

About two thirds of the material in this book is on fluid mechanics and one third on elasticity. Included are a review of vector analysis and an introduction to tensor analysis. Among the topics considered are two-dimensional potential flow, vortex motion, slow viscous motion and lubrication theory, water waves, shock waves, hydrodynamic stability, turbulence, elastic beam theory, Saint Venant torsion theory, deformations of helical springs, crystal elasticity, and waves in elastic bodies with applications to the foundations of the quantum-theoretical thermodynamics of the solid body. A historically interesting chapter deals with the quasi-elastic body (gyroscopic ether) which serves to illustrated the fundamental difference between mechanics and electrodynamics.

The author's intention may be described by the following quotation: "My aim is to give the reader a vivid picture of the varied material that comes within the scope of the theory when a reasonably elevated vantage point is chosen. With this purpose in mind I shall not be too concerned if I have left some gaps in the systematic justification and axiomatic structure of the work.

[6] Professor of Mechanical Engineering, Massachusetts Institute of Technology, Cambridge, Mass. Mem. ASME.

[7] Associate Professor of Mechanical Engineering, Massachusetts Institute of Technology, Cambridge, Mass. Mem. ASME.

[8] Professor of Mathematics, Massachusetts Institute of Technology, Cambridge, Mass. Jun. ASME.

At any rate I have avoided frightening the student with drawn-out investigations of a mathematical or logical nature and distracting his attention from that which is physically interesting." The reviewer feels that in this aim the author has succeeded to a considerable extent.

Mathematics for Engineers

LA MATEMATICA DELL'INGEGNERE—e le sue applicazioni. By Guido Fubini and Giuseppe Albenga. Vol. 1. Nicola Zanichelli Editore, Bologna, Italy, 1949. Paper, 7 × 10 in., viii and 498 pp., illustrations, 4000 lire.

REVIEWED BY W. FLUGGE[9]

A BOOK on mathematics for engineers should be different from the Traités d'Analyse which French authors of the last hundred years have written with so much mastery. It should put less emphasis on minute exactness in the logic structure and more on the physical interpretations of mathematical theorems. The authors realize this situation and have made an attempt to write a reference book comprising those parts of mathematics which the average engineer should have at hand. They treat such subjects as elementary, descriptive and analytic geometry, vectors, complex numbers, linear equations and determinants, limits, elementary functions, and differential and integral calculus. Along with these mathematical subjects, many applications are explained in much detail, such as moments of inertia, center of gravity (in this order), funicular polygons, Maxwell stress diagrams, Coriolis' force, Mohr's circle. Most of these subjects are connected to some part of the mathematical text, but some of them appear as rather isolated items, for example, a chapter on the optics of lens combinations.

The book seems to be the first in Italy which tries to adapt the teaching of mathematics to the needs of the engineering profession, and its merits should be appreciated correspondingly. Looking at it from this country, the reviewer feels that the authors might have gone much further in penetrating the presentation of mathematical theory with the spirit of technical thinking, but that they might have omitted a good deal of the mechanical subjects, which would have a better place in special books on the theory of structures.

However, the book will be of interest to those who teach mathematics to young engineers and who want to know what their colleagues in Italy think about this problem.

Supersonic Aerodynamics

SUPERSONIC AERODYNAMICS—A Theoretical Introduction. By Edward R. C. Miles. McGraw-Hill Book Co., New York, N. Y., 1950. Cloth, 6 × 9 in., 109 figs., index, xi and 255 pp., $4.

REVIEWED BY MORTON FINSTON[10]

THIS book presents the mathematical background to some topics of interest in supersonic aerodynamics. An indication of the subject matter may be gleaned from the titles of the eleven chapters: (1) Fundamental Theory (i.e., thermodynamics, etc.); (2) Divergence and Circulation; (3) The Potential Equation; (4) Characteristics in the Plane; (5) Linear Theory of Plane Flow; (6) The Linear Potential Equation in Three Dimensions; (7) Shock Waves; (8) Cones in Supersonic Flow; (9) The Method of Characteristics for Axially Symmetric Supersonic Flow; (10) Potential Flow in the Hodograph Plane; and (11) Comparisons of Adiabatic and Shock Flow in Two Dimensions. The author addresses his work to two large groups, "seniors and beginning graduate students in aeronautical engineering" and practicing aerodynamicists who might wish "to break the confines of handbook engineering" and he is concerned principally with assembling the mathematical ideas they will find useful in further study. This is quite successfully done. The derivations and explanations suppose only limited mathematical knowledge and proceed in an unusually simple and clear fashion to more advanced ideas.

Some readers might prefer a slightly different emphasis in the selection of subject matter. For example, although linearized supersonic flow is not only comparatively simple but also among the most highly developed and useful branches of the entire theory, it is dealt with very briefly. In fact, some comments might indicate to the uninitiated that it isn't particularly valuable and the book is constructed so the whole subject may be easily eliminated. The reviewer also regrets that some mention, however brief, of the existence and influence of viscosity is not made. It would seem to be important in orienting beginners.

The treatment of the topics covered is clear, simple, and actually at a level which should make it accessible to the intended reader. Each chapter has a number of problems related to and, happily, at the level of the text. Figures are numerous and helpful and the appearance of the volume is very good. The book will undoubtedly be appreciated and used by many instructors and find its way into the hands of many more students seeking an introduction to supersonic flow theory, and that is as it should be.

Statics and Dynamics

STATIK UND DYNAMIK. By Theodor Pceschl. Springer-Verlag, Berlin, Germany, third edition, 1949. Paper, 6½ × 9½ in., 257 figs., viii and 343 pp., Dm 22.50, bound Dm 25.

REVIEWED BY J. P. DEN HARTOG[11]

THIS is a new third edition of a well-known German text on mechanics. It covers the usual subject matter of the elementary engineering course in the subject. Vectors are used from the very start and continue throughout the book. The subject of kinematics is more fully treated than is usual in books of this type. Lagrange's equations are mentioned without proof at the end of the book, and gyroscopes come in for two or three pages. There is a collection of almost 200 worked-out problems or examples throughout the text.

Mechanics of Particles

MECHANIK DEFORMIERBARER KÖRPER. By Friedrich Tölke. Vol. 1, "Der punktförmige Körper. Springer-Verlag, Berlin, Germany, 1949. Cloth, 6 × 9¼ in., viii and 388 pages, Dm 45.

REVIEWED BY A. M. WAHL[12]

THIS is a comprehensive work which deals with the mechanics of particles and comprises the first volume of a series on the general subject of mechanics of deformable bodies. (Other books in this series which are planned include vol. 2 on statically stressed solids, vol. 3 on dynamically stressed solids, vol. 4 on thermally stressed solids, and vol. 5 on fluids and gases.)

The first portion of the volume under review deals largely with the mechanics of single particles under arbitrary motions. Extensive use is made of vectorial methods of representation, and for this reason parts of the book may be rather difficult reading for engineers not too familiar with such methods. However,

[9] Engineering School, Stanford University, Stanford, Calif.

[10] Naval Supersonic Laboratory, Massachusetts Institute of Technology, Cambridge, Mass.

[11] Professor of Mechanical Engineering, Massachusetts Institute of Technology, Cambridge, Mass. Mem. ASME.

[12] Advisory Engineer, Westinghouse Research Laboratories, East Pittsburgh, Pa. Mem. ASME.

the author devotes considerable space in this volume to the development of mathematical fundamentals including those of vector analysis and differential geometry. (This is done in preparation for the later volumes of this series.) Throughout the text, an understanding of the methods used is facilitated by working out in detail a number of examples on subjects of practical interest. Such subjects include for instance: motion of a crank drive, acceleration of a projectile in a gun barrel, motion in gravitational or electrostatic fields.

The second portion of the book is probably of more direct value to mechanical engineers, particularly those interested in vibration theory, since this part deals largely with the motions of groups of particles or masses connected by springs. In addition, the single-mass spring-supported system both with and without damping is also treated rather extensively. Considerable space is devoted to the chain system consisting of many masses connected by springs, and in particular to the case where the masses and spring constants are equal. Other problems include the case of a shaft of constant diameter on which are mounted a number of disks of varying size and that of a stretched cable carrying a number of discrete masses.

The final chapter of the book treats single and multimass systems with different types of damping, including the constant (Coulomb), viscous, and velocity-squared types. Considerable space is devoted to a detailed working out of the equations for the case of a two-mass system, one mass being viscously damped while the other is excited by a rotating mass type of vibrator. Another case of practical importance is that of a damped single-degree system in which the amplitude of the exciting force increases linearly with time. The solution of technical problems for cases involving velocity-squared damping is also facilitated by the tables given.

No literature references are provided in this volume since the author considers that the subject of particle mechanics has long been a closed field within the domain of classical mechanics. The lack of an index may also make it more difficult to use the book as a reference.

Although the solutions to many of the problems appear in rather cumbersome form, it is the reviewer's opinion that many of these solutions may be helpful in treating certain complicated vibratory systems which occasionally arise in mechanical-engineering practice.

Synthetic Resins and Their Molding

KUNSTHARZPRESS-STOFFE UND ANDERE KUNSTSTOFFE: Eigenschaften, Verarbeitung und Anwendung. By Walter Mehdorn. Springer-Verlag, Berlin, Germany, third edition, 1949. Cloth, 5¼ × 8 in., 276 figs., tables, viii and 354 pp., Dm 36.

REVIEWED BY ALBERT G. H. DIETZ[13]

ALTHOUGH this book covers all synthetic resins—their properties and fabrication—most of the emphasis is on the thermosetting resins, as the author himself points out in the foreword to this third edition. Furthermore, the book is written primarily for the technician in the fabricating shop and for the man who has to decide which resin and which method of manufacture should be used for a given application.

Properties—mechanical, electrical, chemical—are described briefly and presented in tabular and graphical form. A considerable section is given over to a fairly detailed exposition of types of presses and molds for the fabrication of thermoplastic and thermosetting resins. Methods of finishing, testing, and inspection are outlined, and examples of typical uses of the various types are given. The book is generously illustrated.

For the American some of the most interesting portions of the book deal with German practice, which was largely unknown outside of Germany during the war years.

[13] Professor of Structural Engineering, Department of Building Engineering and Construction, Massachusetts Institute of Technology, Cambridge, Mass. Mem. ASME.

JOURNAL OF APPLIED MECHANICS

VOL. 18
NOs. 1 – 4
1951

PUB. 575

UNIVERSITY MICROFILMS
ANN ARBOR, MICHIGAN. 1952

RESOLUTION CHART

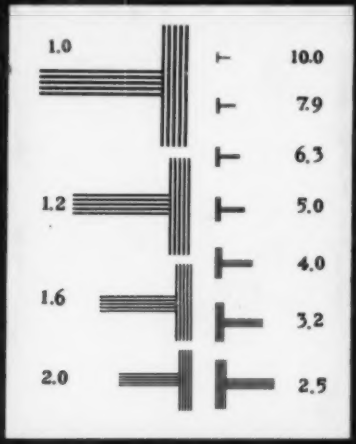

100 MILLIMETERS

INSTRUCTIONS Resolution is expressed in terms of the lines per millimeter recorded by a particular film under specified conditions. Numerals in chart indicate the number of lines per millimeter in adjacent "T-shaped" groupings.

In microfilming, it is necessary to determine the reduction ratio and multiply the number of lines in the chart by this value to find the number of lines recorded by the film. As an aid in determining the reduction ratio, the line above is 100 millimeters in length. Measuring this line in the film image and dividing the length into 100 gives the reduction ratio. Example: the line is 20 mm. long in the film image, and $100/20 = 5$.

Examine "T-shaped" line groupings in the film with microscope, and note the number adjacent to finest lines recorded sharply and distinctly. Multiply this number by the reduction factor to obtain resolving power in lines per millimeter. Example: 7.9 group of lines is clearly recorded while lines in the 10.0 group are not distinctly separated. Reduction ratio is 5, and $7.9 \times 5 = 39.5$ lines per millimeter recorded satisfactorily. $10.0 \times 5 = 50$ lines per millimeter which are not recorded satisfactorily. Under the particular conditions, maximum resolution is between 39.5 and 50 lines per millimeter.

Resolution, as measured on the film, is a test of the entire photographic system, including lens, exposure, processing, and other factors. These rarely utilize maximum resolution of the film. Vibrations during exposure, lack of critical focus, and exposures yielding very dense negatives are to be avoided.

THIS PUBLICATION IS REPRODUCED BY AGREEMENT WITH THE COPYRIGHT OWNER. EXTENSIVE DUPLICATION OR RESALE WITHOUT PERMISSION IS PROHIBITED.